Finite Element Modelling of the Thermal Effects of the Manufacturing Process on the Quality of Electronics Interconnection

by

A.O. Ogunjimi

A Doctoral Thesis submitted in partial fulfilment of the requirements for the award of Doctor of Philosophy of the Loughborough University of Technology

July 1994

Statement of Originality

I am responsible for the work outlined in this thesis, the original work is mine except where explicit reference is made to other sources and that neither this thesis nor the work contained therein has been submitted to this or any other institution for a higher degree.

Acknowledgement

I acknowledge with gratitude, the support, advice and encouragement of my supervisor, Professor David J. Williams, on this project. I am grateful to Mr. Paul P. Conway and Mr. David C. Whalley for their support and advice on various elements of this project and their software administration skills which have been so vital to this work. I will also like to thank Dr. Kevin J. Tilley and Dr. Andrew West for their support and for proof reading this thesis. My gratitude goes to the members of technical staff of the department for their help with the experiments, and to Mr. Jon Petzing of the Mechanical Engineering department for his help with the ESPI experiments.

The financial support of the ACME Directorate of the Science and Engineering Research Council is gratefully acknowledged.

Finally, I will like to express my gratitude to my wife, 'Lola, and my daughter, 'Toni for their patience and motivation and to my family for their continued support throughout the project.

To God who answers prayers

Abstract

This thesis demonstrates the feasibility of using finite element analysis to model the thermo-mechanical effects of manufacturing processes on electronics interconnection. The thesis has two significant complementary parts. The first of these explores the modelling of heat transfer in a commercial solder reflow furnace to contribute to the understanding of the non-uniform distribution of heat on a printed circuit board within the furnace. The second part of the thesis identifies the thermal stresses in a die attach assembly using an electrically conductive adhesive, typically cured in a reflow furnace, thereby indicating potential points of failure.

The first part of the thesis reports the calibrated modelling of a reflow furnace of commercial complexity as part of the demonstration of the feasibility of creating a concurrent engineering design tool for electronic interconnection. The application of a technique using area proportional thermal conductances to model the convective heat transfer between the furnace and board is demonstrated. The model explores the effects of the mechanisms of heat transfer within the oven to show that this is more uniform with the addition of convection and that edge heaters appear to have little effect.

In the second part of the thesis the effect of the material properties of glass transition temperature, Youngs Modulus and coefficient of thermal expansion were quantified using finite element modelling, to show that these properties significantly affect the structural integrity of the interconnections constructed using conductive adhesives. Electronic Speckle Pattern Interferometry (ESPI) methods are also shown to be an effective method of validating such finite element models. This work required the measurement of the viscoelastic properties of typical materials using novel specimen preparation techniques. It is anticipated that the conclusions presented are conservative because of the assumptions and sensitivity analyses made during the modelling activity.

The combined results of the two parts of this work demonstrates the feasibility of modelling the solder reflow process and highlights the potential of electrically conductive adhesives as replacement for solder in high temperature applications. Promising avenues for further work include improved non-linear modelling of interconnection systems and understanding of the effect of rework, including reliability assessment. In addition, further work remains to be carried out in the determination of relevant material properties in representative configurations.

Abbreviations

CAD	- Computer Aided Design
DMTA	-Dynamic Mechanical Thermal Analysis
DSC	- Differential Scanning Calorimetry
ESPI	- Electronic Speckle Pattern Interferometry
FEA	- Finite Element Analysis
FEM	- Finite Element Method
FIP	- Fully Imidised Polyimide
HTE	- High T_g Epoxy
IR	- Infrared
kg	- Kilo- gram
kPa	- Kilo- Pascal
mm	- Milli-metre
MPa	- Mega-Pascal
PCB	-Printed Circuit Board
PLCC	- Plastic Leaded Ceramic Chip
s	- Second
SOIC	- Single Outline Integrated Circuit
TCE	-Thermal Coefficient of Expansion
TMA	-Thermal Mechanical Analyser
T_g	- Glass Transition Temperature
TSOP	- Thin Small Outline Package
PTFE	-Polytetrafluoroethylene
LTE	- Low T_g Epoxy
µm	-Micro-metre

TABLE OF CONTENTS

Chapter 1

Introduction

1.1 Introduction

The quality and long term reliability of electronic interconnections depends, not only on the properties of the components but on the influence of the parameters of the various manufacturing processes to which the components were subjected. Crucial processes in electronics manufacturing are the reflow of solder or curing of adhesives used in the interconnection. These processes are ill-understood and the effect of application of heat (during the processes) on the structural integrity of the resulting interconnection remains unquantified. The size of electronic components and the high component density on a printed circuit board makes the experimental investigation of the various manufacturing parameters difficult. Therefore, the application of modelling techniques similar to those found in structural analysis offers a significant potential in the understanding and control of such processes. Process modelling also promises other economical and technical benefits such as the integration of design and manufacturing activities and a rapid response to a dynamic market demand.

This thesis focuses on the major joining processes for electronics assembly, surface mount soldering and the emerging alternative technology of adhesive joining. The modelling of the soldering process and the effect of curing of adhesives on electronics interconnection are presented as part of efforts towards a better understanding of the physics of these processes. A physics of failure approach was also used to highlight the effects of the manufacturing process on the design variables of a die-attach interconnection. The balance of this chapter highlights the background and the contents of the thesis.

1.2. The Soldering Process

The soldering process has been the most appropriate and economic process for electronics interconnection for many years. In volume production, the surface mount circuit boards are usually assembled by printing or stencilling solder paste onto the printed circuit board followed by component placement, solder reflow and cleaning. Infrared (IR) sometimes in combination with convective heating has become the most

common methods of solder reflow. This is primarily because the method is economical and can be controlled easily. This method has also been found to reduce the occurrence of many reflow defects associated with the older Vapour Phase method. The sub-processes undergone by the components on a board during this reflow method are however, ill-understood. While many complex variables with complex interactions are responsible for reflow defects, the applied temperature during the process is considered to be a major driving factor. Part of this thesis therefore addresses the issue of establishing the temperature distribution on a printed circuit board (PCB) undergoing the reflow soldering process.

Increasing concerns over the severe environmental impact of the process and safety of workers (solders contain lead) has intensified the search for an alternative to the soldering process. Moreover, there is an increasing demand for electronic units capable of operating at high ambient temperatures in automotive and aerospace applications. The near eutectic Tin-Lead solders are unsuitable for temperature cycling above 125°C (170°C to 250°C required). Many of the more robust and high performance electronic assemblies use components with 25mil or smaller pitch in which there is an increasing difficulty in using solder. There is therefore a need for an alternative joining method that will survive high temperature operation, meet the requirements of high reliability over an extended life, that is capable of quality interconnection for fine pitch components and able to meet environmental requirements of most countries. Loaded (conductive) adhesives seem promising a candidate material and an effective alternative to solder.

1.3. The use of Loaded Adhesives for Electronics Interconnection

Adhesives have the potential to combine a high operating temperature with a relatively low process temperature and also remove some of the less environmentally friendly operations such as flux cleaning. They are however more expensive than solder but lower material usage may make the overall cost attractive. Similarly, the surface mount and the die attach processes commonly found in soldered interconnections may be readily modified for conductive adhesives.

The currently available loaded adhesives are capable of continuous operations at temperatures up to 180°C. There are other adhesives claiming the capabilities of operating at temperatures above 200°C and anisotropic adhesives seems a perfect candidate

for fine pitch applications. Apart from the initial trials of the early silver filled epoxies for die attach, very little is known about the applications of conductive adhesives for high temperature interconnection.

1.4. The Approach

The effects of manufacturing processes on a populated printed circuit board (PCB) are difficult to study experimentally because of the cumbersome setups required, the harsh environment for instrumentation and the time scale for the crucial stage of the process. Similarly, there are limits to details obtainable using theoretical methods of analysis, for example, the intricate geometries that characterises modern electronics interconnection are difficult to take into consideration. A helpful option therefore is the computational modelling of the process.

The work outlined in this thesis is that of the use of Finite Element Analysis (FEA) to investigate the effect of manufacturing processes on the quality of electronics interconnection. The Finite element method was specifically chosen because it can fully incorporate the geometry of the interconnect while the results of analysis can also be visualised for any particular instant of the analysis. It is also a step towards the creation of a simulation tool for electronics manufacturing processes. The Finite element models were verified using relevant experimental methods.

1.5. Structure of the Thesis

The work concentrated on two major aspects of electronics interconnection, the macro-level: furnace to board, and the micro level: board to component. This thesis is therefore divided into two broad categories, the first of which is the modelling of a commercial industrial reflow furnace and the second, is the use of loaded adhesives for electronics interconnection.

Chapter 2 reviews the basic principles of the finite element method and relevant work found in the literature on the different approaches to the modelling of electronics manufacturing processes. The appropriate standard methods for the relevant materials property measurements are reviewed and the state of the art methods of model validation discussed.

The thesis, in chapter 3 presents the results of a set of trials carried out on one of the

SENJU Infrared/Convection reflow furnaces at the IBM (UK) Greenock plant. The experiments investigate the effect of features such as the edge heater and convective heating on the temperature distribution of a printed circuit board. Similarly, the effect of tracks on the heat distribution on the surface of the PCB is presented. The results of the experiments are used to calibrate a finite element model of the furnace and of typical product assemblies[1].

Chapter 4, describes the modelling of a commercial state-of-the-art oven. The methods used in combining the effects of the radiation and convection modes of heat transfer are highlighted. The result from the model is compared with the experimental results and the amount of heat transferred by the various mechanisms identified in chapter 3 quantified.

Chapter 5 identifies and discusses the techniques used to measure the relevant material properties needed to model the effect of manufacturing processes on a conductive adhesive interconnection. Issues like sample preparation and the comparison of the material properties to that of solder are discussed. The creep characteristics of a conductive adhesive and solder are also compared.

Chapter 6 examines the variation of residual stresses and the associated potential failure modes based on the mechanical properties of the adhesive matrices. The effect of the die geometry, bond layer thickness, presence of voids and anisotropic properties of the silicon die on the stress distribution in the assembly are examined by conducting model sensitivity, materials property sensitivity and process sensitivity analyses.

Chapter 7 presents the results of the experiment performed to calibrate Finite Element models using Electronic Speckle Pattern Interferometry. The particular model examined is that of an isotropically conducting adhesive, CTC2000, die-attach cooling from the adhesive curing temperature to ambient. The results of the experiment are compared with the finite element analysis of chapter 6.

1. This trials were jointly conducted with D.C. Whalley who later developed a finite element model of a populated PCB.

The concluding chapter 8 discusses the result of this work and conclusions arising from them. It evaluates the authors contribution and suggests directions for further investigations.

Chapter 2

Literature Review

2.1. Introduction

Various methods have been used to study the effects of manufacturing parameters on the quality of interconnection. Thermal equations have been used to model the infra-red reflow soldering process and practical methods using data-loggers have been used to predict temperature distribution of products as they go through the reflow furnace. Similarly, a variety of methods have been used to predict the failure mechanisms in electronics packaging. While a number of reports can be found in the literature about the use of finite elements to model and investigate the reliability of electronics packages in service, less reports are found in the literature that addresses the application of finite element analysis to process modelling, let alone, the specific area of electronics manufacturing process modelling. While there is ongoing analytical work in this area, most industrial product and process specifications are based on experience, without a full understanding of the underlying physics, this is particularly highlighted in most of the experimental reports on the reliability of electronic packages. The demanding nature of today's electronics interconnection calls for a deeper understanding of assemblies which in turn highlights the need for more sophisticated methods of analysis such as the finite element method.

Most of the above methods, have their various strengths and limitations as will be outlined in this chapter. The chapter is divided into three major sections; Overview of the finite element method, electronics manufacturing process modelling, materials property measurement and model validation methods. An overview of the basic principles of finite element analysis, which is used in the core of the work described in this thesis is also included. Different approaches to the modelling of electronics manufacturing processes modelling are discussed. The appropriate standard methods for the materials property measurements are also reviewed and state of the art methods of model validation discussed.

2.2. Overview of the Finite Element Method

The finite element analysis is currently regarded as the most powerful and wide spread numerical method in structural analysis[1,2,3]. The increased popularity of this method is due to the increasing computational powers of modern computers and the availability of software. Computers are faster and more powerful than ever before enabling the application of this method to a variety of industrial problems. Moreover, FEM enables the peculiarities and intricacies of geometries and loading conditions to be taken into consideration. Similarly it can also take into consideration the time and temperature dependence of materials and boundary conditions as appropriate.

The finite element method replaces a continuum, i.e a structure, by a finite number of elements which interact at a number of grid points called nodes[1, 4]. The finite elements are so small such that the displacement or stress fields across the element can be approximated fairly accurately, leaving only the magnitude to be determined. This method is based on numerical methods such as the Rayleigh-Ritz[1, 4, 5] method. Ideally, this step requires a good understanding of the mechanical properties of the structure and insight into the appropriate mesh design, taking into account, for example, that more elements are needed for accuracy in the area with rapidly changing stress and strain fields. This stage of the analysis is called pre-processing.

The elements are then assembled in such a way that the displacements and stresses are continuous across the element interfaces and the applied loads and specified boundary conditions are satisfied. The complete structure is solved typically by determining the displacements at the nodes which is in turn used to determine the stresses.

2.2.1 Stiffness Matrix

There are three types of relationships usually employed in the solution of any structural problem [4- pp9]:

1. Equilibrium: The relationship between the stress, σ, and the applied forces or other stresses, applied are expressed by an equilibrium equation

2. Compatibility: Strain, ε, and displacement are related by the compatibility equation. These two variables are purely geometrical and are more easily determined using the nodes. Compatibility equations are often linear for small displacements.

3. Stress -Strain Law: This constitutive relationship, as it is called, is empirical and is often dependent on experimental evidence. Constitutive relationships may include thermal effects and also reflect the elasto-plastic relationships in metals. This relationship is linear for many structural materials within their useful working range.

The displacement method is a very popular approach in finite element analysis. It is so called because the displacement variables are solved first. In this method the strain is determined from the displacement using the compatibility equation. The stress of the elements are determined from the nodal forces using the equilibrium equation and the stress strain related by the stress strain law.

The relationship between the nodal forces and the nodal displacement is established using the stiffness matrix (also called the compliance matrix). The matrix can be obtained from the Lagrange Theorem ("if a body is in equilibrium, the change in the strain or potential energy caused by a small unit change in the generalised displacement equals the corresponding generalised force"[5]). The theorem is expressed mathematically as follows:

$$\frac{\delta U}{\delta q_k} = Q_k \qquad \text{Eq.2.1}$$

Where U is the strain (potential energy), q is the intensity of the distributed load, Q is the moment of force, F, and k is a numerical factor.

Therefore using the Lagrange theorem, [1], the generalised nodal forces F_k can be represented by the matrix

$$\{F_k\}=\{F_1, F_2, F_3,.....\} \qquad \text{Eq.2.2}$$

and the generalised nodal displacements as

$$\{q\} = \{q_1, q_2, q_3, \ldots\ldots\} \qquad \text{Eq.2.3}$$

therefore,

$$\Sigma F_k \delta q_k = \int_v (\sigma_x \delta\varepsilon_x + \sigma_x \delta\varepsilon_y + \ldots + \tau_{yz} \delta\gamma_{yz})\, dV \qquad \text{Eq.2.4}$$

The above equation expresses the sum of the work of the external force {F} as the sum of the internal forces {σ} moving through a virtual displacement. If the integral is taken throughout the volume of the finite element, the above relationship will become

$$\{\delta q\}^T \{F\} = \int_v \{\delta\varepsilon\}^T \{\sigma\}\, dV \qquad \text{Eq.2.5}$$

The strain, ε, and displacement, q, can be related by the set of matrices

$$\{\varepsilon\} = [\Phi]\, \{q\} \qquad \text{Eq.2.6}$$

Where [Φ] is a rectangular matrix derived from the coordinates of the given points.

Similarly, the stress σ and the displacements are related by the set of matrices

$$\{\sigma\} = [E]\, \{q\} \qquad \text{Eq. 2.7}$$

Substituting for {ε} and {σ} in Eq. 2.5,

$$[K]\, \{q\} = \{F\} \qquad \text{Eq.2.8}$$

where

$$[K] = \int_v [\Phi]^T [E]\, dV \qquad \text{Eq.2.9}$$

[K] is called the stiffness matrix. This matrix is particularly important because it relates the forces to displacements in the finite element model.

2.2.2. Proprietary Software

Finite element software became available in the early 1970's on powerful mainframes and was used in the aerospace, nuclear, defence and automotive industries [6]. The subsequent advances in the computer industry has however led to the development of newer and more powerful software capable of running on personal computers. Numerous modern finite element proprietary software packages are now available in the market. The software packages can be categorised into two major types; Pre/Post processors and finite element solvers. Often a finite element package consists of the pre/post processors and a solver as is the case with I-DEAS, ANSYS and PATRAN, and are compatible with general purpose finite element solvers like ABAQUS, MSC/NASTRAN, MARC, TMG. Some solvers like ABAQUS also combine a solver with a post-processor.

Pre-processor modules are used to prepare the geometry and to define the relevant materials properties and boundary conditions. Such modules also contain the algorithm to subdivide the geometry into finite elements. The method of geometry preparation varies across packages, it varies from the use of solid modellers to simple point and curve generators. Some packages also have the facilities for importing geometries prepared in other Computer Aided Design (CAD) software. The prepared geometry is discretised into finite elements, material properties are defined and the boundary conditions and relevant loadings applied. This module generates a file containing the geometry, finite element, materials properties and boundary conditions data used by the solver. There are facilities in modern softwares for writing these data in a format compatible with the different solvers available.

The solvers are mainly general purpose, capable of handling mechanical, thermal and coupled thermal-mechanical problems. However there are specialised solvers such as FLOTHERM for computational fluid dynamics and TMG for thermal analysis. The solver is at the heart of the analysis because it generates the results. The solver takes the output from the pre-processor for analysis based on the relevant information such

as the geometric locations of the nodes, the boundary conditions and the applied loadings. Solvers often allow the use of user written subroutines, a set of codes written by the user to perform special functions unique to the particular application. The output from the solver module is the displacement, temperature, heat, stress and strain distribution of the finite element entities as appropriate.

The Post-Processor module is used to present the results of the analysis in a user friendly format. A typical post-processor module has the capabilities to translate the result files from a variety of solvers. The format for presentation of results includes a plot of the exaggerated displacement superimposed on the original structure, a contour plot of displacement, temperature, stress and strain, and XY or XYZ graphs of the relevant data. The use of tensors to indicate direction of action of vector quantities is also a common practice. Modern post processors also have facilities for importing experimental data for comparison with analysis results and to create derivatives of the original results. In most cases it is also possible to generate a hardcopy of the display of results.

2.2.3. Overview of I-DEAS Finite Element Software

I-DEAS Finite Element software used in this work is a complete finite element package with the three generic modules described earlier. It allows the analyst to build a complete finite element model, including the physical and materials properties, loads, and boundary conditions. It is also compatible with a variety of solvers.

2.2.3.1. Geometry Modelling

Geometry creation in I-DEAS can be done in three ways:

1. The Solid Modeller from which solid geometries are created. Each solid geometry can be interpreted as lines, points and surfaces that is easily accessible in the FEM module.

2. Geometry Modelling Task in which geometries are created from a series of curves and points recognised by the FEM module.

3. The Pearl relational database can also be used to import geometric datasets created in other softwares.

2.2.3.2. Pre-processing

The pre-processing module descretises the created geometry into finite elements by first dividing it into regions called mesh areas for planar geometries and mesh volumes for solids. Materials and physical properties can be allocated to either the mesh areas or the elements created in the mesh area, either way, the properties are assumed the elements during analysis. The models can be checked, at the discretion of the analyst, for ill-conditioned elements or duplicate nodes. The boundary conditions are applied as constant or variable (described by equations) displacement, forces, temperature and heat fluxes. Files compatible with a variety of solvers can be written from this module for analysis. In this study, the ABAQUS solver was used hence the pre-processor was set up to write files for the solver.

2.2.3.3. Post-Processing

The post processor is versatile. The solutions are translated into I-DEAS format by this module and a wide variety of methods can be used to display the results. Deformation plots imposed on the original model can be used to view displacements. Similarly, contour plots are used to view displacement, strains and stresses. Vector plots can also be used when the direction of stresses and other vector quantities are critical.

I-DEAS Finite Element software has been chosen in this work because of its versatility and its compatibility with a wide variety of software and the ease of use because it is menu driven.

2.3. Modelling of the thermal effects of manufacturing process on electronics interconnection.

The thermal effects of the manufacturing process on electronics interconnection mainly arises from the reflow of solder or the cure of conductive adhesives used in the assembly of the interconnection system. This stage of manufacturing is the most heat intensive and often involves the heating of the entire assembly leading to the thermal coefficient of expansion mismatch in the assembly which in turn leads to thermal stress. Most of the manufacturing methods applicable to the use of solders in

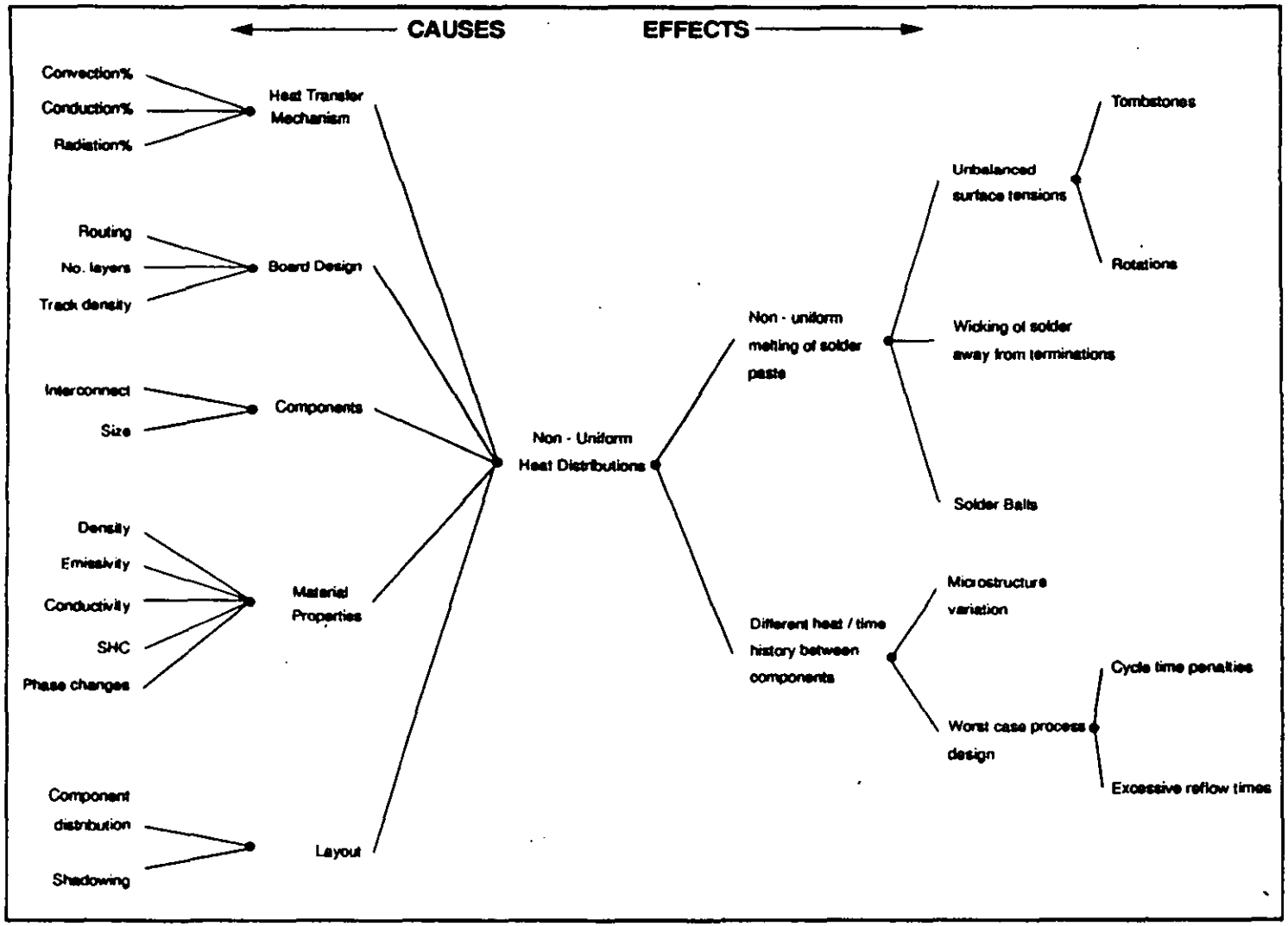

Figure 2.1: Causes and effects of Heat distribution during the reflow process
(P.P. Conway et al)

electronics manufacturing were found to be applicable to the use of conductive adhesives[7]. The infrared and conventional (dry) oven systems used for solder reflow are also used for conductive adhesives, hence a study of the effect of the heating method is applicable to both materials.There are four categories of Infrared reflow: the Lamp IR or radiant IR, Reflector/Lamp IR, Natural convection/IR or Panel IR and the forced air convection/IR. The infrared/ convection process has however become the most dominant of the reflow technologies.

Most manufacturers are aware of the complex variables that interact in the production of surface mount assemblies, it is however difficult to evaluate or quantify the effect of each variable. P.P Conway et al. [8] have identified that most of the process variables (causes in figure 2.1) affect heat distribution on the surface of the printed circuit board which in turn leads to defects (effects) in the manufactured joints. It therefore follows that a better understanding of the temperature distribution within the oven and across the PCB is needed to reduce defects in the manufactured joints.

2.3.1. Oven Systems

The literature on oven systems is mainly dominated by manufacturers of reflow systems to promote their technology [9,10,11]. More realistic appraisals of reflow systems have been undertaken by users [12, 13, 14].

The two most frequently used methods of solder reflow are vapour phase and infrared reflow. Many improvements have been made to these methods over the years with the sole aim of achieving thermal equilibrium. While the vapour phase process has been found to have many drawbacks [8] and given rise to a series of problems such as wicking, tombstoning and component rotation, it still finds application in small volume and critical applications where high component density may result in shadowing with infrared heating[8]. Another great advantage of the vapour phase system is in its inherent predictability[8].

Infrared heating has however over the years gained a wider acceptance than vapour phase. While the merits of IR over vapour phase method is summarised in Hey [13], Gothard [14] and Walton [15], the increasing use of IR is predominantly due to the

preference for the dry heating of IR when compared to the wet system of the vapour phase.

2.3.2. The Modelling of the Infrared Reflow Process

There are several examples of the use of finite element analysis to examine power dissipation and thermal characteristics under environmental test condition of products in service [16, 17, 18, 19]. However very little can be found in the literature on the application of finite element analysis to reflow process modelling.

Eftychiou et al. [20] developed a numerical model of the transient thermal response of a prewired circuit in a converted wind tunnel fitted with infrared panel heaters (to simulate the conditions in a reflow furnace). An heirachical approach, which divides the system into oven condition and thermal response of the board, was taken. Numerical analysis and finite difference methods were used to solve for a 2-Dimensional steady state heat transfer and relevant boundary condition equations. The oven model ignores the presence of the card assembly in predicting the air velocity and the temperature distribution in the oven. The predictions of the oven model are then used to determine the boundary condition for the card assembly model. The assemblies modelled are not typical of the real industrial situation. The components used are materials with established properties, for instance, aluminium sheet modules were substituted for electronic components and lexan sheets for FR-4 board. The assemblies in some instances were also coated to alter the emisivities of the assembly to that of a known material.

Whalley et al. [21] developed a finite element process model of a three zone, six infrared heater panel, purely radiative reflow machine by Surf Systems. The model was developed using Structural Dynamics Research Corporation(SDRC) I-DEAS Finite element Pre/post processing software and MAYA Thermal Model Generator (TMG), finite difference solver.

The model consists of two structures, the furnace and the PCB, thermally interlinked by radiative heat transfer relationships. Unlike the approach by Eftychiou et al., this model takes into consideration, the continued presence of the PCB at every stage of the analysis. Similarly the motion of the PCB through the furnace was mimiced by

varying the temperature of the individual heater panels, hence a transient analysis was carried out for the entire duration of the PCB in the furnace. The work presented in this thesis builds upon this earlier work by Whalley et al.

2.3.3. Thermal Stress Analysis of Die-attach Assembly

Considerable work has been carried out on the thermal stresses in die attach assemblies. Reports in the literature show the application of various methods applied in the past varying from qualitative experiments[22, 23, 26] to the use of constitutive equations [24, 25, 26, 27, 28, 29]. The literature on the application of finite elements to modelling die attach has mainly addressed the reliability of the electronic packaging during service as opposed to the effect of manufacturing processes on the reliability. Most of the reports likewise did not address the use of conductive adhesives in electronics manufacturing and their peculiarities except for the reports [22, 23, 26] in which experimental work arising from accelerated testing is used to investigate the performance of the early generations of adhesives in electronic packages. The work from CALCE Electronics Packaging Research Centre[26], carried out at about the same time as the research reported here was undertaken, uses constitutive equations and experiments to investigate the failure mechanisms in die attach assemblies utilizing both solder and conductive adhesives. Driemer et al. [24] used a different approach to model thermal stress in layered structures. The approach uses a three-terminal equivalent electrical circuit to represent elastic tensile, shear characteristics and thermal coefficient of expansion. Equivalent circuits of several layers are used to simulate laminates. Current and voltage obtained from the equivalent circuits using electrical network analysis are used to derive thermal stresses and thermal coefficient of expansion respectively. This method however depends on numerical methods to determine the effect of geometry and interfacial stresses.

Overall, experimental work identifies the common modes of failure but gives no explanation for the source of failure, while constitutive equations can predict mechanisms of failure but are unable to map stresses to specific locations on the assembly. Finite element analysis can predict the mechanism of failure and map stresses to the particular point of occurrence from which the modes of failure can be deduced. The latter method was chosen by the author.

2.4. Materials property measurements

Accurate material property values are crucial for a reliable finite element analysis. However, they (material properties) are often difficult to obtain especially for commercial materials. This is mainly, for example, because most of the modern generation of conductive adhesives are both relatively new and include undisclosed proprietary materials. The relevant industrial standards such as military standards also do not often necessitate the measurement of elastic properties of the particular material therefore the onus of measurement of such properties often rests on the user. This section therefore concentrates on the relevant documented work on the techniques for measuring the relevant materials properties. The relevant properties in this work being the modulus of elasticity, Poisson's ratio, thermal coefficient of expansion (TCE), glass transition temperature (T_g) and creep properties for polymers. These properties are for the purpose of this thesis, classified as either thermal or mechanical properties. Application properties such as thermal conductivity and dielectric constants (although not relevant to the work in this thesis) are often given in technical literature that accompanies these products.

There are several sources that give lists of the important properties of electronics packaging materials [30, 31, 32, 33, 34]. However detailed documentation of testing methods is mainly found in the annuals of the American Society for Testing and Materials[35] and the Institute for Interconnecting and Packaging Electronic Circuits[36].

2.4.1. Thermal Properties

The expansion of a material being heated ideally occurs in three dimensions, however the thermal coefficient of expansion (TCE) is usually measured in one direction. The main method used in measuring TCE of electronic packaging material is dilatometry [37]. Other methods such as telemiscroscopy, interferometry, capacitance and X-ray diffraction for crystalline materials [37] are also used. Capacitance and Laser interferometry techniques [38, 39] are usually applied for precision measurements and for measuring the TCE of films.

The dilatometric technique uses a probe made of a material of known thermal expansion characteristics whose end touches the specimen held in a heating or cooling chamber. The other end of the rod protrudes from the chamber such that the expansion of the specimen upon heating or cooling can be determined by measuring the movement of the rod. Dilatometric techniques are similarly used for bulk polymers in the form of the Thermal Mechanical Analyser (TMA).

2.4.2. Mechanical Properties

The mechanical properties of a material are determined by measuring the stress-strain response of the material. The relevant stress-strain response in this work is the elastic response and time dependent properties such as creep for polymers. Uniaxial tensile testing of flat or cylindrical materials [35, 36] is widely used for measuring the elastic properties of the metals and polymers used in electronics packaging, and techniques are being developed to enable the use of specimens with micrometer dimensions as found in electronics packaging [40]. Three or four point flexure techniques are used for ceramics, laminates and other solid polymers found in electronics packaging. The elastic strength properties are reported as the ratio of stress to strain referred to as Young's modulus of elasticity. Above the elastic limit, the results are reported as a graph of stress versus strain. These results are often presented to show variation with temperature and rate of loading [41] and tests could be carried out in shear, double lap shear and torsion [42]

The viscous or time dependent behaviour of polymers introduces a complex response to mechanical excitation. Therefore, a more sophisticated method of measuring the elastic modulus is required. Dynamic mechanical thermal analysis (DMTA) is used to measure both in-phase and out of phase (with the applied stress) components of the elastic response of polymers in oscillating flexure or shear [43, 44, 45, 46]. The test is also used to detect the glass transition (T_g) temperature. The TMA and Differential Scanning calorimetry are other methods used to determine the T_g of polymers [47].

The Poisson's ratio is determined by measuring the change in dimension of the specimen in a direction perpendicular to the direction of the applied stress. The perpendicular change in dimension is then expressed as the ratio of change in the direction of

application of the stress. Bauer at al. reported the use of a gas dilatometer to determine the Poisson's ratio of polyimide films [48].

Creep and stress relaxation are used to determine the long term reliability of materials (usually, solder or polymers) in packaging often operating at temperatures close to their maximum operating temperature. Creep is the extension of a specimen under constant load or stress while stress relaxation is the stress under constant extension. The loading can be either in tension, compression, flexure or shear. The same equipment as is used to determine the modulus of elasticity can be used for creep and stress relaxation tests.

2.5. Overview of Model Validations

The electronics industry has seen a gradual transition from a responsive problem solving approach to mechanical issues, to predictive mode of operation in which numerical analysis especially, finite element modelling is playing a significant part. However, for accuracy of numerical analysis, the models used need to be verified or calibrated as appropriate. A variety of methods are used for model validation. These methods are typically used to measure temperature history, in and out of plane displacement measurements and stress-strain components of a specimen or system. Model validation includes the use of thermocouples and dataloggers to record temperature history of a specimen or system[10, 49, 50], the use of strain guages[51, 52] and optomechanics [53, 54] for stress strain verification.

Studies involving reflow often require the measurement of the temperature variation across the reflow furnace. The method often employed, and the most effective method, is the use of thermal dataloggers to record the temperature-time variations as measured by an attached thermocouple passing through the furnace [9, 10, 49, 50]. There are more records of the use of the method by manufacturers promoting their products rather than the verification of an analytical method. This method however was applied by the author (chapters 3 and 4) to validate the finite element model of an infrared reflow furnace. A similar experiment is described in [49] which was subsequently used in the validation of an analytical model.

2.5.2. The use of electrical strain gauges to validate modelled stresses

The bonded electrical resistance strain gauge has been one of the most frequently applied tools for experimental stress analysis since 1940 following its successful application at the Massachusetts and California Institutes of Technology in 1938 [55, 56]. The advent of the thin foil strain gauges in the early 1950's subsequently lead to wider application (because of its reduced size and ease of bonding to specimen) in industry. These are now widely applied.

The application of electrical strain gauges in electronics packaging can be found in the literature since the early 1960's [57, 58]. More recent applications are reported by R.B Jordan [59], Usell et al. [60], Gee et al. [53, 61] and Lanchberry et al. [62]. Common problems in the application of strain gauges have always been:-

1. The large quantity of measurement and calculations required for effective stress mapping [53]

2. The effect of the properties of the materials from which the strain gauge is made e.g the need for temperature compensation for the resistor by pre-determining the temperature coefficient [53] or the use of external dummy gates to achieve temperature compensation. Likewise the anisotropic effect of the materials in which the resistors are implanted.

3. The presence of a foreign body can also affect stress transmission in the body under test.

4. Because of the finite size of the strain gauge its application in miniaturised electronic packages of today may be limited.

Errors in strain gauge mapping of stresses as explained above are inevitable due to the technique and the materials used. Therefore the validity of the results of stress-strain mapping using strain gauges can be limited. Optical methods offer a whole-field displacement measurement with greater accuracy and are capable of measuring the smaller components as found in today's electronic components. They are often preferred to the less accurate and more restricted strain gauge methods.

2.5.3. Optical Methods for Model Validation

Advanced optical methods now form a major validation tool for stress-strain analysis. The "displacement and deformation method" as this is known, starts from the use of laser holograms and interferometers to measure vibrations in a wide variety of applications ranging from breast cancer detection [63] to mechanical component vibration and deformation [64, 65]. This method measures the wholefield displacement and hence the strain of a component or system. The measured strain is then compared with predicted strain or displacement of an analytical method. The sensitivity of this method makes it very popular for the continually miniaturizing electronics packaging, for example, the microscopic Moire interferometry is capable of 20nm displacement sensitivity [66]. The most widely applied method is the Moire interferometry.

The Moire interferometry utilizes the diffractive properties of light to produce a whole-field contour map of the in-plane displacement of a specimen. This method has been applied sucessfully by Bastawros et al. [67, 68] to verify an FEM model of the low cycle thermal fatigue of solder ball connections. The method was also used at the IBM Corporation to study the strain and bending characteristics of a Thin Small Outline Package (TSOP) module and the effect of anisotropic properties of the materials of a Printed Circuit Board (PCB) on its mode of deformation. The results were subsequently used to verify finite element models [69].

Other optical methods similar to Moire interferometry are being used for measuring the out of plane displacement of electronics packaging. Classical Holography and interferometers [70] are common methods used for measuring out of plane displacement under thermal and mechanical loading. A modified and relatively modern type of interferometry is the Electronic Speckle Pattern Interferometry [71] applied in this work for the verification of the later models. This method compared with classical holography enables real-time display of deformation (displacement) mode directly on a television screen. A full account of the use of ESPI to measure the static and dynamic surface displacements is given by Wykes et al. [72, 73].

2.6. Conclusions

The use of computational modelling in the electronics industry is changing from problem solving to prediction. Similarly, it is becoming clearer from works like that of Conway et al. [8] that the manufacturing process plays a very important role in the reliability of electronic packages. The shortage of literature (compared to issues like fatigue and creep failure of solder) showing experimental or modelling work in this area shows that it has not been well addressed, supporting the value of the work reported here.

This literature review has highlighted the background on which the work reported in the subsequent chapters of this thesis is based. It also shows that experimental stress analysis identifies mode of failures but cannot explain the mechanism. Constitutive equations can be used to identify mechanisms of failure but it is often difficult to map stresses to particular locations on the assembly. This work serves as a bridge between scattered island of works by identifying relevant and effective methods and the technology required to address the issues of the effect of the manufacturing process on electronics interconnection.

Chapter 3

Reflow Furnace Trials

3.1. Introduction

A crucial process variable in the reflow soldering of surface mount assemblies is the non uniform heat distribution on the printed circuit board (PCB) as it goes through the reflow furnace. This subsequently leads to various effects as identified in Figure 2.1, by P.P. Conway et al[8]. This chapter presents the results of a set of trials carried out on one of the SENJU Infrared/Convection reflow furnaces at the IBM(UK) Greenock plant. These experiments were conducted to enhance understanding of temperature related manufacturability issues and to study the heat distribution on the PCB within the furnace. The effect of features such as the edge heater and convective heating on the temperature distribution of a printed circuit board assembly was also studied by varying the furnace parameters. The size/type of the PCBs were also varied to study the effect of tracks on the heat distribution on the surface of the PCB. The result of these experiments are used to calibrate a finite element model of the furnace and of typical product assemblies, this is presented in chapter 4. The experiment is described following a discussion of the effects of various heat mechanisms on the design of reflow ovens

3.1.1. Thermodynamic Principles of Heating in Reflow Furnaces

The three modes of heat transfer, namely conduction, convection and radiation are inherently present in any reflow furnace. The processing capabilities of any system are dictated by the dominant mode of heating which in most reflow furnaces is either radiation or convection, the conductive mode of heat transfer is considered a minor contributor (except within the PCB). The system is said to be in equilibrium when there is a balance of heat flow across the system. The dominant heat transfer mechanism primarily defines the equilibrium conditions of the given system. The nearer to equilibrium a system operates, the more uniform the temperature of the assembly to be heated because heat transfer is driven by the temperature differences (temperature gradient) between heat source and the target. Unfortunately, thermal gradients, a

function of the heating rate, are created on components being heated as the system gains heat before its peak temperature[10]. These gradients can be reduced by allowing the assembly to stabilize to the temperature of the actual heat source at a particular point in the system [15]. However, in practical conditions, application of thermal energy will have to cease before equilibrium can be reached in order to give realistic processing times and prevent overheating of some components. It is also worth mentioning geometric effects at this point [74]. The elements of the edge of the PCB have a higher surface area to volume ratio compared to those in the centre, they are able to absorb more heat and get hotter. Therefore before the temperature of the PCB attains equilibrium, the edges will be hotter than the middle of the board

The above thermodynamic principles of heating form the basis of using a combination of infrared and convection in reflow furnaces. The air as a fluid has the ability to maintain the temperature around the assembly at a temperature near that of the source, which in most state-of-the-art furnaces, is an array of infrared emitters or a heater coil in the fan duct. The use of other components like the edge heaters does not only supply heat to the edges, but maintains a constant supply of heat to the whole system while the assembly stabilizes.

Much has been written, especially by their manufacturers, to encourage the use of forced convection ovens for equilibrium heating[9, 10, 11]. However most users consider that better heating can be achieved by a combination of one or more modes of heating[12, 15, 75]. Even vapour phase processes are being improved upon by using a combination of IR and convection as pre-heat before reflow.

3.2. The SENJU Reflow Furnace

The SENJU reflow furnace is a state-of- the-art reflow furnace used in the IBM Manufacturing plant at Greenock. It combines infrared and convective heating with the use of conveyor edge heaters. There are six heater zones within the furnace, comprising of twelve individually controllable heater panels, six below the conveyor supporting the printed circuit board and six above. The 'finger type' conveyor has adjustable width and is capable of supporting printed circuit boards 120mm to 410mm wide. IBM however uses work holders allowing the same conveyor width setting for all the

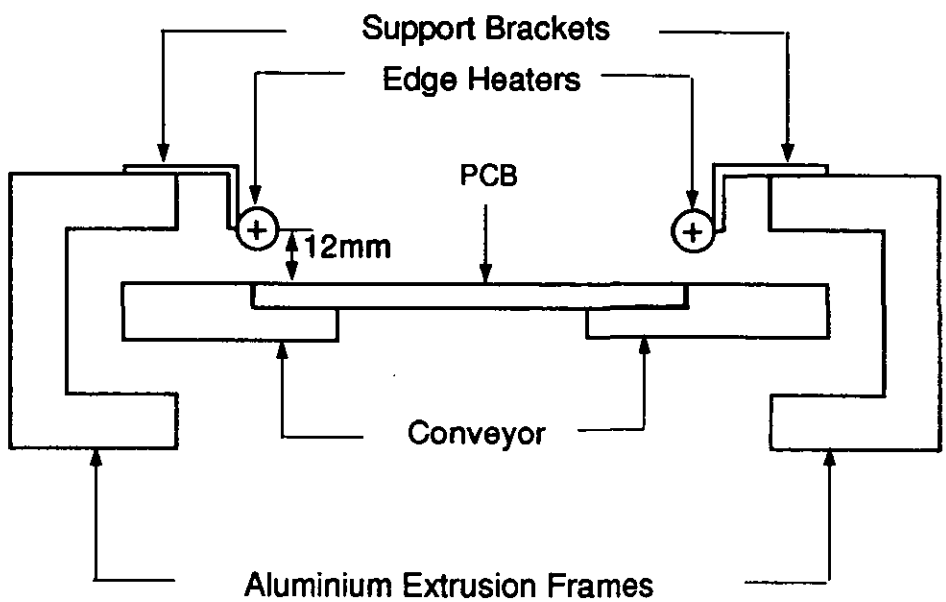

Figure 3.1: Cross section of the conveyor/edge heaters set-up

different types of PCB processed at the factory. However, because one side of the conveyor is fixed and the other movable, the position of the workholder is not always symmetrical about the centre of the furnace.

The area comprising the first two heater zones is called the pre-heat section, the next two heater zones is the mid heat section while the last two heater zones is called the reflow section. These sections are so named because of the activities within the different sections. The PCB is gradually heated from ambient temperature to a temperature close to that of the reflow temperature in the pre-heat section (which is longer than the other sections), further heat is applied at the mid heat section to further raise the temperature of the PCB nearer to the reflow temperature. This section is shorter than the pre-heat section but longer than the reflow section. The reflow section is where the actual solder reflow takes place. The temperature in the furnace is highest in this section. It is therefore the shortest section to prevent prolonged exposure of components on the board to high and damaging temperature.

Forced convective heating is achieved in the furnace by compressed air blown through the porous infrared heater panels by a system of duct and fans. The air supply can be adjusted to supply maximum (100%)[1], half (50%) or no air at all. The edge heaters run parallel to the conveyor and are suspended at a height of 12mm above it (Figure 3.1). They are capable of delivering a maximum heat flux of 2.4KW uniformly distributed along their length.

3.3. Experiment Description.

The experiment described below was carried out using the equipment from the main facility at the IBM manufacturing plant at Greenock, Scotland. The objective of the experiment is to investigate the heat distribution on the PCB within the furnace and to study the effect of features such as edge heaters and convective heating on the heat distribution on the PCB. The effect of tracks on the temperature distribution of the PCB and the components on the PCB was also investigated. Other experimental variables identified during work planning were the effect of workboard holders and the

1. 100% airflow is equivalent to full convective capacity in this particular furnace while 50% is equivalent to half the capacity.

variation in the airflow characteristics in the different sections of the furnace. These were investigated by using a bare board without a workboard holder as control and by measuring the airflow rate in the different sections of the furnace.

Four types of circuit boards (all FR4 base material) were used for the experiment:

a. An unpopulated IBM standard size (356 x 502)mm board with tracks, held in the workboard holder and a bare sheet of FR4 same size as the workboard holder.

b. Eurocard size (230 x 160) mm bare board suspended in a workboard holder, six (2 x 3 sets) eurocard size boards with components but without tracks and three eurocard size boards with components and tracks (same layout as without tracks).

c. A typical assembled IBM product in a workboard holder.

Other experimental hardware, consisted of a Datapaq reflow tracker kit which was used to record the temperature history of points on the PCB as it travelled through the furnace. The data from the reflow tracer kit is transferred on to a computer disk for analysis and long-term storage using an IBM laptop personal computer. The airflow rate in the different sections of the furnace was measured using a airflow meter.

3.4. Procedure

Six thermocouple probes from the Datapaq data logger were attached to the boards and components using either high temperature solder or heat resistant adhesive tapes as appropriate. The datalogger, which can be triggered manually or automatically by heat, is used to record the temperature of the relevant points on the board as it passes through the furnace (The datalogger, when fully charged is capable of reading 2040 data points on each of the 6 channels). The recorded temperature history of the board is then transferred from the datalogger into the personal computer for analysis and long-term storage on disk. The heating parameters were varied by controlling the level of convection from natural convection (fans off) to 50% and subsequently 100% air. The edge heaters were also switched on and off as appropriate. Figures 3.2 and 3.3 illustrates the position of the of the thermocouples on the board. Temperatures in the gaps between the heater panels and of the edge heaters were measured. The air velocity in the various sections of the furnace was also measured using the air flow

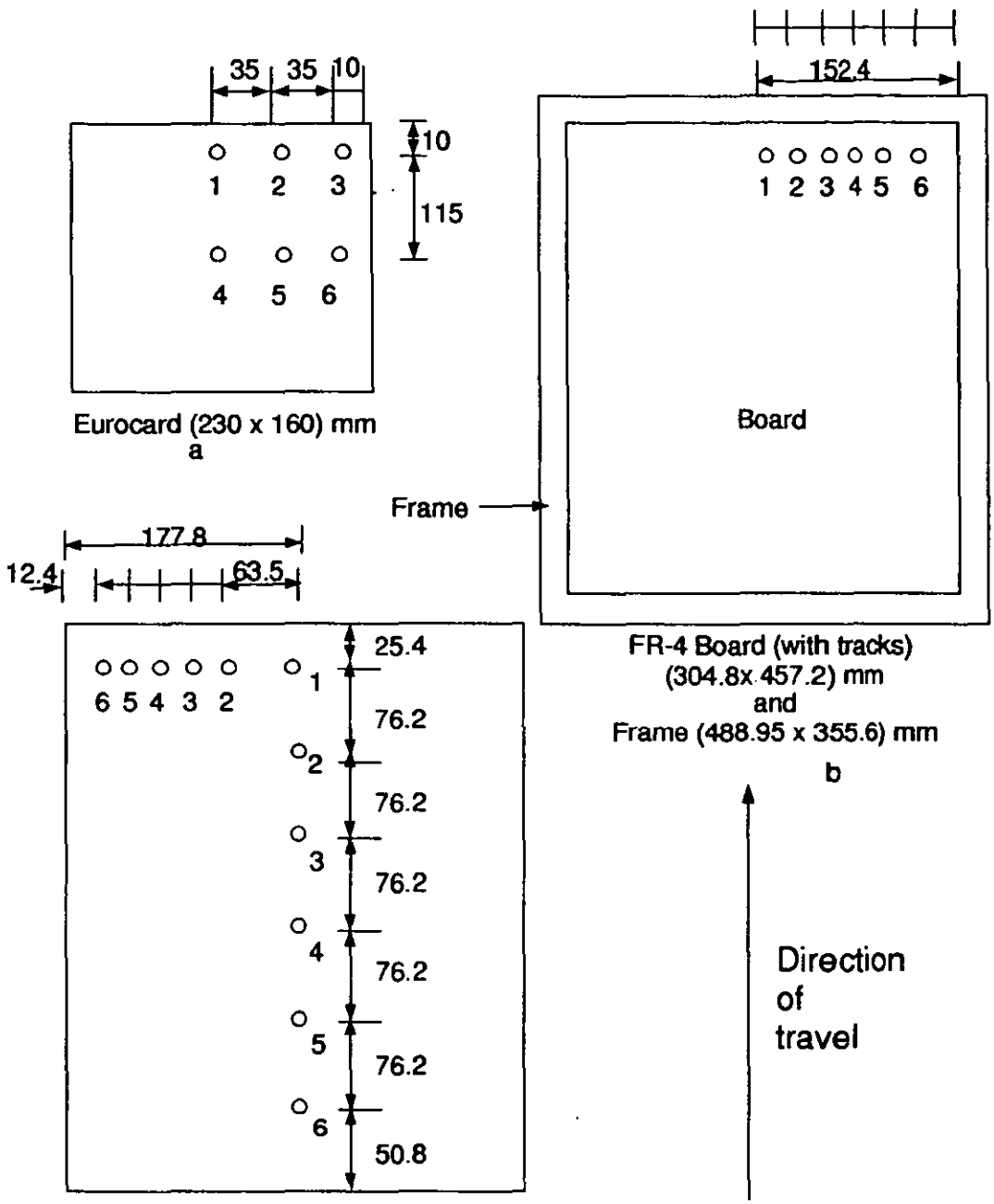

Figure 3.2: The layout of positions of thermocouples

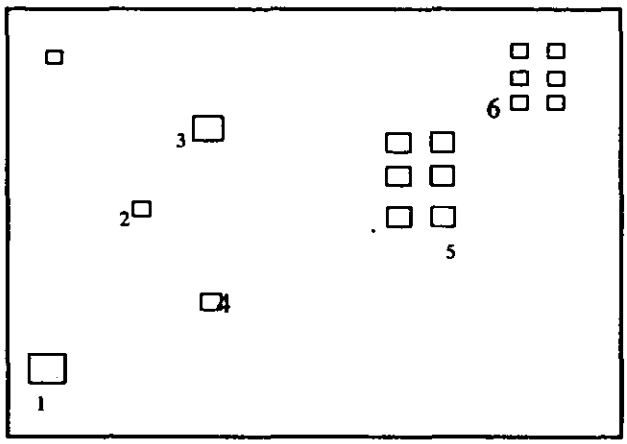

Passive Components: Resistors and Capacitors

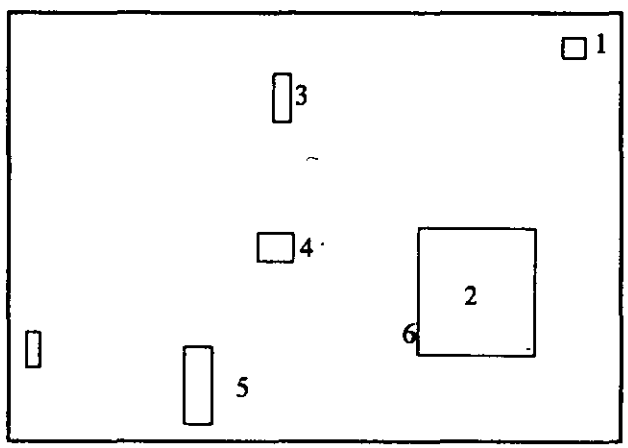

Active Components: SOICs and PLCCs

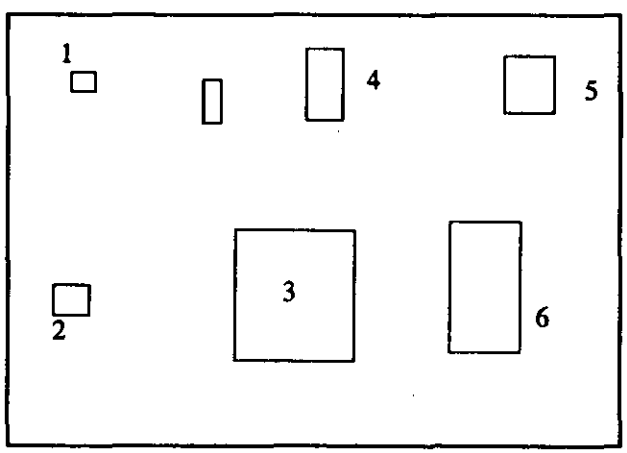

Product : Combination of Active and Passive Components

Key:

1,2,3,4,5,6 - Position of thermocouples

Resistors

Capacitors

Small Outline Integrated Circuit (SOIC)

Plastic Leaded Chip Carrier (PLCC)

Thermocouple mounted on lead

Figure 3.3: Components Layout

Table 3.1: The first set of trials at IBM

		Convection			Edge Heaters		
		0%	50%	100%	On	Off	Thermocouples
1	Full size FR-4	Standard Profile					Leading edge
2	Full size FR-4						Trailing edge
3	Ascot						Component bound
4	Full size FR-4						Front to back
5	Eurocard						3 front, 3 middle
6	Eurocard	x				x	3 front, 3 middle
7	Empty carrier	x				x	Along edges
8	Carrier & card	x				x	Along edges
9	Eurocard		x			x	3 front, 3 middle
10	Eurocard			x		x	3 front, 3 middle
11	Full size FR-4			x		x	Front to back
12	Full Size FR-4 & tracks only			x		x	Horizontal, 1 inch from the leading edge
13				x		x	
14				x		x	Horizontal, 4 inches from the leading edge
15				x		x	Horizontal 4 inches from the trailing edge
16				x		x	
17				x		x	Horizontal, 4 inches from the leading edge
18				x		x	Front to back
19	Carrier & card			x		x	
20	Full size FR-4			x		x	Leading edge
21	Full size FR-4 & tracks only			x	x		Front to back
22	Full size FR-4	x			x		Leading edge
23	Carrier & Card	x			x		
24	Full size FR-4 & tracks only	x			x		

meter.

The furnace setting used by IBM for the standard sized board was used for some of the trials. The settings include some convective heating, with the edge heaters on and the zones set at different temperatures to achieve more uniform heating. Most of the tests were conducted with all the heater zones set to a temperature of 200°C with the convection either partly or fully on or off, thus allowing evaluation of the contribution of each of the features. The tests carried out are outlined in Tables 3.1 and 3.2.

		Convection			Edge Heaters		
No	Type	0%	50%	100%	On	Off	Thermocouples
1	Full size FR-4	x				x	As shown in Figure 3.3
2	Board with tracks only	x				x	
3	Passive components I	x				x	
4	Passive components II	x				x	
5	Product I	x				x	
6	Active components I	x				x	
7	Product II	x				x	
8				x	x		
9	Passive components II			x	x		
10	Passive components I			x	x		
11	Active components II			x	x		
12	Product I			x	x		

Table 3.2: The second set of trials at IBM

3.5. Analysis of Results

The major output of the experiment is the temperature profile of the board over the time interval. The effects of convection and edge heaters on the temperature distribution of the board were evaluated together with the influence of PCB tracks. The eurocard board is small enough to be suspended in the middle of the workholder, hence

the effect of the edge heater is minimal. The eurocard and standard sized boards were used for the bare board analysis. The results are summarised in Figures 3.4, 3.5, and 3.6. Figures 3.4a-d show the results of tests 6,9 and10 which enables the evaluation of the effect of convection. Figures 3.5a-e shows the result of tests 12, 18, 21 and 24 used for the evaluation of the effect of the edge heaters. Figures 3.6a-c shows the effect of copper tracks.

The average temperature, over the length of the edge heaters was 355°C. The rate of airflow between the gaps cannot be measured with the furnace in a closed position due to the short length of the hose on which the sensor was mounted. by raising the top half of the furnace, the air flow characteristics was found to vary from 0.1m/s at the inlet to 0.5m/s from one end of the furnace to the other.

3.5.1. The effect of convection

The results presented by figures 3.4a-d were conducted using the eurocard size PCB and were of purely radiative, radiative plus fifty percent convective and radiative plus one hundred percent convective heat transfer modes respectively. The six thermocouples were arranged as shown in figure 3.2a with three thermocouples (1, 2, 3) in front and three (4, 5, 6) at the middle. The behaviour of the board as depicted in figure 3.4a is typical of radiative heat transfer where each sets of three thermocouples at places of equal emissivity and with a similar view of the infrared heaters have the same temperature. As expected, the three front thermocouples in each of these tests showed an earlier rise in temperature than the rear three. The peak temperature for the front three was also higher than the middle three. The case of radiation plus fifty percent convection, (figure 3.4b) shows a wider range of heat distribution across the thermocouples indicating the effect of the variation in air flow characteristics due to the position of the air ducts. The radiation plus one hundred percent convection has a similar characteristics although the temperature achieved is higher (Figure 3.4c).

A comparison of the three modes of heating in figure 3.4d shows that the profile with convective heat transfer reached a higher temperature suggesting a greater amount of heat transfer to the board. The highest temperature occurred on the board with 100% connection. The temperature recorded at each of the thermocouples placed across the

Radiation only

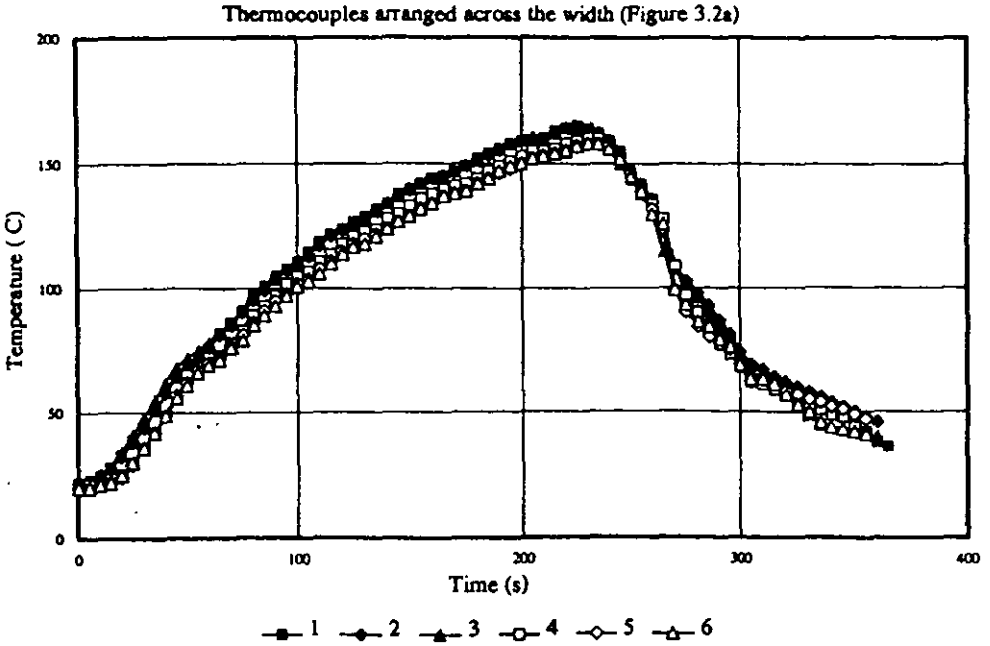

a

Radiation + 50% Convection

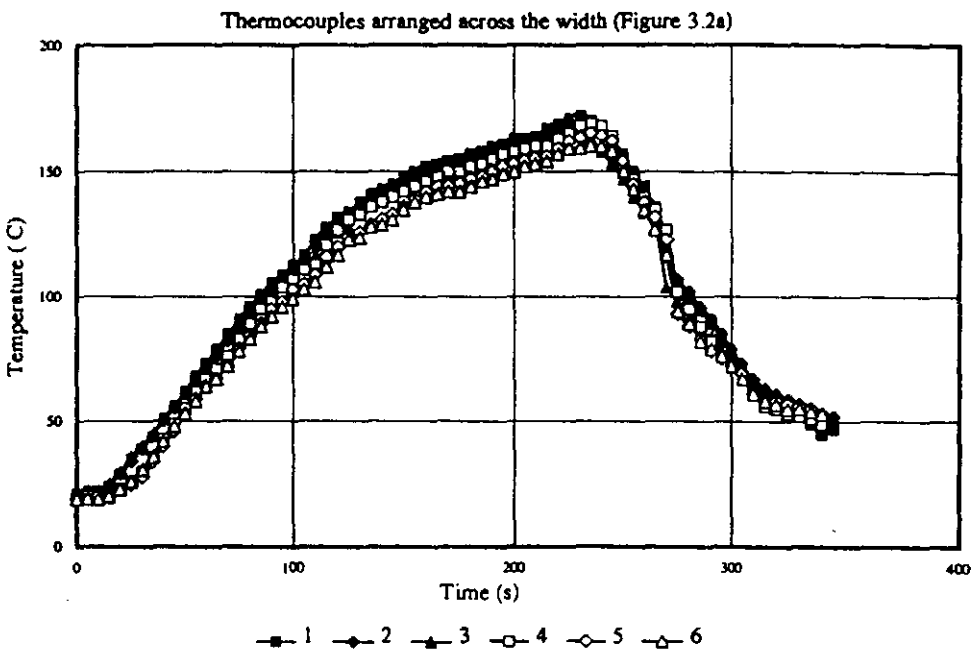

b

Figure 3.4 a & b: The effect of convection

which board?
3.2 or 3.3
(3.2 (a) only)

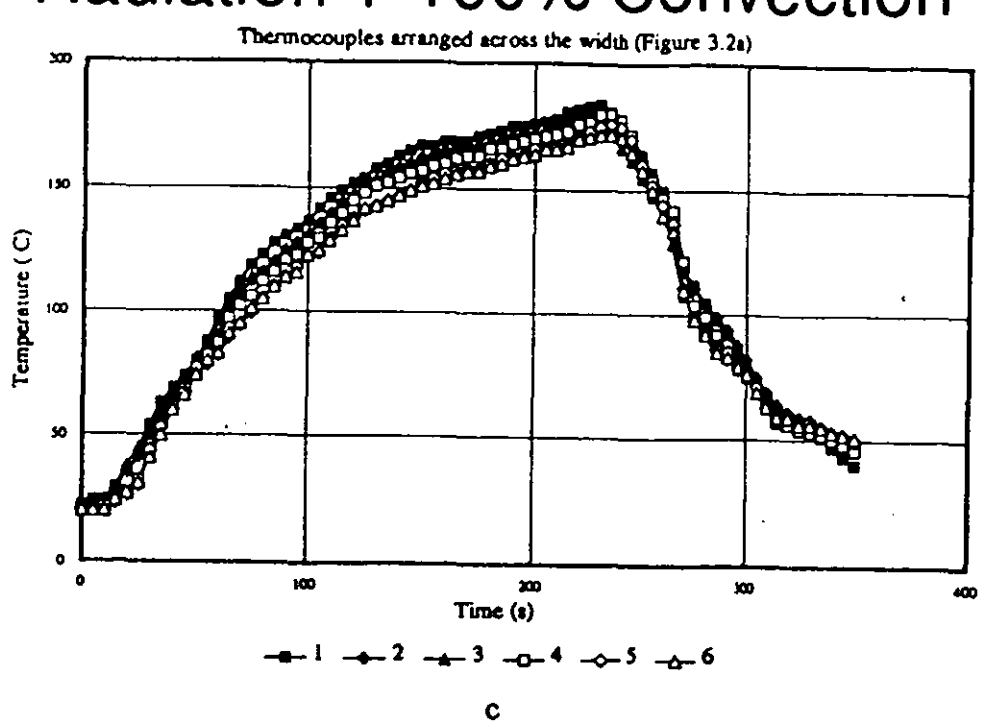

c

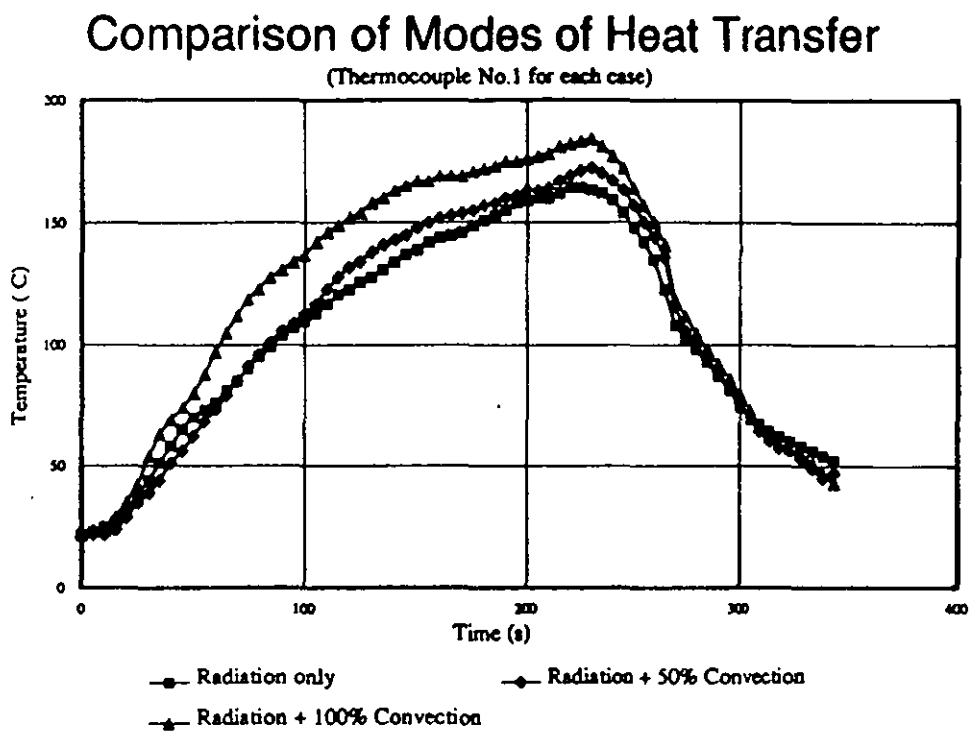

d

Figure 3.4 c & d: The effect of convection

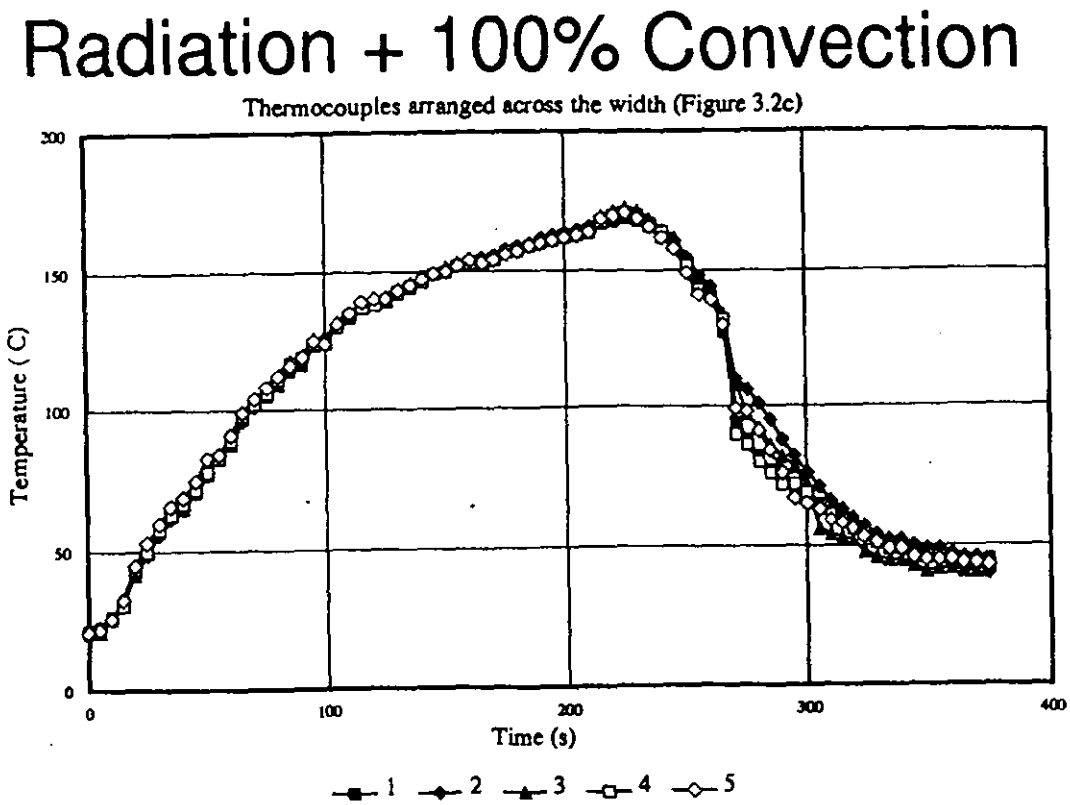

a

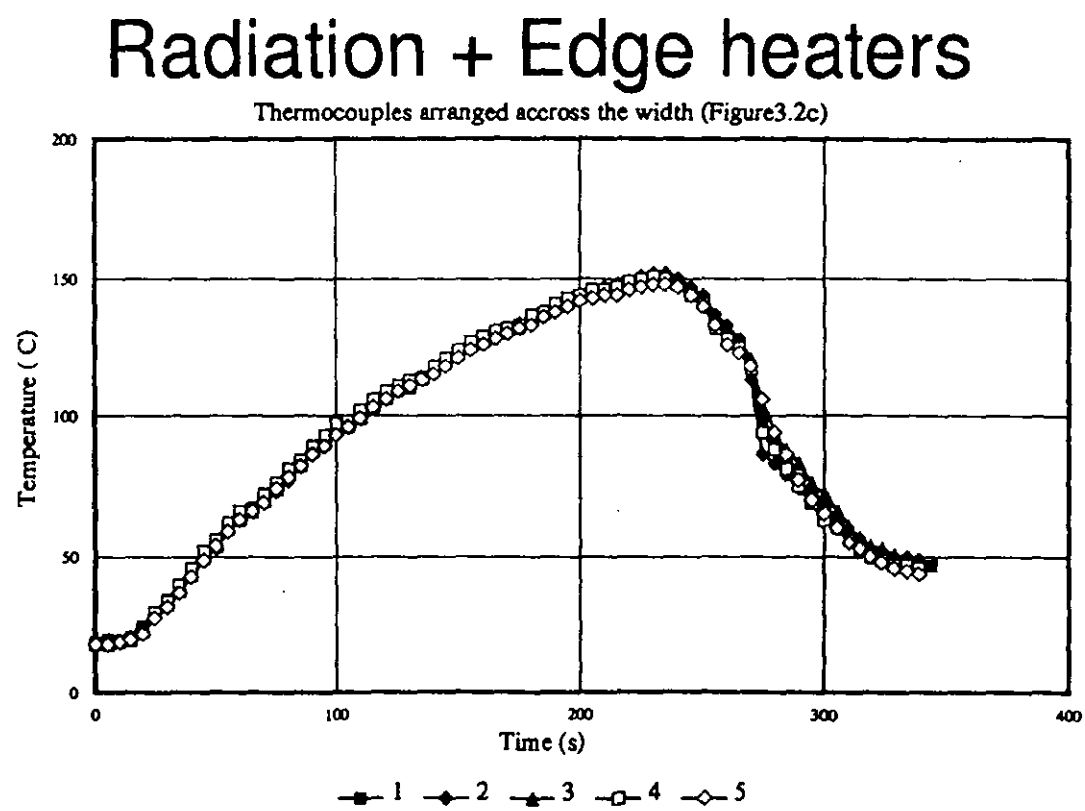

b

Figure 3.5 a & b: The effect of edge heaters

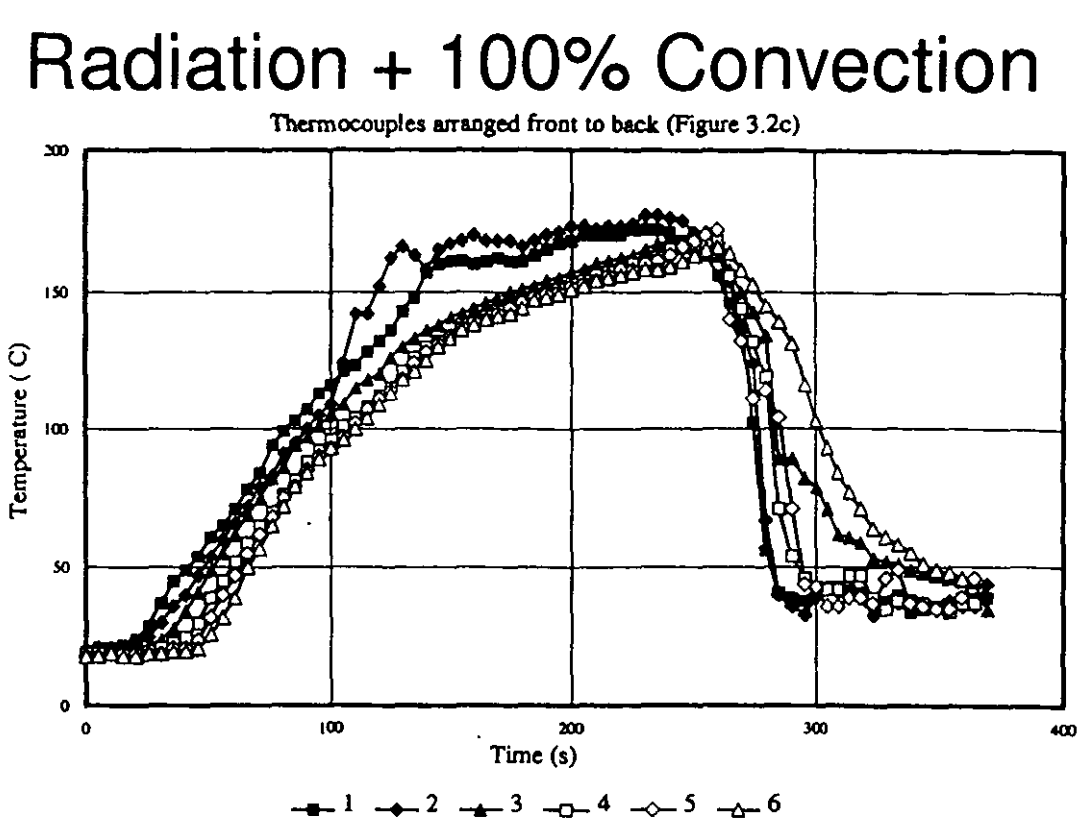

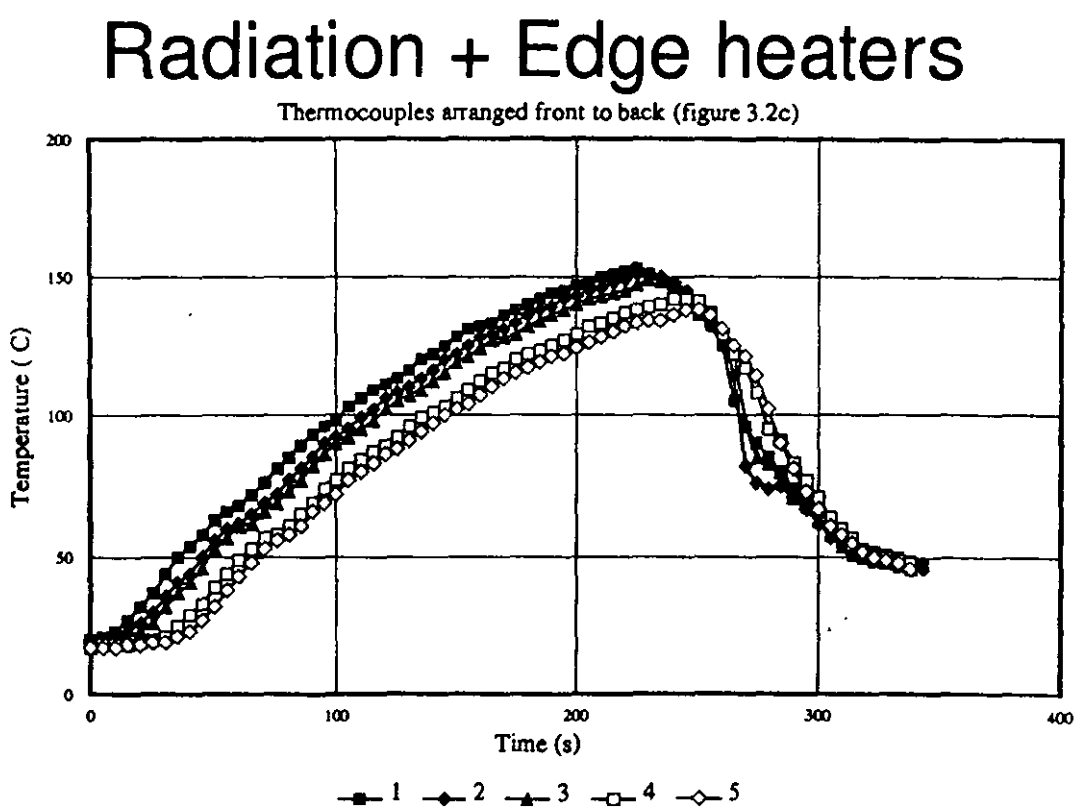

Figure 3.5 c & d: The effect of edge heaters

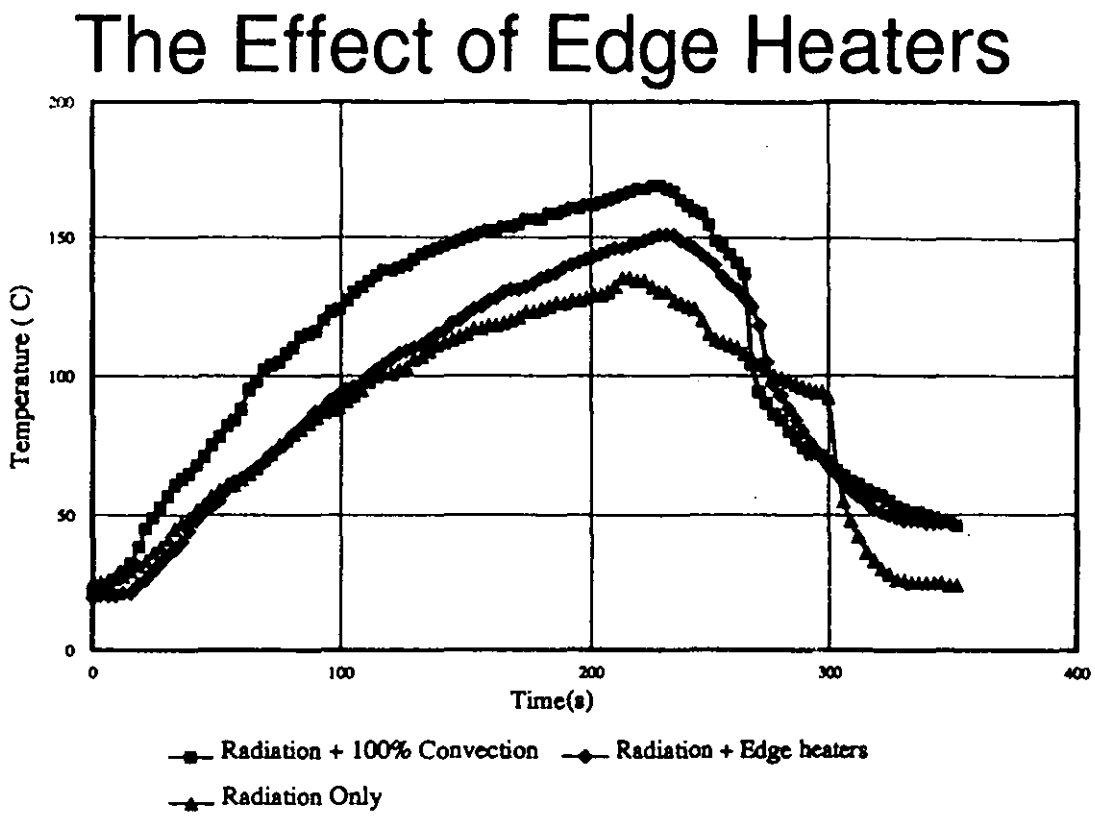

Figure 3.5 e: The effect of edge heaters

board (in the directions 1-3 and 4-6, figure 3.2a) shows a gradual variation in temperature with position. This is in contrast with the radiation only which shows little variation. It can be seen from the graphs that the higher the convection the steeper the temperature profile in the pre-heat zone suggesting that the rate of heating is greater with convection. This is more noticeable for the second heater zone. The three different profiles also suggest 20-30% more heat is applied as a result of the 100% convection. There is little difference between purely radiative and radiation plus 50% convection. At some stages in the cycle the purely radiative system appears to have heated up faster than that of radiation plus 50% convection.

3.5.2. The effect of edge heaters

The case of the edge heaters is presented as graphs of radiation plus 100% convection and radiation plus edge heaters in figures 3.5a and b respectively. The graphs are results of test 12 and 24 conducted on the full size FR-4 board with the probes arranged across the leading edge of the board sideways as shown in figure 3.2c. It is observed that, with the edge heaters, the radiative component of the furnace plays the dominant role in heating up the PCB as the temperature profile of the PCB is very similar to that of radiation only, figure 3.4a. There is no evidence of the contribution of the heat supplied by the edge heaters to the temperature of the PCB. The heater zones, and consequently the position of the fan ducts are more noticeable with convection, while there is a smooth transition with the edge heaters as shown in figure 3.5e. Figures 3.5c and d however shows a smoother heat gradient across the board from front to back with edge heaters.

3.5.3. The effect of PCB copper tracks

Figure 3.6a shows the effect of the copper tracks on the temperature distribution on the PCB. The components whose terminations are mounted on copper tracks heated up faster, got hotter, and cooled down faster than those not mounted on tracks. This observation is more obvious for the active components which are bigger compared to the passive ones. The general trend in all the boards, however, is that the bigger components, because of their higher thermal mass, take longer to get hot (Figure 3.6b). Although the passive components followed a similar trend to that of the active components, the effect of tracks is less noticeable. While the temperature difference

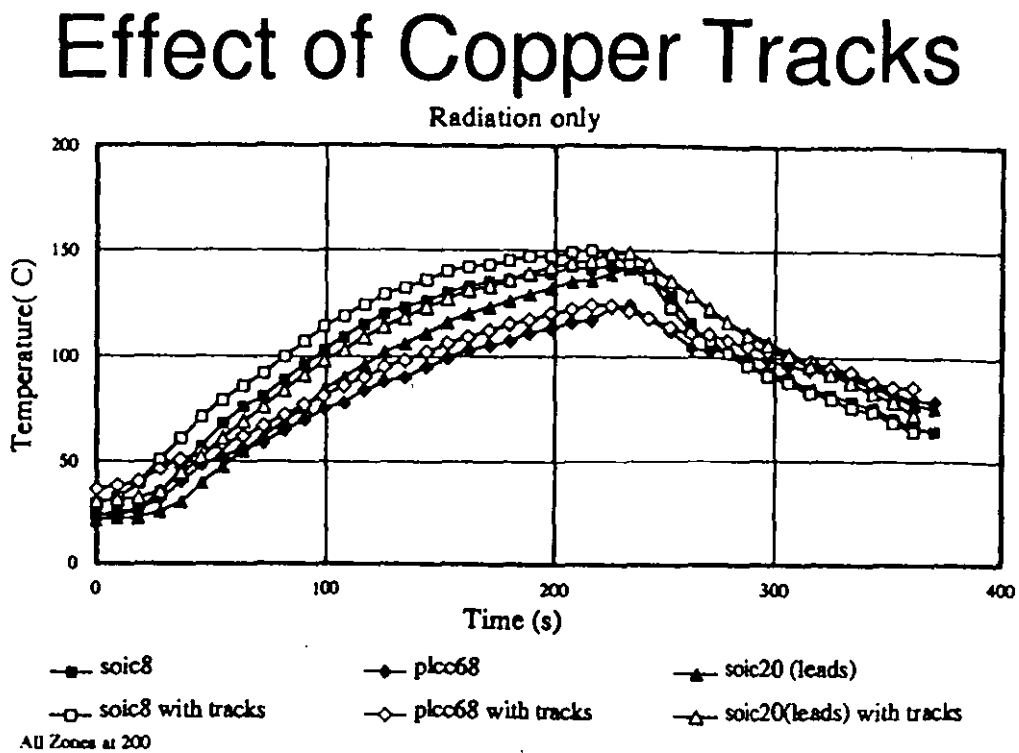

a

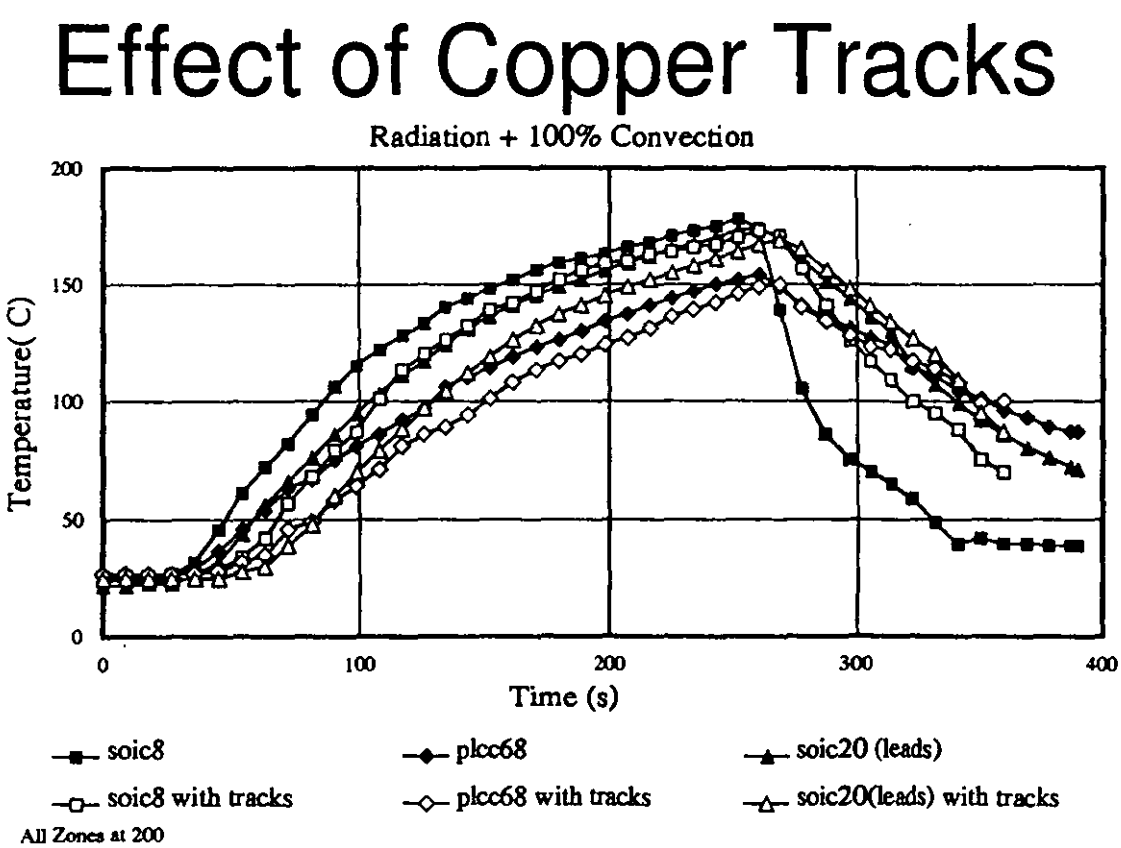

b

Figure 3.6 a & b: The effect of copper tracks

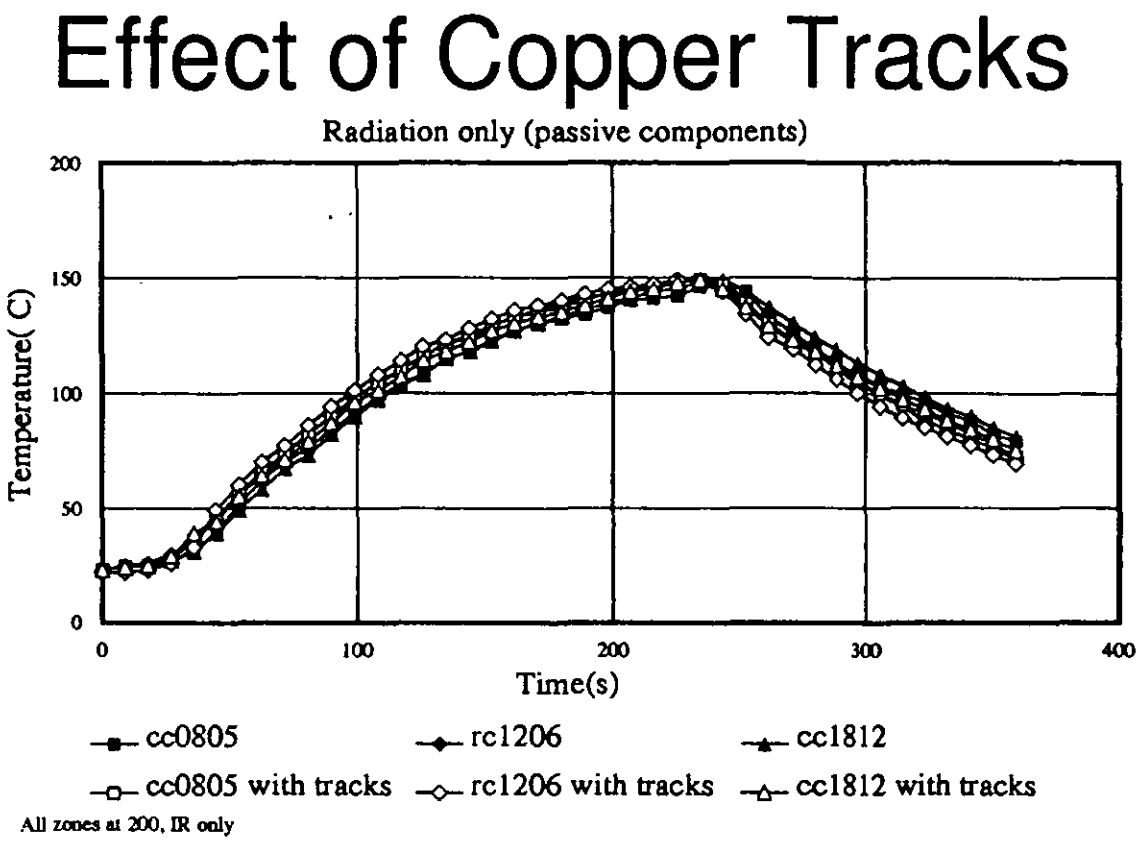

Figure 3.6 c: The effect of copper tracks

between components with tracks and those without is about 10°C for the active components, a difference of 1°C was observed for the passive components.

3.6. Discussion

These experiments have demonstrated the effects of convection, edge heaters and infrared radiation on the temperature distribution of a PCB as it goes through an industrial reflow furnace. The trials give a representative view of the situation in the furnace and not a complete view of the problem. Data has been gathered for very specific points on the PCB at considerable expense (3 days of production distruption on an industrial furnace!).

The amount of heat absorbed by the board in a purely radiative environment depends on the emissivity (or absorptivity) of, and view factors between, the PCB and the IR emitters. This is evidenced by the curves of figure 3.4a, where points at the same distance from the front, and hence, similar view factors, are seen to cluster together. This characteristic of the curves suggests that there is no variation of heat across the width of the board leading to bands of isothermal points (sharp thermal gradients) across the board from front to back. The geometric effect also comes into play with the two front corners getting hotter than any other point on the board. In contrast to the IR only, the addition of convection introduces an effect that reduces the uniformity of the temperature distribution across the width of the board, similarly the temperature between thermocouples at similar positions i.e. 1and 4, 2 and 5, 3 and 6 (figure 3.4b), are closer together than a similar situation in the IR only mode of heating. This suggests a smoother thermal gradient from front to back. In contrast to IR only heating (figure 3.4a), the gradient of the heat profile of figure 3.4c is steeper showing that the convective medium, air in this case, aids in the fast rise of the temperature of the board. Therefore the system operates at a temperature nearer equilibrium thereby reducing the temperature gradient across the PCB. The effect of the edge heaters on the temperature profile of the PCB cannot readily be assessed by these trials. However, the results indicate that the edge heaters give a more uniform supply of heat to the board, this seem particularly significant in smoothing the effect of the heater zones and gaps. Another argument in favour of the heaters is that most FR-4 boards (of which most PCBs are made) have copper exposed at the edges. Copper is a good conductor of heat and in most cases well distributed within the substrate. Therefore more heat can

be supplied to the PCB via the copper network in the substrate. There was, however, no evidence of this in these trials.

It was observed that there is a negligible difference in the temperature of the passive components irrespective of their size or position on the board, in contrast, a bigger temperature difference was observed for the larger active components. The surface area and emissivity of the components are the dominant factors in the predominantly radiative environment. The smaller components get hotter faster and cool down faster. In a board comprising of SOICs and PLCCs, the SOICs got hotter faster than the PLCCs in the ascending order of their sizes.There is a remarkable difference between the lead and the epoxy part of the PLCC during pre-heat. The leads on the large components (PLCC68) were colder than any other component on the board. Tracks do not have much effect on the amount of heat supplied to the components but they can affect the rate of heating or cooling.

An interesting phenomenon however, is the fact that equilibrium was not achieved at the reflow (maximum) temperature but shortly afterwards. Perhaps if the board had been left longer, equilibrium would be achieved by which time the components could have been damaged. It therefore shows that there will always be a thermal gradient across the board and on the components before reflow. There is a need to quantify the size of this thermal gradient and to be able to design the process with adequate knowledge of the state of the board during the process. Experimental trials are very costly and do not give a full picture of the process, a better and cheaper method may therefore be the computer simulation of the process.

3.7. Conclusion

Pure IR heating, because of its sharp thermal gradients, can result in component damage on the PCB assembly. A combination of IR and convective heating however may reduce this effect. The function of the edge heaters in this furnace is not clear, they do however appear to reduce temperature gradients somewhat.

This set of trials gave an understanding of the effects of the different modes of heat transfer in the furnace on the reflow assembly. This is a time consuming method with

a limited view of the state of the assembly at any point in time because of the restricted number of data points that can be collected. This however, is the best available to the electronics manufacturing industry at this point in time. A suitable computer simulation of the process can give a more complete picture of the state of the assembly at any point in time, hence a better understanding of the process. This improved understanding will help in the design of heat profiles for reflow.

The trials described in this chapter and the data collected give the major parameters for a computer model of the furnace and its calibration.

Chapter 4

The Development of a Process Model of the Senju Reflow Furnace at IBM Greenock

4.1. Introduction

In order to understand and to potentially provide a tool to reduce the effects of the non-uniform heat distribution on a printed circuit board as it goes through the reflow furnace, a computer process model of the SENJU infrared / convection reflow furnace has been constructed. More over, the design of a new reflow profile is often a difficult task for process engineers in the industry because there are no methods, at present, for predicting, in advance, the thermal response of the printed circuit board(PCB) to the modes of heating in the furnace. It is necessary to therefore conduct a set of extensive trials, similar to those described in chapter 3, to determine the appropriate furnace settings to achieve the desired reflow temperature of the PCB. These trials are time consuming and result in wastage of products and resources. They are also not capable of predicting the thermal response of alternative assemblies to different furnace conditions or of quantifying the heat transfer mechanisms within the furnace. It is therefore desirable to have a more versatile, more efficient and predictive method of studying the process. This type of method is offered by computer modelling of the furnace system.

This chapter presents the development of the process model of the SENJU Infrared / convection reflow furnace described earlier in chapter 3. The trials described earlier in this thesis gave a guideline to the model development and will therefore be referred to frequently in this chapter. The chapter begins by reviewing similar work in the literature and goes on to describe the development and calibration of the model. The profiles determined from the earlier trials are then compared with the predicted profiles. The work in this chapter will therefore demonstrate the feasibility of modelling the reflow process and will enhance the understanding of the temperature related issues in the solder reflow process.

4.2. The Thermal Process Model

The critical process issues in an IR/convection furnace are complete solder reflow at each joint and ensuring that the maximum temperature the components can withstand without experiencing permanent damage is not exceeded. In practise therefore, the heating parameters of the furnace are set such that the temperature reached by the PCB is high enough to reflow the solder joints and the time at peak temperature is sufficiently short to not damage the components. The aim of any model is therefore, to mimic the reflow process and be able to predict the transient thermal response of the PCB to the heat parameters within the furnace. The output of the modelling exercise will therefore be the temperature distribution across the PCB as it travels through the furnace.

4.2.1. The Modelling System

The finite element - finite difference approach similar to that of Whalley et al [21] was adopted in building this model. The SDRC I-DEAS Finite Element Modelling software was used to capture the geometrical relationships between the PCB assembly and the furnace. The geometry created is then divided into a finite number of discrete variables called finite elements by a process called meshing. The process generates the appropriate elements for thermal analysis and defines the location of nodes for each of the elements. Relevant physical and material properties are then defined for the different components of the geometry.

The Thermal Model Generator(TMG), a thermal analysis tool, utilizing a finite difference method, converts the finite element geometry to a finite difference model by converting the finite elements to geometric points (grids) connected by thermal conductances. A set of simultaneous equations expressing the relationship between heat flow and temperatures at each grid is then solved to determine temperature and heat flow within the system. TMG is capable of steady state or transient solutions for conduction and radiation calculated from geometry and for free and forced convection. It is also capable of integrating, for special cases, user written programmes.

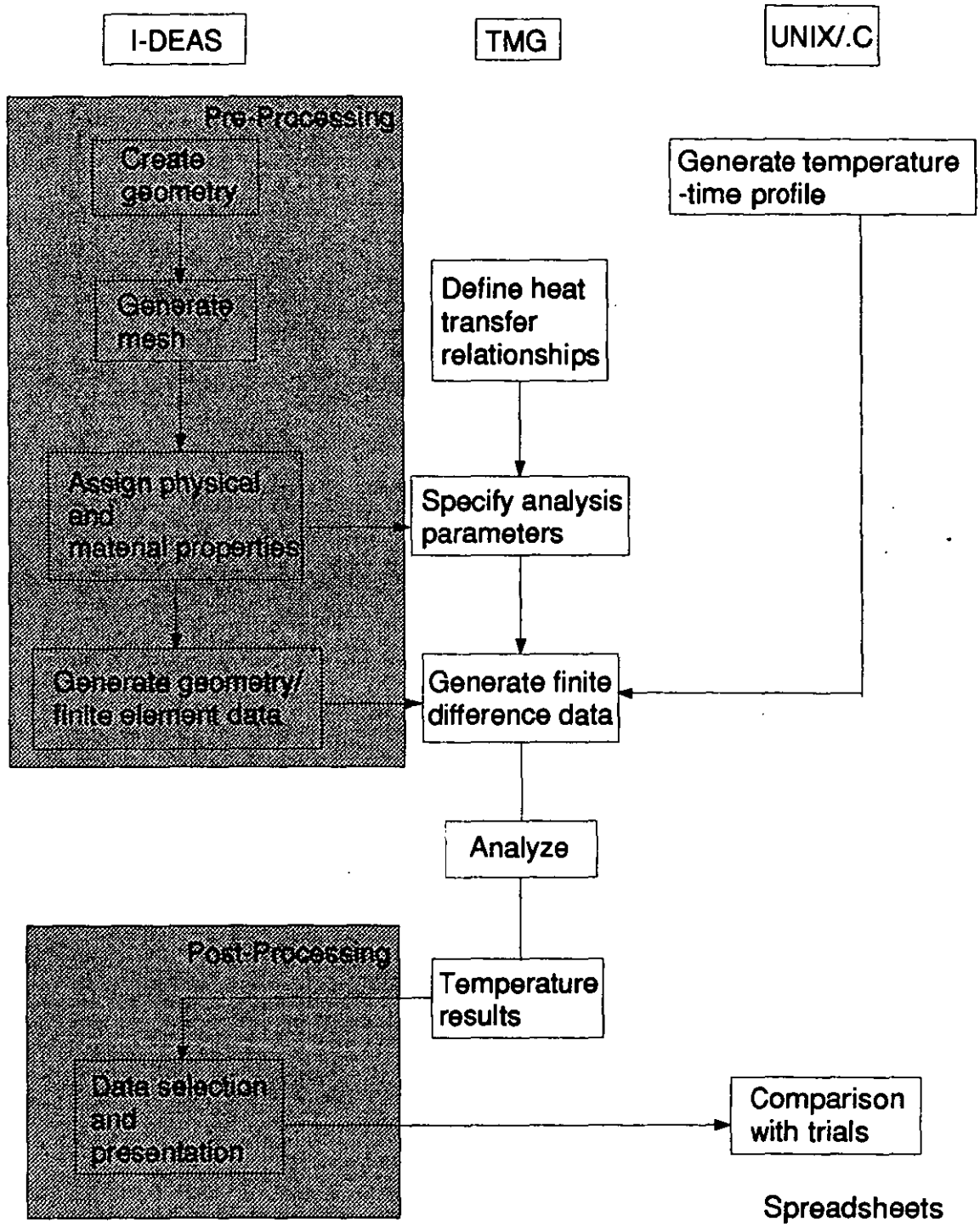

Figure 1: Stages of Modelling

The results from TMG, the temperature history and associated heat flows are then post processed in I-DEAS so that the results can be displayed as temperature profiles superimposed on the original geometry. Figure 4.1 shows the various stages of modelling at which the different softwares are used.

4.2.2. The Model

The model is made up of two main structures, the furnace and the PCB. The objective of the model as stated previously, is to mimic the reflow process. The relevant issues are therefore the dynamics of the system in terms of the movement of the PCB through the furnace and effective definition of the thermal relationship between the furnace and the PCB.

4.2.2.1. Simulation of the Dynamics of the PCB.

The analysis of the model requires the definition of thermal links between the furnace and the PCB at different positions during its movement through the furnace. This will result in the generation of a large amount of geometrical data and a cumbersome computation. In order to avoid this, the furnace was modelled to be twice as long as the real one and the PCB fixed at the centre. The movement of the PCB in the oven was therefore mimiced by applying a time varying profile to the IR emitters. Appendix I shows the programme written to generate the profile data.

4.2.2.2. The Pure Radiation Model

The first model developed was that of a purely radiative (equivalent to the real furnace system with the convective heating turned off) heat transfer from the IR emitters to the PCB. This was done because it provided an appropriate starting point for the model, and the feasibility of it has been previously demonstrated [21]. There are 6 heater zones with gaps between them. Each heater zone is made up of 2 IR emitter panels (one each at the top and bottom) making a total of 12 IR emitters. The gaps between each IR emitter were each modelled as separate zones and an extra zone was added at the end to model the ambient temperature of the environment. In order to present the simplest case for modelling, and to be consistent with trials of chapter 3(the model was calibrated using the trials), all the heater panels were set to 200°C. Figure 4.2 shows the plan view of the heater zones in the real furnace.

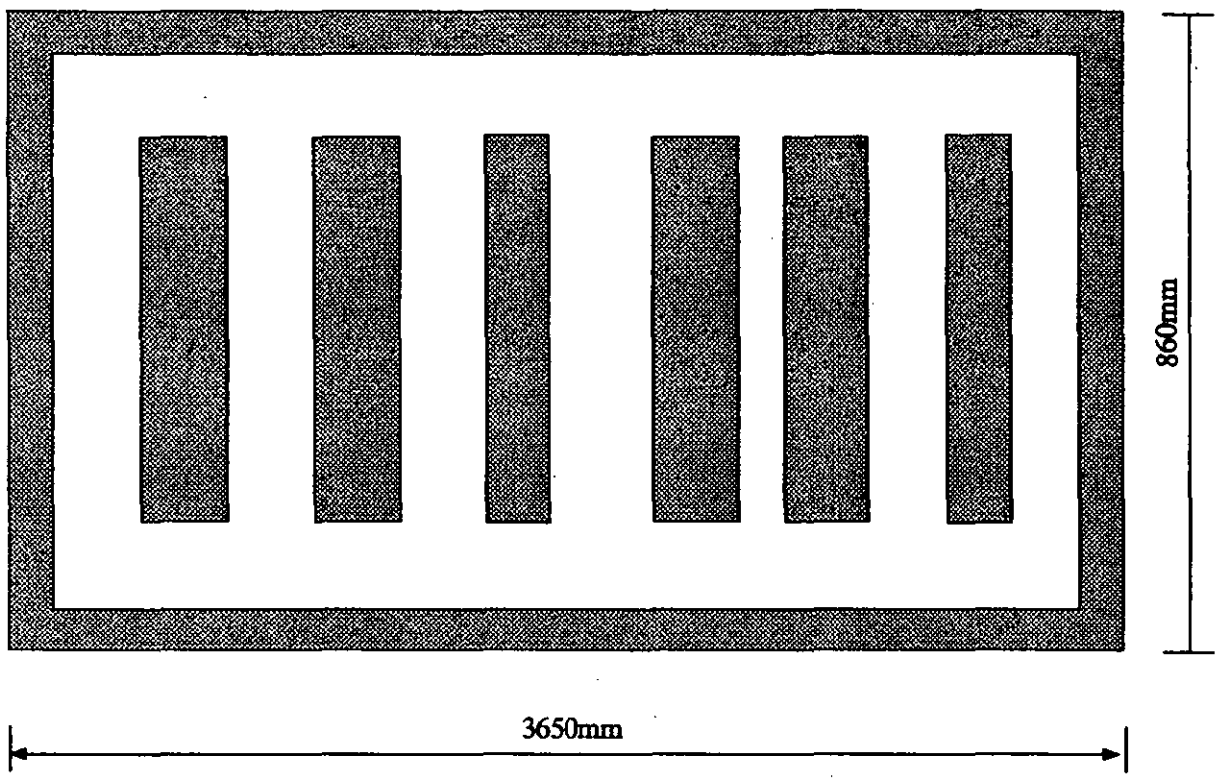

Figure 4.2: Plan view of the heater zones in the real furnace

A Eurocard sized PCB, 230mm by 179mm and made from 1.6mm thick FR-4 was modelled to be consistent with trials described in chapter 3. The analysis of the model requires calculation of the view factor, v_{ij} (defined as the fraction of the radiation emanating from a surface i intercepted by surface j), between elements of the furnace and those of the PCB. The heat flow through a radiative conductance is given by

$$Q = \sigma a_i e_i v_{ij} (t_i^4 - t_j^4) \qquad \text{Eq. 4.1}$$

where:

σ is the Stefan-Boltzmann's constant

a_i is the area of node i

e_i is the emissivity of node i

v_{ij} is the is the grey body view factor between nodes i and j and

t_i and t_j are the temperature of nodes i and j

The matrix form of the above equation relating temperature and heat flow in the model is generated and subsequently solved for the temperature and heat flow variables to predict the temperature distribution on the PCB.

Figure 4.4 shows a comparison of the model with experimental results (taken from test 6 in chapter 3).There is a good correlation between the predicted profile and the experiment up till the peak temperature after which discrepancies are apparent. This is because the PCB is cooled by cooling fans (forced convection cooling) at the outlet of the furnace. Forced convection cooling is not included in the model. Notice the steps in both profiles due to the spacing of the IR emitters. Figure 4.3 shows a diagram of the furnace model while the predicted temperature distribution on the PCB is shown in figure 4.5. Also notice the hot spots at the edge of the PCB replicating the geometry effect observed in the experimental program in Chapter 3.

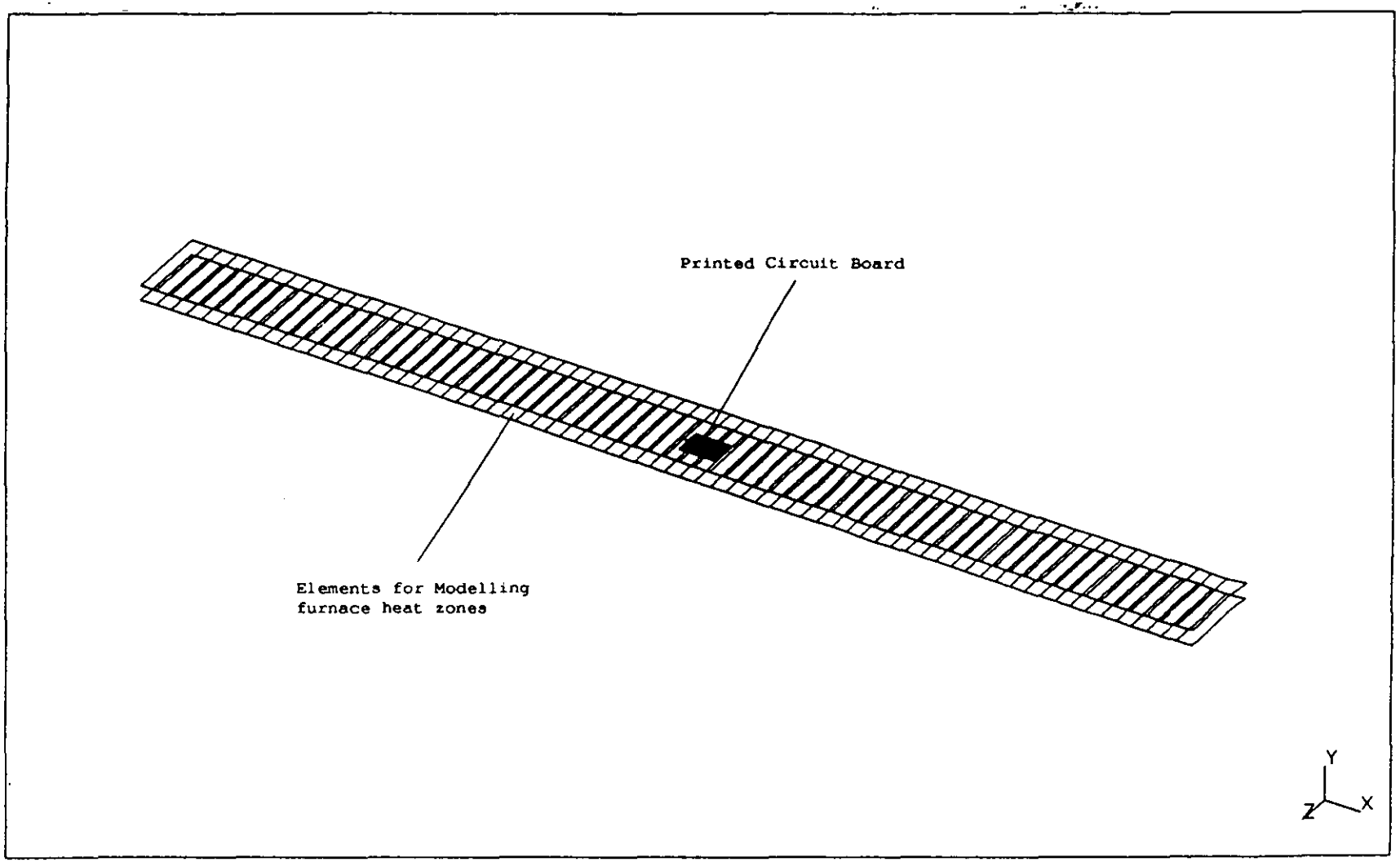

Figure 4.3: Isometric view of the furnace and PCB model

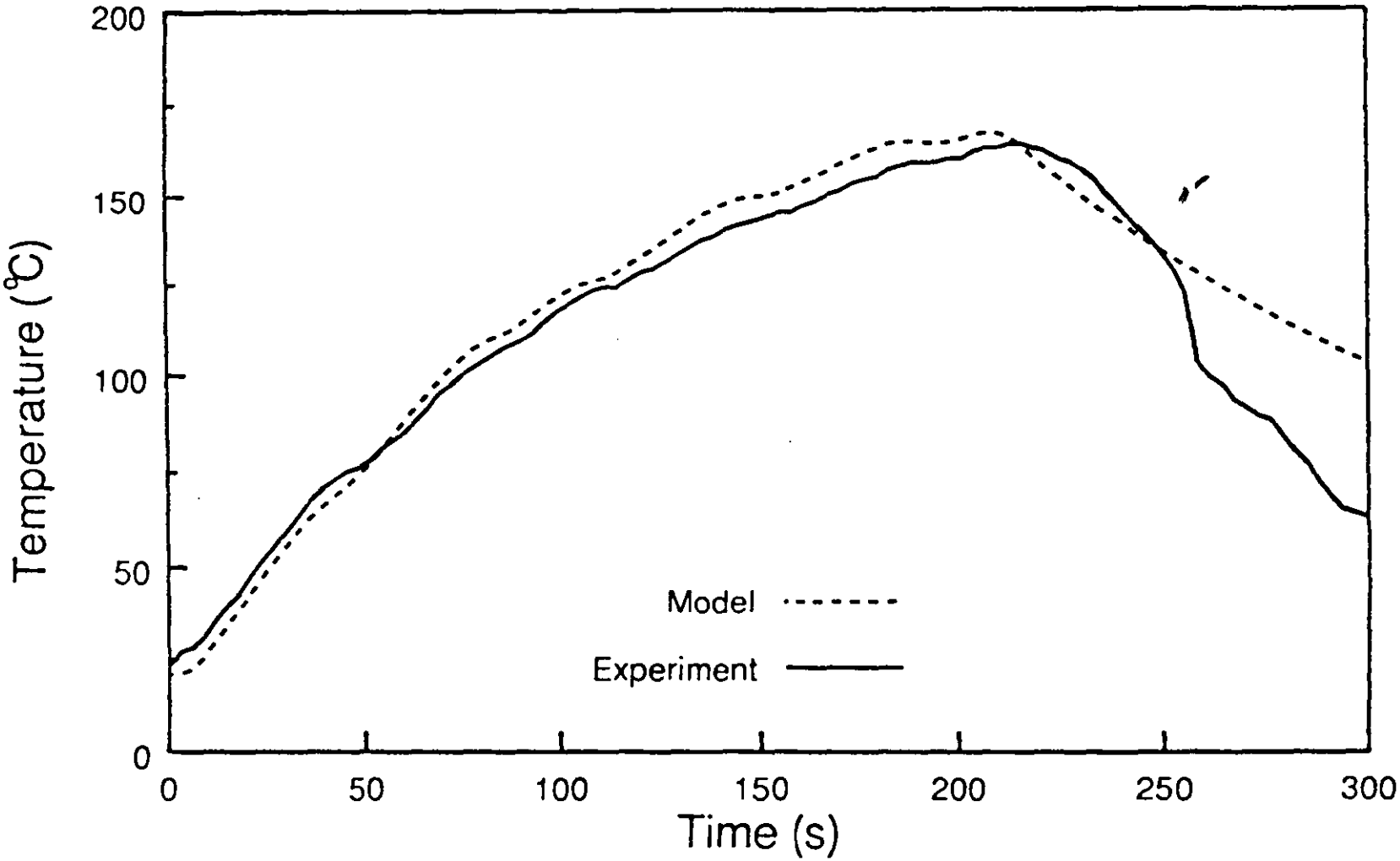

Figure 4.4: Comparison of model with experiment for SENJU furnace with radiative mode of heat transfer only

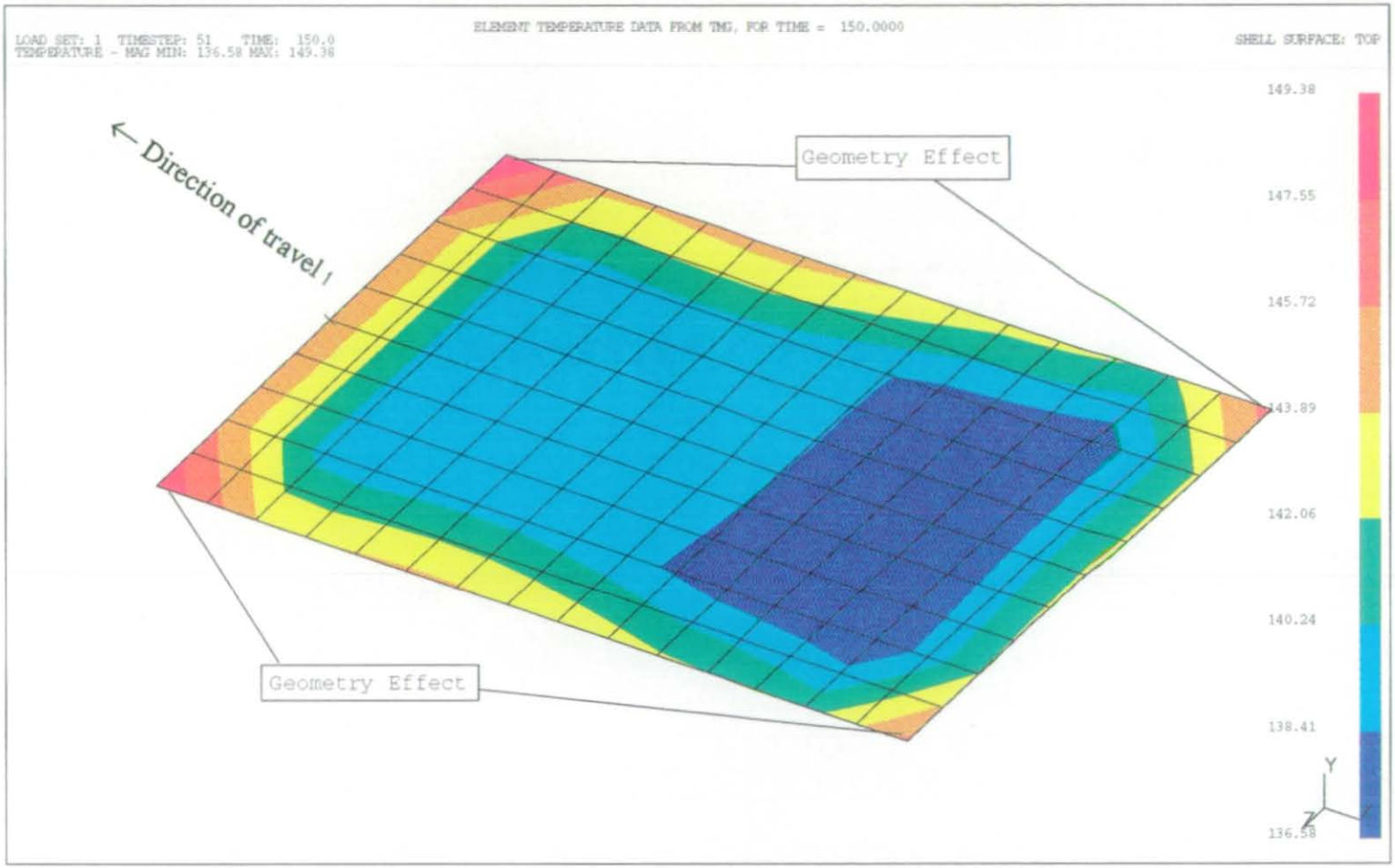

Figure 4.5: The predicted thermal response of the PCB to IR only mode of heat transfer

4.2.3. Modelling the Edge Heater

The edge heaters were subsequently built into the model. The edge heater models were built to optimise analysis time and computer disk space by ignoring the parts of edge heaters with negligible view factors. A time varying profile was used to simulate the movement of the PCB past the edge heaters in a similar manner to that used for the IR heaters. A listing of the program for generating the time varying profile for the edge heaters can be found in appendix II.

There are two approaches to defining the heat transfer from the edge heaters. The first, is to assume direct application of 2.4kW heat flux to the furnace system via the edge heaters and the second, is to assume heat transfer to the PCB and the IR emitters by radiation. An attempt to use the first approach introduced instability (the iterative algorithm for solution could not converge) in the model. This is probably due to the fact that introducing the heat flux upsets the energy balance in the system: The surface area of the edge heaters is small compared to the IR emitter panels and the PCB. Most of the radiation from the edge heaters will ideally go to the IR panels since they have a greater view factor, but the temperature of the panels are set to a fixed value, hence they cannot absorb any more energy from the edge heaters. The proportion of the energy absorbed from the edge heaters by the PCB is also limited by their view factors. Since this is a transient analysis, the time was too short for the temperature within the system to equilibrate. The predicted temperature of both the PCB and the edge heaters was much higher than experimental results (chapter 3).

The explanation above suggests a heat loss from the edge heaters that is not provided for in the model. The alternative approach taken was to fix the temperature of the edge heaters at the value measured during the trial of chapter 3. Two elements were created to model the loss of heat energy by making them a heat sink at the ambient temperature of the factory environment. The extra heat energy introduced by the edge heaters is then diverted to the two elements by creating a thermal link between the edge heaters and the "loss" elements.

Figure 4.6 shows the position of the edge heaters in the furnace and the predicted temperature distribution of the PCB is shown in figure 4.7.

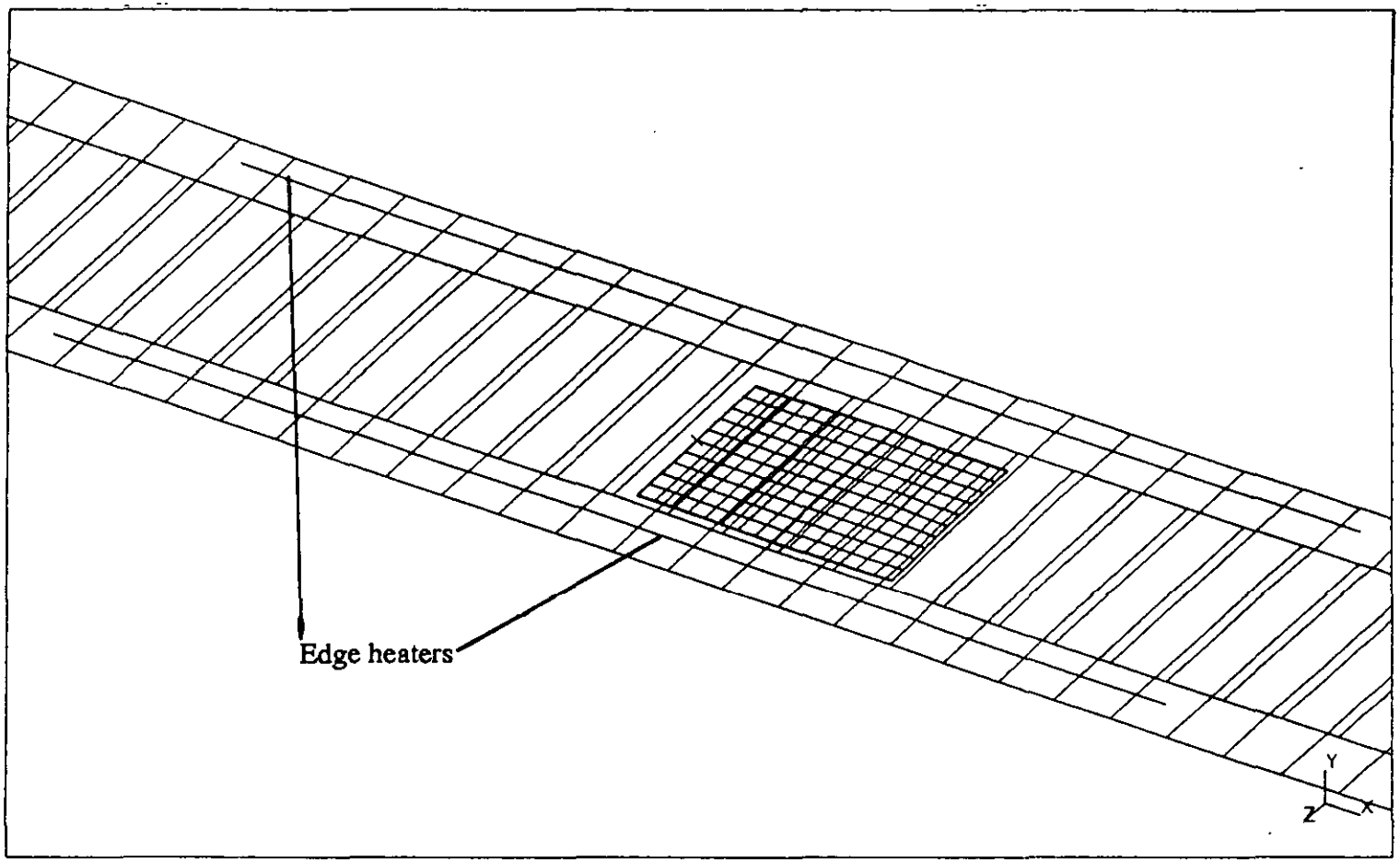

Figure 4.6: Position of the edge heaters in the furnace model

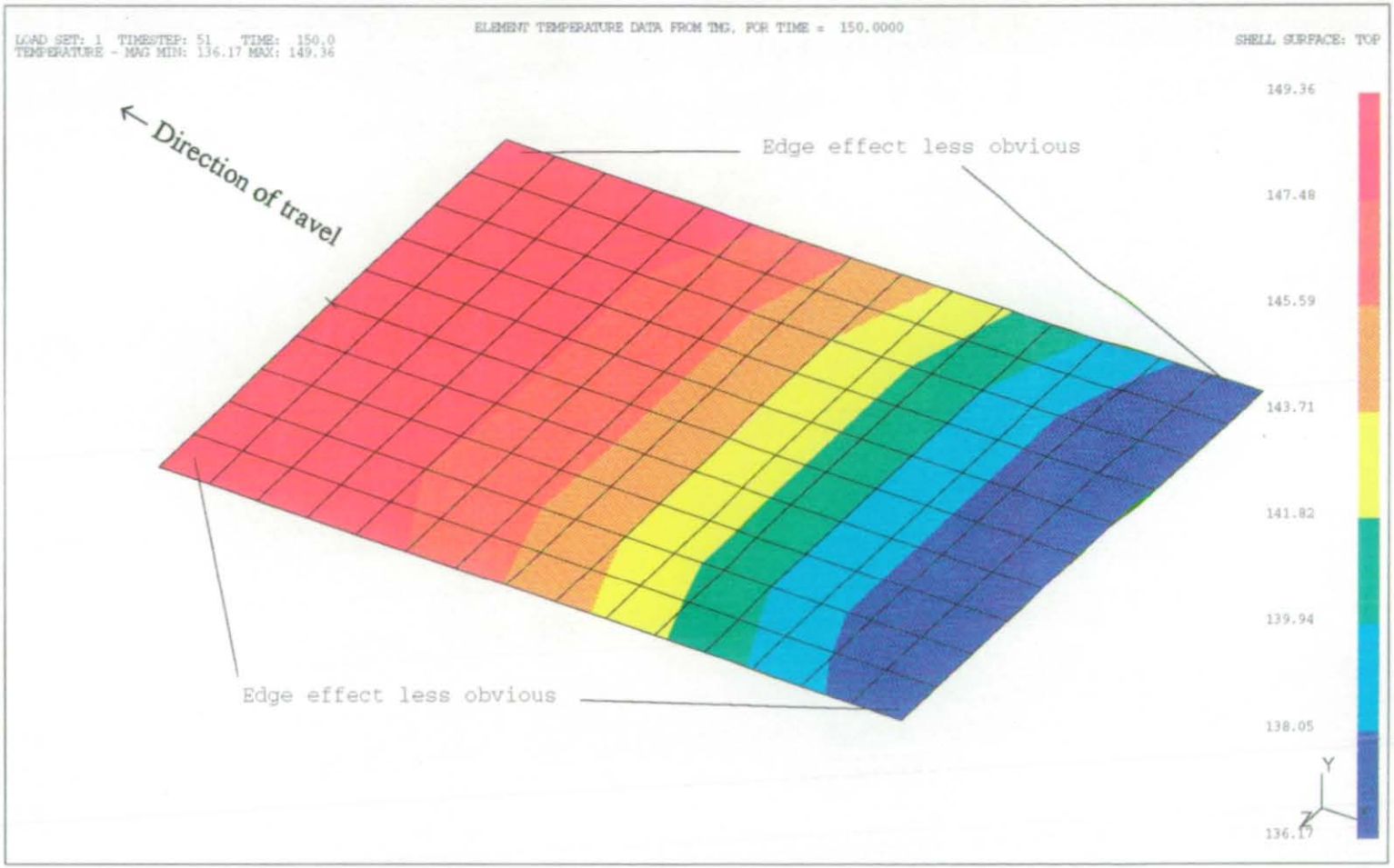

Figure 4.7: The predicted thermal response of the PCB to IR + edge heaters mode of heat transfer

4.2.4. Addition of Convection

The addition of convective heating to the model was significantly more complex than the addition of edge heaters. As stated previously in chapter 3, the rate of air flow in the different heater zones varies as the PCB moves through the reflow furnace. This means that a profile has to be created that describes the change of coefficient of convection with time. This is difficult to do as there was no means of practically measuring the necessary parameters needed to determine the coefficient. The coefficient was therefore determined empirically from the results of the trials in chapter 3.

NOT TRUE.

Since air is blown into the furnace through the porous IR panels and recirculated via the gaps, it was assumed that coefficient of convection is the same under each of the IR panels and zero in the gaps. The air circulation blower in the furnace pumps at the rate of 0.23 m^3/min. [75] at a speed of 0.1 m/s (Chapter 3) hence there is a 0.3kg mass of air in the furnace at any particular instance during operation. The effect of convection (air in the system) was modelled by using finite elements whose properties are defined solely by mass (Lumped mass elements). The mass of the air was distributed between the lumped mass elements and the IR panels connected to the lumped masses by means of linear conductive conductances to model the heating of the air, while linear conductances whose value depends on the surface area of the elements of the PCB were used to model heat transfer between air and the PCB.

Figure 4.8 illustrates the use of linear conductances and lumped masses to model convection

Conductive conductances are used to model conductive heat flow through nodes. The heat flow Q_{ij} through a conductive conductance connecting nodes i and j is described by:

$$Q_{ij} = \frac{t_i - t_j}{\frac{l_i}{a_i k_i} + \frac{l_j}{a_j k_j}} \qquad \text{Eq. 4.2}$$

where

k_i, k_j are thermal conductivities of the nodes i and j respectively

a_i, a_j are the cross-sectional areas of the nodes

l_i,l_j are the distances from the node centres to the nodal boundary

t_i,t_j are the temperatures of nodes i and j

A time varying profile was applied to the linear conductance between the IR panels and the lumped masses to simulate the effect of the gaps in the furnace. The value of conductances used in the model was empirically determined based on experimental data as the coefficient of convection was not known. Figure 4.9 shows a comparison of the predictions with experimental results. Although the model is reasonably successful, as can be seen from Figure 4.9, it fails to fully reflect the furnace behaviour through the reflow cycle. The reason for this discrepancy can however be explained by examining the experimental results more closely. Figure 4.10 shows the rate of change of temperature in the furnace against time. Variations in the rate of change of temperature, signified by the various peaks on the graph, shows a varying amount heat input from zone to zone. This suggests that the difference in duct work associated with the air system are resulting in non-uniform air distribution within each zone. It will be necessary to measure the air flow characteristics through out the furnace in order to accurately model the forced convection. The sharp spike at time=260s shows the effect of the cooling fans. The gradual reduction in the rate of change of temperature between time=100s and 200s indicates that less is absorbed by the PCB as it approaches the temperature of the heat source (peak temperature occurred at time = 200s, and temperature of the source = 200°C). Figure 4.11 shows the predicted temperature distribution after 150 seconds of the PCB entering the furnace.

4.2.5. The complete SENJU model

The final model incorporated all the components and the corresponding heat transfer modes to model a standard IBM reflow profile[1]. Figure 4.12 shows the components of the complete model. The profile of the model heater zones are shown in figure 4.13. The predicted profile on the PCB (figure 4.14) was then compared with trials from chapter 3 (Figure 4.15). The PCB modelled was a bare IBM standard sized board.

1. The details of the profile cannot be outlined here because of its commercial sensitivity.

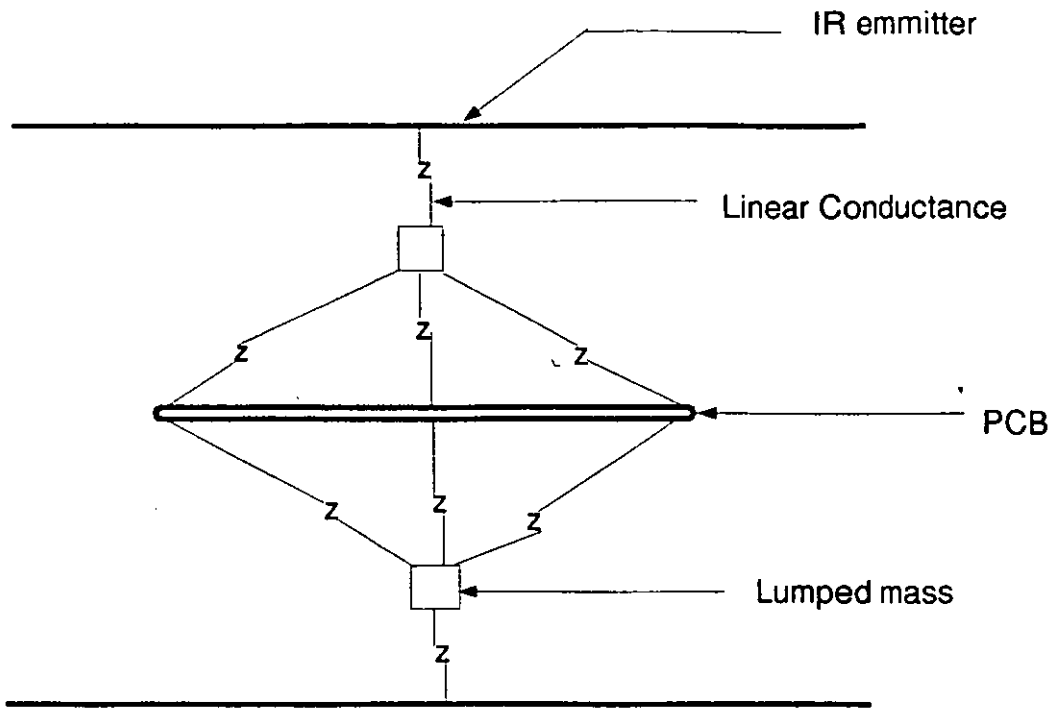

Figure 4.8: The use of linear conductances to model convection

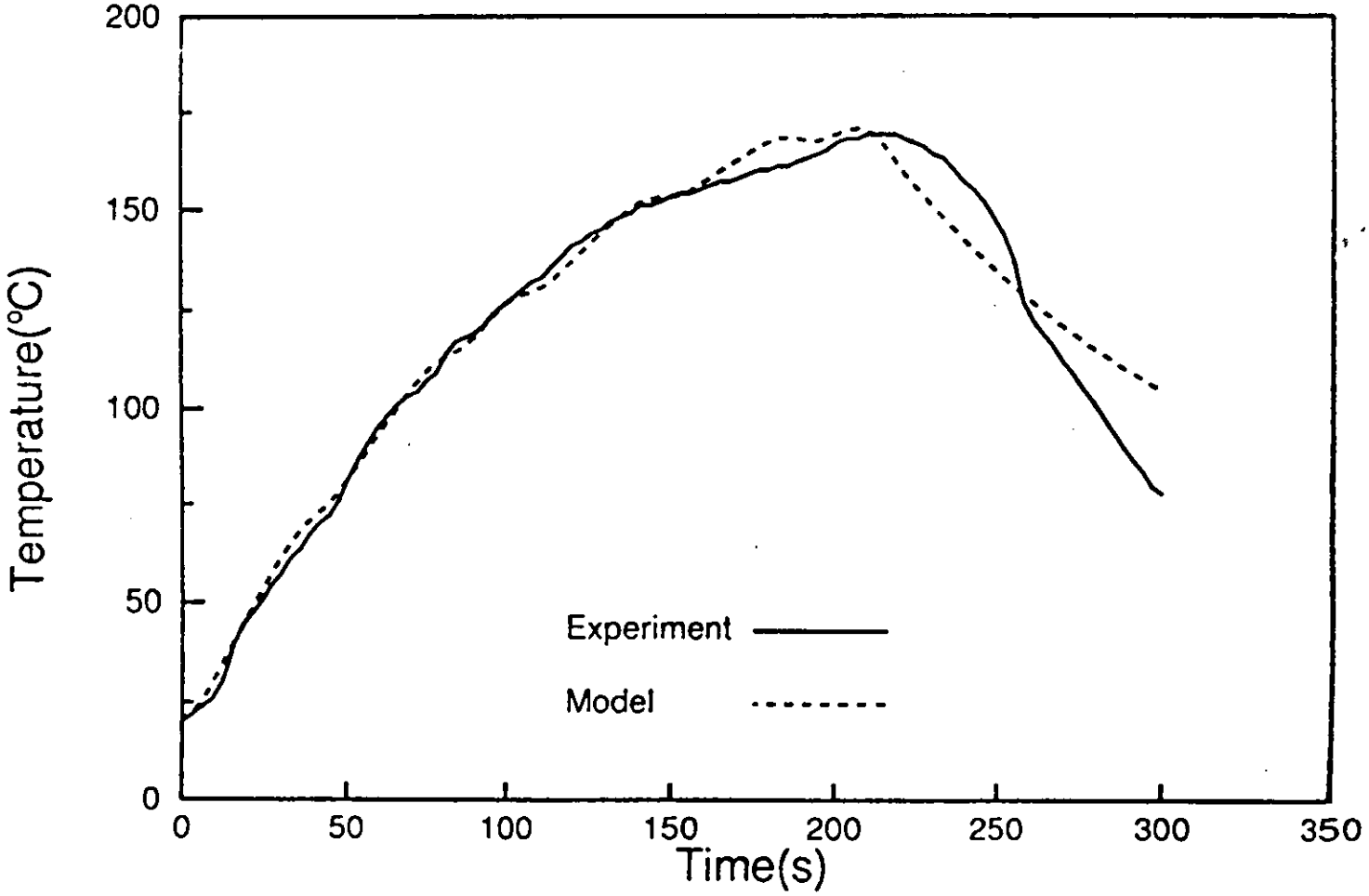

Figure 4.9: Comparison of model results with experiment for the SENJU furnace with convective heating

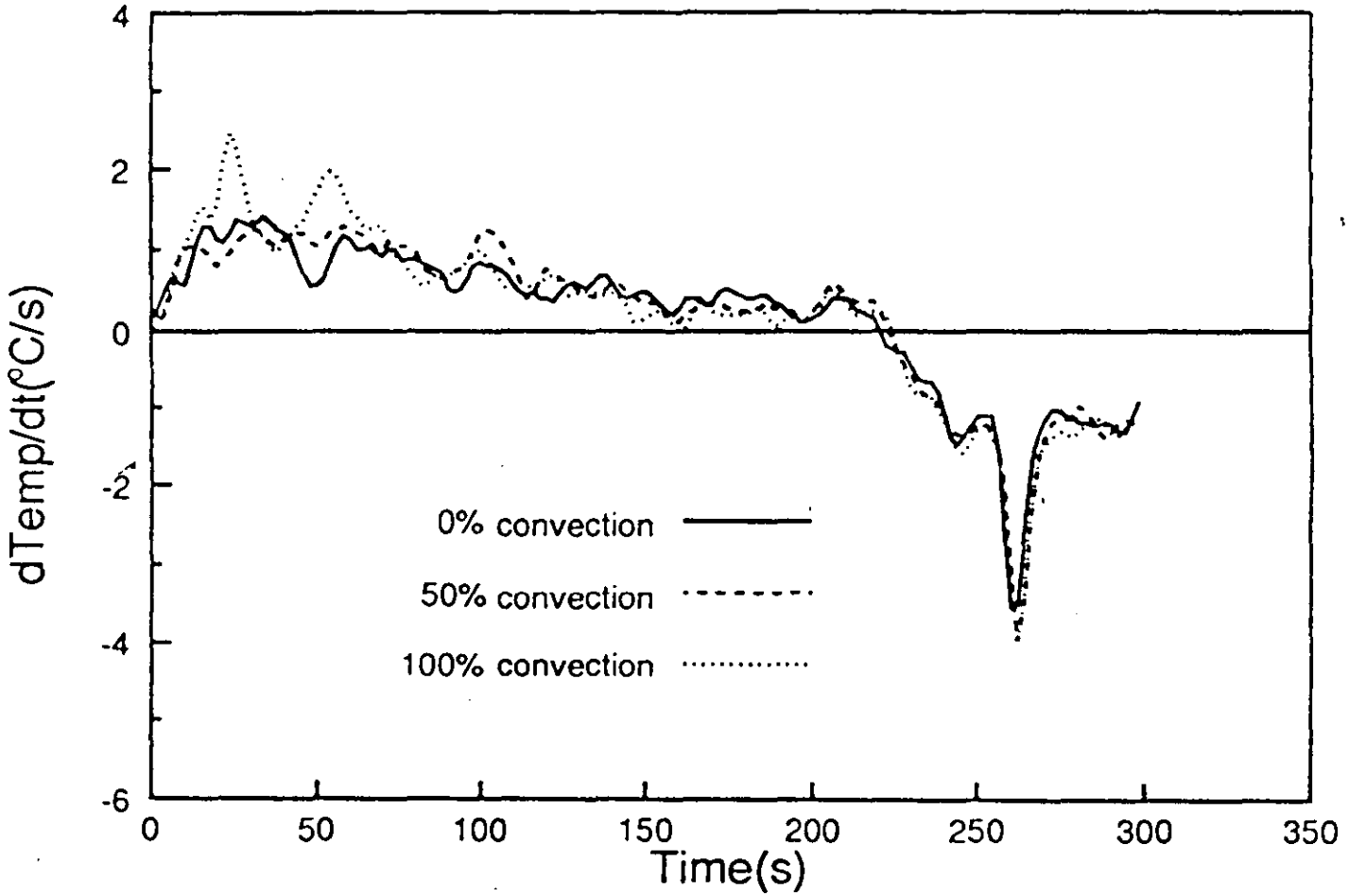

Figure 4.10: The effect of convection on the rate of change of temperature in the SENJU furnace

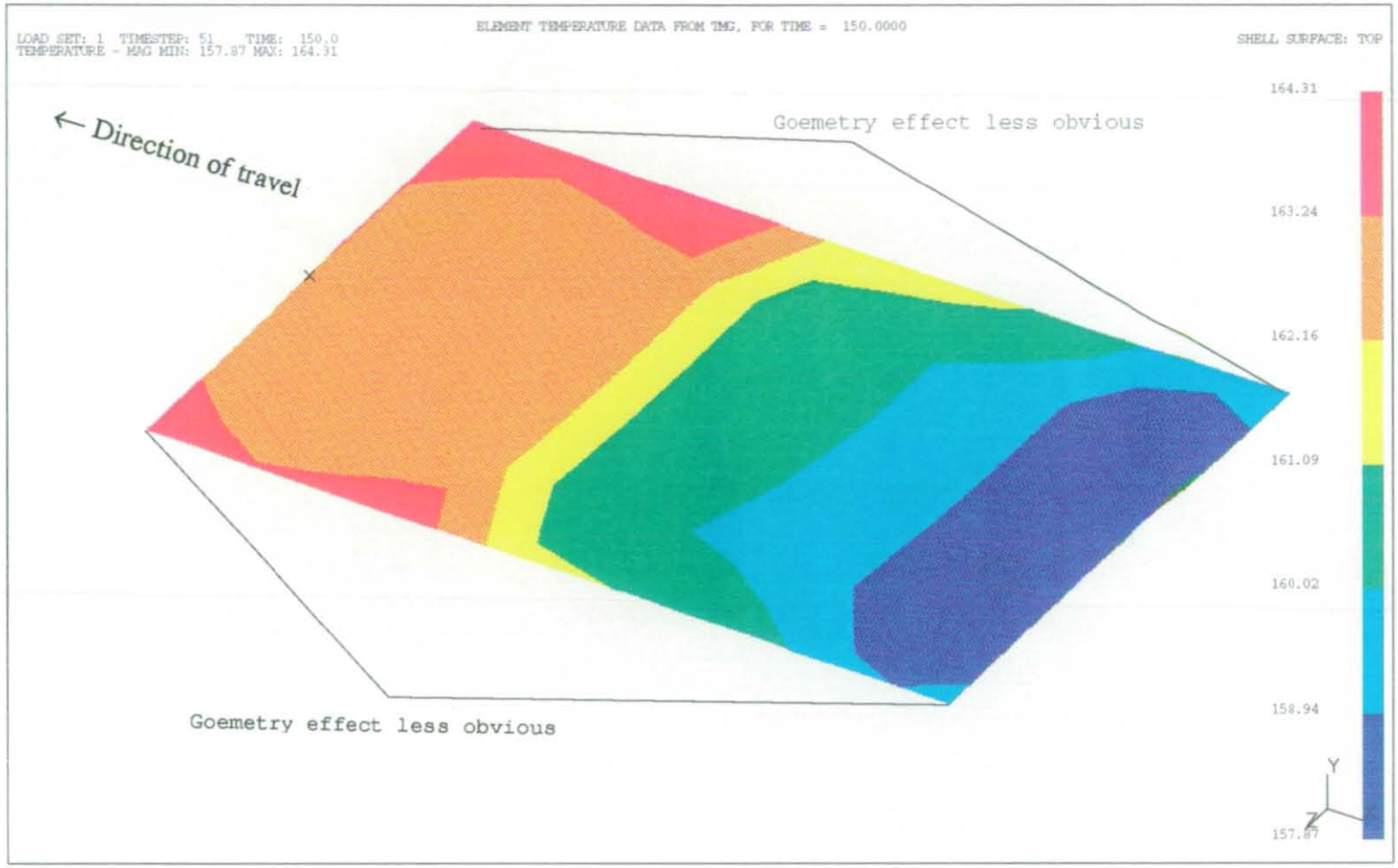

Figure 4.11: The predicted thermal response of the PCB to IR + convective mode of heat transfer

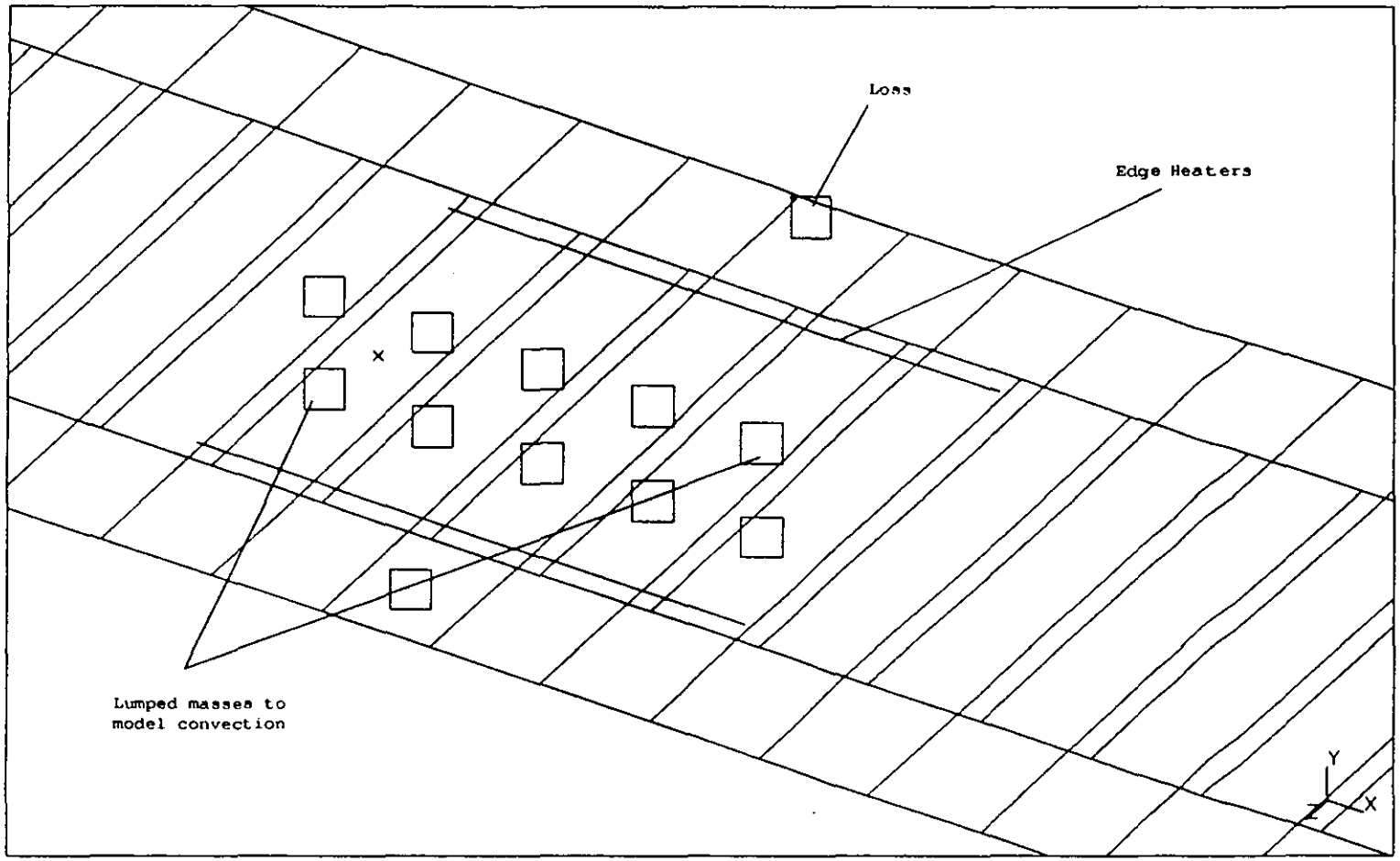

Figure 4.12: The components of the complete furnace model

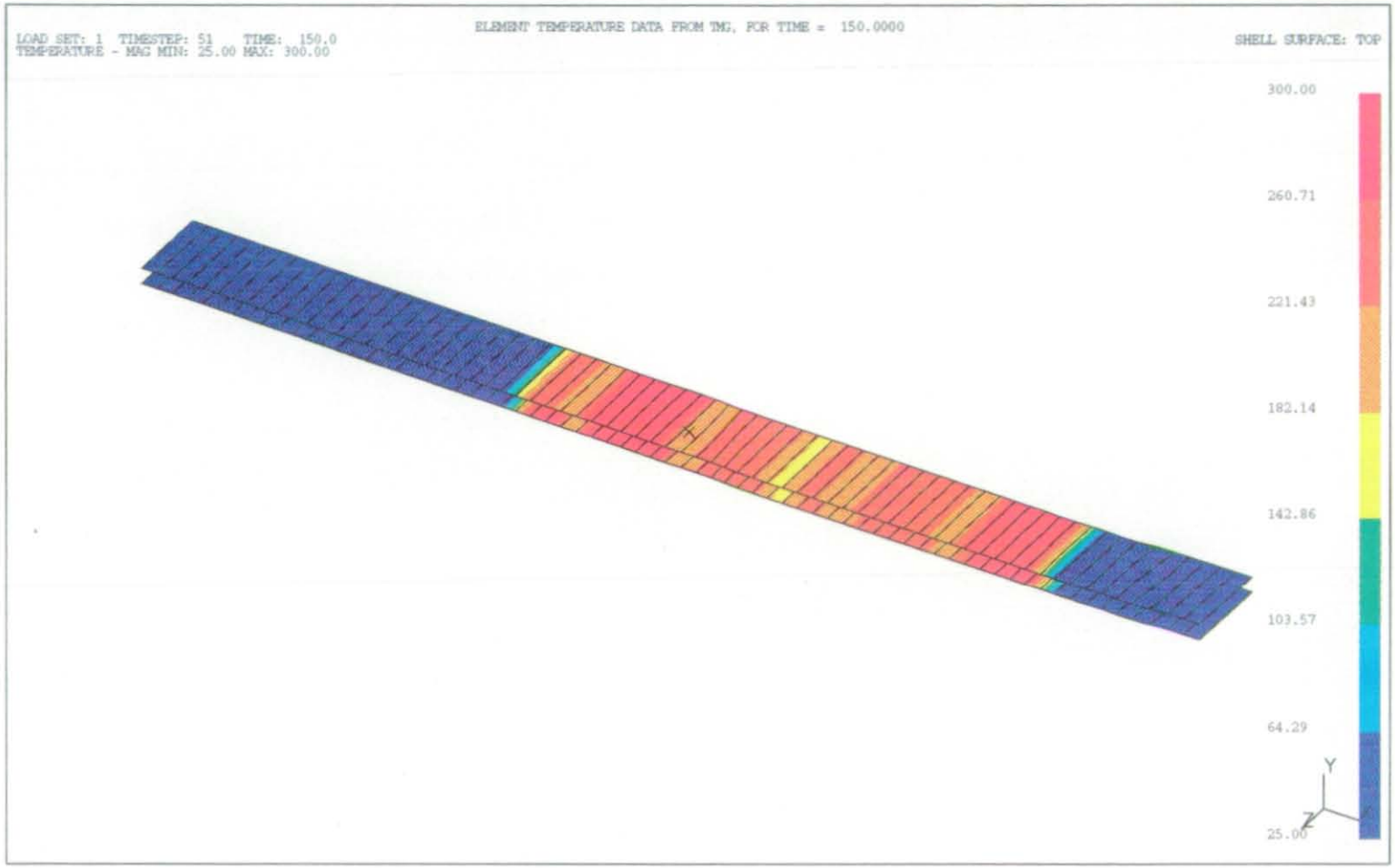

Figure 4.13: The Profile of the model heater zones

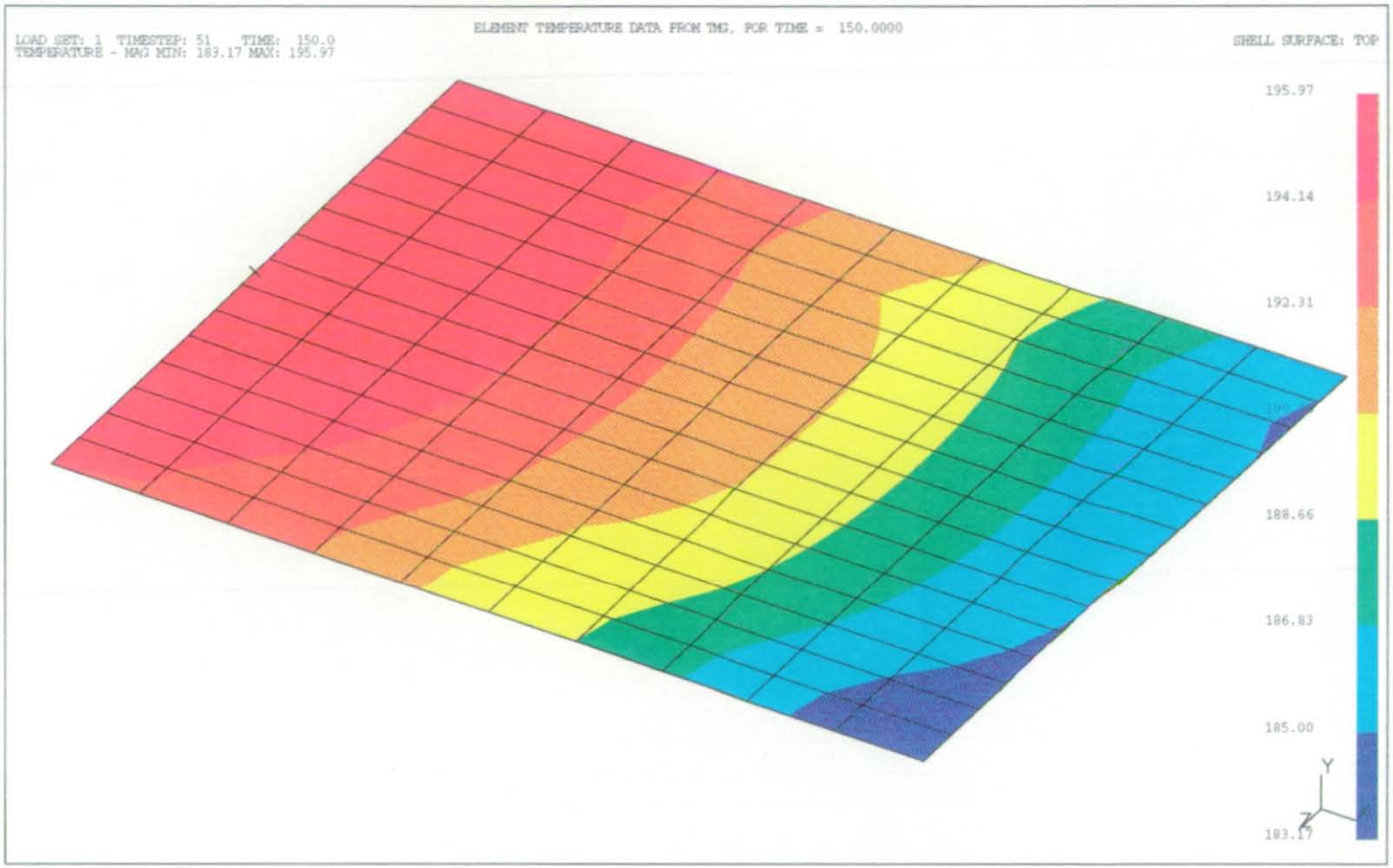

Figure 4.14: The predicted thermal response of the PCB to the mode of heat transfer in the SENJU model

4.3. Discussion

One of the major advantages of the finite element model over the experiment is the possibility of visual display of the temperature distribution on the PCB. The different heat transfer modes in the furnace can be assessed by taking snap shots in time, of the temperature distribution of the board, with the appropriate heater components active.

Figure 4.5 shows the effect of pure radiative heat transfer on the PCB. The geometry effect is very obvious as hot spots are clearly visible at the corners of the PCB where the surface area of elements are greater. Similarly, areas with similar view factors are seen have similar temperature distribution. Overall the edges are hotter than the inner part suggesting smaller components could be damaged during reflow, if placed near the edge. The big dark patch in the middle shows the coldest region on the board. This is expected since the front end has been in the furnace longer. The variation of temperature from the coldest to the hottest is about 13°C

The addition of edge heaters did not raise the temperature but altered the distribution across the board (Figure 4.7). The geometry effect becomes less obvious because there is more heat going into the edge along the length of the board. This observation explains the presence of the edge-heaters which was not detected in the results of the trials in chapter 3. However the temperature gradient across the board (from hottest to the coldest) increased by about 4%.

Addition of convection (Figure 4.11), similarly reduces the geometry effect while increasing the temperature gradient across the board. There is about 50% reduction in the temperature gradient resulting from a maximum temperature of 164.31°C and a minimum of 157.87°C. The reduction in the thermal gradient indicate a better heat distribution across the board.

The thermal response of the PCB to the complete furnace shows the combined effect of the edge heaters and convection (Figure 4.16). The heat distribution on the PCB is not symmetrical because one side of the conveyor is fixed while the other can be moved to accommodate different sizes of boards. Therefore the PCB is not symmetrically located in the furnace. The temperature differential across the board is about 13°C however, this figure should not be used as a direct comparison with the other models as the profile in question was completely different.

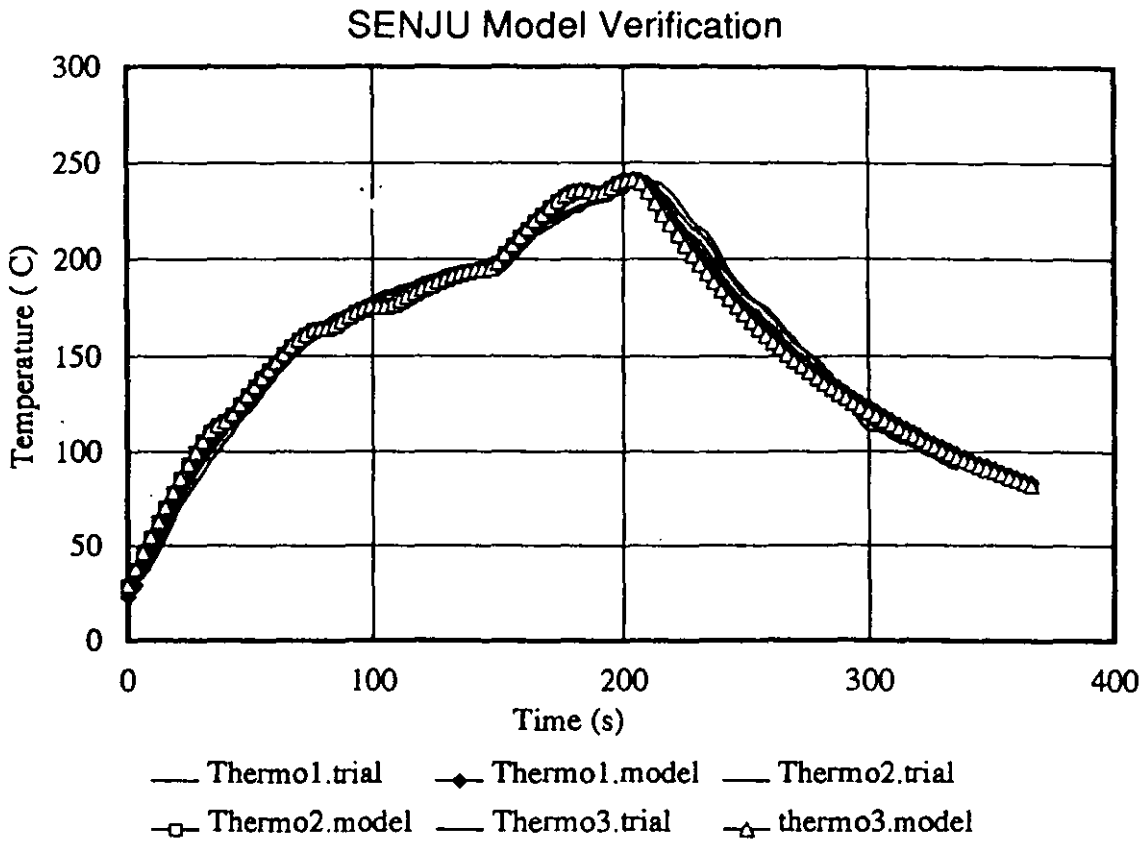

Figure 4.16: The temperature profiles for the different components of the model

4.4. Limitations of the Model

Although there is a good correlation between the model and experiment, a discrepancy is noted at the peak temperature in the reflow cycle. This discrepancy can be attributed to the fact that some factors influencing heat loss from the furnace cannot be modelled: The model assumed a closed system while in reality heat is lost to the environment through the two open ends (entrance and exit ends) of the furnace. Similarly there will be heat loss by conduction through mountings in the furnace.

The air flow rate in the different zones of the furnace was assumed to be the same which is not true in the real furnace. Perhaps a better correlation in experiment and model will be achieved if the variations in the flow rate can be incorporated in the model.

4.5. Conclusion

The combination of infrared and convection has proven to be an ideal one because the temperature differentials across the board are lower and the geometry effect is minimised. The need for the edge heaters still remains difficult to justify. The only obvious advantage is the reduction of the geometry effect. There is a good correlation between the model and the experiment during the heating cycle (figures 4.3, 4.9 and 4.15), however there is a more obvious discrepancy on the cooling cycle due to the use of cooling fans on the exit of the real furnace. The model assumed free convection cooling to ambient as opposed to forced convection of the cooling fans in the real furnace as there was no means of determining the convection coefficient. The use of linear conductance and lumped masses is however a unique way to model convection in the furnace. The effect of the variation in the airflow characteristics across the furnace could not be incorporated into the model. Similarly, the effect of heat loss at the two ends of the furnace was not accounted for resulting in a discrepancy in the predicted maximum temperature of the board.

Chapter 5

Materials Property Measurement

5.1. Introduction

The preceding chapters have dealt mainly with the issues associated with heat transfer to the assembly, this and the following chapters will deal mainly on the effect of the heat on the components of the assembly. Solder has been the traditional medium of component attach. Recently conductive adhesives have indicated a potential to replace solder in the attachment of components. Adhesives have the ability to combine a high operating temperature with a low processing temperature and also remove the need for a flux cleaning operation. These features are particularly attractive to manufacturers because of the demand for high temperature applications and more robust performance from electronic products in the automotive and aerospace industry. Current surface mount technology and die-attach processes may be readily modified for the application of conductive adhesives. The same reflow furnace is used for curing adhesives and a low process temperature minimizes damage to components during curing. A review of the impact of conductive adhesive technology on electronics interconnection was reported by Ogunjimi et al. [77].

Solder applications are better understood than conductive adhesive applications, many issues must therefore be resolved for conductive adhesive technology particularly the effect of the processing parameters on the quality of interconnection. There are on-going efforts addressing soldering process problems and its effect on surface mount components [78, 79], the author has therefore chosen, as part of an investigation of the use of conductive adhesives for electronics interconnection, to study, using finite element analysis (FEA), the effect of manufacturing parameters on the final quality of the conductive adhesive joints.

An important step in finite element modelling is the definition of the material characteristics, the constitutive equations and the materials properties of the model. These are important because they dictate the mechanical behaviour of the system. For instance, the most significant material characteristic for a stress analysis is the stress strain law governing the behaviour of the material. The method of stress application also determines other properties that might be required e.g thermal coefficient of expansion must be specified for thermal loads and material density for dead weight and centrifugal loads. Thermal stress analyses were undertaken in this work, therefore the relevant material properties are Young's Modulus of Elasticity, E, Thermal Coefficient of Expansion,α, and Poisson's ratio, υ,. A knowledge of the variation of these properties with temperature will be advantageous for the study of high temperature capabilities of the conductive adhesive joint. Similarly, there is a need to understand the visco-elastic properties of the conductive adhesive to give some understanding of stress relaxation properties, hence a knowledge of the creep properties of the adhesive is required.

Determination of the material properties is a frequent bottleneck in finite element analysis as they are rarely available. The properties of the standard components of a die-attach assembly (described later in chapter 6),such as the silicon die and alumina substrate are available from literature and from manufacturers as they are mature products. Conductive adhesives, however, are relatively new and usually contain proprietary materials whose properties are only known to the manufacturers because of commercial pressures. The conductive adhesive used in this study was an experimental product developed by Cooksons Technology Centre for high temperature applications. Most of the material properties had to be experimentally determined by the author.

This chapter discusses the techniques used to measure the relevant material properties outlined above. The major methods used are simple tensile tests and Dynamic Mechanical Thermal Analysis (DMTA). The simple tensile test was used to measure the modulus of elasticity while DMTA was performed to measure the glass transition temperature, T_g, of the adhesives, the variation of the Modulus of Elasticity with temperature and the creep characteristics of the adhesive. The method of preparation of the thin specimens

used is also novel.

5.2. Mechanical Testing of Polymers

Isotropically conductive adhesives are composite polymers usually consisting of a metal filled epoxy matrix, with the ratio of metal to epoxy of approximately 20:80% by volume. The epoxy matrix is therefore the dominant component. Most commercially available conductive adhesives are engineered to address specific problems of the use of conductive adhesives in electronics manufacturing. The application of the adhesive therefore determines the mechanical properties. Such problems include high temperature performance, minimisation of residual stresses due to curing, ease of processing and ability to "rework" bad joints. Three main types of adhesives that are identified are low Tg, thermosetting (a polymer that hardens when two components, a resin and a hardener are heated together) epoxy for thermal stress management, high Tg thermosetting epoxy and polyimides for high temperature application, and thermoplastic (a polymer that softens on heating) adhesives for ease of rework. Epoxy based adhesives were found to be easier to process than other materials such as polyimide which are solvent based. The author had direct access to a large quantity of the experimental high Tg thermosetting epoxy, CTC2000, this material was chosen as the main test material for this work as it was of most interest to the industrial partners in the work. Other adhesives are tested for comparison as appropriate.

5.3. Mechanical Properties of Conductive Adhesives

The measurement of modulus of elasticity is perhaps the most important variable for an elastic stress analysis. Modulus of elasticity are easily measured for simple elastic materials such as metals and ceramics. This is usually done by loading a bar of the material in tension with a known force while observing the resultant extension. The Young's modulus of elasticity, E, is defined as

$$E = \frac{stress}{strain} \qquad \text{Eq. 5.1}$$

where

$$stress = \frac{force}{area} \qquad \text{Eq. 5.2}$$

and

$$strain = \frac{extension}{length} \qquad \text{Eq. 5.3}$$

The strain in the material is however governed by the Poisson's ratio of the material.

Polymers like conductive adhesives are however visco-elastic (a term chosen to describe their intermediate position between viscous liquid and elastic solids[80]) in nature because they exhibit time dependent properties. Their mechanical properties are dependent on the conditions of test. At low temperatures or high frequencies of testing, a polymer exhibits a brittle glass-like characteristics with a high modulus of elasticity and will fail at strains greater than 5%. At higher temperatures or low frequencies, the same polymer may exhibit rubber-like characteristics, with a modulus of about three orders of magnitude lower, and the ability to withstand large extensions of up to 100% without permanent deformation. Permanent deformation occurs under loadings with the polymer behaving like a viscous liquid at a higher temperature still [80].

Polymers like conductive adhesives exhibit an intermediate temperature range called the glass transition temperature range at which the polymer is neither glassy or rubbery. This is a range of an intermediate modulus at which the polymer may dissipate a lot of energy on being strained. This range can be identified by a change in the volume/linear coefficient of expansion, normally used to identify a glass transition temperature, T_g, or a drastic change in modulus of elasticity the onset of which can also be used to determine T_g. The mechanical behaviour of polymers is critically related to the glass transition temperature (or temperature range) because the properties below and above this temperature are totally different, and this temperature defines the point of transition.

The visco-elastic or time dependent behaviour of polymers makes simple tensile tests an inadequate method of characterisation because of different behaviours at different conditions of testing i.e temperature and strain rate. It is difficult to use simple tensile tests to explore combinations of any of these conditions as a considerable amount of data and specimens will have to be generated to give a reasonable result. Dynamic mechanical testing on the other hand applies a sinuosidual load to the sample, this load results in a real, or in phase modulus E_1, and an imaginary or, out of phase modulus, E_2 obtained as follows[80]:

By subjecting the specimen to an alternating strain, ε, while measuring stress, σ, the stress and strain properties of a visco-elastic material will both vary sinuosidually with the strain lagging behind the stress, therefore, if

$$\varepsilon = \varepsilon_0 \sin \omega t \qquad \text{Eq. 5.4}$$

and

$$\sigma = \sigma_0 \sin (\omega t + \delta) \qquad \text{Eq. 5.5}$$

where

ε_0 is the initial strain

σ_0 is the initial stress

ω is the angular frequency

δ is the phase lag

t is time

By expanding σ,

$$\sigma = \sigma_0 \sin \omega t \cos \delta + \sigma_0 \cos \omega t \sin \delta \qquad \text{Eq. 5.6}$$

i.e

$$\sigma = \varepsilon_0 E_1 \sin\omega t + \varepsilon_0 E_2 \cos\omega t \qquad \text{Eq. 5.7}$$

The stress therefore can be seen to consist of two components E_1 in phase with the strain and E_2 out of phase, where

$$E_1 = \frac{\sigma_0}{\varepsilon_0}\cos\delta \qquad \text{Eq. 5.8}$$

and

$$E_2 = \frac{\sigma_0}{\varepsilon_0}\sin\delta \qquad \text{Eq. 5.9}$$

If we write

$$\varepsilon = \varepsilon_0^{i\omega t} \qquad \text{Eq. 5.10}$$

and

$$\sigma = \sigma_0^{i(wt+\delta)} \qquad \text{Eq. 5.11}$$

Then

$$\frac{\sigma}{\varepsilon} = E^* = \frac{\sigma_0}{\varepsilon_0} e^{i\delta} \qquad \text{Eq. 5.12}$$

$$= \frac{\sigma_0}{\varepsilon_0}(\cos\delta + i\sin\delta) \qquad \text{Eq. 5.13}$$

Where E* is a complex modulus,

$$E^* = E_1 + E_2 \qquad \text{Eq. 5.14}$$

The real part of the modulus E_1 is often called the storage modulus (because it defines the energy stored in the specimen due to the applied strain). It represents the elastic behaviour of the material and is equivalent to the static modulus measured in simple tensile test. The imaginary part of the modulus, E_2 represents the viscous behaviour of the material and is often referred to as the loss modulus. The ratio E_2/E_1 is often referred to as tan δ, the loss tangent. Increases in E_2 can represent microscopic factors such as molecular relaxations or macroscopic factors such as phase boundary motion [81]. The ability to measure both of these moduli enables the full characterisation of polymers. Detailed information on the use of dynamic mechanical testing can be found in [44,45,46]

5.4. Modulus of Elasticity Measurements

The post cure properties of the adhesive needed to be determined so that they can be used to model the effect of curing parameters on the adhesive joint. In order to do this three principal material properties were needed, the thermal coefficient of expansion, the Young's modulus of elasticity and the Poisson's ratio. The material used is a developmental product from Cooksons Technology Centre, CTC 2000, supplied in paste form. The thermal coefficient of expansion was measured by Cooksons personnel using dilatometry leaving the modulus of elasticity and the Poisson's ratio to be determined.

The major issues in the measurement of the Modulus of Elasticity for conductive adhesives is the preparation of the specimen to represent the material in service (for example the adhesive thickness may vary from about 50 to 100μm), to fully reflect the visco-elastic properties of the polymer and the direct interpretation of the measured property. It was therefore decided to use two methods to arrive at a representative value. The first approach was to use the simple tensile test and the second was Dynamic Mechanical Thermal Analysis

5.4.1. Preparation of Specimens

Preparation of specimens is an important issue because of the nature of the samples to be tested. Conductive adhesives have very strong adherence to many surfaces except tin and polytetrafluoroethylene (PTFE). Since the adhesives are supplied in uncured paste form, there is the need to prepare the appropriate shape of specimen and cure (the specimen) in a mould to which it will not adhere. PTFE moulds were therefore chosen.

Similarly, voids are a major concern in bulk specimens. It was found difficult to make acceptable bulk samples using polyimides and other high solvent loss adhesives. The samples made with this category of adhesives were unsatisfactory, being very porous (about 25% of voids) due to the volatile gases given off and are therefore not good enough for the test. The epoxy based adhesives were however better with less pores (about 5%). The pores are caused by gases given off at high temperature during the curing process and little can be done to minimise these voids. An attempt was made to reduce voiding by filling and part curing the adhesives in layers, however, this resulted in adhesive laminates rather than bulk samples, hence the process was discontinued. The larger samples prepared for simple tensile tests are more porous than those prepared for DMTA.

The specimens were prepared by cutting out the shape of the specimen from a 2mm thick, 100mm x 100mm (PTFE) sheet to generate a mould. This mould is then filled with the adhesive and sandwiched between two other PTFE sheets (to prevent the adhesive from flowing out during cure) to be cured in a conventional oven. After curing, the specimen is then extracted from the mould. Figure 5.1 shows the process of making bulk material samples for tests.

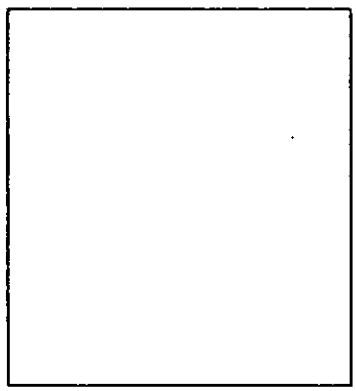

a. Plain PTFE Sheet

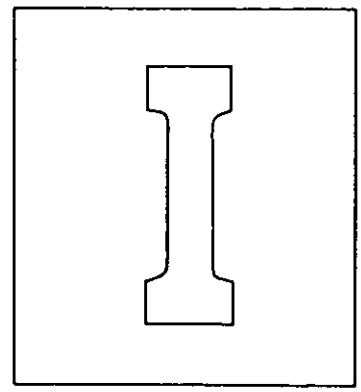

b. Specimen shape cut out of plain PTFE sheet to make a mould

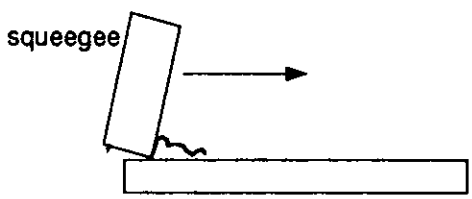

c. Adhesive printed into the mould

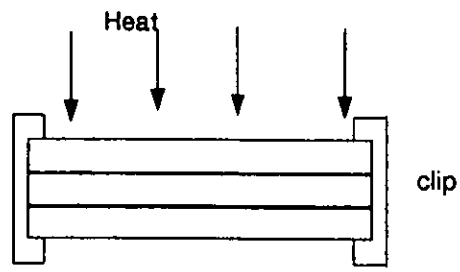

d. Mould sandwiched between two other PTFE sheets to prevent adhesive flow-out during cure.

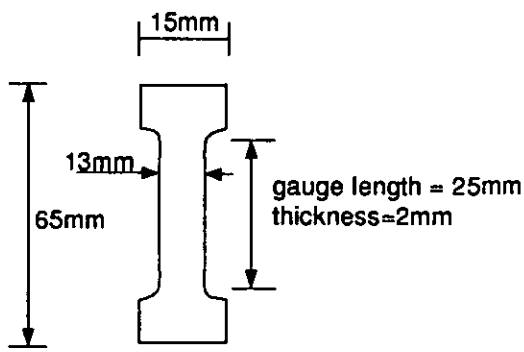

e. Cured specimen extracted from the mould

Figure 5.1: The process of making specimens for material testing

5.4.2. Simple Tensile Test

The simple tensile test was used to measure the Youngs modulus of elasticity of the adhesive CTC2000.

5.4.2.1. Equipment

Simple tensile test was carried out on a JJ Instruments MK5 tensile testing machine on which the force is applied through the cross head. The extension of the specimen during the application of the force was measured using an Hounsfield 100R extensometer and the results plotted on a JJ Instruments PL3 Chart plotter. Twenty dog-bone shaped samples of CTC2000 were prepared for the experiment.

5.4.2.2. Procedure

The experiment was performed on the 15 best (least porous) "dog-bone" shaped specimens of cured CTC2000 adhesive paste, The size of a typical specimen is shown in figure 5.1. The specimens were so shaped to provide a wide surface area to be gripped by the jaws of the machine during the test and to strengthen the two ends so that failure occurs only within the gauge length. The minimum gauge length required by the machine is 25mm. The specimens were prepared over a period of time and the time of preparation of each specimen was noted so that the effect of aging on the properties of the adhesive could be taken into consideration. The rates of application of the force (strain rate) was varied from 2mm/min to 8mm/min in steps of 2mm/min.

5.4.2.3. Results of simple tensile test

Figure 5.2 shows typical force versus extension curves for bulk specimens. The modulus of elasticity was calculated by measuring the gradient of the curve and multiplying by the machine constant.

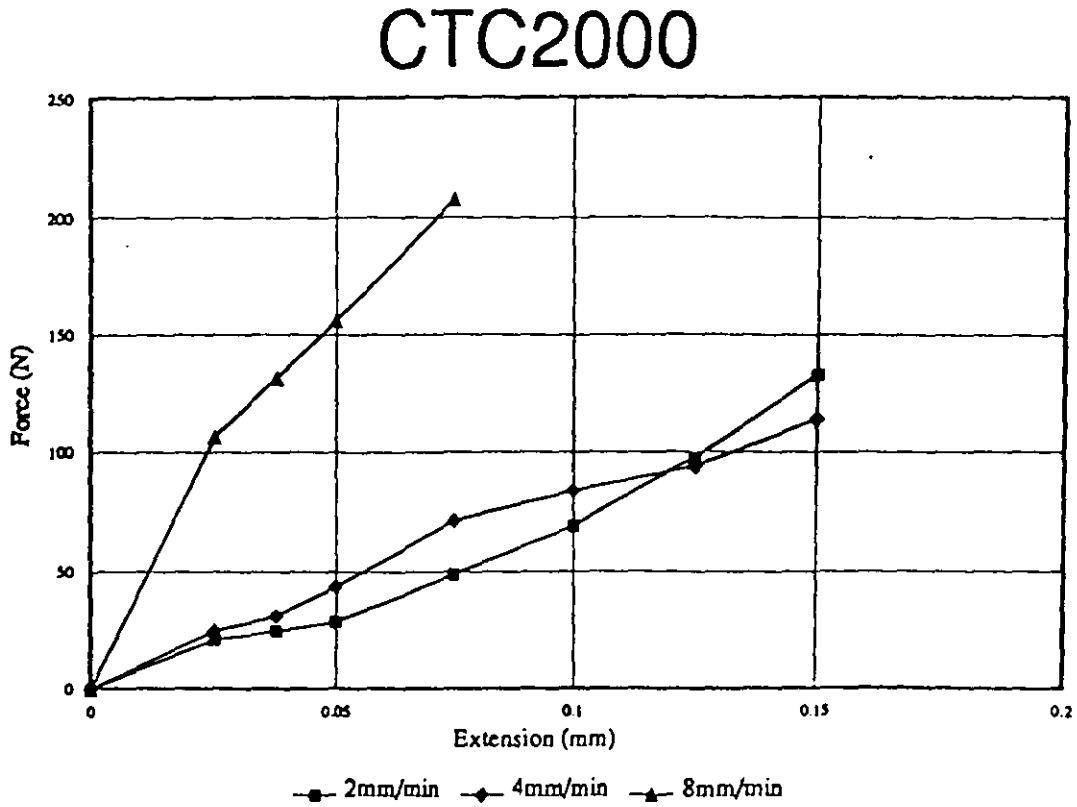

Figure 5.2: Typical Force versus Extension curve for the simple tensile test

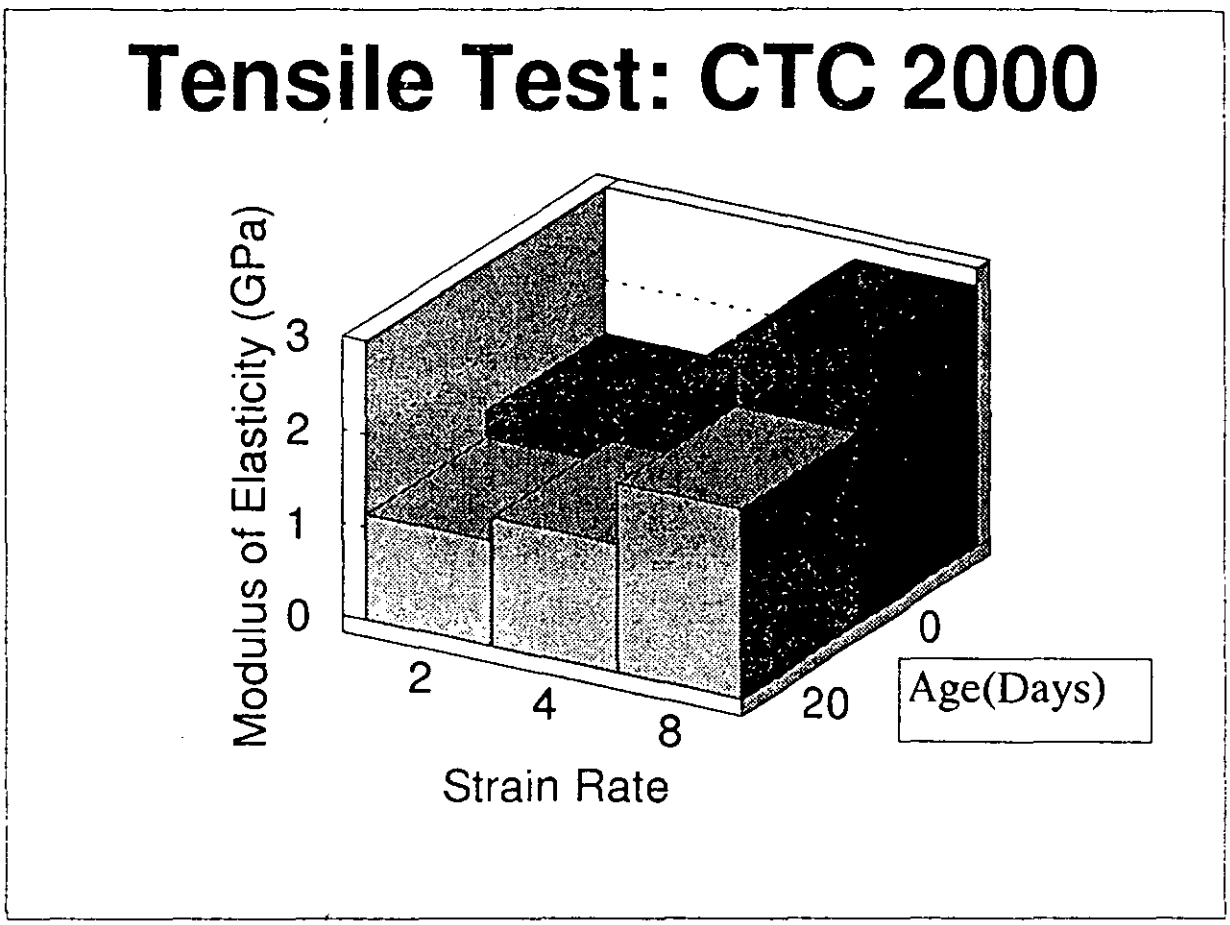

Figure 5.3: Simple tensile test result for CTC 2000

The result presented in figure 5.3 comprises the average of the values measured for the relevant conditions. As expected, it could be seen from the figure that the modulus of elasticity of the material is strain rate dependent. This is particularly apparent in the variation in the stress strain behaviour of the material as the strain rate increases i.e. the apparent modulus of elasticity increases with strain rate. This is illustrated in figure 5.2 where the force -extension curve increases in slope with increasing strain rate. Similarly the modulus of elasticity is seen to decrease with age suggesting a reduction in stiffness (bond relaxation of the material with age).

Voids were very visible on the cross section after breakage. The porous nature of the sample is a great cause for concern and therefore puts the integrity of the results in doubt. Similarly, it is very difficult to assume a typical strain rate for the operating strain rate of the adhesive in service. Due to the afore-mentioned problems, the results of the simple tensile test was not used in the models. The DMTA approach was therefore used to measure the relevant properties used in the model.

5.4.3. Dynamic Mechanical Thermal Analysis

While the simple tensile load applies a direct static tensile stress to the material, DMTA applies a sinuosidual load to the sample enabling the measurement of both the elastic and viscous behaviour of the material. Samples of two adhesives were prepared. The adhesives tested were thermosetting CTC2000, a high Tg adhesive manufactured for high temperature applications, and a thermoplastic, Staystik 101, manufactured for ease of rework.

5.4.3.1. Procedure

DMTA was performed on the DuPont Instruments 983 Dynamic Mechanical Analyzer. The sample size required needs to be sufficiently large to allow for the resolution of the machine but small enough to minimize the effect of voiding. Bar samples of size 2mm x 10mm x 40mm prepared as illustrated above (Figure 5.1). The samples were clamped between the two test jaws of the machine and a sinuosidual strain applied with the aid of

synchronised motion of the two jaws. In order to measure the modulus within the linear visco-elastic range, it is important that the applied strain level is kept small. Therefore the amplitude of oscillation was held at 0.20mm at a frequency of 1Hz. The test was carried out between -100°C and 250°C for the Staystik sample to study subzero temperature variation of modulus. The test however showed that the variation of modulus with temperature is minimal between -100°C and ambient temperature and hence the test was conducted between room temperature and 250°C for CTC2000.

5.4.3.2. Results of DMTA

Figures 5.4 and 5.5 shows the variation of modulus of elasticity with temperature for Staystik 101 and CTC200 respectively. Table 5.1 shows a comparison of the results of the two specimens. The glass transition temperature, T_g, is the temperature at which turning points (peaks) occur in the curve for tan δ .The observed T_g for CTC 2000 was 225°C. Staystik 101 on the other hand has two peaks for Tan δ suggesting the matrix consists of copolymers with different glass transition temperatures. These materials are proprietary and the compositions are not known to the author. The high temperature performance of the two adhesives were compared by comparing the ratio of the modulus at 200°C to that of 100°C (high temperature performance is defined in excess of 175°C in the context of solder replacement). This ratio indicates that the modulus of elasticity at 200°C for the Staystik adhesive has reduced to 0.32% of its value at 100°C compared to 24% for CTC2000. This suggests that the thermoplastic adhesive does not have good mechanical stiffness at 200°C

	CTC2000	Staystik 101
T_g (°C)	225	130.40 186.33
E_{100}(GPa)	3.1	3.98
E_{200}(GPa)	0.75	0.126
E_{200}/E_{100}	0.24	0.0032

Table 5.1: Comparison of DMTA results for CTC2000 and Staystik 101

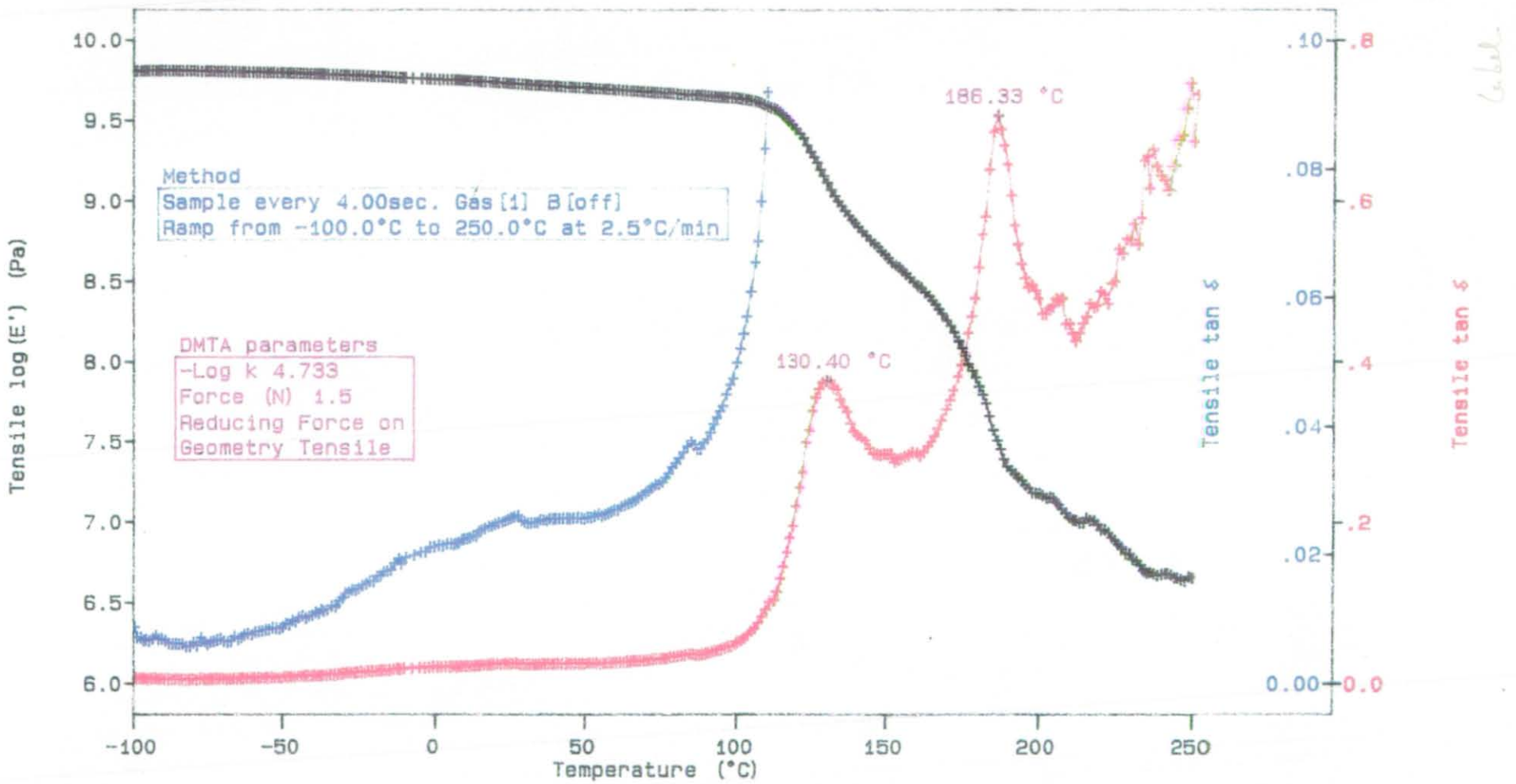

Figure 5.4: Variations of Modulus of elasticity with temperature for Staystik 101

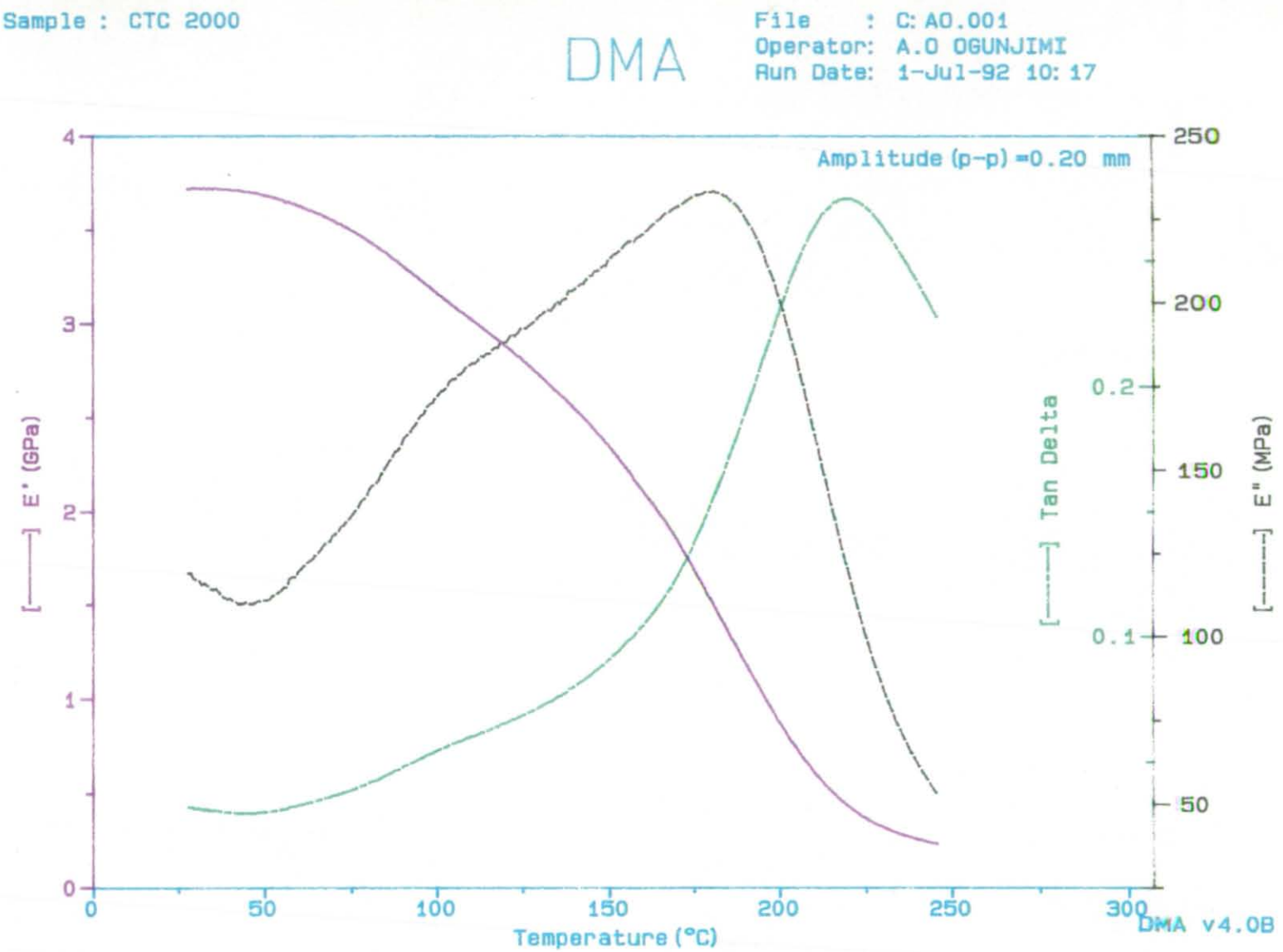

Figure 5.5: Variations of modulus of elasticity with temperature for CTC2000

5.5. Creep Testing

While the tests described above measure the linear (assuming small strain) visco-elastic properties of the adhesive, the non linear effect of the visco-elastic properties of the adhesive was studied by DMTA creep testing. Creep is the deformation under constant load occurring over time. It is important to undertake creep testing because it indicates the behaviour of the materials in service. In order to fully reflect the behaviour of the adhesive in operation, typical bondline thickness value was determined for specimen preparation. Therefore the specimen in this case was stencilled to a thickness of about 230μm this being the lowest thickness achievable by the method of specimen preparation. The adhesives selected for test were identified for qualities such as ease of processing, potential high temperature application, ease of rework and low residual stress. Creep tests were carried out on five commercially available and the experimental CTC2000 conductive adhesives.

5.5.1. Results of creep test

The output of the creep test is a plot of displacement against time. Figures 5.6-5.8 show plots of the raw data of the test results. These results are then compared in Table 5.2 from which it could be seen that the high temperature, high T_g, adhesives exhibit the best creep characteristics. The thermoplastic adhesive, Staystik 101 has the worst performance at high temperature, in fact, the sample fractured at 150°C. A comparison of the creep strain rate of the adhesives (Figure 5.9) with that of solder indicates that the adhesives are about an order of magnitude lower. This suggests that adhesives have a higher strength at high temperatures than solder, indicating that they will be more reliable than solder. Similarly, as it will be expected from earlier discussion of T_g, there is a significant increase in displacement at temperatures above the T_g of the adhesive. This indicates that high T_g adhesives have a better creep properties at higher temperatures than low T_g adhesives.

Figure 5.6

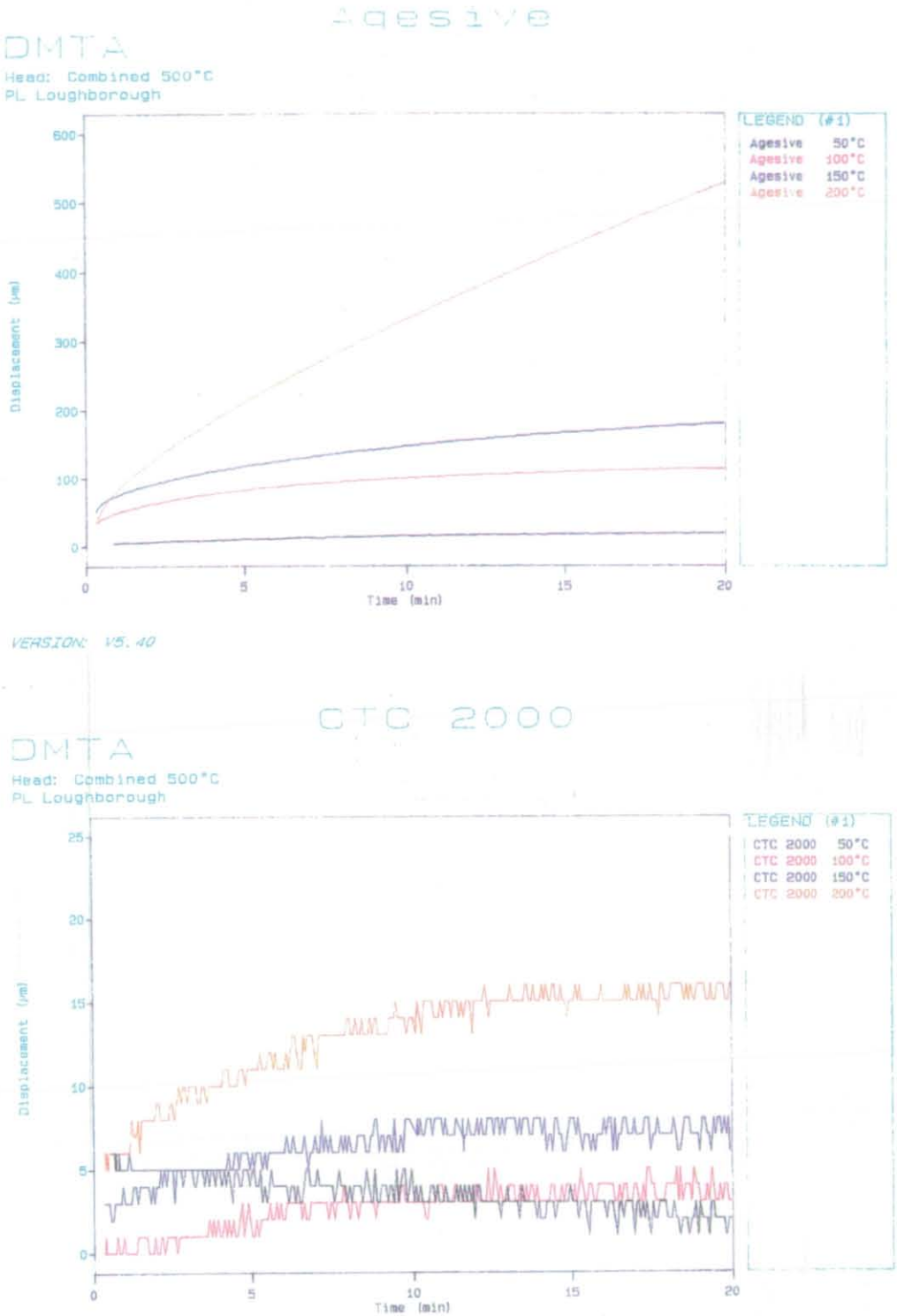

Figure 5.6. Creep test results for Agesive and CTC2000

Figure 5.7

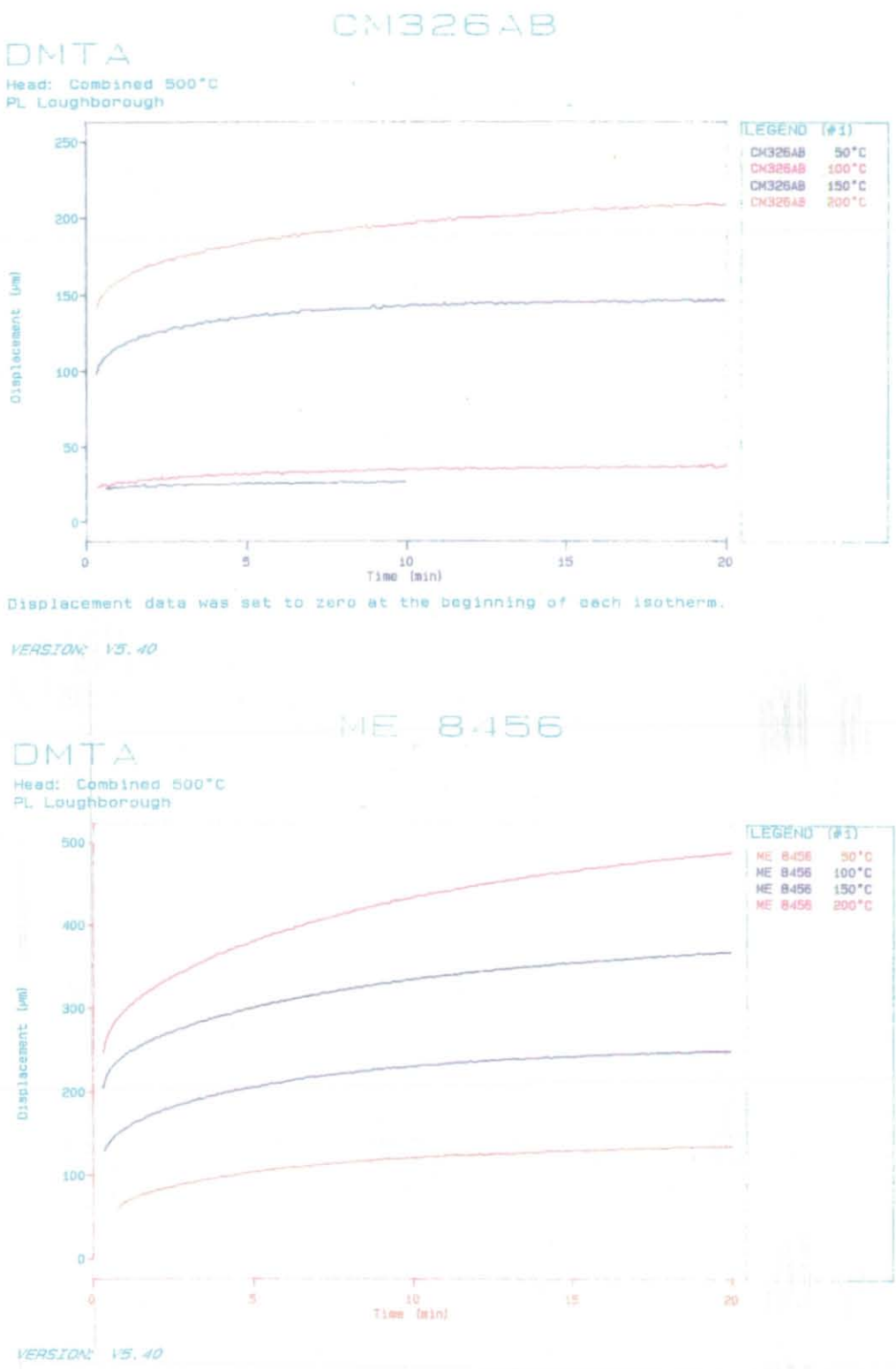

Figure 5.7. Creep test results for CM326AB and ME8456

Figure 5.8

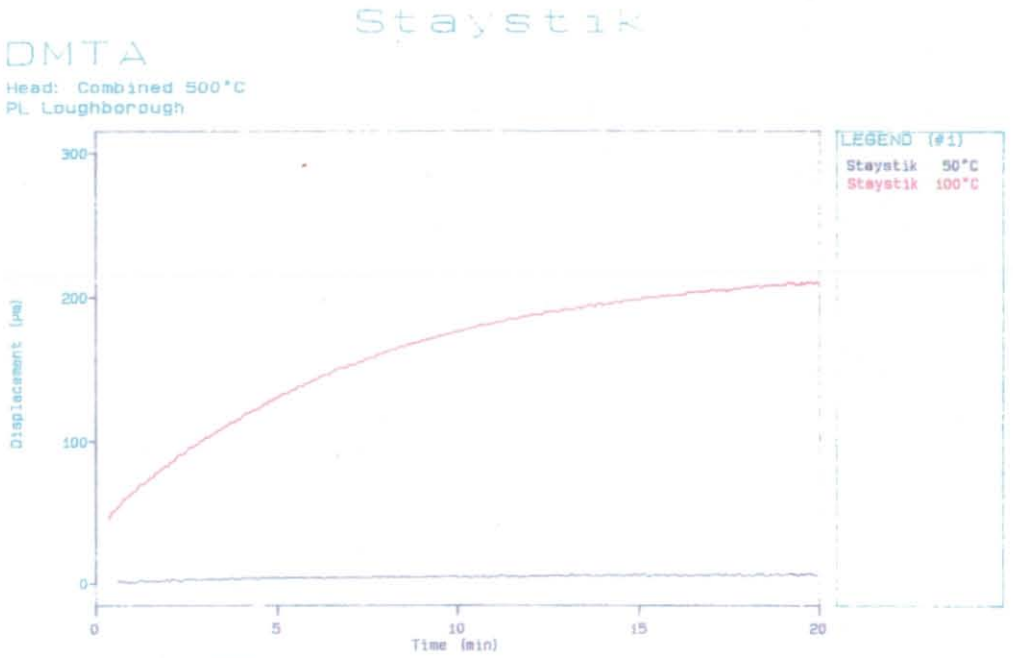

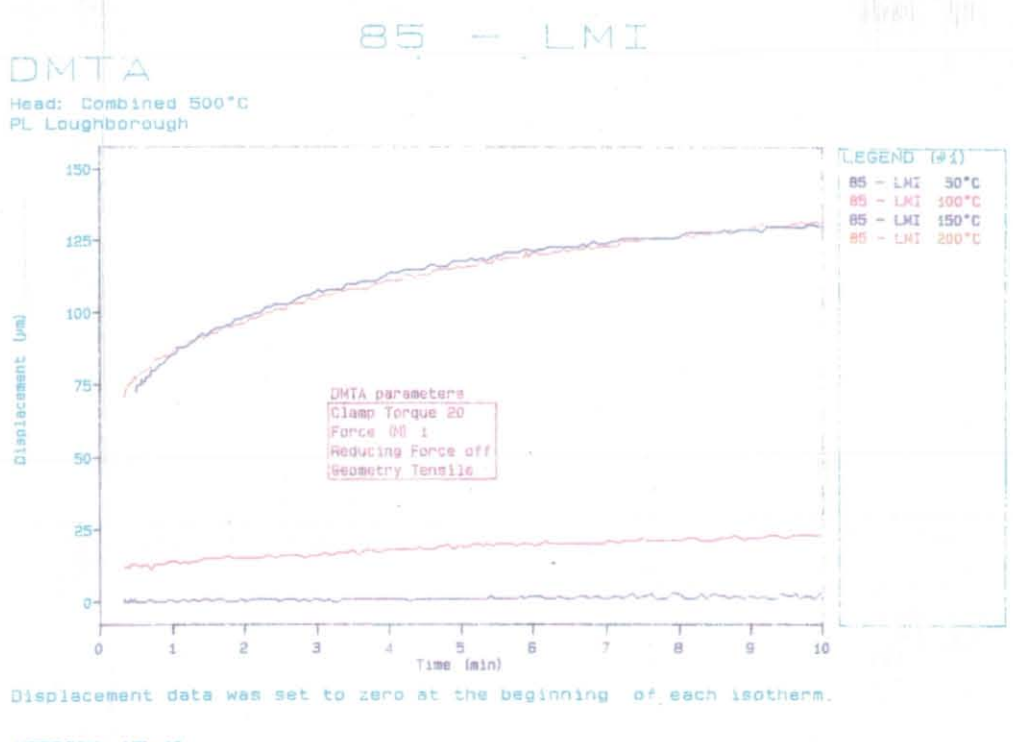

Figure 5.8. Creep test results for Staystik and 85-LMI

Adhesive	T_g(°C)	Maximum Displacement (μm)	Maximum Micro-Strain	Specimen Thickness (μm)	Comment
AgEsive	150?	520	42.80	214	Rate of creep greater after 150°C
CTC2000	230	15	1.39	310	Excellent creep characteristics
CM326AB	79	200	16.12	220	Creep greater after 100°C
ME 8456	-25	500	40.65	215	Progressive increase in creep with temperature
Staystik101	>150	200	18.35	225	Sample fractured at 150°C
84-LMI	103	125	9.87	224	Creep greater above 100°C

Table 5.2: A comparison of Creep results

5.6. Discussion

The methods and material properties measured as outlined above give a better understanding of the material and consequently, the relevant material properties to be used for modelling. The inherent problem in testing conductive adhesives stems from their viscoelastic properties which means properties measured are only valid for the test conditions and not universal. This means that relevant properties have to be measured for the appro

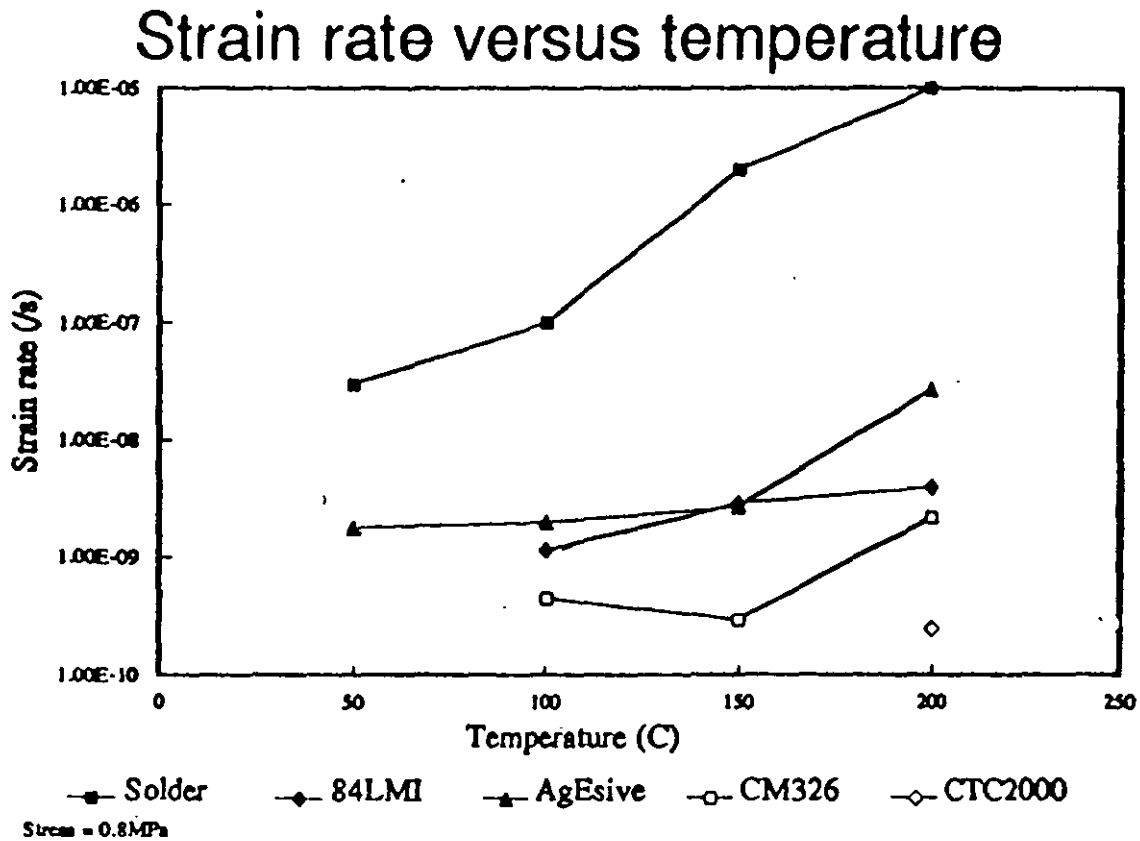

Figure 5.9: Comparison of strain rates of conductive adhesives with solder

priate application. Test samples are also difficult in adhesives and the chemical properties of these materials can cause them to adhere to the mould or attack it.

The simple tensile test solely measures the elastic properties of the adhesive, it is therefore not an effective method for characterising this type of material. The samples required for test are large and therefore difficult to make without voids. The lack of control over the quality of the samples and the inherent variation in the measured values makes the results of the simple tensile test in this case, questionable. The qualities of the samples for DMTA were much better and the results more comprehensive. The measured glass transition temperature was in agreement with that determined by the manufacturers using Differential Scanning Calorimetry (DSC). The values measured using DMTA are however subject to errors from the machine as follows [5].

The sample is clamped between two arms as shown in figure 5.10 below and a bending stress applied to it. The modulus of elasticity is calculated from stiffness of the bar sample, using a constant, K, according to the following expression

$$K = w\left(\frac{t}{l}\right)^3 \qquad \text{Eq. 5.15}$$

Where w is the width, t is the thickness and l is the length of the sample between the clamps.

$$stiffness = KE_1 \qquad \text{Eq. 5.16}$$

The potential source of error is the length used in calculating K. Referring to figure 5.10, it is assumed that the stress under the clamp is zero therefore the length used in calculation is l. But in actual fact there is still some deformation up to the centre point (point of contact) of the clamp as shown. This means that the effective length of the specimen is l' as shown, introducing an error $(l'-l)^3$ into the expression for K. This can result in a mod

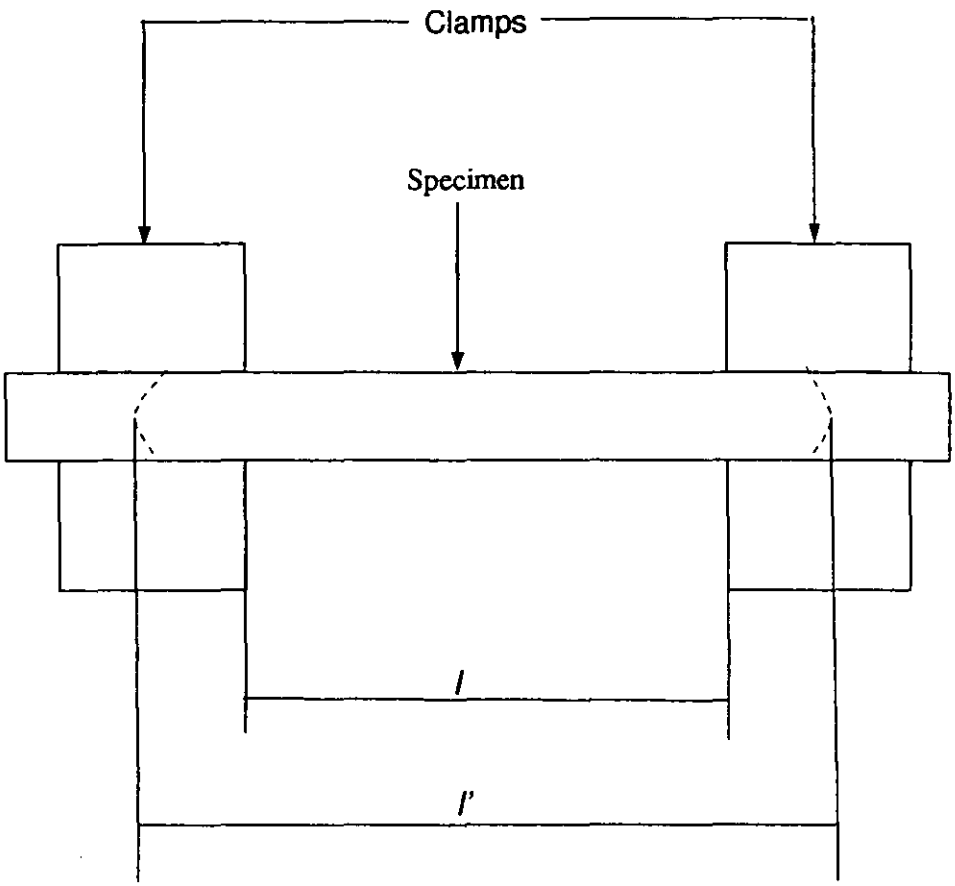

Figure 5.10: Error in DMTA measurement

ulus value 25% lower than the true value. Therefore the result of the DMTA was calibrated by carrying out a similar analysis on a material of known modulus of elasticity from which the error is then estimated. The material used to calibrate the result was Nylon 66. The measured value using DMTA was 2.65GPa while the quoted value from the manufacturers (Goodfellows Metal Ltd. Cambridge, U.K) was 3.3GPa, 20% more than the measured value. This correction factor was then applied to the measured values for the adhesive for modelling purposes.

5.7. Conclusion

The measured glass transition temperature for the experimental product, CTC2000 was 230°C and the modulus of elasticity at room temperature was 3.7GPa (4.651GPa after error correction). The thermal coefficient of expansion was measured by the manufacturer and quoted at 36 x 10^{-6} /°C before Tg and 114.05 x 10^{-6} /°C after Tg. The Poisson's ratio was assumed as 0.35 [10]. A novel method was developed for preparing specimens for test.

Finite element models (described in Chapter 6) were used to analyze the effect of the postcure residual stresses in the system due to manufacturing processes, the most relevant material properties are those at room temperature. The creep results were used to model non-linear effects and reliability over a range of temperature in which case the variation of other properties with temperature becomes relevant.

Chapter 6

Modelling of the Conductive Adhesive Die Attach Assembly

6.1. Introduction

Thermally and electrically conducting adhesives are currently being used for component and die-attach applications in the automotive and aerospace industries. They have the potential to combine a high operating temperature with a relatively low process temperature and also remove the need for a flux cleaning operation. Conducting adhesives have the potential to replace soft solders in component attach since soft solders are unsuitable for use in the more aggressive environments which future automotive and aerospace products will be required to endure. This has led to a demand for adhesives with an improved high temperature performance (typically capable of reliable operation over a temperature range of -65°C to +250°C). The introduction of ultra fine pitch semiconductor packages is also stretching the capabilities of soft solders. Anisotropic adhesives offer the potential to over come some of the manufacturing problems associated with fine pitch technology by avoiding the need for fine pitch printing and by eliminating the hazard of solder bridging.

Conductive adhesives are usually supplied in a paste form which is applied to the substrate by screen printing or syringe dispensing. Components are placed upon the printed adhesive which is then cured by the application of heat in an oven or belt furnace. The curing process can lead to significant residual stresses which may influence the quality of the manufactured joint and its subsequent reliability. The mechanical properties of the assembly and curing temperature of the adhesive combined with the joint geometry including, for example, the shape of the silicon die, bondline thickness and other process variables such as voids are important in determining such stresses. The finite element method offers a valuable tool for analysis of such joints since features such as adhesive fillets and the precise geometry of the components of an assembly

can be taken into consideration during modelling.

This chapter examines the variation of residual stresses and the associated potential failure modes based on the mechanical properties of the adhesive matrices. The effect of the die geometry, bondline thickness, presence of voids and anisotropic properties of the silicon die on the stress distribution assembly were examined by conducting a sensitivity analysis. The sensitivity analysis conducted can be divided into three major areas; modelling approach sensitivity, materials property sensitivity and process sensitivity. Modelling approach sensitivity examines the use of different modelling techniques, and the arrangement of elements in the critical areas of the model. Materials property sensitivity analysis examines the variation of stress level in the assembly with variation of critical material properties and the anisotropic properties of silicon. Process sensitivity examines the effect of the manufacturing parameters such as silicon wafer preparation and voids in the conductive adhesive layer.

6.2 Mechanisms and Modes of Failure in Conductive Adhesive Bonds

The identified primary causes of mechanical failure in conductive adhesive interconnections are [83]:

a. Thermal stress due to thermal expansion mismatch between component, substrate and adhesive.

b. Voids under the die (due to solvents and other volatile chemicals released during cure) which may either lead to weak bonds or "die popping", (a situation where, because of the trapped gases under the die, there is no adhesion between the adhesive and the die which results in the die becoming detached from the substrate).

The modes of failure which may occur are:

a. Die cracking or distortion:

b. Adhesive failure at the adhesive/substrate or adhesive components interface: and

c. Failure of the bulk of the adhesive

These modes of failure are related to the fundamental and physical properties of the materials used in the interconnection particularly those of the adhesive. An attempt to alter these properties can result in a compromise in bond strength and long term reliability. In order to investigate the effect of variation of these properties, the finite element (FE) method was chosen since carefully refined FE models can be built to closely reflect the real geometry and material properties and allow a wide variety of data to be gathered cheaply and within a short time. Visualisation of the problem at hand is another important aspect of the analysis technique used.

6.3. The Modelling Strategy

The models described in this chapter were developed using Structural Dynamics Research Corporation (SDRC) I-DEAS Finite Element Package Pre and Post processors. The initial models were analysed using the ANSYS Finite Element Solver. The restrictions on the size of the model that can be handled under the academic license of the ANSYS software subsequently led to the use of ABAQUS solver for the other models.

Figure 6.1 shows the strategy applied to the work reported in this chapter. The preliminary model utilized linear material properties taken from literature. The model was built expressly to identify the stress pattern in the assembly and potential points of failure to determine an appropriate simplified approach to modelling. The model was progressively improved as is shown in figure 6.1. Experimental methods as discussed in chapters 5 and 7 were used to refine the preliminary model by determining more accurate material properties and identifying the appropriate and more realistic model geometry. The improved model was used to undertake both material and geometric sensitivity analyses for the die attach system. The final stage of model can also be used for service reliability analysis as outlined in Figure 6.1. The final stage described above was not undertaken in this thesis and strategies for this will be discussed in the concluding chapter.

THE MODELLING STRATEGY

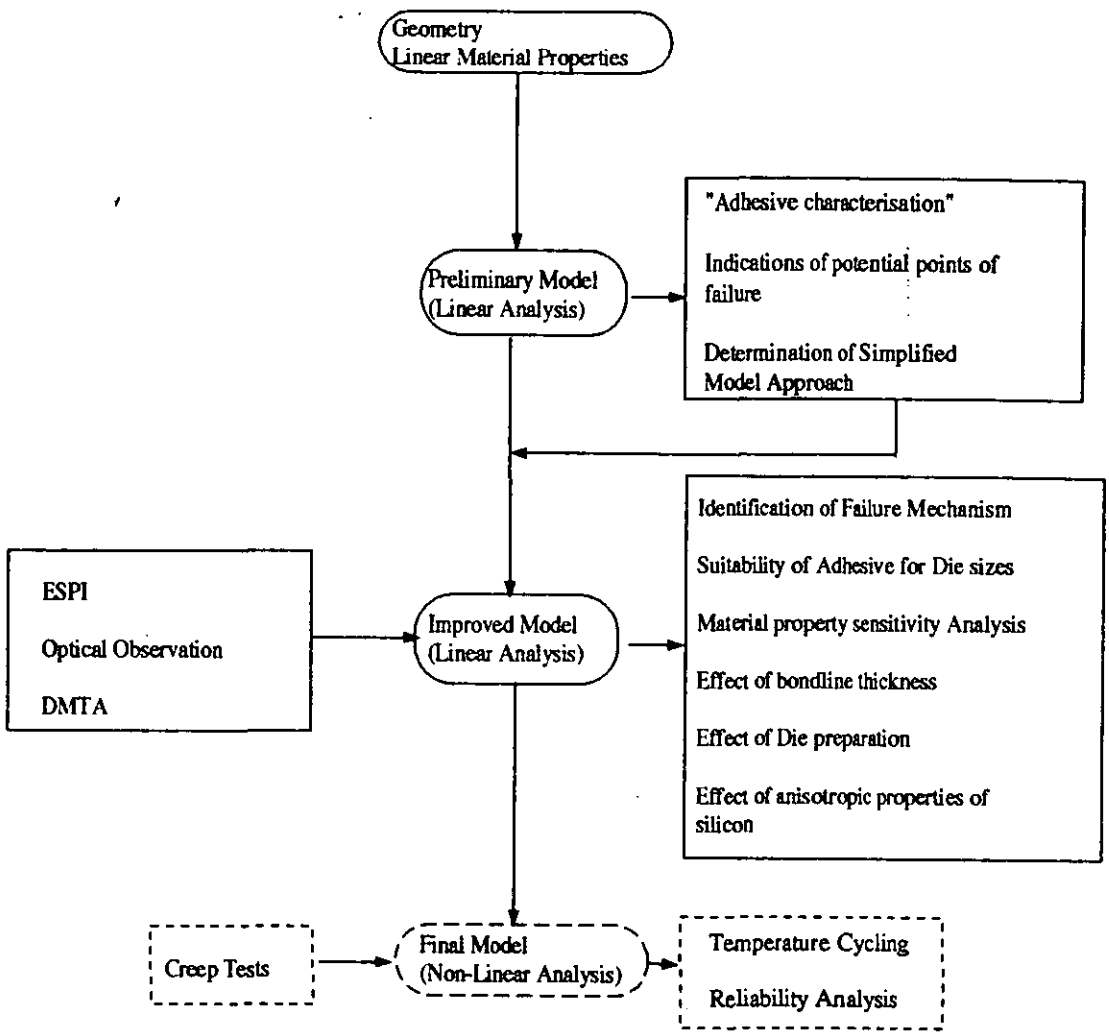

Figure 6.1: The approach to modelling

6.4. Adhesive Properties and Modelling Methodology

Linear structural analyses of the induced thermal stress due to cooling of the interconnection assembly from cure temperature to ambient (taken as 25°C) were undertaken for each case discussed in this chapter. Accurate representation of the components of the interconnection assembly is crucial for a successful analysis. The materials used in the analysis are well known in the micro electronics industry except the adhesives which are relatively new and are proprietary materials. Therefore material properties used in the models were gathered from a combination of literature search and experiments as discussed in chapter 5. The relevant material properties required for this type of analysis are:

1. Youngs modulus of elasticity:
2. Poisson's ratio
3. Glass transition temperature for the adhesives, and
4. Linear thermal coefficient of expansion.

The glass transition temperature is particularly important as most of the adhesives have markedly different thermal coefficient of expansion above T_g to that below T_g. The thermal coefficient of expansion (α) actually used in the analyses however, is the average over the temperature range for the analysis derived as follows:

$$\alpha = \frac{\alpha_0 (T_g - T_0) + \alpha_1 (T_1 - T_g)}{T_1 - T_0} \qquad \text{Eq. 6.1}$$

where

α_0 is the thermal coefficient below T_g

α_1 is the thermal coefficient of expansion above T_g

T_0 is the ambient temperature, and

T_1 is the final temperature

The modulus of elasticity used for silicon in the adhesive characterisation models were

those quoted in literature until experiments were conducted using silicon wafers from Wacker (the silicon wafer fabrication company), the material properties supplied with the silicon dies were then used for the sensitivity analysis in order to be consistent with experiments in chapter 7:

Elastic constants supplied by the manufacturers were used to investigate the sensitivity to silicon orientation.

The models as explained previously were developed using the SDRC IDEAS pre and post processor. The underling assumptions in all the models are as follows except otherwise stated:

1. All material properties were considered to be linear (i.e stress relief due to plastic deformation of any component of the adhesive was not taken into consideration).
2. The adhesive layer is homogeneous and void free.
3. The system is in thermal equilibrium (all components are at the same steady temperature) at the curing temperature.
4. The system is strain free at the curing temperature such that all the computed stress is a result of the cooling action.

The four major steps taken in the modelling are as follows:

6.4.1. Definition of the physical problem

The definition of the physical problem includes establishing the geometry and the loading (i.e the boundary conditions), selection of the type of analysis required and providing the relevant material properties. The geometry in this case is a square silicon die mounted on a square alumina substrate with the aid of a conductive adhesive. A standardised dimension for the assembly is shown in Table 6.1.

	Silicon Die	Conductive Adhesive	Alumina Substrate
Width (mm)	10	10	25.4
length (mm)	10	10	25.4
Thickness (μm)	640	50	500

Table 6.1: Standard dimension for the die attach assembly modelled

The loading on the structure is primarily thermal arising from changes between the curing temperature and the room temperature. There is a restraint on the structure imposed by gravity i.e the structure is not floating in space. There are no constraints on the edges of the structure as they are allowed to deform freely.

6.4.2. Creation of a Finite Element Model

Creation of a good model is crucial to the success of a finite element analysis. The model is created to represent the behaviour of the physical structure as accurately as possible. The efficiency of the analysis can be measured in terms of the trade-offs between the required degree of accuracy, computer time and disk space and time taken to create the model. The models presented here have been simplified by employing symmetry as appropriate thereby saving time and computer resources. Also the models are refined appropriately by creating more and smaller elements in key areas of interest such as those near geometric discontinuities or where high stress intensity is anticipated. This helps to increase the accuracy of the results.

The boundary conditions imposed on the model are such that all the structure was assumed to be at room temperature prior to the analysis and that the temperature of the finite element nodes was uniformly increased to the curing temperature. Out of plane displacements were also restrained on the planes of symmetry and the nodes at the origin were also restrained from vertical displacement.

6.4.3. Analysing the Model

The first set of analyses (characterisation of adhesives) were undertaken using the ANSYS finite element solver and the later analyses used ABAQUS. The resident algorithm in I-DEAS post processor was used to check for ill-conditioning (excessive element distortion, incorrect element connections, gaps or unconnected interfaces) in the model. The cost of analysis in terms of time and computer resources was minimized by optimizing the node numbering thereby minimizing the bandwidth of the equations to be solved. This is done by evoking an algorithm that makes the difference between the highest and lowest node numbers for each element as low as possible.

In all cases, linear structural analyses of the thermal stress induced by cooling the assembly from the cure temperature to ambient (25°C) was undertaken. The solutions were performed solely by the software without the need for any intervention from the analyst except to check for error messages in order to verify the credibility of the result and hence the model.

6.4.4. Interpretation of Results

The purpose of analysis is essentially to determine the engineering performance of the structure in question, under the service conditions (loads). The results of the analysis therefore have to be interpreted to be relevant to the appropriate use of the structure. The analysis in this case has been used to determine the mechanism and modes of failure in the die attach system by studying the stress distribution and stress level in the structure. The sensitivity analyses were performed to study the response of the stress levels to the various factors affecting stress distribution in the system. Nodes along the paths of high stress intensity (suggesting possible paths of failure) are selected and graphs of the appropriate stress component against the appropriate variable. Visualisation of the results was also enhanced using stress contour plots. The computed values are compared with experimental values in chapter 7.

6.5. Adhesive Characterisation

There are four major factors which may limit the use of conductive adhesives for electronics interconnection:-

a. High temperature performance

b. Residual stresses due to curing

c. Processability

d. Reworkability

It is virtually impossible to find an adhesive that addresses all the above issues satisfactorily. The most popular adhesives are silver filled epoxies because they possess good strength, good adhesion to a wide range of materials and can be processed easily. However, their performance at high temperature has been found to be limited (to about 150°C) and they are difficult to rework. Silver filled polyimides are known to offer a long time to failure in accelerated temperature-humidity tests [22], but being solvent based have inherent processing problems such as excessive void formation during cure. High curing temperatures (typically 275°C) are also required for these materials thereby resulting in high (thermal) residual stresses. Cured polyimide adhesives also have a high modulus of elasticity, which means that significant thermally induced stresses can be transmitted to the die and substrate and may lead to residual stress related failure. These materials are also difficult to rework. Silicone based adhesives offer the potential for good thermal stress management because of their compliance (glass transition temperature, T_g, of -55°C to -100°C) [84]. They do however have problems of molecular migration which may result in degradation of adhesion and may result in contamination of other parts of the assembly, e.g. wire bonding pads. They have therefore not found wide application within the industry.

These problems have led to the development of adhesives engineered towards specific applications. The three main types compared in this studies are: the low T_g epoxy (LTE) for thermal (stress) management; high T_g epoxy (HTE) for high temperature application and fully imidised polyimide (FIP) for ease of rework (these materials are thermoplastics), for thermal stress management (flexibility and low curing tempera-

ture) and thermal stability [85]. The drive for high quality and reliable electronic interconnection also calls for an understanding of the various parameters involved in the design and manufacture of such joints.

6.5.1. The Model

A linear structural analysis of the induced thermal stress due to cooling of the assembly from the cure temperature was undertaken for typical examples of adhesives mentioned above. The material properties used in the analysis have been gathered from a combination of manufacturers technical data and experiments and are as shown in Table 6.2.

The die attach assembly was modelled in 3-dimensions. A one eighth segment of the assembly was modelled as the assembly symmetrical across the middle and the diagonal planes as shown in Figure 6.2 The model consists of three major parts with dimensions as shown below:-

a. The die, silicon: 4mm x 4mm x 0.50mm

b. The adhesive layer of bond line thickness 50μm

c. The substrate: 99% Alumina: 8mm x 8mm x 0.64mm

		Conductive Adhesive			Silicon Die	Alumina Substrate
Property		FIP	HTE	LTE	Silicon	99% Alumina
T_g(°C)		230	230	-25	-	-
Youngs Modulus(MPa)		3000	4651	68.95	130000	380000
CTE (ppm/°C)	<Tg	55	45	-	3.061	6.800
	>Tg	216	170	110		
Poisson's Ratio		0.30	0.35	0.45	0.279	
Cure Temperature		275	300	150	-	-

Table 6.2: Materials property used for modelling

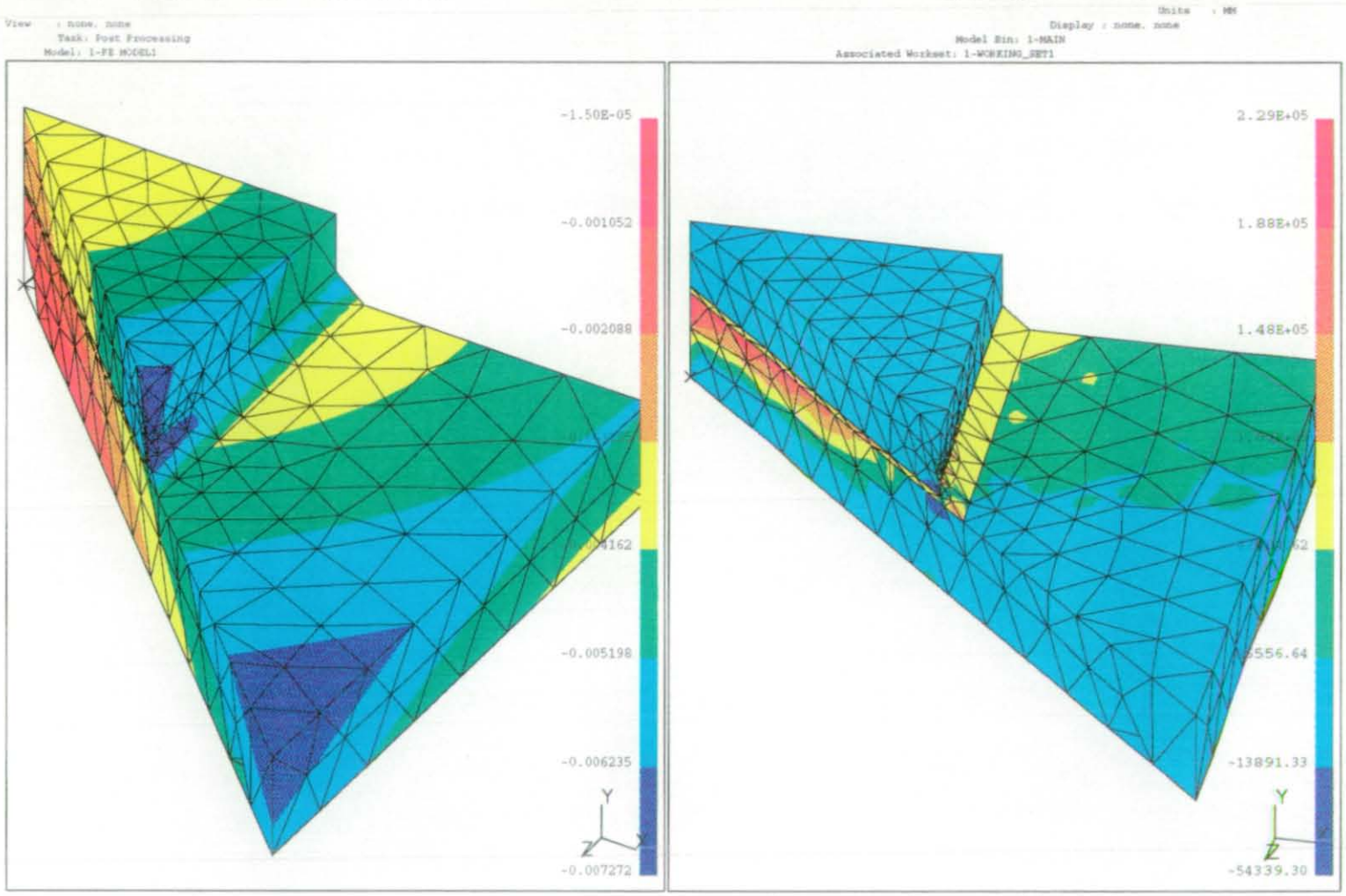

Figure 6.2: The predicted displacement and maximum principal stress distribution in the Low T_g epoxy

For accurate stress prediction, care was taken to use a high element density at regions of expected high stress. The amount of elements used was however limited by the academic license restriction on the size of the problem that can be handled by the ANSYS finite element solver.

6.5.2. Results

The outputs from the analysis are the displacements and stress distribution in the system. Three possible regions/mechanisms of failure are addressed in these analyses.

a. The die: by fast fracture, in which the magnitude and direction of stress at the die surface is vital.

b. The die-adhesive or substrate-adhesive interface: either by peeling or by shear failure in which the directions of stresses are also important.

c. The bulk of the adhesive through plastic deformation where the Von Mises stress in the material becomes critical.

A comparison of the stress distributions for all the adhesive types at the potential points of failure are illustrated in figures 6.3 to 6.4. The 'spikes' in the graphs indicates that the level of stress refinement could be improved upon, however, element quality checks and stress averaging across the elements indicates an acceptable level of mesh refinement. Subsequent models were more refined.

6.5.2.1. The Die

The stress distribution in the die, as predicted in the analysis is such that the top surface is under tension. A plot of the maximum principal stress on the surface as depicted in figure 6.3a reveals that, for all adhesive types, the maximum stress in the die occurred at a distance of approximately $w/4$ from the edge where w represents half the width of the die. The HTE imposed the highest level of stress on the surface of the die followed closely by the FIP and the thermosetting polyimide and epoxy respectively. There is however a large difference (about three 3 orders of magnitude) between the stress level observed for LTE and the other materials. A similar plot of the principal stress along the vertical edge of the die, figure 6.3b, shows that the maximum stress occurred at

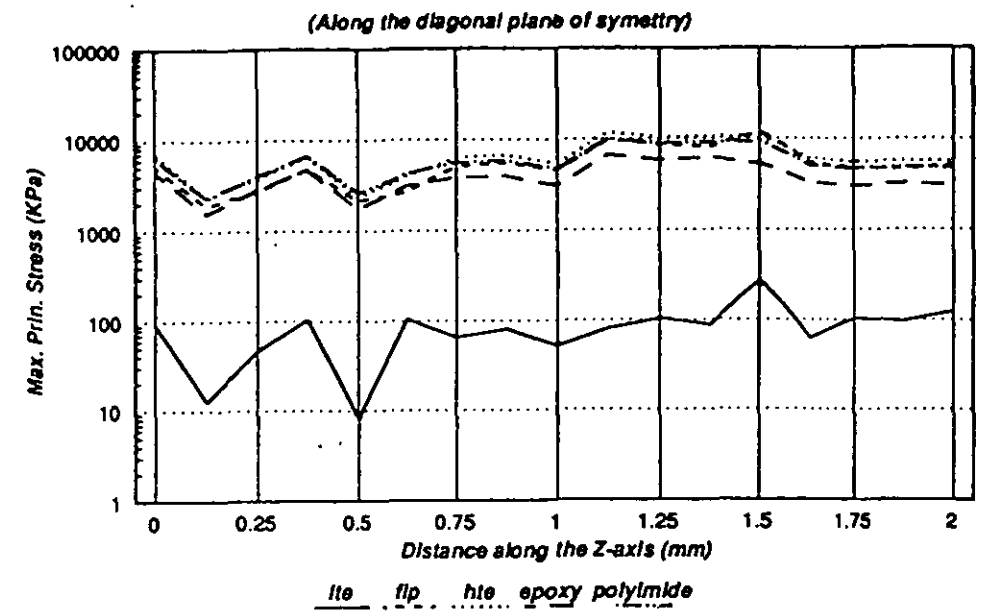

a

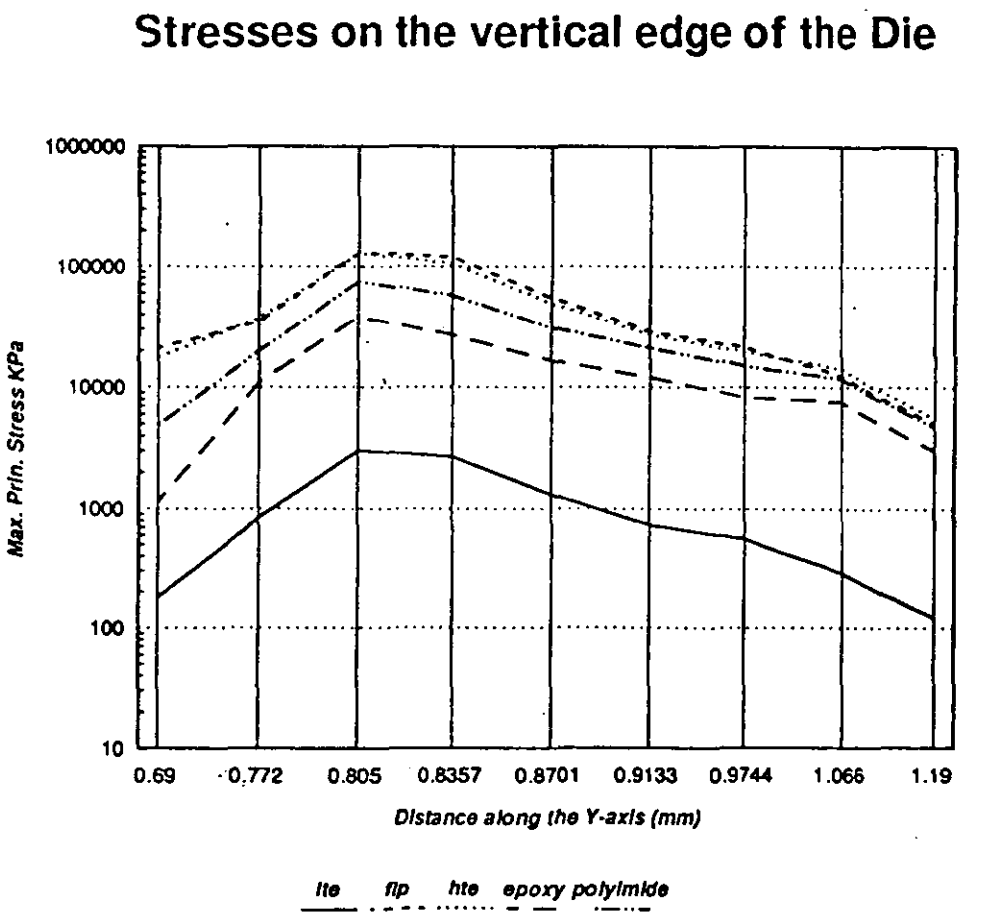

b

Figure 6.3 a&b: Stress distribution on the surface of the die

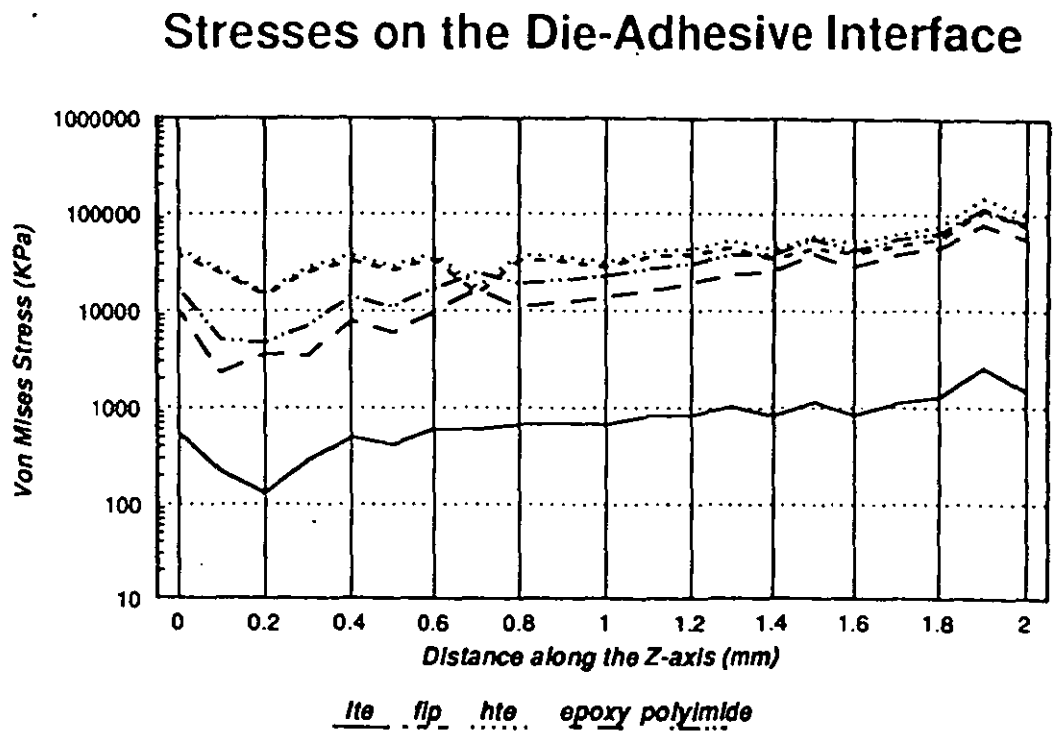

a

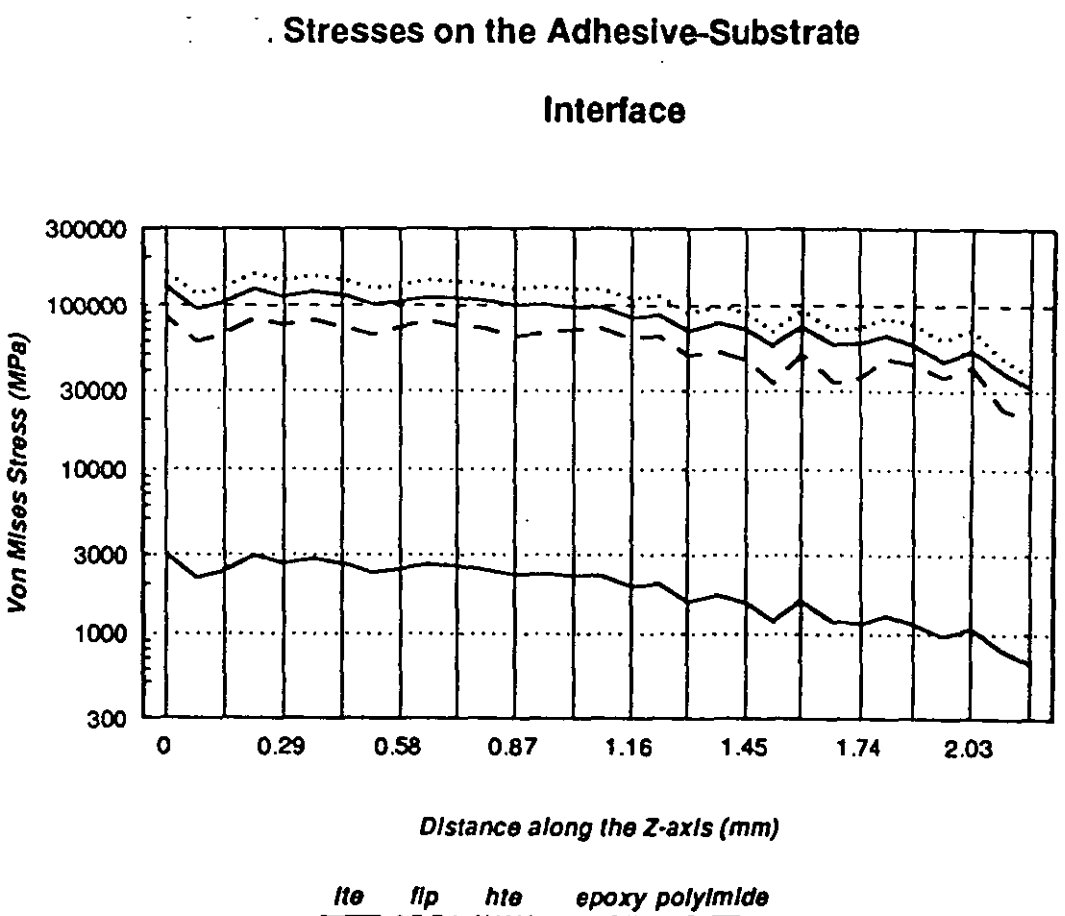

b

Figure 6.4 a&b: Stress distribution on the die-adhesive-substrate interfaces

about $h/4$ from the base of the die where h is the height (thickness) of the die.

6.5.2.2. The Die-Adhesive-Substrate interfaces.

The relative stresses between different adhesive materials predicted at the die-adhesive interface show a similar pattern to the stress predicted in the die. A plot of the Von Mises stress in the interface (figure 6.4a) reveals that the highest level of stress was observed with the HTE while the others followed in the same order as the die. The level of stress was observed to rise gradually from the centre towards the edge of the die with the highest level of stress occurring just before the edge. The level of stress at the adhesive substrate interface (Figure 6.4b) is approximately ten times that at the die-adhesive interface and the stresses are higher towards the centre of the die.

The overall pattern in the results indicates that the higher the processing temperature, the higher the residual stress. However, the residual stress was not found to be directly proportional to the process temperature since the adhesive mechanical properties also influence these stresses. Adhesives with high T_g exhibited the higher stress level those with lower T_g.

6.5.3. Discussion.

The bulk ultimate tensile strength of a material compared with the amount of stress applied to a specimen of that material does not give a unique criterion on which to evaluate the probability of failure. The specimen preparation plays a very important part in the observed strength because of the potential generation of surface flaws, especially in a brittle material like silicon. Potential causes of surface flaws in silicon dies includes processes such as grinding, preferential etching, sawing, device processing and handling. Fracture will occur in a brittle material when the uniform tensile stress perpendicular to a flaw, with size 2a, reaches a critical value [3], σ_c, given by

$$\sigma_c = m.k_{ic}.[pa]^{-1/2} \qquad \text{Eq. 6.2}$$

where m is a geometry factor (1.20 for a surface flaw with a semi-elliptical shape) and k_{ic} is the fracture toughness of the material (k_{ic}~25.9N/mm$^{3/2}$ for silicon). The large difference in the magnitude of stress induced in the die by the LTE compared to the others indicate that the LTE adhesives can accommodate dramatically larger flaws in the die without necessarily leading to die failure.

The mechanical state of the polymer depends largely on the closeness of its temperature to the glass transition temperature (T_g). Polymers are relatively stiff when operating below their T_g but the modulus of elasticity drops steeply above T_g. The analysis undertaken has assumed linear material behaviour and has included material properties only at the two extremes of temperature, the results therefore does not present a complete picture of the state of the system over the entire temperature range as the viscoelastic properties [86] of the adhesive were not taken into consideration. The HTE adhesive is known to be more compliant than the polyimide based adhesive. Results of Dynamic Mechanical Thermal Analysis in chapter 5 imply that the high T_g epoxy will probably still be strain free at a lower temperature than the processing temperature. The predicted stress could therefore be slightly exaggerated. While the thermal coefficient of expansion has been averaged over the temperature range, there is a very drastic change in thermal coefficient of expansion above the T_g.

The two most likely ways in which adhesives may fail in operation are by plastic deformation and initiation and propagation of flaws [87]. Sources of naturally occurring flaws in the adhesive may be voids, cracks, dirt particles, additive particles, and inhomogenuities in the adhesive for example [87]. Most of these flaws can be prevented by good manufacturing practices. Interfacial debonding is also possible but rarely happens unless the presence of dirt, grease or other materials that can prevent proper adhesion. Moisture can also initiate debonding.

The performance of these adhesives or their suitability for a particular process cannot be solely based on the level of residual stresses. The ease of processing must also be considered. The high T_g epoxy, while retaining the good adhesion and ease of process-

ing associated with epoxy adhesives has also good performance at higher than normal temperatures for epoxy based adhesives making it suitable for high temperature application. The fully imidised polyimide, while retaining good strength at high temperature, combines the ease of rework with flexibility and low residual stresses. The low T_g epoxy seems ideal for thermal stress management showing a low level of stresses, it is however very rubbery (Poisson's ratio= 0.45), and its appropriateness for particular applications needs further investigation.

6.6. Model Sensitivity

The accuracy of a finite element analysis, like all other computational methods, depends entirely on the input from the analyst. Input parameters need to be specified to reflect as closely as possible the real system behaviour. The intricate nature and increasing sophistication of electronic interconnections are making such structures more difficult to model accurately. The use of finite element analysis in a research environment where the impact of a large number of parameters must be investigated necessitates the creation of multiple models and analyses. This results in large computer memory and disk space requirements and is very labour intensive. While the accuracy of the results is vital, overall analysis efficiency must be traded off against the computational resource required and the speed of analysis iterations. Similarly, as can be seen from the preceding section, the previous set of analyses exhausted the solver capabilities (academic license limit) leading to a compromise in the accuracy of results. There is therefore, a need to develop approximate methods that can adequately represent the real system whilst minimising computer processing time and memory requirements and the overall cost of the analysis.

Similarly, the adhesive is a very important component of the assembly however, it is a very thin layer compared to the thickness of the other components. The modelling of such a thin layer can introduce problems of scale in finite element mesh refinement. In order to optimize the final model the adhesive layer has been modelled using a single layer of elements. As the major and most crucial component of the entire assembly is the silicon die. There is a need to investigate the compromise in accuracy of results

(for the silicon die) by using this method.

This section presents a comparison of three modelling approaches for the analysis of thermally induced stress in a die attach system. The three types of models considered were 3-dimensional (3D), axisymmetric and 2-dimensional (2D) models. Similarly the adhesive layer was modelled using 1-6 layers of finite elements and the results compared.

6.6.1. The Die Attach Models

Three models of the die-attach system were analysed using the SDRC I-DEAS finite element modelling system and ABAQUS finite element solver. The adhesive considered was the high T_g epoxy engineered for high temperature applications. The dimensions and material properties are as shown previously. A linear analysis of the thermally induced stress created by cooling the system from the curing temperature (275°C) to ambient (taken as 25°C) was performed.

Figure 6.5 shows the plan view of the 3D geometry of the die attach assembly with the axisymmetric and 2-dimensional approximations highlighted using dashed lines.

6.6.2. The 3-Dimensional Model

The problem was modelled using 3D geometry taking planes of symmetry along the diagonal (z'y-plane) and mid-plane (xy-plane) of the assembly. This reduces the model size by a factor of 8. A total of 3038 10-node tetrahedral triangular solid elements were employed. Attention was paid to generating an effective distribution of elements to ensure good element density for a good degree of accuracy.

6.6.3. The Axisymmetric Model

A 2-dimensional axisymmetric model of the problem was also built. The origin of the axes was taken to be the centre of the structure, with the vertical (y) axis as the axial direction and the horizontal (x) axis as the radial direction. A total of 860, 6-node par-

abolic axisymmetric solid elements were used, ensuring adequate mesh density. As this model is 2-dimensional an approximation has to be made to allow the prediction of the stresses along the diagonal of the real assembly. This was achieved by choosing the length of the model to be the same as the length along the diagonal of the real assembly.

6.6.4. The 2-Dimensional Model

A 2D model of the same problem was built using 6-node plane stress parabolic triangular elements. The structure was modelled in the xy plane with a plane of symmetry at the centre of the structure. A total of 926 elements were used.

There are two possibilities for modelling the two dimensional stress system. The out of plane thickness stress, s_{zz}, is assumed to be zero or the through thickness strain, e_{zz}, is assumed to be zero. The first case is the plane stress situation. While this assumes the out of plane stress to be zero, the thickness of the model and hence the effect of the strain out of plane is not totally ignored in the calculation of the stiffness matrix of the model. Hence the variation in thickness of the various components of the model influences the stiffness. The latter case, the plain strain situation, is appropriate when the model is of a large and uniform thickness and hence the out of plane component of strain can be safely ignored. In view of the varying layer thicknesses in the structure being modelled the plane stress case was considered most appropriate.

6.6.5. Results

The output from the models are stresses and displacements. The results were therefore compared by examining the stress distributions and the displacements in the system. The maximum principal stress distribution the vertical component of displacement in the 3D model are similar to that in figure 6.2.

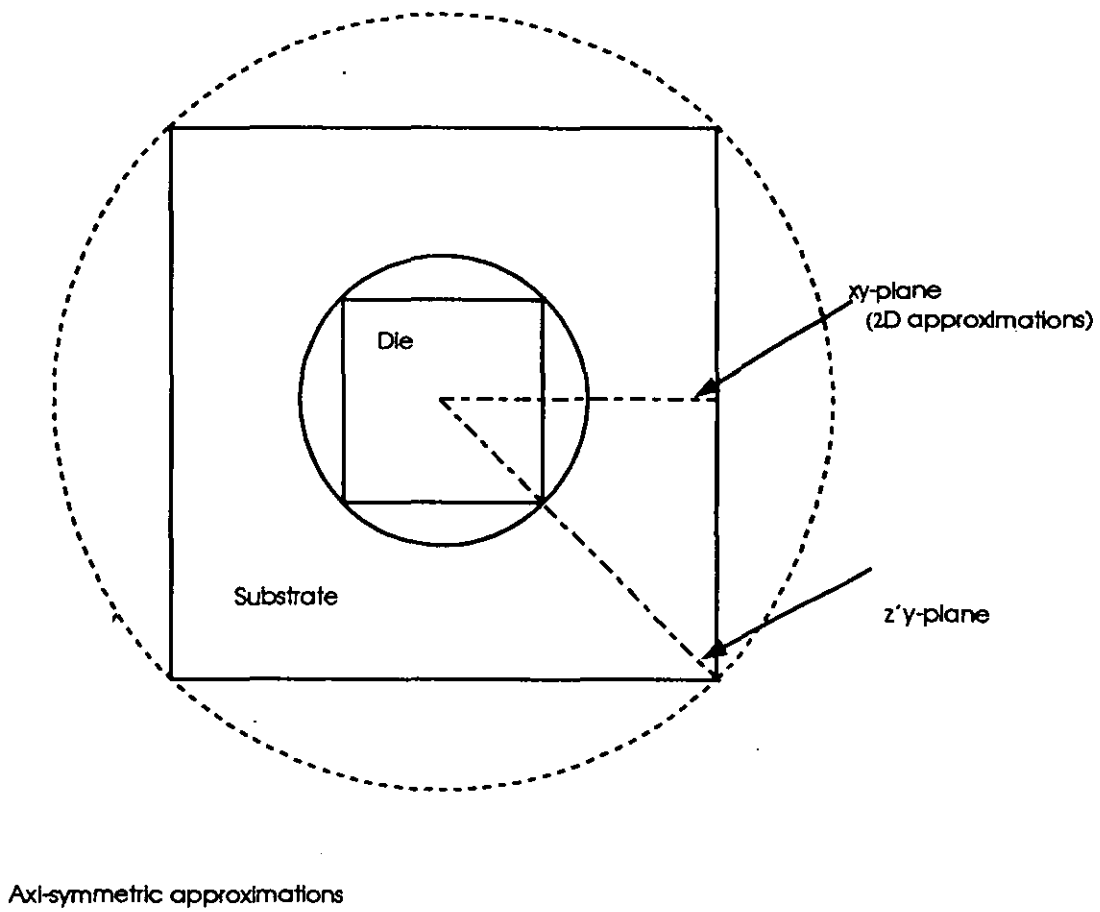

Figure 6.5: Plan view of the model of the die attach assembly

6.6.5.1. Displacements

The primary result of an FEA is normally the nodal displacements of the structure from which the stresses are then calculated [8]. Accurate prediction of displacements is usually readily achieved and reasonable displacements may be predicted even with a coarse mesh. Figure 6.6 shows the vertical component of displacements in the die. There is a clear correlation in the displacements predicted by the 2D model and the xy-plane of the 3D model on one hand and between the axisymmetric and the z'y-plane of the 3D model on the other. This therefore implies that, since the largest displacements occur along the diagonal of the die, the axisymmetric model is better than the 2D model at predicting the worst case displacement in the die.

6.6.5.3. Stresses

The stress distributions in the models are as shown in figures 6.7 and 6.8. Figure 6.7 shows the maximum principal stress component of the stress distribution on the top of the die. As expected, the worst case once again occurred along the diagonals of the die as shown by the z'y-plane of the 3D model. There is a large difference in the stress predicted by the 2D models when compared with the axisymmetric and the 3D models. Where maximum stress is the criterion for evaluation of possible failure modes, the axisymmetric model predicts a closer value to that expected on the xy plane of the structure. The correlation in the position of the maximum stress between the axisymmetric and the z'y plane of the 3D model is as a result of the length of the diagonals assumed in the axisymmetric model. The stress level in the axisymmetric model is however closer to that predicted along the mid-plane of the 3D model. The average stress predicted by the 2D model on the other hand is higher than the 3D model suggests. A plot of the stress on the edge of the die as shown in figure 6.8 reveals that the axisymmetric models give a closer and a more similar distribution to the true case along the diagonal of the die while the 2D model, although having a similarly shaped stress distribution, predicts a stress level that is neither close to the value on the xy nor the z'y planes.

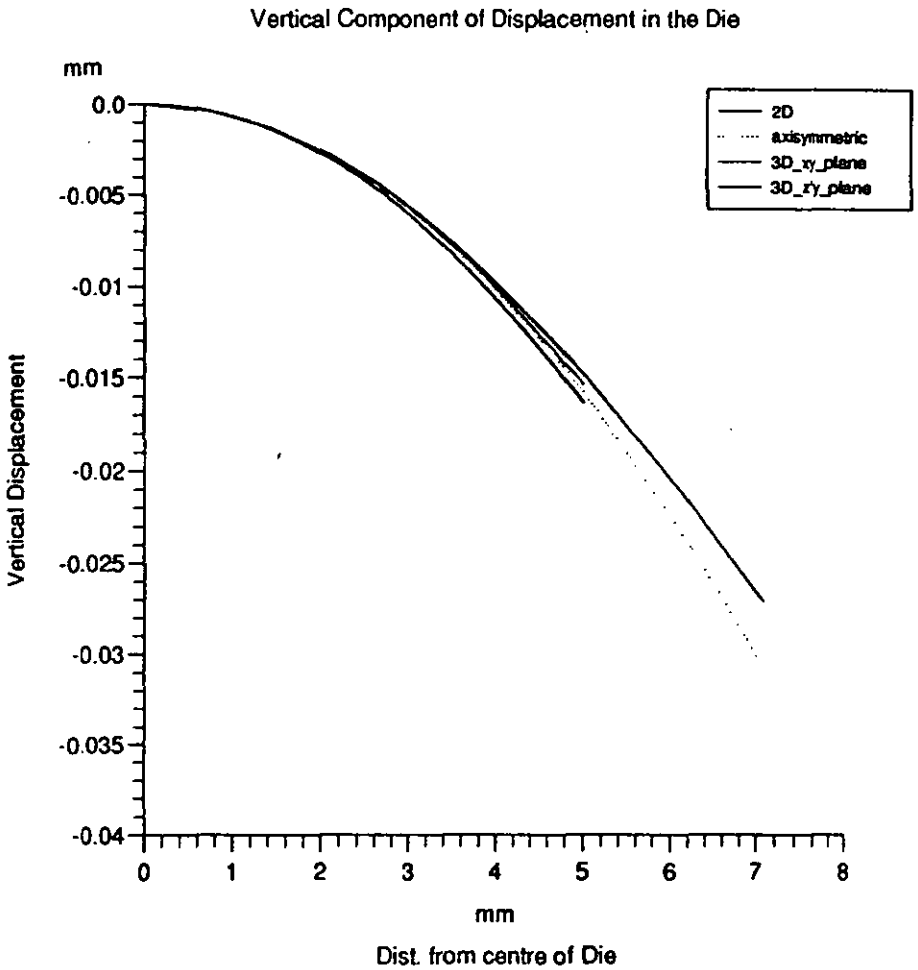

Figure 6.6: Comparison of predicted displacement

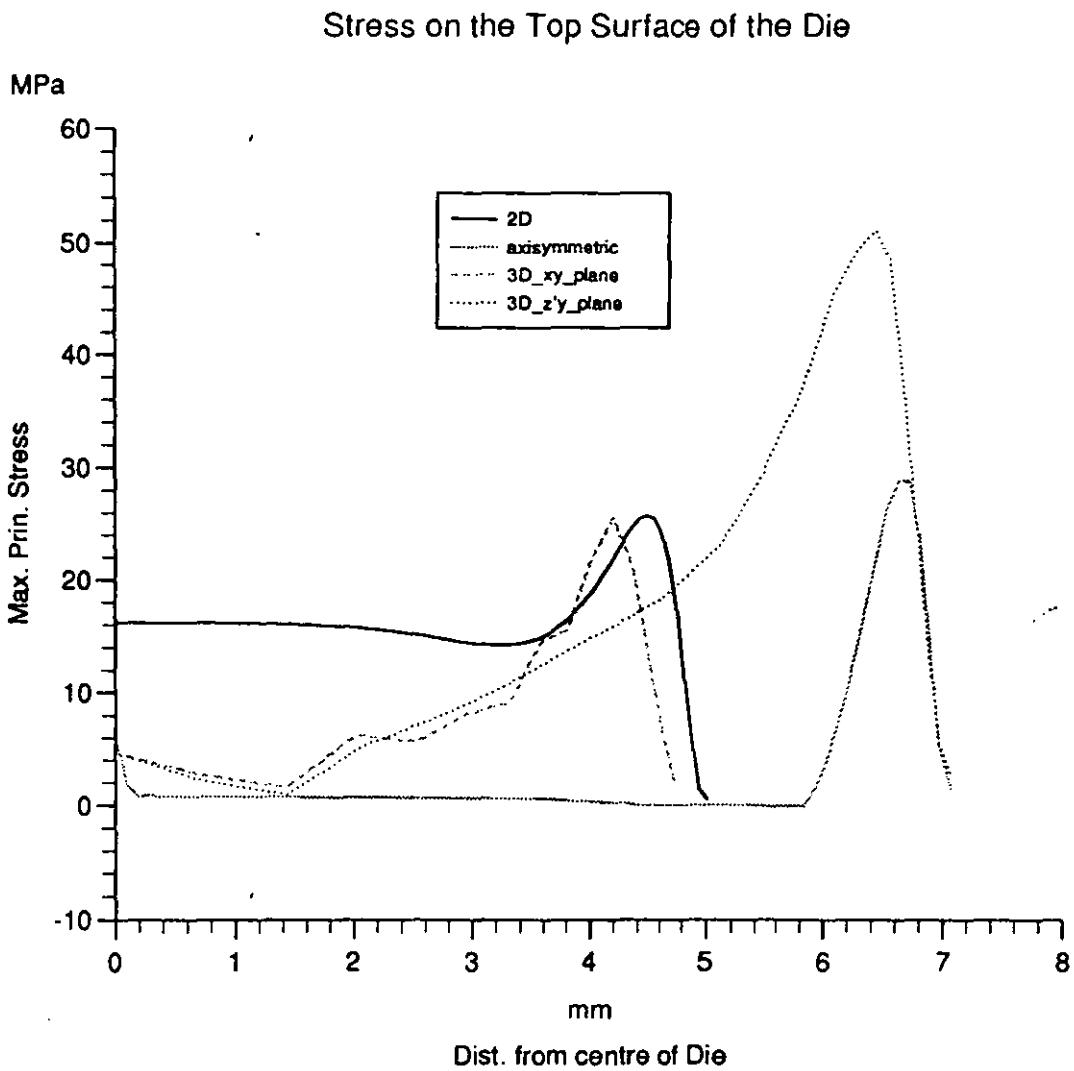

Figure 6.7: Comparison of the predicted stress on the top surface of the die

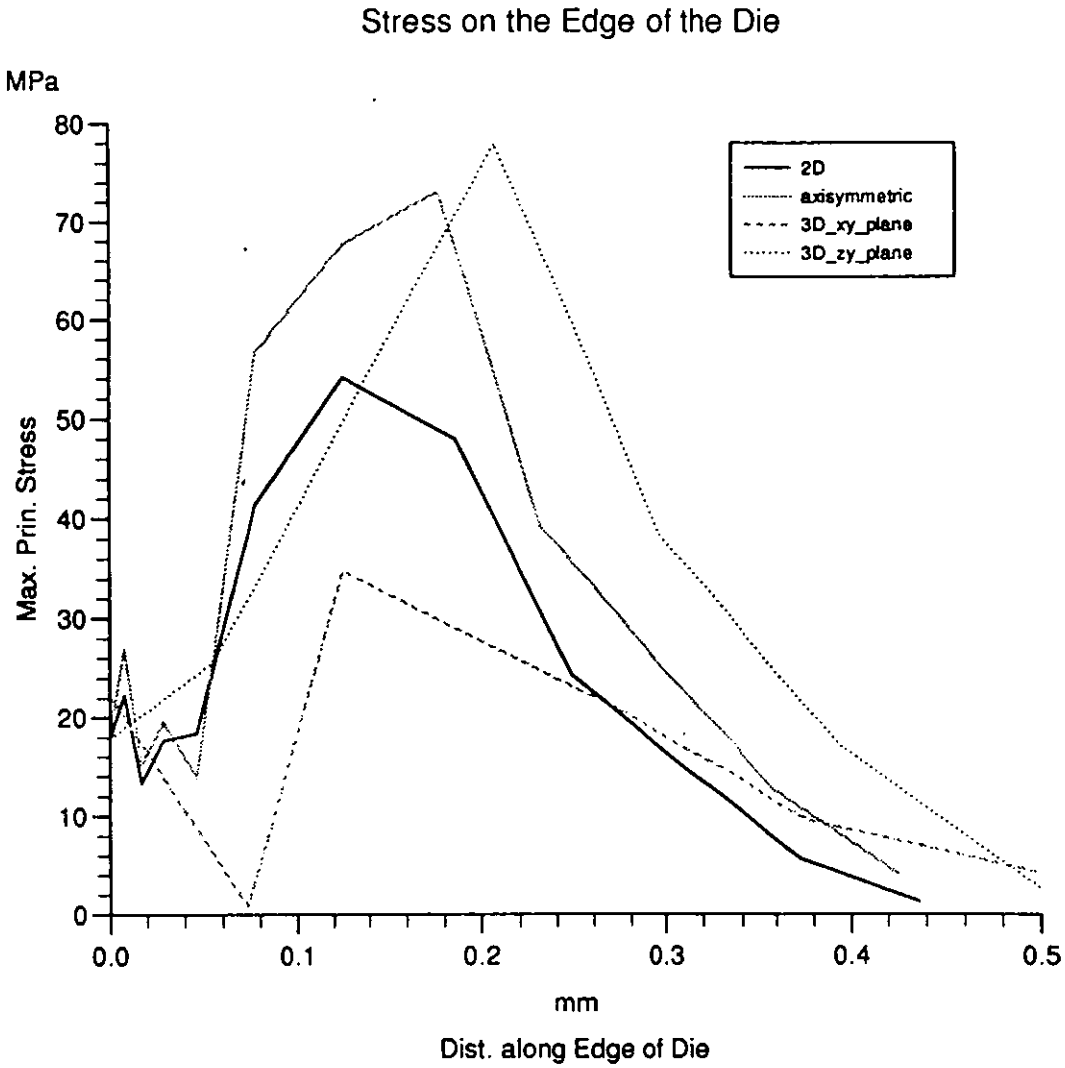

Figure 6.8: Comparison of the predicted stress on the vertical edge of the die

The stresses on the interface, figures 6.9 and 6.10 show a better correlation between the axisymmetric and the 3D models except for the stress level at the edges. The worst case, as expected, occurs along the diagonal of the die.

6.6.6. Discussion

There are four significant regions of interest in the die-attach assembly modelled.

a. The surface of the die; to predict whether stresses are high enough to cause cracking.

b. The edge of the die; to investigate the possibility of cracking.

c. The two interfaces of the adhesive; to check for the possibility of failure by peeling.

d. In the bulk of the adhesive to check for the likelihood of plastic yielding of the resin.

Whilst a 3D model will give the most accurate results, considerable savings can be made by using the two approximate models. Figure 6.11 shows a comparison of the computer time taken for the three models on a SUN SPARC 1+ workstation. The total time is a summation of the system and analysis time. The system time is the time used in file handling and associated processes while the analysis time is the actual time taken to analyse the model. It is apparent that a substantial amount of computer resource is required for the analysis of the 3D model. Furthermore, a considerable amount of engineering time (not included in the figure!) was spent in preparing the mesh for the 3D model, in contrast to both the axisymmetric and the 2D models which took very little time to build and mesh. In a research environment, in which sensitivity and similar studies are conducted on a regular basis, computer memory and disk space requirements and speed of analysis are limiting factors.

In all instances the axisymmetric model predicted closer values to the 3D model when compared to the 2D model. The major discrepancy between the 3D and axisymmetric models occurred in the stress level predicted on the surface of the die. This is due to

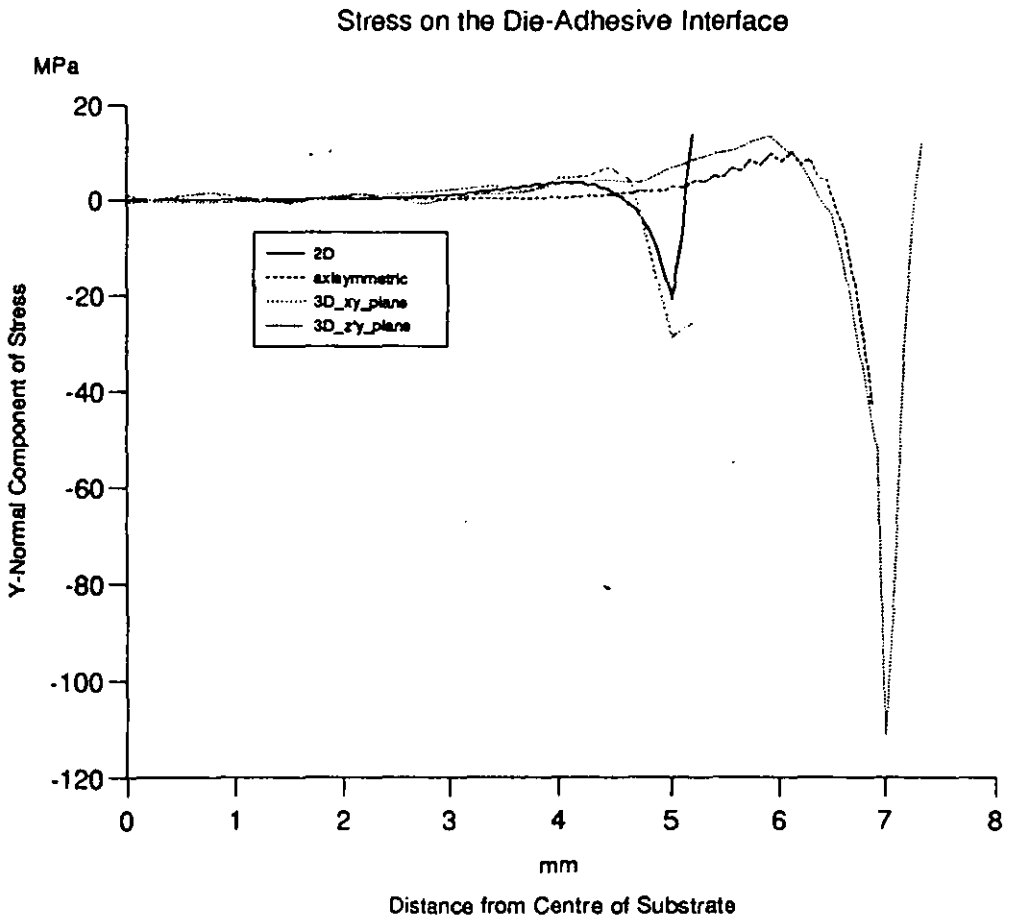

Figure 6.9: Comparison of the predicted stress on the die-adhesive interface

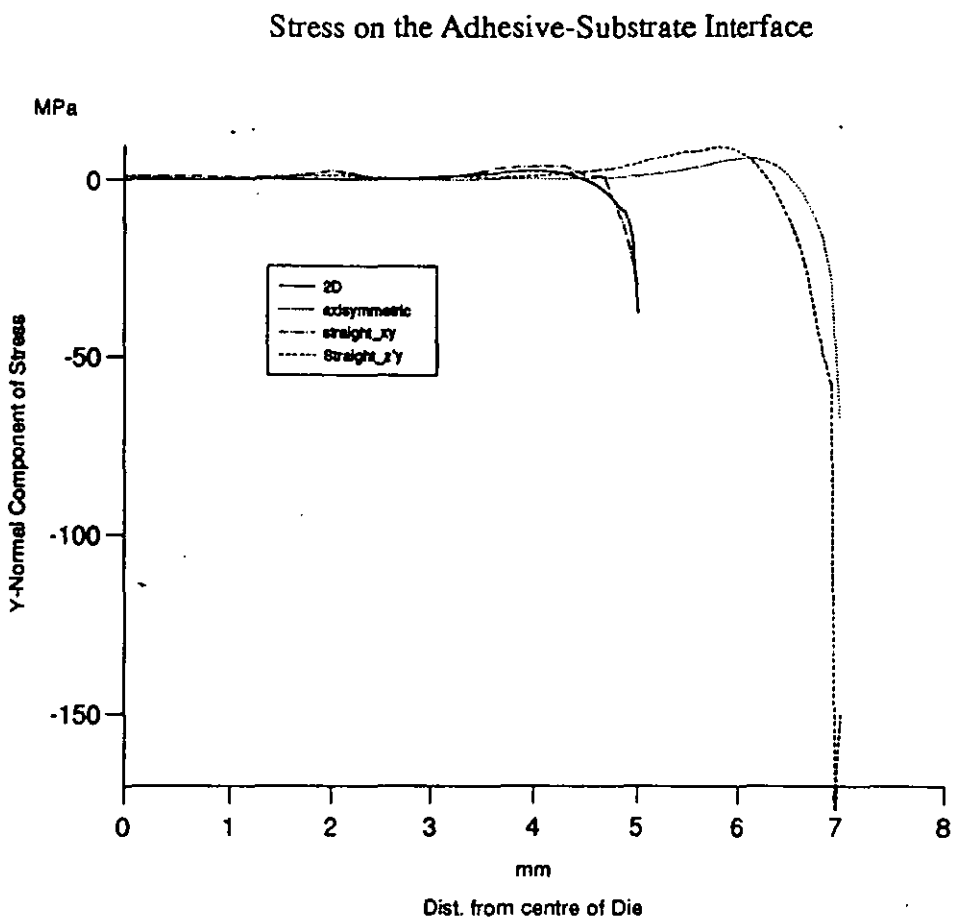

Figure 6.10: Comparison of the adhesive-substrate interface

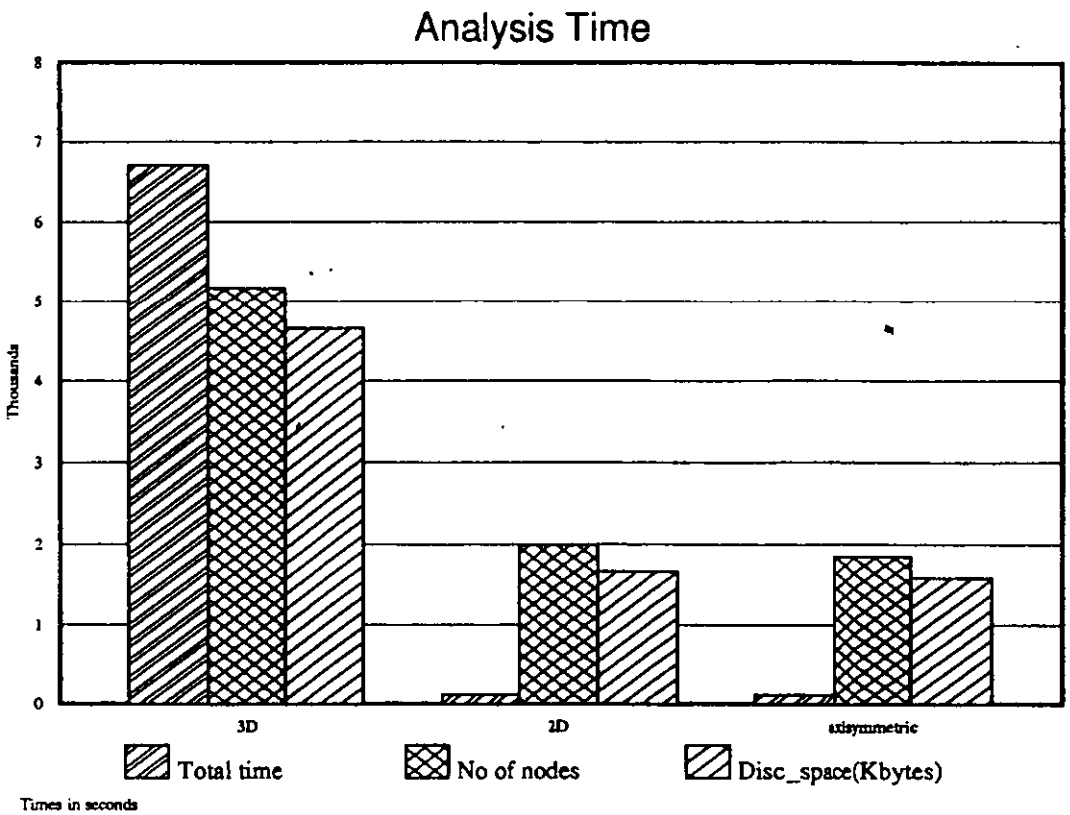

Figure 6.11: Comparison of the time taken for analyses

A. 3-D Geometry

1. True representation of geometry
2. Very expensive to analyse
i.e Large time, computer resources requirement

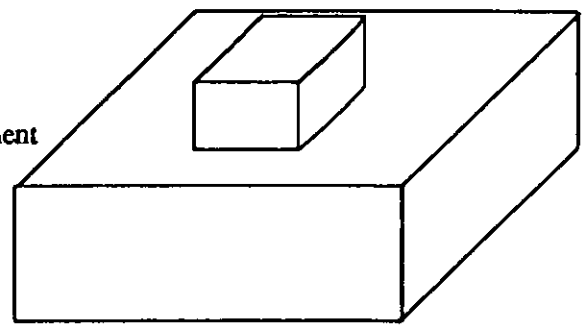

B. Axisymmetric Geometry

1.Axisymmetric representation of structure
2. Easy to construct and to mesh model
3. Ignores the effect of corners
4. Cheap to analyse

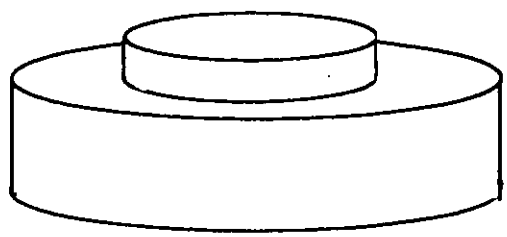

C. 2-D Geometry

1. Planar representaion of structure
2. Easy to construct and to mesh model
3. Incomplete picture of structure
4. Cheap to analyse

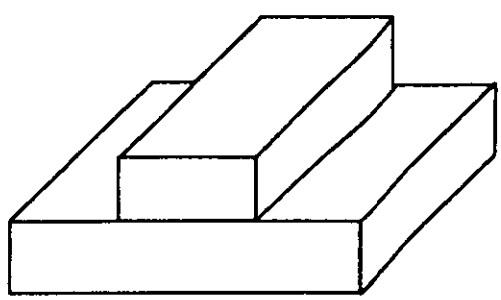

Figure 6.12: Comparison of models geometry

the fact that the axisymmetric model does not take into account the stress raising effect of the corners of the rectangular die. The displacement plots of the 3D model suggest a largely axisymmetric pattern of displacement. The subsequent results also justify the use of axisymmetric geometry for modelling surface mount components by Hall [88]. It should, however, be borne in mind that the peak stress along the diagonal of the square could be as high as 1.85 times that predicted by the axisymmetric model (which is the same level of stress predicted for the mid-plane). Similarly the position of occurrence of the peak stress is geometry dependent and will therefore depend on the length of the model. Figure 6.12 shows a comparison of the structures that the different models actually represent.

6.7. Material Sensitivity

Of great interest to the manufacturers of conductive adhesives is the need for a better understanding of the effect of the mechanical properties of the conductive adhesives on the interconnection. Certain properties like the modulus of elasticity determine the rigidity of the interconnection while the thermal coefficient of expansion gives an indication of thermal mismatch between components and hence residual stresses due to thermal processing operations.

Most of the mechanical and electronic properties of silicon are orientation dependent and therefore many of the fabrication processes are orientation sensitive, as are the different applications of silicon. For instance, the {111} plane exhibits the smallest separation [89], therefore the growth of silicon crystal is most easily accomplished along this plane, which means the <111> silicon is the least expensive and is used mainly in bipolar devices and microcircuits. Similarly, dicing silicon wafer into its individual microcircuits is done by scribing its surface with a diamond tool or by sawing into a rectangular pattern. The weakened slice is then deformed until it breaks apart into individual circuits.[1] The ultimate tensile strength of silicon is a maximum in the <111>

1. The effect of this method on the geometry of the silicon die produced is discussed in the process sensitivity section.

directions (350MPa)[89], and the modulus of elasticity is higher in this direction than the <110> or the <100> directions(190, 170, and 130GPa), therefore silicon tends to cleave on the {111} plane.

As a result of the afore-mentioned it becomes imperative to investigate the sensitivity of the interconnection system to the material properties above therefore, sensitivity analyses were carried out for the thermal coefficient of expansion and the modulus of elasticity of the adhesive. The effect of silicon orientation was also investigated.

6.7.1. Materials properties of the adhesives

The typical range of thermal coefficient of expansion for the adhesives currently in the market is 10 - 70 (10^{-6}/°C) [Market survey conducted by the author for ACME project on the use of Loaded adhesives for electronic interconnection in October 1991], similarly the modulus of elasticity ranges from 1 to 7 GPa. Therefore analyses were conducted between these ranges.

As can be seen from the results of the analysis in section 6.4. the axisymmetric models offers a good approximation to the 3-D model therefore axisymmetric models as described in section 6.4. were used for these analyses. Analyses were conducted for each of the material properties by varying the relevant material property of the adhesive between the specified range.

6.7.2. Effects of the orientation of silicon

There are three major planes of orientation of silicon. The {100},{110} and the {111} planes. The difference in their mechanical properties is highlighted by the different modulus of elasticity exhibited in the different directions; 190, 170 and 130 GPa in the <111>, <110> and <100> directions respectively. Therefore the approach to modelling the effect of the orientation of silicon is to define the elements of the silicon in an appropriate orientation while maintaining the orientation of the other parts of the model.

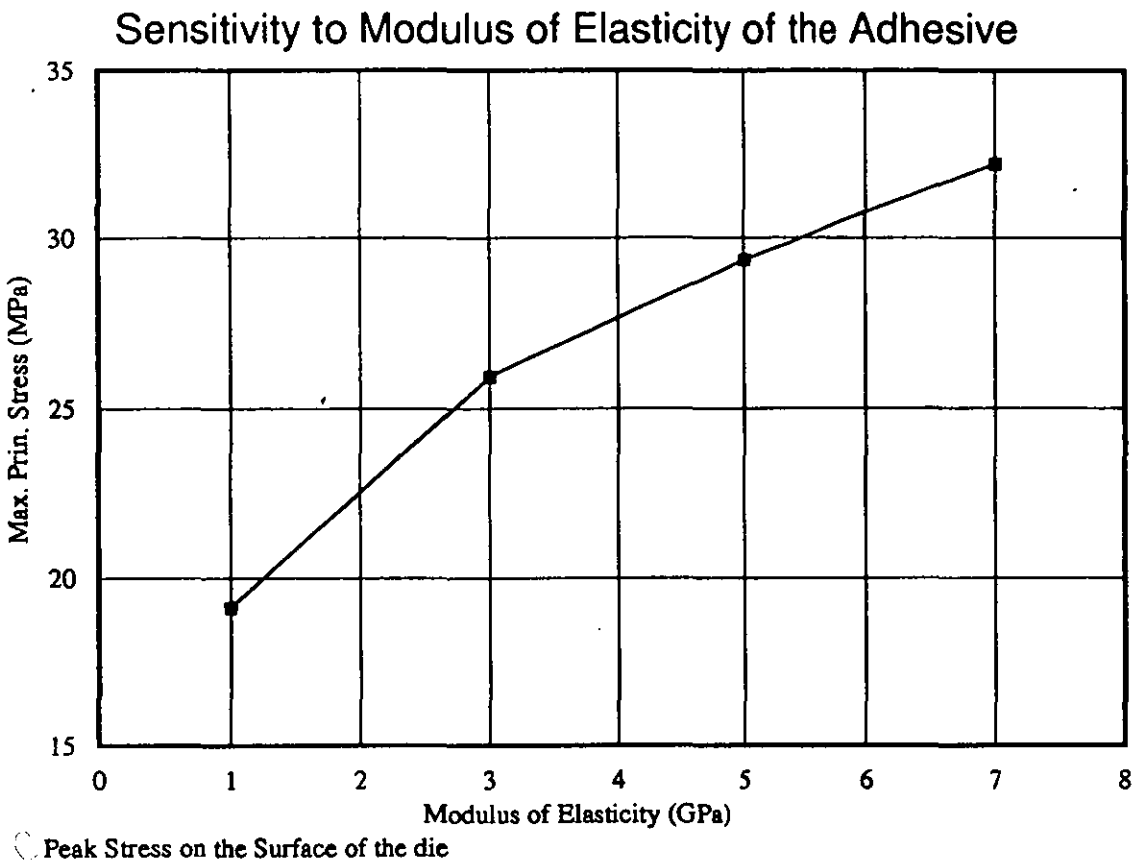

Figure 6.13: Sensitivity to modulus of elasticity of the adhesive

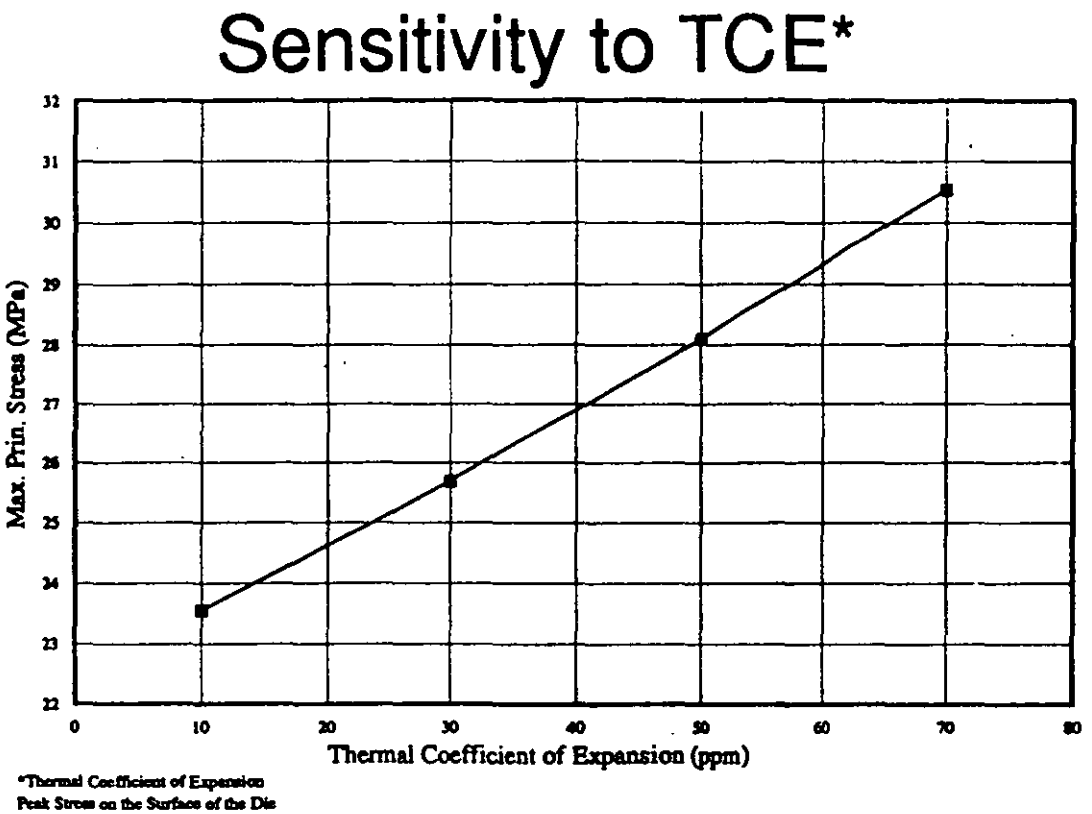

Figure 6.14: Sensitivity to the thermal coefficient of expansion

6.7.2.1. The models

Three models were used for these analyses, each a 3-D model (as described in section 6.4.) for the desired plane. The silicon die were given the desired orientation by creating coordinate systems normal to the desired plane and aligning the elements of the silicon die to this. The elastic constants [30] as shown below (Table 6.3) were used in order to reflect the anisotropic properties of silicon. The models were developed in I-DEAS finite element pre and post processor and solved using the ABAQUS finite element solver.

	E(GPa)	$\alpha(10^{-6}/°C$	υ
Silicon	C11=165.64 C12=63.94 C44=79.51	3.06	-
Epoxy	4.65	55.9**	0.35
Alumina	380	6.80	0.34

Table 6.3: Materials property showing elastic constants for silicon

E-Young's Modulus of Elasticity

α- Thermal Coefficient of Expansion

υ-Poisson's Ratio

**Average over the temperature range considered

6.7.3 Results

As stated previously, the silicon die is considered to be most costly element of the assembly and previous analyses have shown that the most likely failure is the cracking of the die either on the surface or the edge of the silicon, The results of the sensitivity analyses are therefore presented for the surface of the die. Figure 6.14 shows that the peak maximum principal stress on the surface of the die increases linearly with increasing thermal coefficient of expansion. Similarly, the graph of the variation of the

peak maximum principal stress on the surface of the die (figure 6.13) showed a steep increase in stress up to 3 GPa after which the increase becomes less steep. Both graphs suggests that the lower the values of these material properties the lower the residual stress in the die.

The effect of the orientation of silicon is shown in Figures 6.15 to 6.18. The effect of the orientation is more visible at the die-adhesive interface, however these stresses are low and compressive and do not offer any threat of failure to the assembly. The graphs of stresses on the vertical edge and the surface of the silicon die shows that the <110>, orientation exhibits higher stress followed closely by <100> while <111> is the more conservative of the three. This therefore suggests that the silicon die with <110> orientation will be prone to failure.

6.8. Process Sensitivity

There are two relevant stages in preparation of the die attach assembly that are crucial to the subsequent reliability and quality of the manufactured joints; preparation of the silicon die and the printing of the conductive adhesive.

As discussed earlier, the most frequently used technique for dicing a silicon wafer into individual silicon die is by sawing. It is either partially sawn and the weakened wafer cleaved into its individual chips or completely sawn through. This method of silicon die preparation introduces a peculiar geometry to the die which can influence the stress distribution. For a silicon wafer with a <100> orientation (as in the die of interest), it is expected that the cleavage after scribing or part-sawing perpendicular to the flat surface will reveal the {111} plane. Hence the side of the cleaved walls will be at 56.4° [89] to the flat surface. Three types of geometry were observed for silicon dies: straight edge (Fig.6.19a), undercut edge (Figure 6.19b), and bevelled edge (Figure 6.19c). The bevelled and undercut edges resulted from the partly sawn then cleaved method of preparation while the straight edges resulted from a sawn through wafer. The general belief of the bigger the die, the greater the stress, supporting the argument that conductive adhesives may be inappropriate for large area die attach, was also investigated.

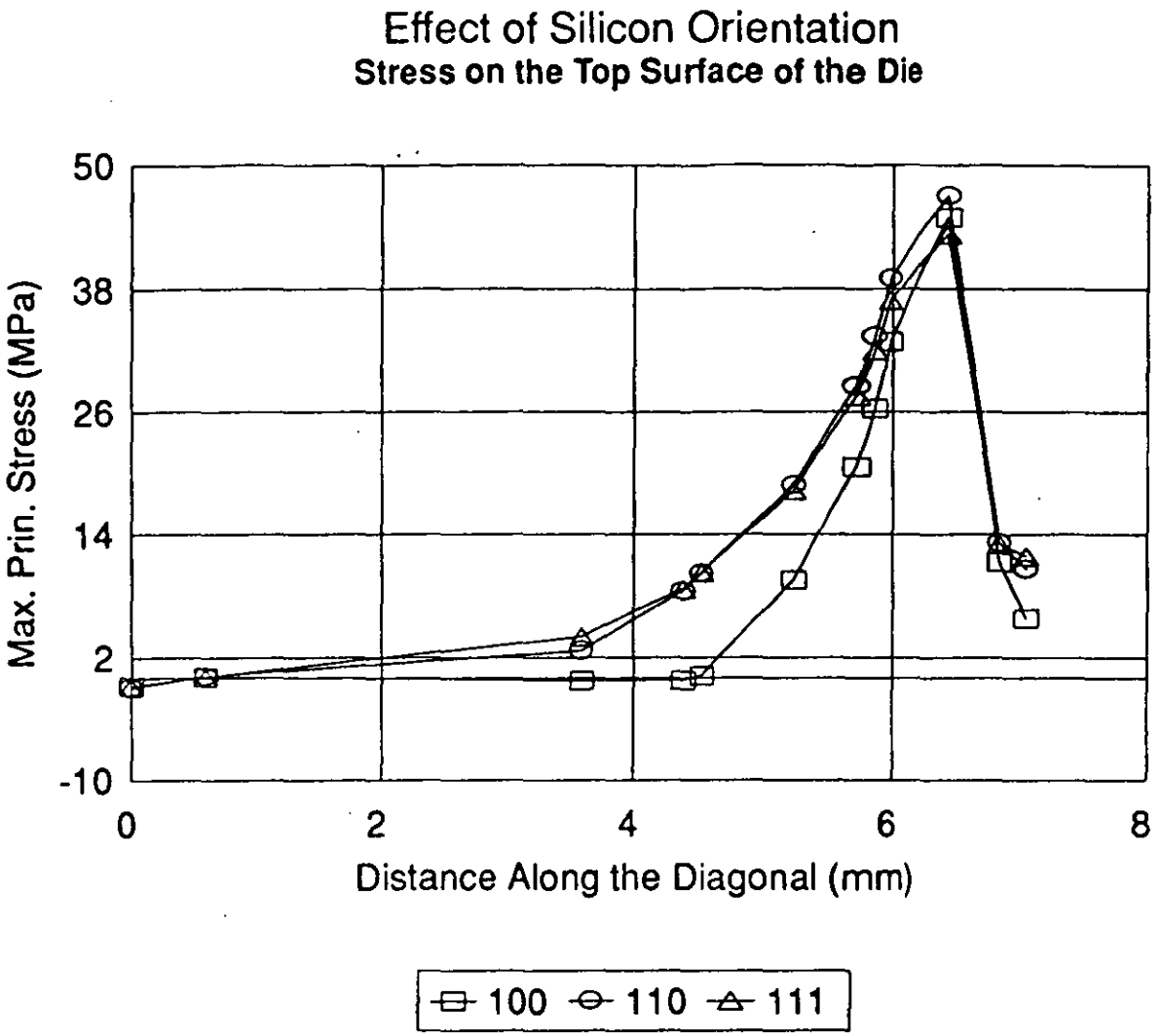

Figure 6.15: Effect of the orientation of the silicon die

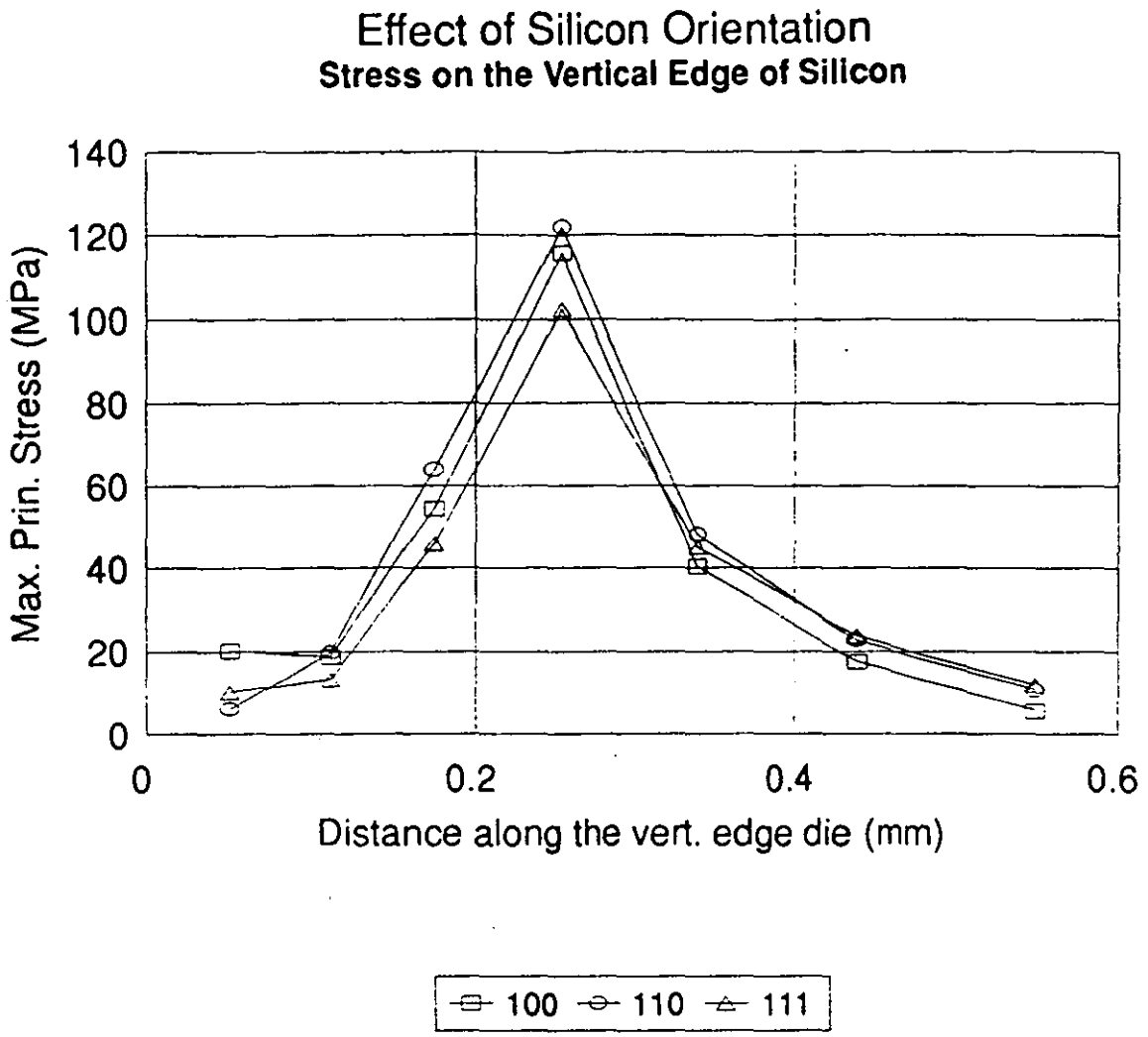

Figure 6. 16: Effect of the orientation of the silicon die

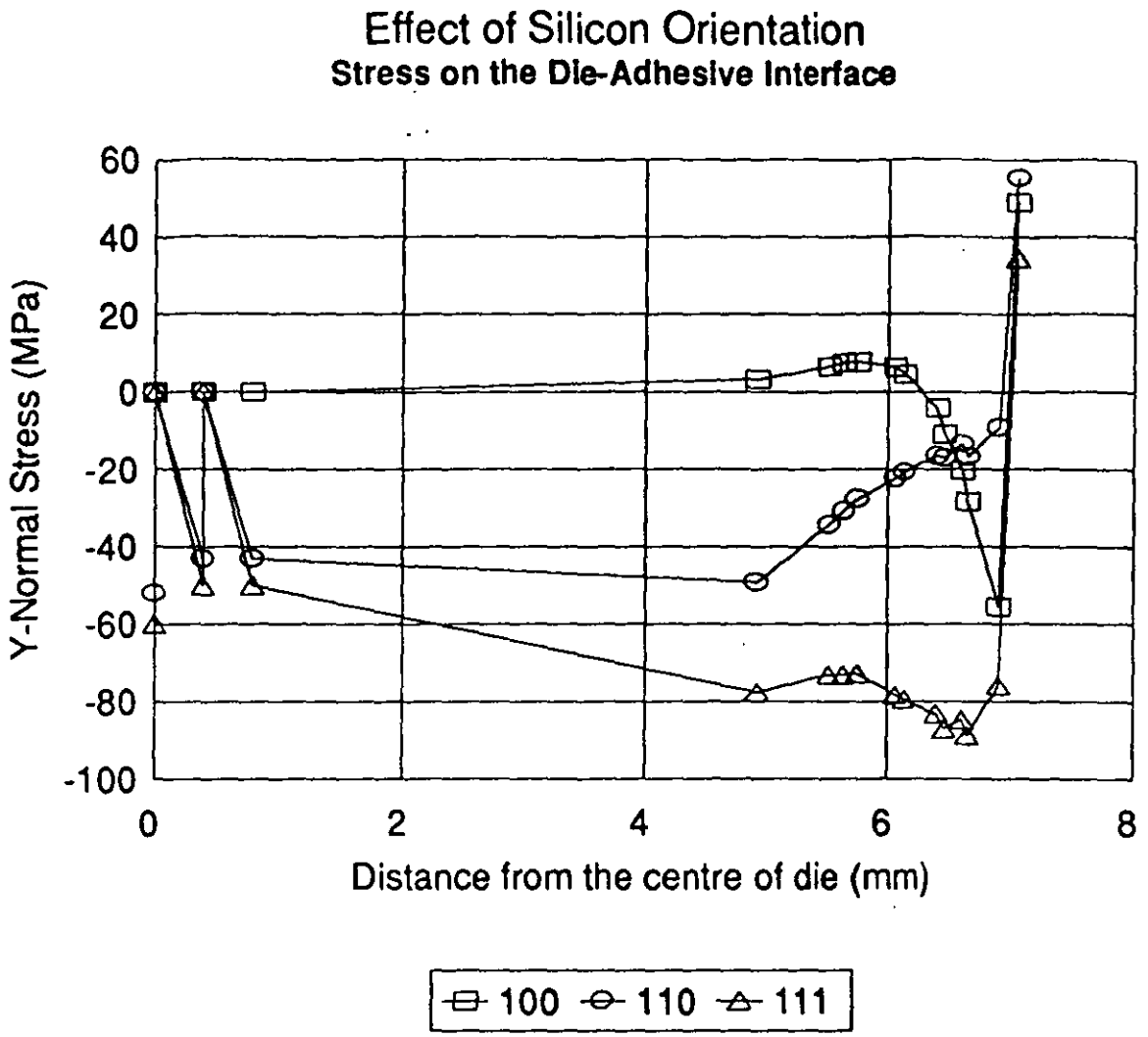

Figure 6.17: Effect of the orientation of the silicon die

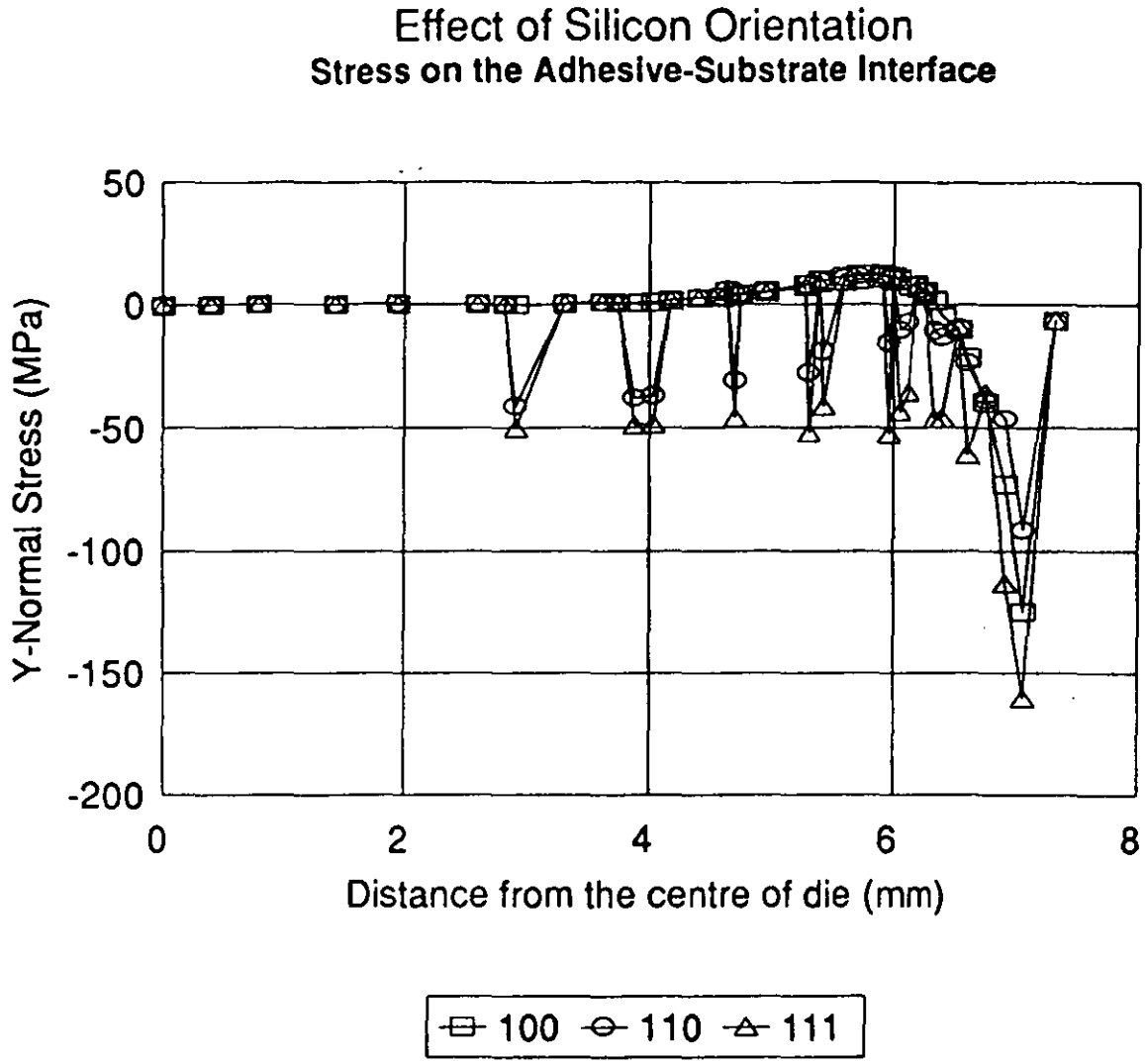

Figure 6.18: Effect of the orientation of the silicon die

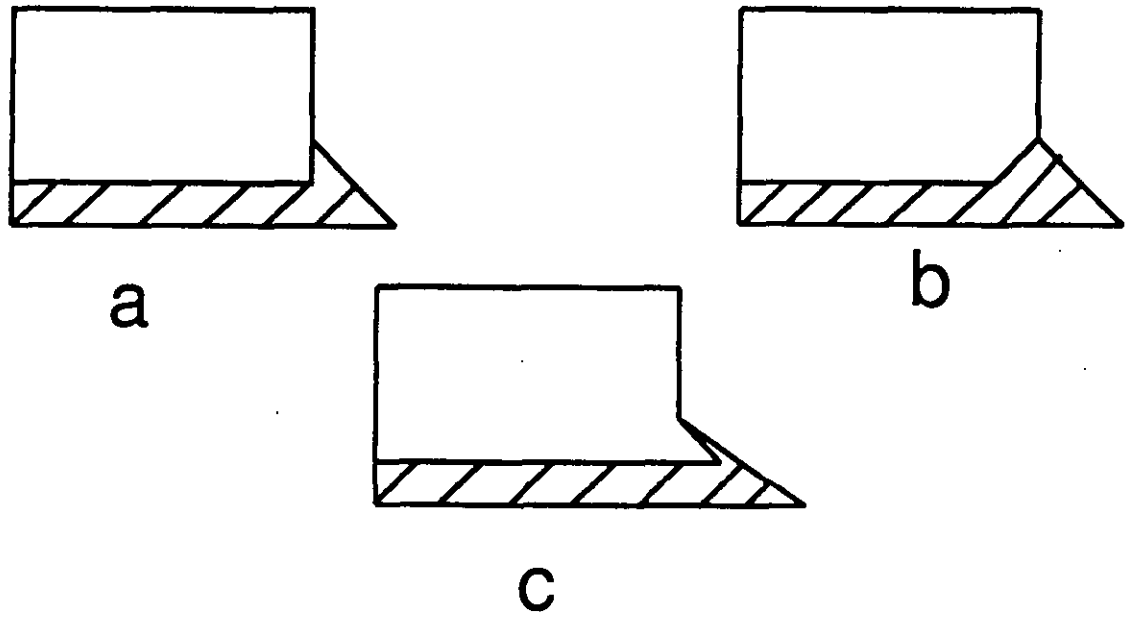

Figure 6.19: Variation in geometry of silicon dies

Similarly, the preparation and screen printing of the conductive adhesives often results in trapped gases, dirt or air during the assembly. This create voids in the adhesive layer. The effect of voids in the layer has not been quantified previously but they are generally believed to be stress raisers. The bondline thickness in conductive adhesives assemblies also needs to be optimized for stress and thermal management. The general belief is that a thicker bondline serves to stress relieve the silicon die, however thinner bondlines are better for thermal management. There is a need to address the sensitivity of stress in the silicon die to the bondline thickness and the presence of void in the adhesive layer.

6.8.1. The Models

Three 3-dimensional models similar to those described earlier were used to investigate the effect of die geometry. The observed silicon die geometries were modelled. The fillet was modelled as an isosceles triangle of height 0.125 mm and the die cleavage angles were 56.4°.The model was discretised using the meshing algorithm in the software to ensure a good element density around areas of stress intensity such as geometric discontinuities. A linear analysis of the thermally induced stress created by cooling the die attach assembly from the curing temperature (275°C) to ambient (taken as 25°C) was performed with the assumptions used in the model as before namely:-

1. All material properties were considered to be linear (i.e. stress relief due to plastic deformation of the adhesive was not taken into consideration).
2. The adhesive layer is homogeneous and void free.
3. The system is in equilibrium at the curing temperature (i.e. strain free).
4. Isotropic material properties were assumed for silicon.

Five axisymmetric models with varying bond-line thickness (10 μm to 50 μm) were analysed for the sensitivity of the assembly to bond-line thickness. Similarly five models ranging from 2 x 2 mm to 10 x 10 mm were used to investigate the sensitivity to die size.

The models for the analysis of the effect of voids had different assumptions from the previous models. It has been observed that voids are generally randomly distributed in the adhesive layer, the pattern is such that there are small voids surrounding a large void [Personal Communications with LUCAS Electronics, December 1992] and also, the total area of the void in the layer does not exceed 35%of the entire adhesive surface area.Voids were simulated by creating cylinders distributed as shown in figure 6.20 with areas ranging from 5% to 35% of the adhesive layer. A total of four models with voids were developed and analysed. The fourth model was used to investigate the effect of location of the void. A void was deliberately situated under the die to correspond with the position on the die, at which maximum stress on the surface was predicted.

6.8.2. Results

The results of the analysis are presented by evaluating the relevant component of stress levels in the previously identified potential failure points in the assembly.The effect of die size and bond-line thickness was evaluated using the stress level in the die as this gave a more easily comparable set of data. The four areas outlined above were examined for each die geometry modelled. It should be noted that the substrate in this analysis is allowed to deform freely without the constraints of any form of packaging as might occur in a real product. The situation described above assumes the manufacturing situation in which the product is not yet packaged, therefore it may not apply to a product in service in which the substrate may be constrained to remain flat.

6.8.2.1. Sensitivity to die geometry

A comparison of the predicted stress level on the surface of the die (Figure 6.21) for the different die geometries indicates that the maximum stress level occurred in the die with the undercut edge. The bevelled-edge die has the lowest level of stress. However, it should be borne in mind that a bevelled and an undercut edge are likely to occur at opposite ends of the same die. This indicates that a sawn through die is better than scribed-cleaved die for stress management.

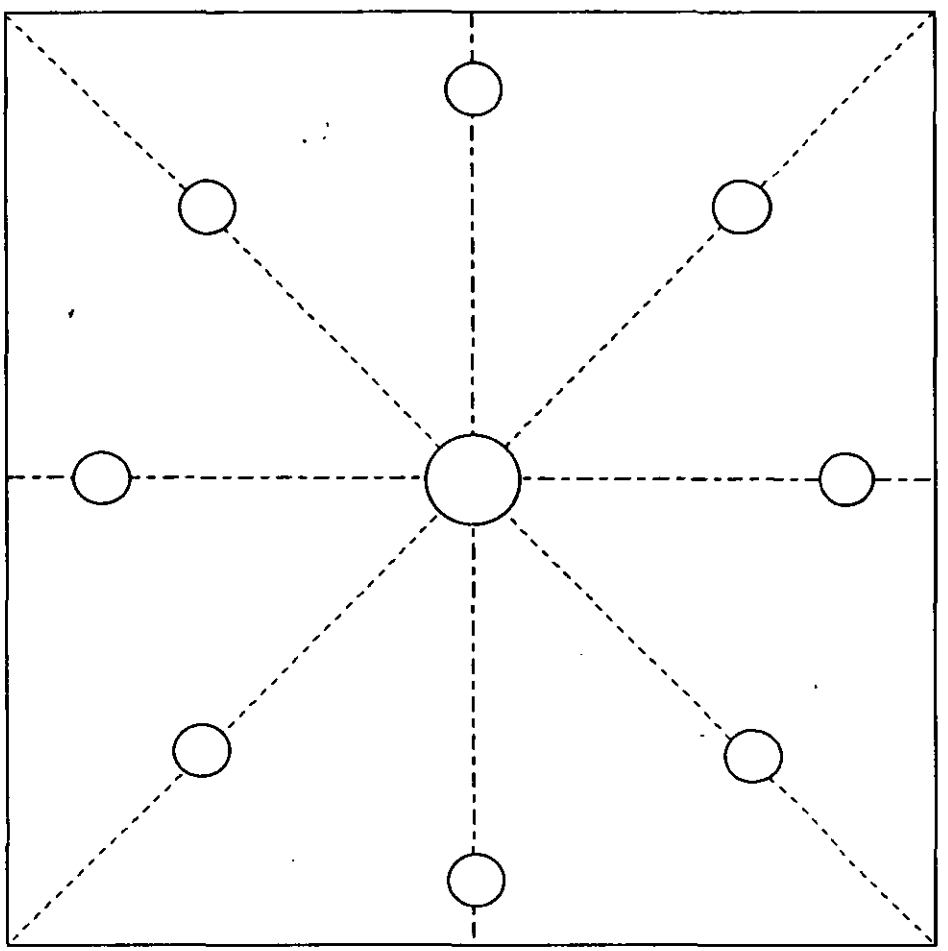

Figure 6.20: Plan view of simulated voids in the adhesive layer

A graph of the stress on the edge of the die, Figure 6.22, shows that the maximum stress occurred in the undercut edge die, followed by the straight edge and finally the bevelled edge die. The stress level observed, when compared with the ultimate tensile strength of silicon (the horizontal line on the graph), indicates that there is only a small margin of safety for the undercut geometry. It was also observed that the peak stress on the edges did not occur at the start of the fillet (0.175mm) which shows that the stress resulted from the geometry of the die itself. Furthermore, variation in stress distribution resulting from differences in geometry is observed in the fact that some of the edges resulted in compressive stresses and the peak stresses occurred at different heights for different geometries and planes.

The graphs of stresses at the interfaces (Figures 6.23 and 6.24) show very little difference in stress level between the three different geometries. Differences are however obvious in the level of stresses observed for the different planes. It was also noticed (as indicated for the undercut edge) that the maximum tensile stress normal to the interfaces occurred at the die-adhesive interface suggesting that peeling will probably initiate at this interface. It is also worth observing here that the stress on the Die-Adhesive interface plotted in Figure 6.23 is for the portion of the die resting vertically on the adhesive and not necessarily to the tip of the fillet except for the die with the undercut edge.

6.8.2.2. Sensitivity to Die Sizes

A plot of the peak stress along the die surface for different square die sizes ranging from 2x2mm to 10x10mm (Figure 6.25) reveals that the maximum stress to be expected on the xy-plane occurred with the 4mm square die. It can be seen from the graph that the peak stress occurs closer to the perimeter of the die therefore the effect of the peak stress over the whole die seems to be balanced by a bigger low stress region in the larger dies. The graph therefore shows a situation where above a certain size the peak stress does not increase with increase in die size. The small differences in peak stress predicted for die sizes greater than 4mm square (observed from the graphs) is not significant and could have resulted from the level of refinement of the mesh.

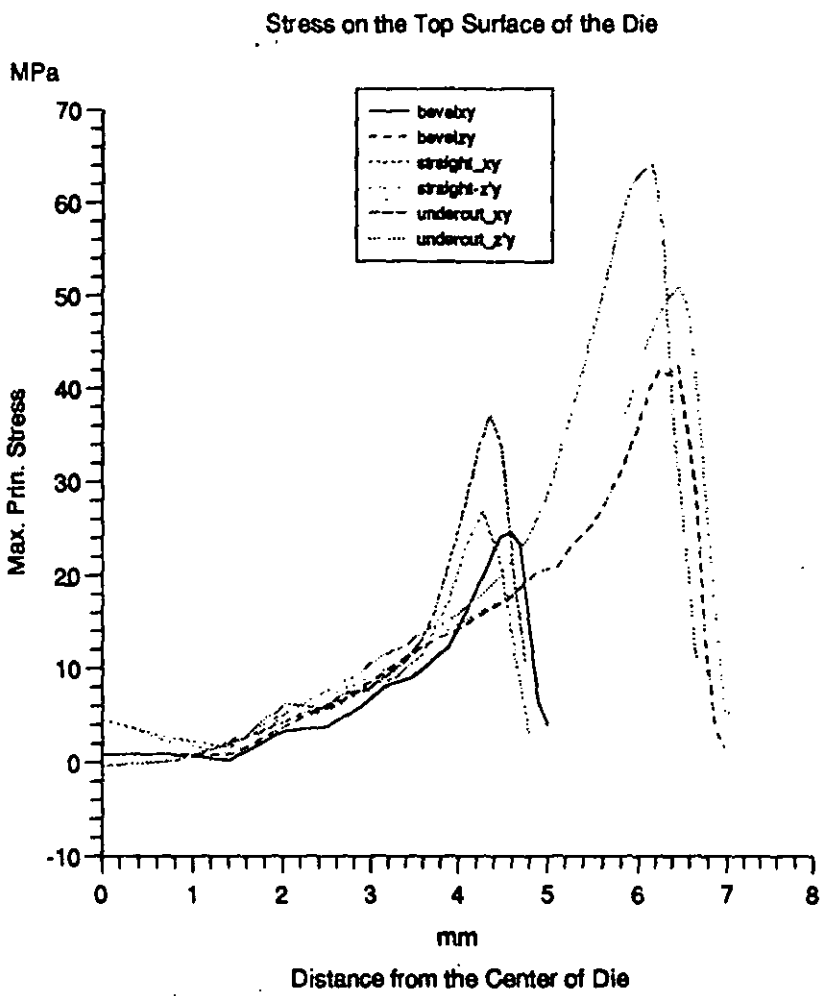

Figure 6.21: Sensitivity to die geometry

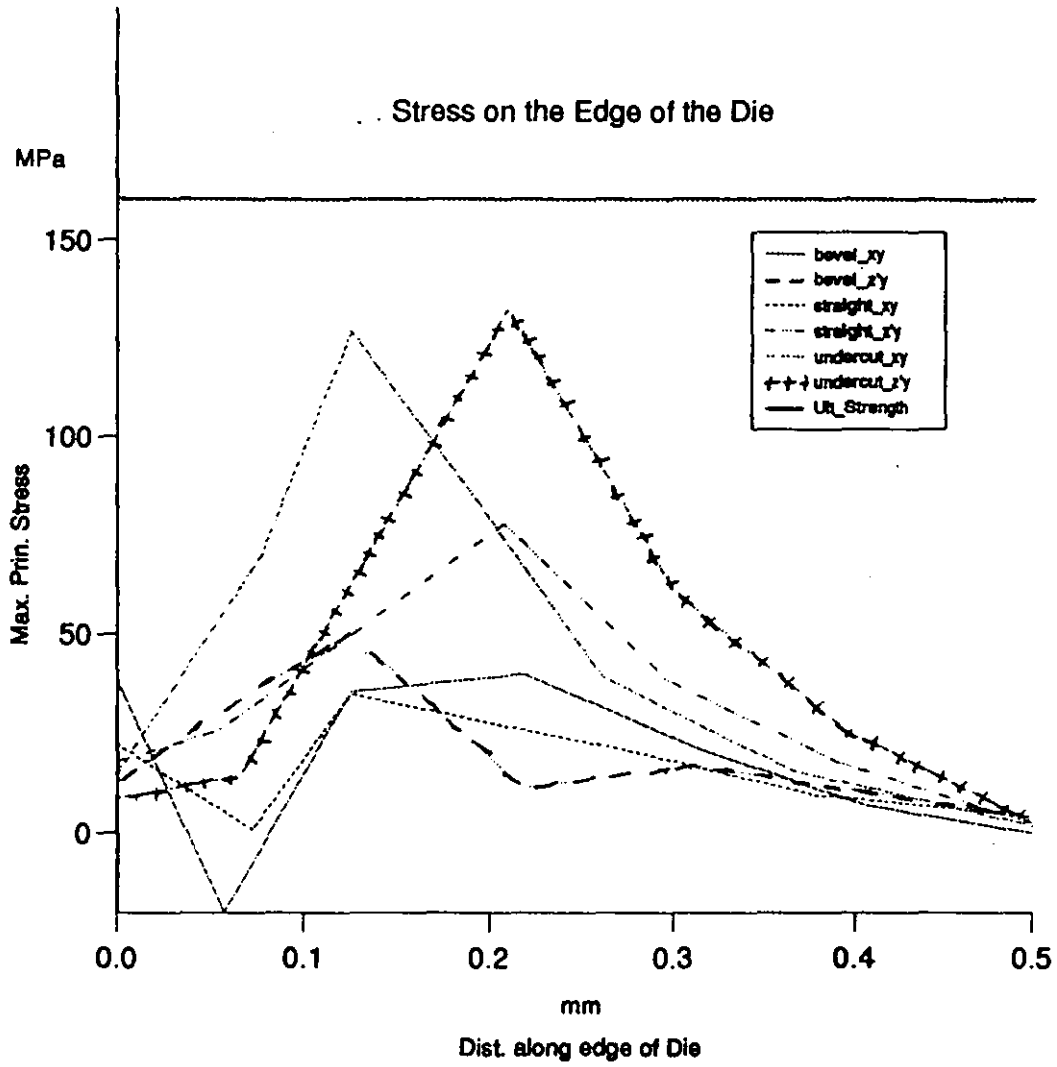

Figure 6.22: Sensitivity to die geometry

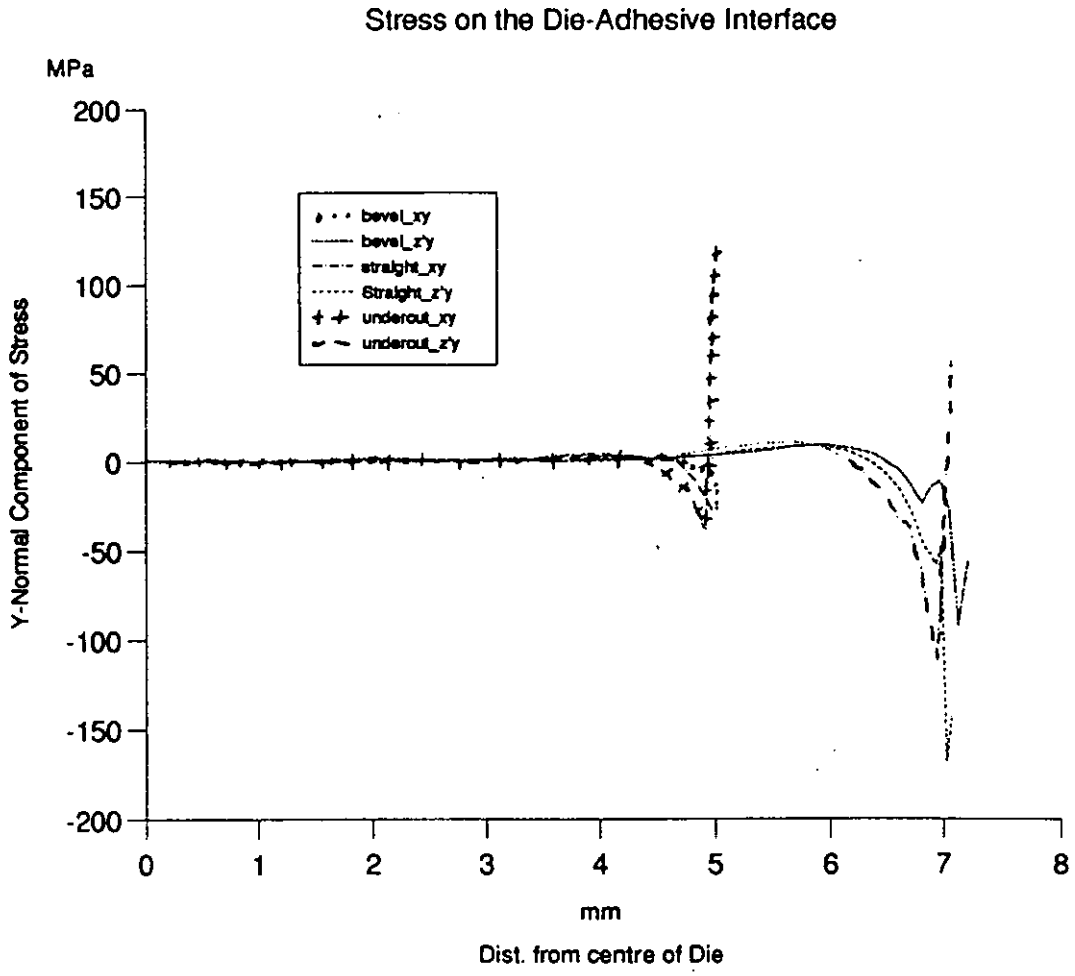

Figure 6.23: Sensitivity to die geometry

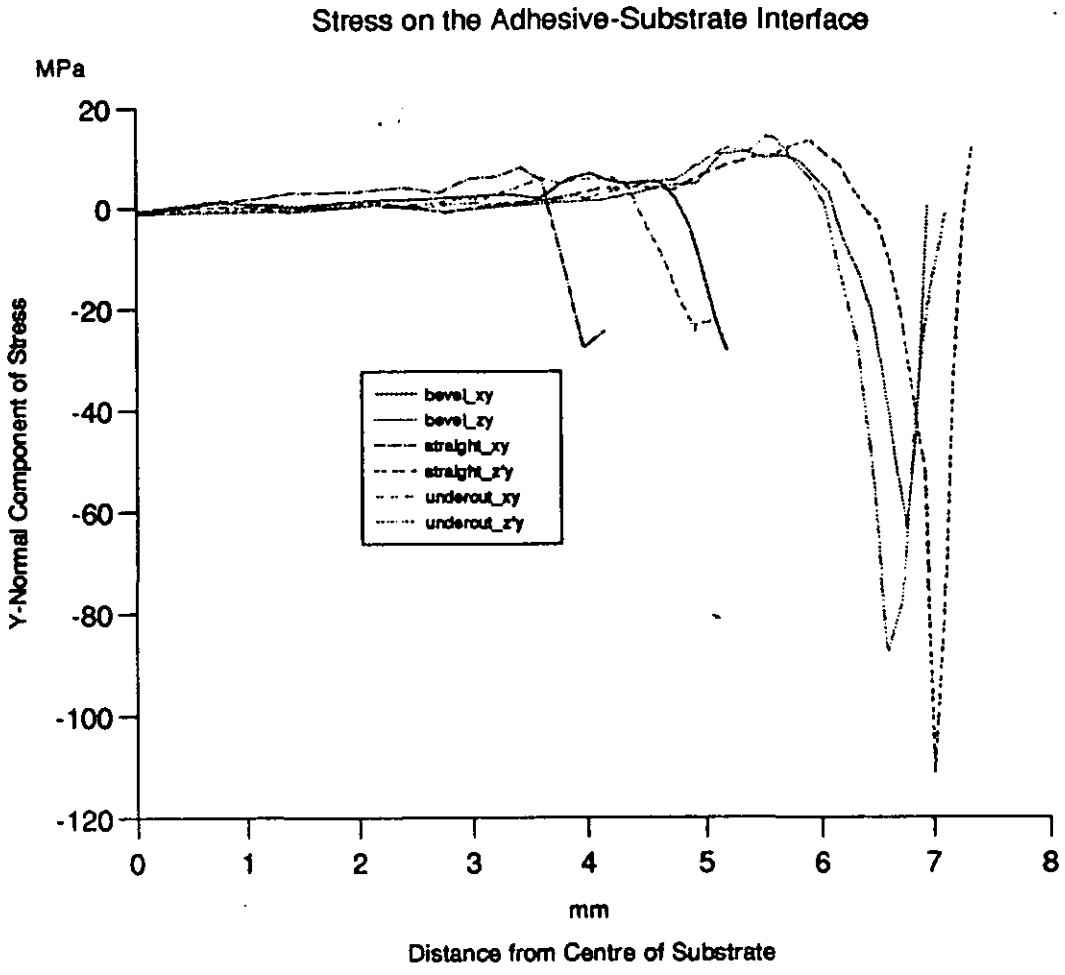

Figure 6.24: Sensitivity to die geometry

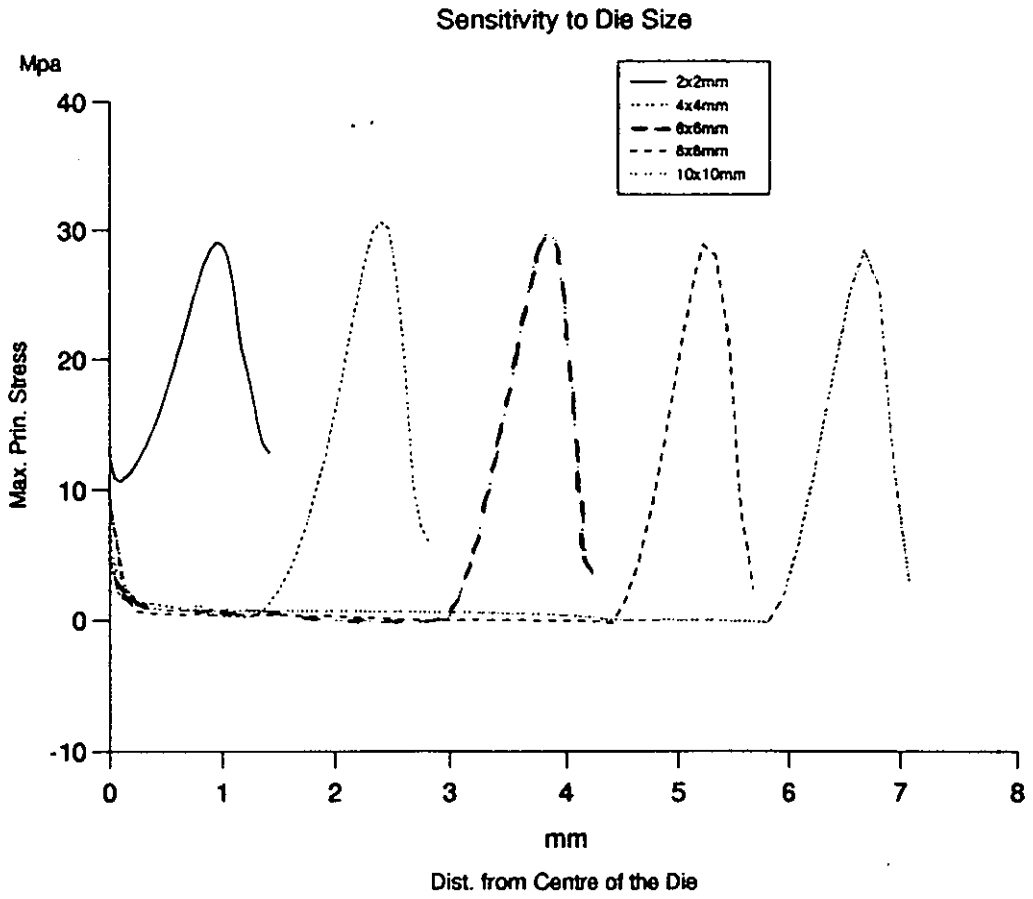

Figure 6.25: Variation of stress level with die size

6.8.2.3. Sensitivity to Bondline Thickness

Figure 6.26 shows the peak maximum principal stress on the surface of the die for the different bondline thicknesses. It is apparent from the graph that the thinner the bondline the greater the stress on the surface of the die. The stresses shown are those expected along the mid-plane of the assembly. A higher stress level of about 1.6 to 1.85 times those shown in Figure 6.26 is expected along the diagonal [90]. It can also be seen that the rate of change of stress begins to decrease above a bondline thickness of 20μm and is actually lowest between 30 and 40μm. The differences in stress level above the 30μm thickness could include an artifact of mesh fineness. It may therefore be concluded that, for stress management, the bondline thickness should be greater than 30μm since the lower the bondline thickness, the better the thermal conductivity.

Examination of the stress normal (in the Y-direction) to the interfaces (Figures 6.27 and 6.28) reveals that there is very little variation in the level of stress for the different bondline thicknesses. However, figure 6.28 particularly shows that the tensile stresses observed in the interfaces have some sensitivity to bondline thickness, but this effect is very small in comparison with the compressive stress at the edge of the interface.

6.8.2.4. Sensitivity to voids

The effect of voids in the adhesive layer is depicted in figures 6.29-6.31. The effects of voids are more apparent in the graphs of the silicon die. However these graphs also show that the greater the percentage of the conductive adhesive covered by voids, the lower the level of stress on the surface of the silicon die. This is further shown in Figure 6.30 graph for the vertical edge of the adhesive. Furthermore, the location of the void at the stress critical point, figure 6.31 shows that the predicted stress is even lower for the model without a void.

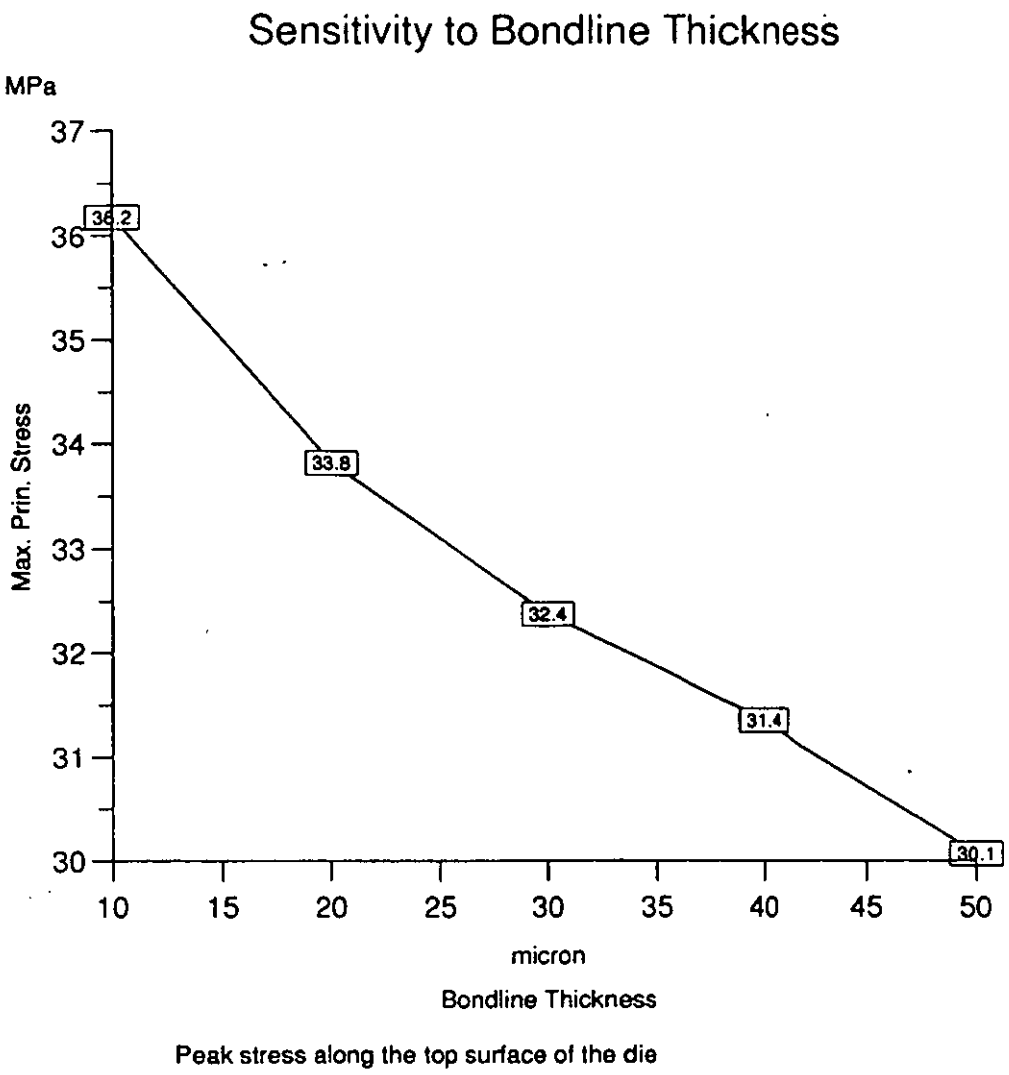

Figure 6.26: Variation of stress level with bondline thickness of the adhesive

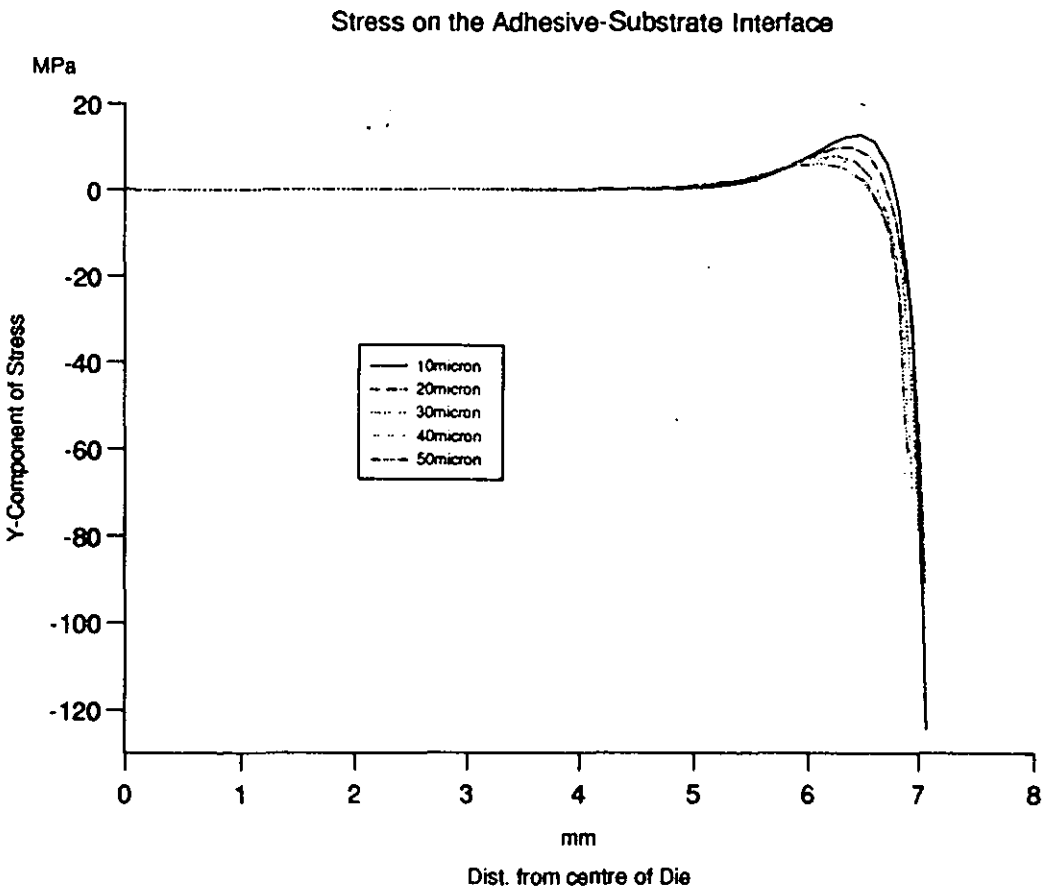

Figure 6.27: Variation of stress level with bondline thickness of the adhesive

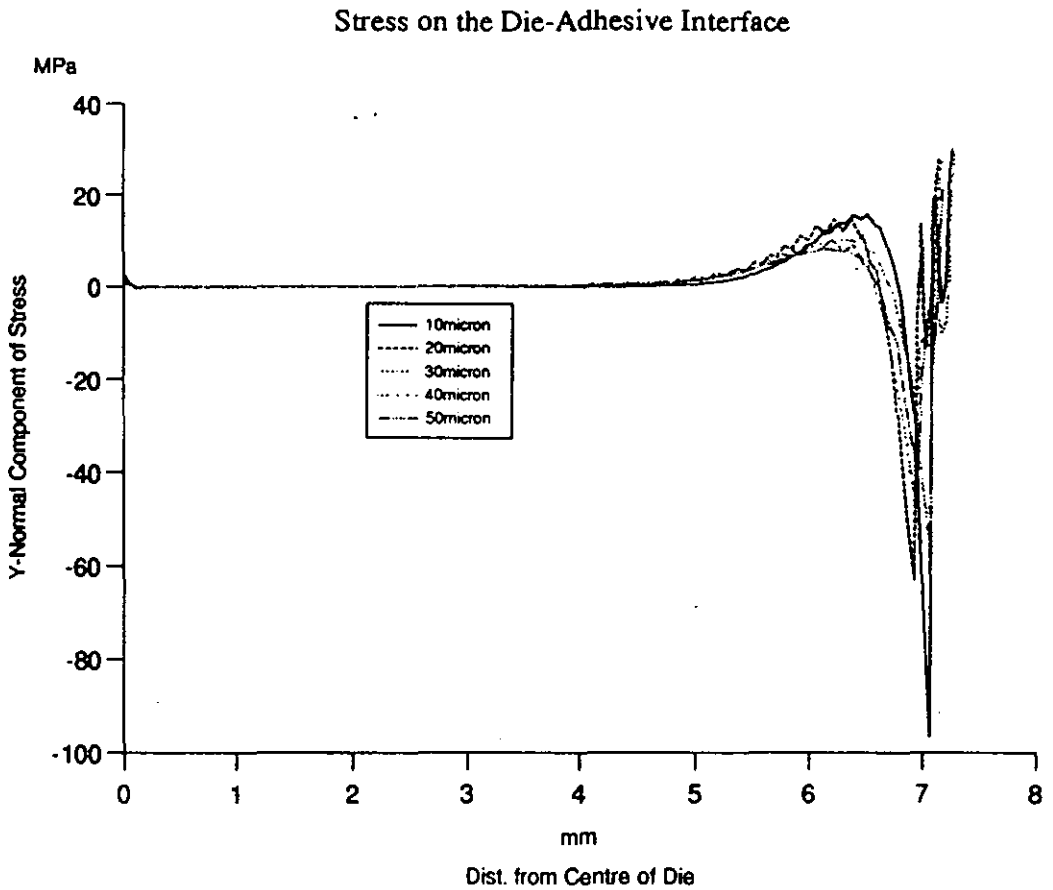

Figure 6.28: Variation of stress level with bondline thickness of the adhesive

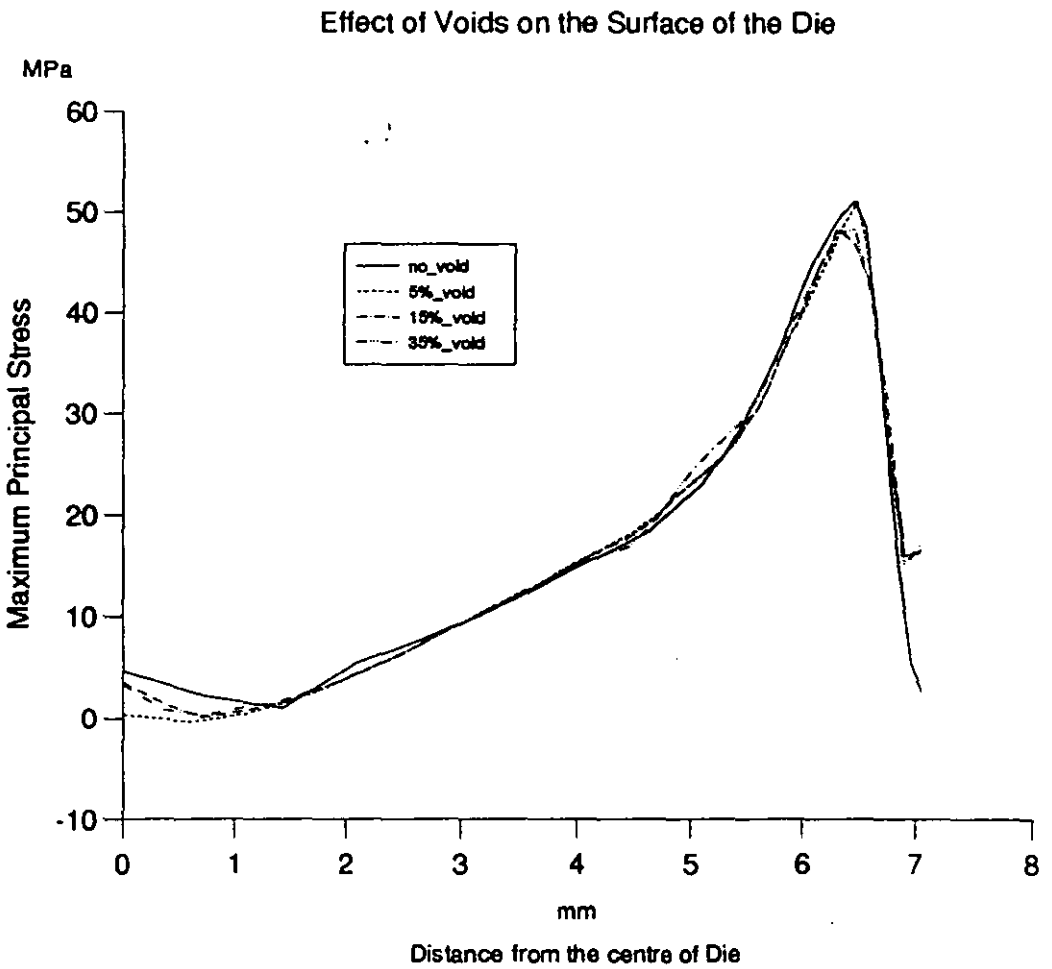

Figure 6.29: Effect of voids

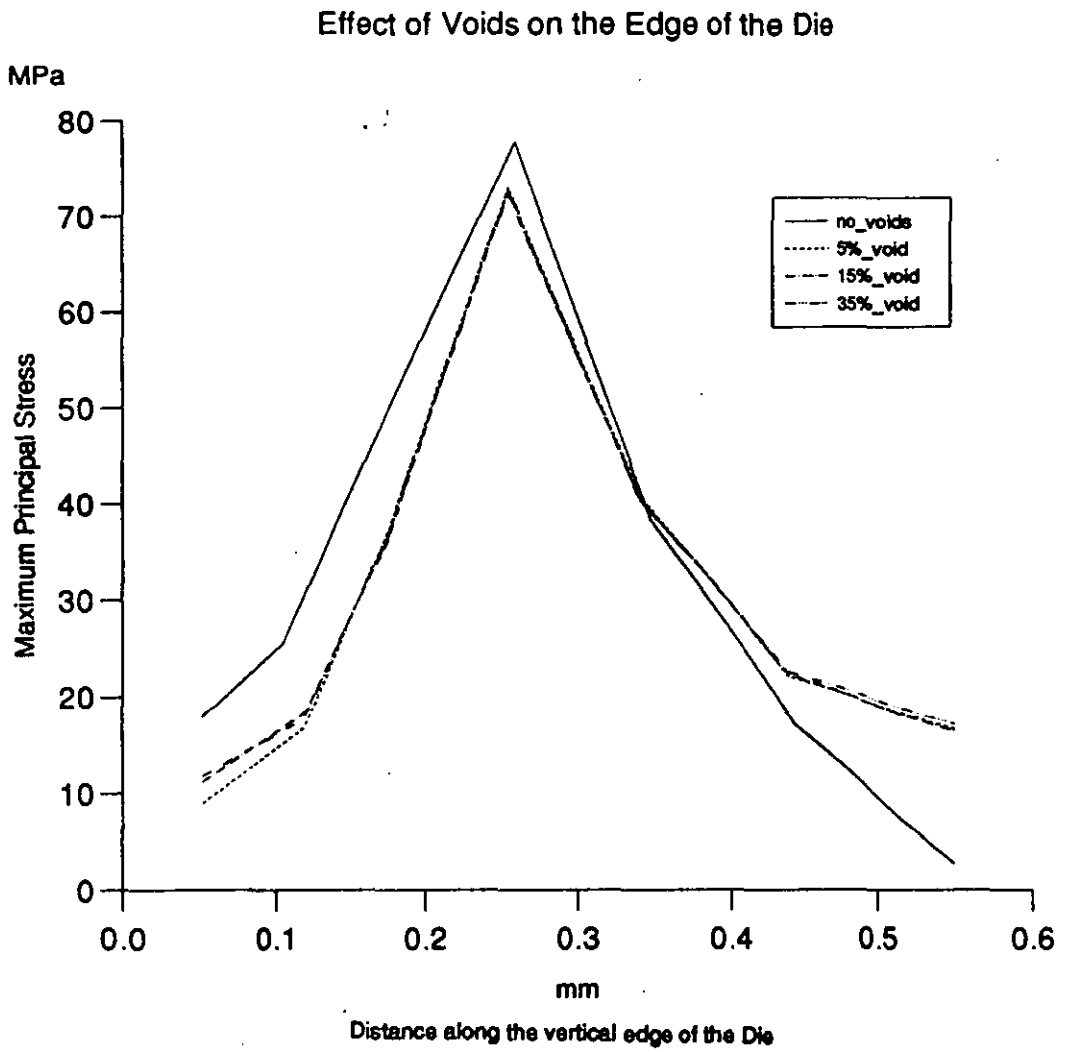

Figure 6.30: Effect of voids

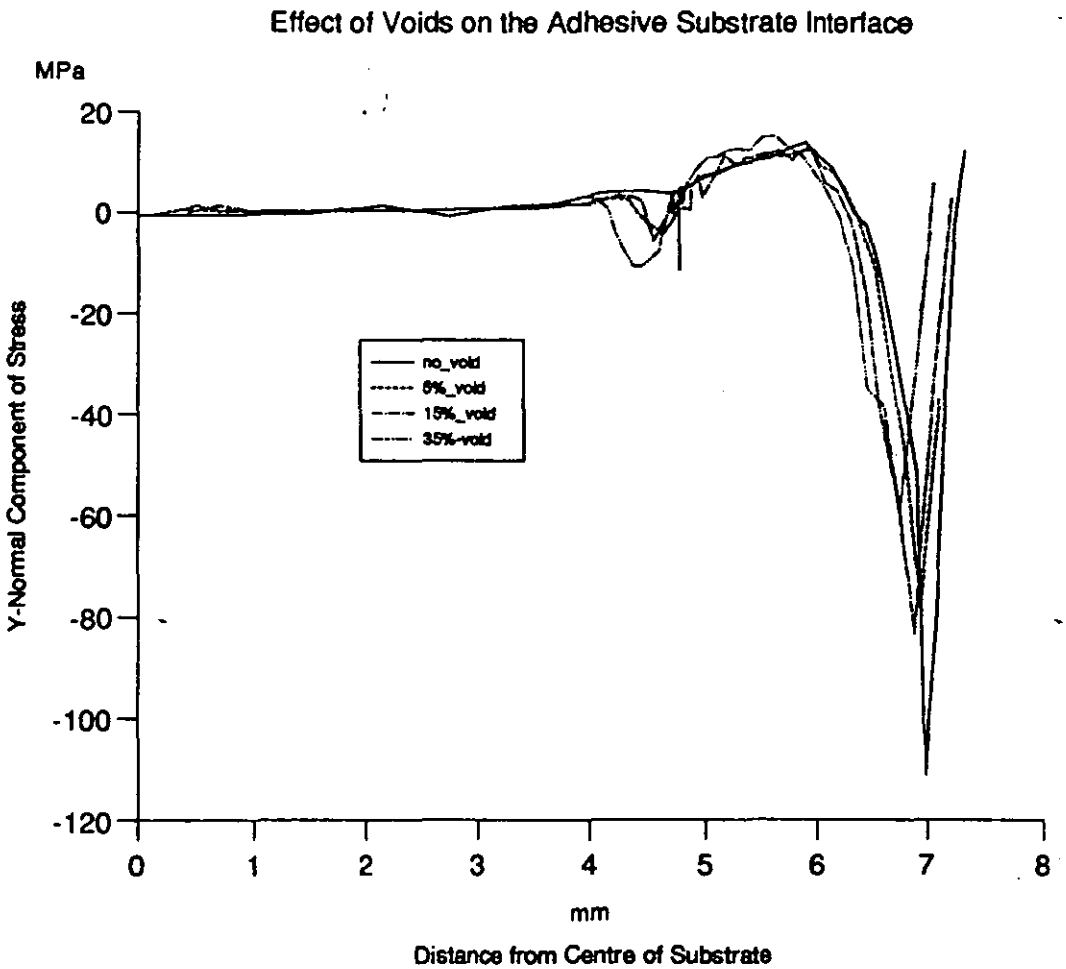

Figure 6.31: Effect of voids

6.8.3 Discussion

There are four significant regions of interest in the die-attach assembly modelled:

a. The surface of the die; to predict whether stresses are high enough to cause cracking.

b. The edge of the die; to investigate the possibility of cracking.

c. The two interfaces of the adhesive; to check for the possibility of failure by peeling.

d. In the bulk of the adhesive to check for the likelihood of plastic yielding of the resin.

The predicted stress level in the die can be compared with the ultimate strength of silicon in order to determine the likelihood of failure. From all the analyses it can be seen that the highest stress occurred along the vertical edge of the die. In fact the stress at the vertical edge of the bevelled die geometry is very close to the ultimate strength of silicon suggesting a greater possibility of failure at the vertical edge of the silicon die than anywhere else in the model. The graphs of the results of the die geometry also show that the sawn through die is better for stress management. This is so because a bevelled edge will inevitably result in an undercut edge on another die as a result of the cutting process. The result of the variation of stress with die size allays the fear that the bigger the die the greater the stress. A comparison with a fixed substrate also predicts a similar stress pattern except that the stress levels are higher in this case (figure 6.32). This result is consistent with observations from analytical methods at CALCE Electronics Packaging Research Center [91]. Where the stress level increases until a die size of 8mm in length across the diagonal and no significant increase is observed. However, there may be other factors during service that may lead to observed failures of large area die attach in service.

Similarly, the result concerning the voids also challenges the wide spread belief that voids act as stress raisers in conductive adhesive die attach assembly. The mechanical properties of the void as shown in this analysis support stress relief. However voids in real life may not be as modelled, and the presence of voids may alter the modulus of elasticity of the adhesive and also affect the thermal behaviour of the assembly leading to small heat pockets that may significantly increase the thermo-mechanical stress around such voids.

There is no single criterion for evaluating peel at the interfaces. Peel is governed by a combination of the different components of stress in the materials at the particular interface. The resultant stress acting perpendicular to the surface has been used in this analysis as it is a major component of stresses leading to peel. The observed stress curves at the interfaces are consistent with observations in other published works as noted by Kinloch [92]. Some of the main points that emerged from previous contributions were that the in-plane normal stress in an adhesive joint is tensile in nature and are uniform near the interface and may be given by

$$\sigma = E_a D_{at} DT$$

where:-

E_a is the Modulus of Elasticity of the adhesive;

D_{at} is the difference in linear thermal coefficient of expansion between the adhesive and substrate;

DT is the change in temperature between the stress free temperature and the temperature of interest.

This formula was proposed for structural adhesive joints in which the adherents are both made of the same materials. It gives an approximate value that takes no account of the geometry factor. Using this formula, the estimated tensile normal stress should have been 86Mpa compared with the 130Mpa predicted by the finite element analysis.

It should be noted that the results presented in this section are for models of a freely deforming assembly except for that shown in fig 6.32. The stress levels and perhaps the stress distribution may change when the assembly is packaged as constraints may be imposed by the packaging. Similarly, linear elastic properties have been assumed throughout the models so if plasticity or creep occur in the real materials the actual stress levels will be lower.

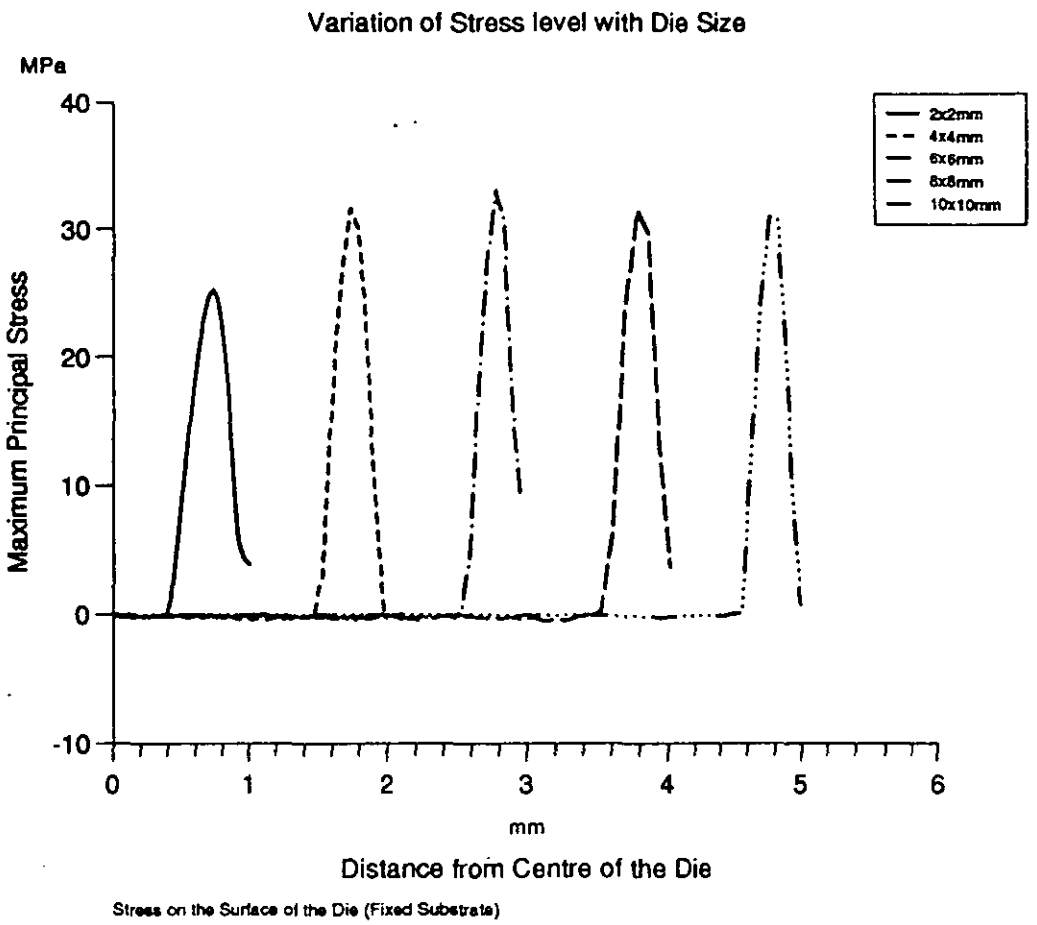

Figure 6.32: Variation of stress level with die size (fixed substrate)

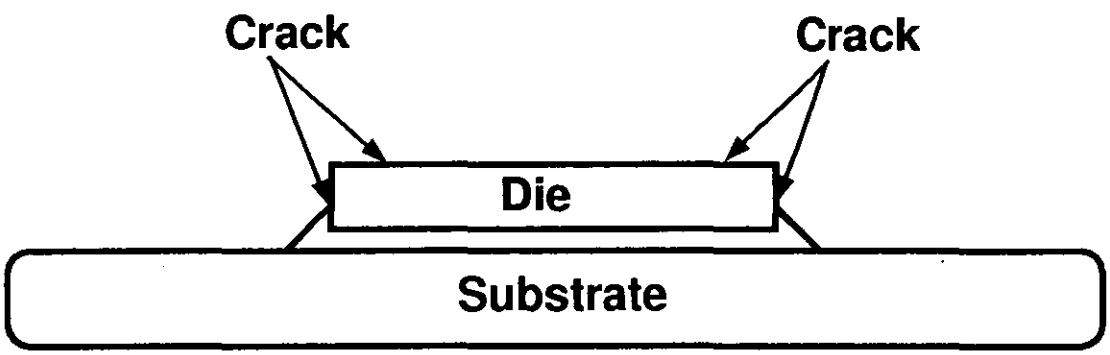

Figure 6.33: Possible effects of thermal stress on a die attach assembly due to the adhesive curing process

6.9. Conclusions

A comparison has been made between the use of 2-dimensional, axisymmetric and 3-dimensional geometry in the finite element analysis of a die attach assembly using conductive adhesives. The axisymmetric geometry was found to be a good approximation to the 3-dimensional geometry and gave considerable savings in computer resources and human effort. In this work, the axisymmetric model has proved to be an acceptable approximation to the 3D model with the advantage that it reduces the total computer time taken by 98%. The true effect of the corners of the square die modelled was, however, not reflected in the stress level predicted by both of the more computationally efficient but simplified 2-dimensional and axisymmetric models. The stress level at the surface of the axisymmetric die when compared with a rectangular die is much lower suggesting that a circular die is better than rectangular die for stress management.This result also encourages the use of axisymmetric models in sensitivity analysis in which geometric parameters such as the die size, bond-line thickness etc. for the assembly must be investigated. This approximation method can be applied to the analysis of structures having similar geometry in the manner of that already applied to the simplified analysis of surface mount joint deformation [88].

The result of the analyses indicate that the bondline thickness should be above 30μm for good stress management. There are also indications that there is an increase in peak stress in the die with increasing die size up to about 4x4 mm after which the level of stress remains approximately constant. Analysis has also shown that a sawn through die is much better for stress management and that voids as a geometrical entity in the adhesive layer does not necessarily serve as a stress raiser. Other factors such as change in thermal characteristics of the adhesive due to the presence of the void are likely to alter the thermal and mechanical behaviour of the adhesive layer. The expected modes of failure in a die attach assembly are shown in figure 6.33

Chapter 7

The Use of Electronic Speckle Pattern Interferometry to Calibrate Finite Element Models

7.1. Introduction

A process model needs to be calibrated to avoid unreliable predictions. Calibration of FEA models of thermal processes that result in strains can be carried out by comparing the real to the modelled displacement characteristics. Experimental analysis of object deformation relies on either contact or non-contact techniques. Traditionally, strain gauges and accelerometers have been utilised in order to determine displacement characteristics, see for example, S.A. Gee et al.[1], but these methods only provide point source information, and can in certain circumstances distort test-object behaviour by their presence. In most cases results have always confirmed predictions qualitatively with considerable variance in quantitative correlation. The major problem with strain gauges has been the calibration of the strain gauges prior to the experiment. The advent of the laser has created a growing family of experimental equipment, both point source and whole-field based, which are all non contact devices. Hence object behaviour can be evaluated with the knowledge that the detection method is not interacting with the test piece.

This chapter presents the results of the experiment performed to calibrate the Finite Element models using Electronic Speckle Pattern Interferometry(ESPI). The particular model examined is that of an isotropically conducting adhesive, CTC2000, die-attach cooling from the adhesive curing temperature to ambient. The die attach assembly was subjected to similar thermal conditions as in the manufacturing process while measuring the out of plane deformation. The experimental result was then compared to a finite element model of the same situation.

7.2. Displacement approach to Solution in Finite Element Analysis

An important aspect of the finite element analysis that enables calibration of models by measuring the deformation, is the displacement approach to solution [see Chapter 2]. In this system, the displacement variables are solved first, by using compatibility relationships between disablements and strains, the relationship between applied forces and stresses can be established using the appropriate stress-strain law. Therefore, as long as the appropriate stress-strain law and relevant material properties are used, if reasonable assumptions about the structures are made, a good displacement prediction should guarantee a reasonable prediction of stress.

7.3. Electronic Speckle Pattern Interferometry

Electronic Speckle Pattern Interferometry (ESPI) is an 'off- shoot' of Holographic Interferometry (HI), first reported separately by Leendertz [3] and Macovski [4]. ESPI relies on the 'speckle effect' observed on objects illuminated with coherent monochromatic light, most commonly supplied by lasers. Instead of holographic recording media, a CCD camera is used, linked to a monitor, providing real- time analysis of object deformations which are statically or dynamically induced. This has several immediate advantages over HI. Instant processing of results via the associated electronics removes chemical processing uncertainties. Each interferogram is replaced every 40ms (at a 25Hz frame rate), hence allowing virtually instantaneous visualisation of behaviour changes caused by alterations to the test specimens boundary conditions.

ESPI can resolve displacement out-of-plane and in-plane, via the use of specific interferometer designs for each axis, as explained by Wykes [4]. The choice of ESPI configuration can be chosen to examine specific object displacement, or three interferometers can be used simultaneously to provide spatially discrete but comprehensive analysis. ESPI is inherently less sensitive to environmental disturbances because of the rapid image plane refresh rate. However, the fringe patterns, whilst of a similar nature to HI results, are generally of lower contrast and quality by virtue of the optical physics involved.

ESPI utilises the granular speckle caused by the reflection of a coherent light from an optically rough surface. The light is not reflected from points but areas on the object surface, the smallest being the resolution limit of the lens of the imaging system. Each area will have its own unique combination of amplitude and phase, with the phase varying by 2π or more between areas, thus causing random intensity of reflected laser light across the object surface. Figure 7.1 shows a schematic representing the layout of the optical elements of an out-of-plane interferometer.

In order to observe changes of phase and amplitude, a reference beam is required, split from the original laser source. This is combined with reflected object light at the image plane, such that the intensity of any point on the image plane of the interferometer (I_A) will be:

$$I_A = I_o + I_r + 2\sqrt{I_o I_r}\cos\psi \qquad \text{Eq. 7.1}$$

Where I_O and I_r are the object and reference beam intensities respectively and ψ is the phase.

Hence a unique recording of phase and amplitude is produced. Displacement of the object caused by part of a thermal cycle will result in a phase change $\Delta\phi$, thus altering the intensity at the point to I_B:

$$I_B = I_O + I_r + 2\sqrt{I_o I_r}\cos(\psi + \Delta\phi) \qquad \text{Eq. 7.2}$$

By subtracting Eq.7.2 from Eq.7.1 correlation subtraction fringes are produced, delineating between areas which have and have not altered during the change of state:

$$I_A - I_B = 2\sqrt{I_O I_r}(\cos\psi - (\cos(\psi + \Delta\phi))) \qquad \text{Eq. 7.3}$$

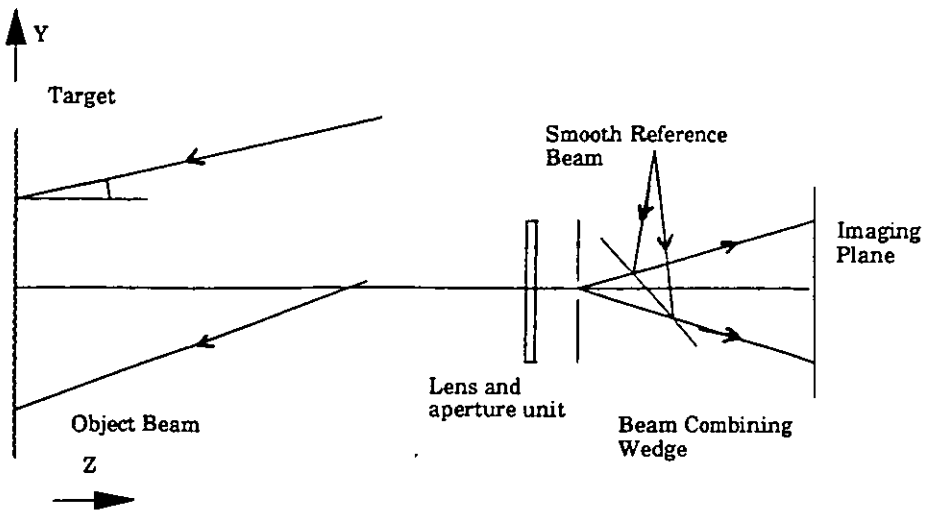

Figure 7.1: The basic elements of an out of plane speckle pattern correlation interferometer

These three equations govern the formation of correlation fringe patterns for subtractive speckle interferometry. When a target is illuminated with the object beam, there is a fixed path length from laser source to viewing optics. An object displacement will cause a change of path length and an associated change of phase, as described by Wykes(4). Hence out-of-plane object displacement, *d*, can be represented in terms of wavelength and fringe order, *n*, as shown in equation 7.4

$$d = \frac{n\lambda}{2} \qquad \text{Eq. 7.4}$$

If accurate results are to be obtained, then viewing and illumination angles require optimisation, otherwise more than one component of motion will be observed. The sensitivity vector (n_i - n_v), where n_i is the illumination direction and n_v is the viewing direction) should be as close to zero as possible with departure beyond 10° - 15° leading to in-plane components being visualised concurrently. Much of this potential experimental uncertainty can be removed by using commercially available interferometer designs. An in depth analysis of the mathematics and physics involved with speckle interferometry, is provided by Jones & Wykes[6].

7.4. The Model

A model of the die-attach system was developed on the SDRC I-DEAS Finite Element modelling system. The die-attach system modelled employed a silicon die bonded to a 99% Alumina substrate by electrically conductive adhesive (the same model used to conduct sensitivity analysis on the effect of silicon die orientation in chapter 6). The adhesive considered is CTC 2000, a thermoset epoxy engineered for high temperature applications. The real dimensions of the assembly are as shown below. The problem was simplified to reduce computation time by modelling a quarter of the whole assembly because of its symmetry along the xy and yz planes. Issues in the modelling of such systems have already been discussed in chapter 6.

7.4.1. Dimensions of the Model

Die (Silicon): 10mm x 10mm x 0.5mm

Adhesive (Silver filled Epoxy): 50μm thick + Fillet

Substrate (Alumina): 25.4m x 25.4m x 0.64mm

A linear analysis of the thermally induced stress, due to the cooling of the system from the curing temperature of 300°C to ambient (25°C), was performed. The curing temperature of 300°C was chosen for experimental convenience. The anisotropic properties of silicon were taken into consideration by using the stiffness coefficients [8]. The main assumptions in the model are as follows:

1. All material properties were assumed to be linear
2. The system is in equilibrium at the curing temperature.
3. The adhesive layer is homogeneous and void free.

The material properties are as shown in Table 7.1:

	E(GPa)	$\alpha(10^{-6}/°C)$	υ
Silicon	C_{11}=165.64 C_{12}=63.94 C_{44}=79.51	3.06	-
Epoxy	4.65	55.9**	0.35
Alumina	380	7.80	0.34

Table 7.1: Materials property

E-Young's Modulus of Elasticity

α-Thermal Coefficient of Expansion

υ-Poisson Ratio

**Average over the temperature range considered

7.5. Equipment

The equipment consist of an out of plane Ealing Optics Vidispec Interferometer used to measure the out of plane displacement. The image captured by the interferometer is stored on an A-four video frame storer and is then recorded on a VHS video cassette using a Sony U-matic video recorder. A special jig was made to hold the die attach assembly vertically while the laser beam was focused on to it. The silicon die used in the die-attach assembly was mounted on an alumina substrate coated at the back with a thick film resistor for heating the assembly. A power supply unit is used to supply power to the assembly and the temperature regulated using a Eurotherm thermal control unit. A schematic of the equipment is shown in figure 7.2.

7.6. Procedure

The adhesive employed requires heating at 275°C for 25 minutes for a full cure, further heating to 300°C for 5 minutes enhances high temperature performance. The heating of the adhesive was achieved by plating the back of the alumina substrate with a thick film resistor with a value of approximately 10Ω per square mm with silver palladium electrode strips at either ends. Electric current was supplied to the substrate via a Eurotherm thermal control. The sensor of the thermal control is then placed in contact with the adhesive fillet on the silicon die for temperature feed back. The temperature, using the thermal control, was ramped up to 300°C at the rate of 10°C per minute. The temperature is allowed to stabilise at 300°C for about 5 minutes before switching off the power.

The specimen (still at 300°C) was illuminated with an Helium Neon (λ=632.8nm) object beam of the out-of-plane Ealing Optics Vidispec interferometer, whilst the camera was focused on and around the silicon die. Care was taken to optimise the interferometer, in terms of reference beam path length compensation (vital for speckle correlation to be achieved) and reference beam intensity. Figure 7.3 shows a live image of one of the die-attach system analysed.

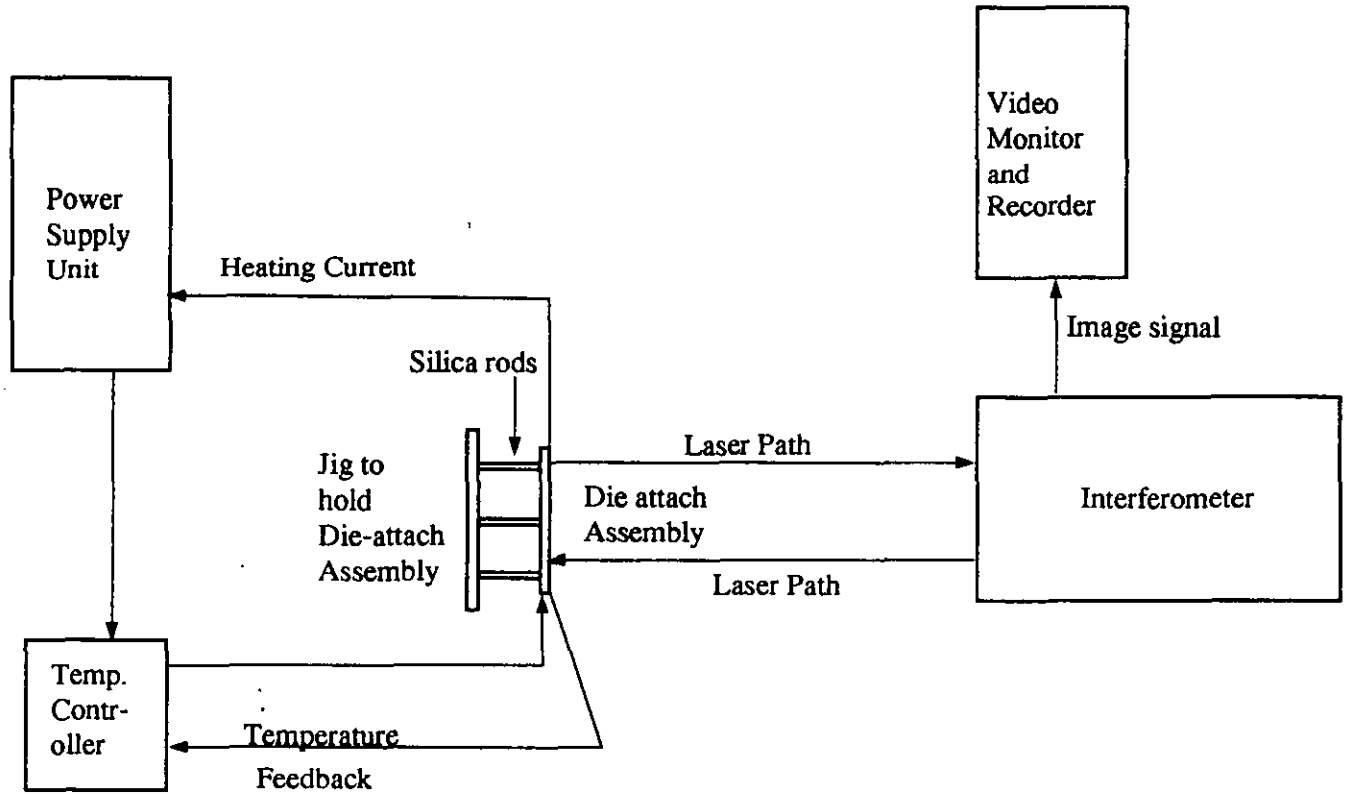

Figure 7.2: Schematic of the equipment set up for ESPI

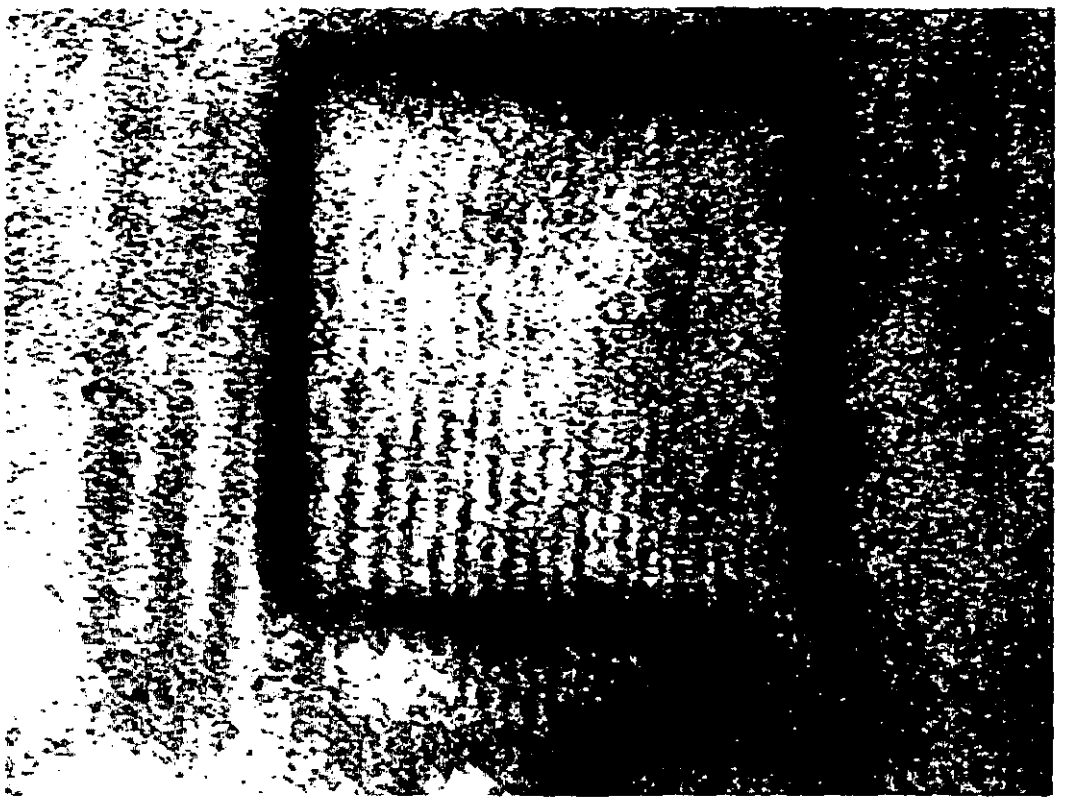

Figure 7.3: A live image of the die-attach assembly

Correlation fringes were obtained by taking an initial reference image of the specimen before deformation (i.e cooling), which was stored in a solid state frame memory store. Cooling initiated thermally induced contraction of the substrate, adhesive layer and silicon die, thus altering the speckle pattern. At frame rates (25Hz), each subsequent speckle image was subtracted from the stored reference image, producing real-time correlation fringes, displayed on the video monitor.

Rapid cooling causes large displacements and consequently a high number of fringes (up to 300). Realistically, it becomes difficult to observe more than twenty fringes on a monitor screen. This problem is solved by refreshing the frame store memory at appropriate intervals. Continuity of experimentation is maintained by adding each set of fringe patterns together. Hence an initial out- of-plane deformation of 6μm will produce approximately 19 fringes. If the subtraction unit is refreshed at this stage and a further displacement of 5μm (16 fringes) is observed, then a total deformation of 11μm or35 fringes is recorded. In this manner, by repetitively resetting the frame store during the cooling cycle, the total experimental deformation is recorded in ten to fifteen stages.

Analysis of the data is difficult in real-time, because the initial cooling rate is very rapid, causing intense fringe activity and consequently frequent refreshing of the frame store. Thus all of the monitor data is stored on video tape for examination. For this application, it is necessary to interrogate the video tape, frame by frame, manually observing and counting the build-up of fringes, during each correlation sequence.

7.7. Results

The linear Finite Element Analysis predicted a bowing mode of deformation similar to that observed using ESPI (Figure 7.4). The analysis was conducted considering cooling from a temperature range of 300°C to 25°C with the assumption that the whole system is in equilibrium at 300°C. The Finite Element Analysis predicted a total displacement of 71.8μm. Fringe counts have been obtained from analysis of the video tape data. Three separate experiments produced counts of 266, 265 and 267 fringes. Using equation 7.4, these values can be converted into the respective displacement values, 84.2, 83.8 and

84.5μ m (Table 2)

	Model μm	Experiment μm	Difference μm	%Error
Exp. 1	71.8	84.2	12.4	15
Exp. 2	71.8	83.8	12.0	14
Exp.3	71.8	84.5	12.7	18
Mean	71.8	84.2	12.4	15

Table 7.2: Comparison of results

The cooling curves can be seen to have a good correlation as they all follow the exponential characteristics expected of cooling curves. It should however be noted that there are fewer data points for the cooling curve for EXP.1. hence the discrepancy between the curve and the other curves.

The displacement-time curves (Figures 7.5a&b) followed the same trend as the cooling curves because of the linear proportionality of the coefficient of expansion of the two dominant components of the system, namely the silicon die and the alumina substrate, to temperature. The discrepancy between EXP. 3 and the other two is due to the rapid initial deformation during the first 20 seconds leading to potentially large uncertainties of fringe counting in these regions. Fringe counting becomes more accurate as cooling rate decreases. This is shown by the graph lines converging.

7.8. Discussion

Ideal cooling of a plate element produces uniform contraction. In this study, the silicon die was bonded on the underside to the alumina substrate, hence in-plane strain was restricted, whereas out-of-plane movement was the dominant deformation. An example of uniform contraction is represented by the fringe pattern shown in Figure 7.4b. A series of circular fringes can be observed overlying the die and continuing on the substrate,

showing the components to be contracting at approximately the same rates and in a similar manner. Real time viewing of the correlation fringes reveals the formation characteristics. The fringes evolve from the centre of the picture, spreading out as more are formed, due to the bending of the substrate with the thermal gradient. Each fringe represents a line of isoamplitude, the distance between one fringe and the next representing a displacement in that region of $\lambda/2$. Hence from the centre of the die to the outside edge, it can be estimated that there is a displacement difference of 1.5μm. This behaviour is typical of thermally loaded constrained plates or membranes, during their heating or cooling cycles.

Uniform contraction of the test specimens is an ideal scenario, and one not often encountered during experimentation. Due to differing coefficients of thermal expansion, and inconsistencies of bond quality, the symmetrical pattern presented in Figure 7.4b can be completely distorted. Figure 7.6 depicts such an event, with a clear discontinuity of the fringes occurring at the lower die/substrate boundary, but not at the upper boundary. This behaviour suggests poor bond quality at the lower boundary region, causing differential contraction of the specimen to occur.

Circular fringe patterns are associated with the initial cooling stages of the specimens, emanating from the centre of the die, but at lower temperatures, asymmetric cooling becomes more apparent. This is evident as parallel straight or curved fringe sets moving across the specimen, in particular directions. Contraction of this nature is a function of the boundary conditions, in this case, as the system is well insulated, conductive cooling to the base plate of the apparatus via the silver palladium electrodes, and convective cooling to the atmosphere. The change of direction of the fringes can also be associated with the differential cooling of the different components of the die-attach assembly and the degree of freedom offered by the method of restraint. Since the heat comes directly from the resistor film on the back of the substrate, a thermal gradient is created from the substrate to the silicon die.

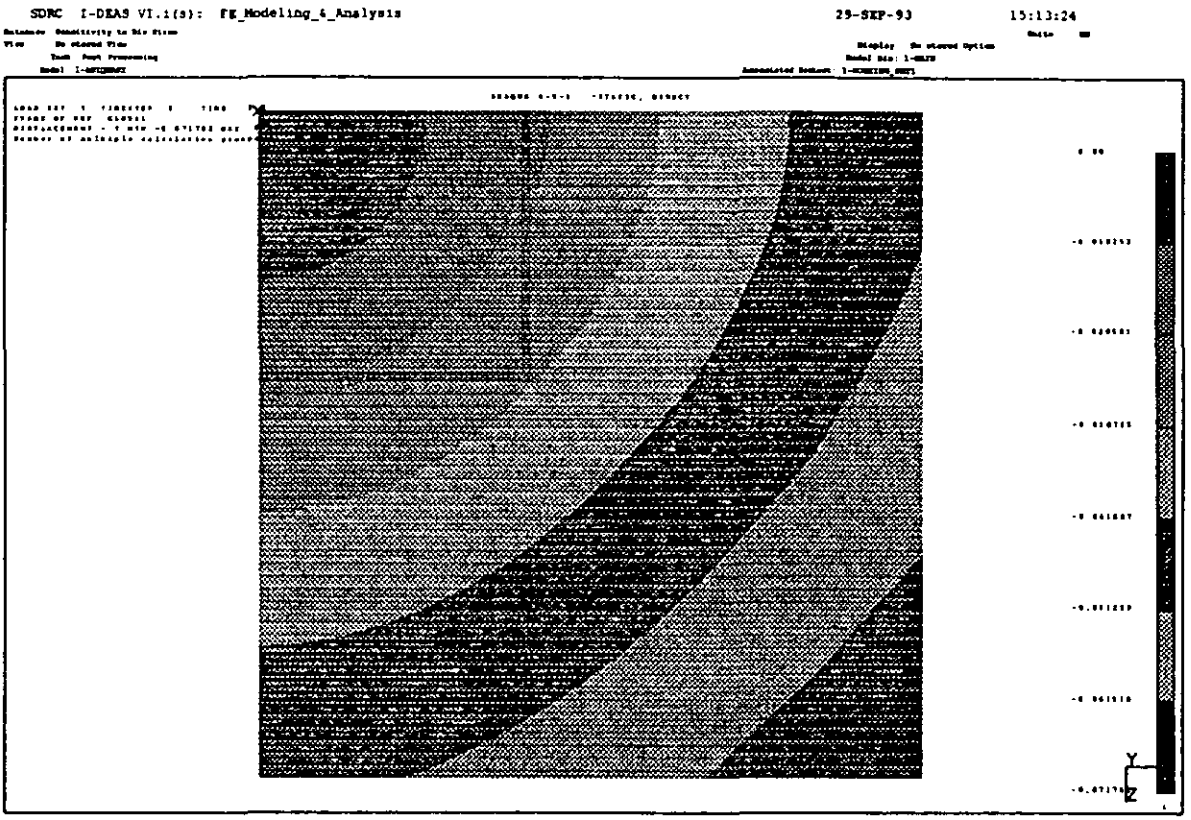

a

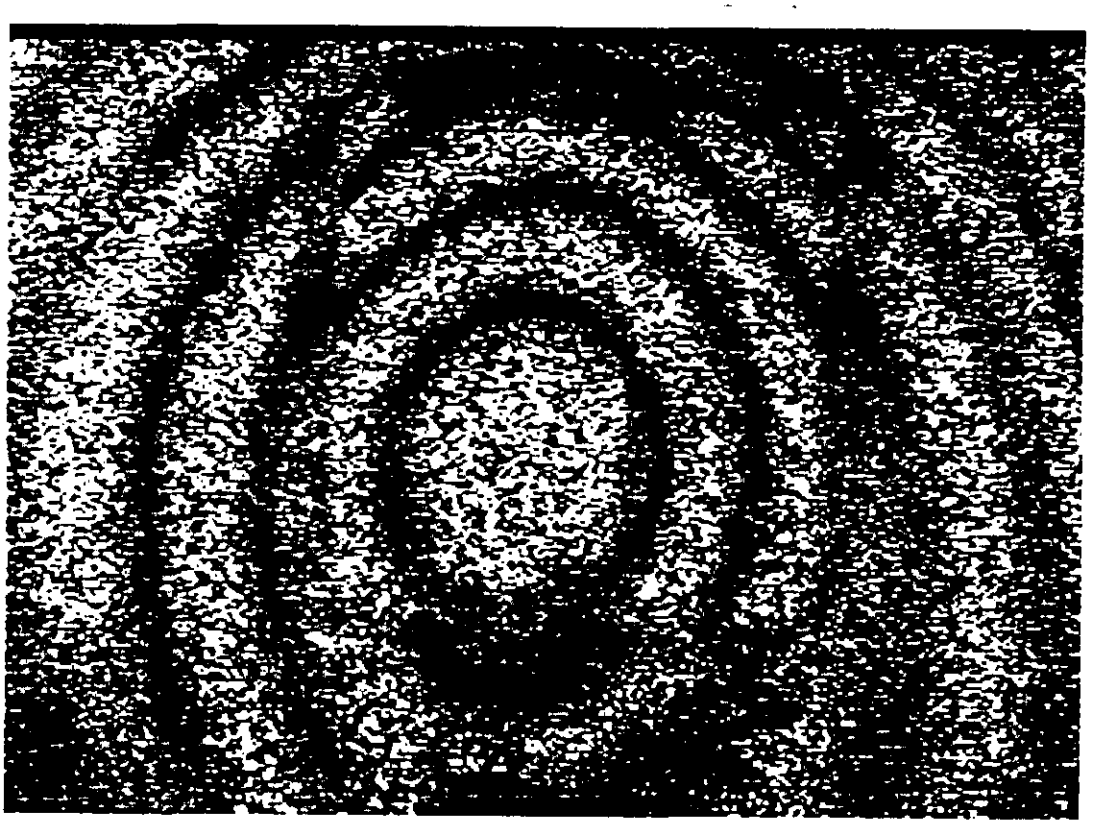

b

Figure 7.4 a&b: Modes of deformation

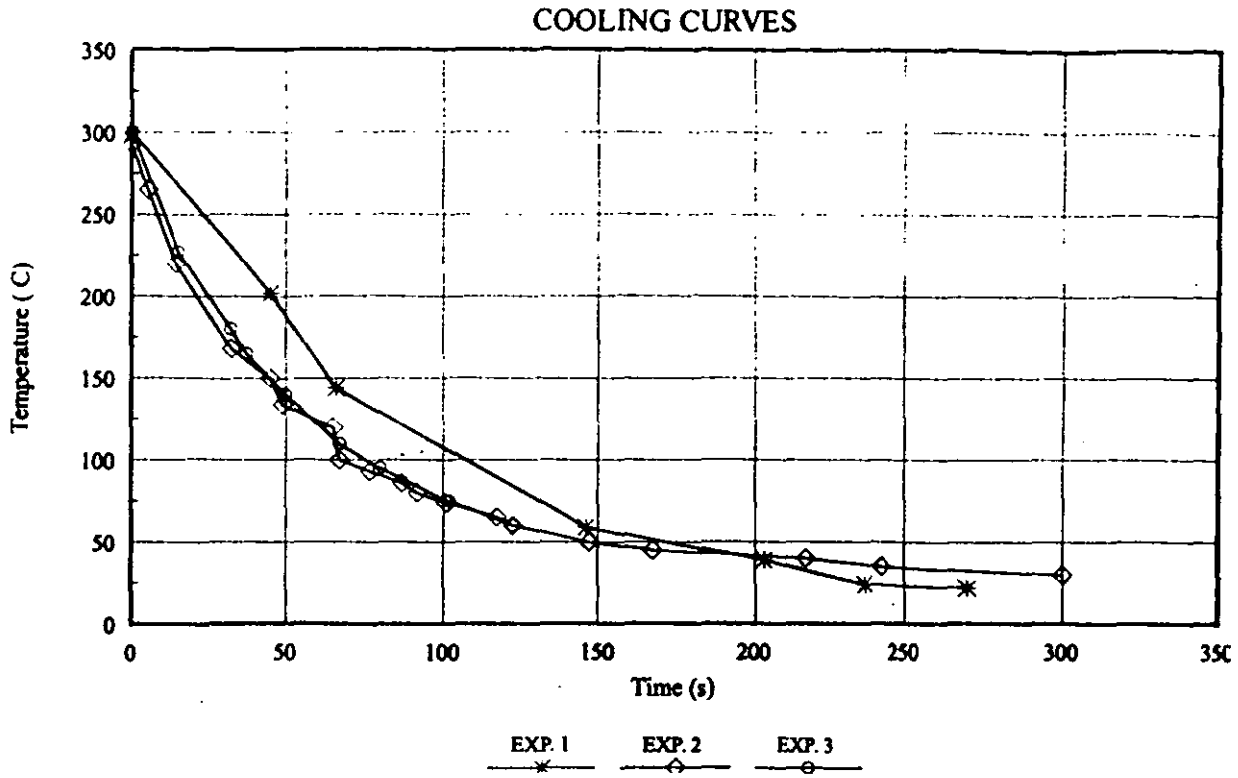

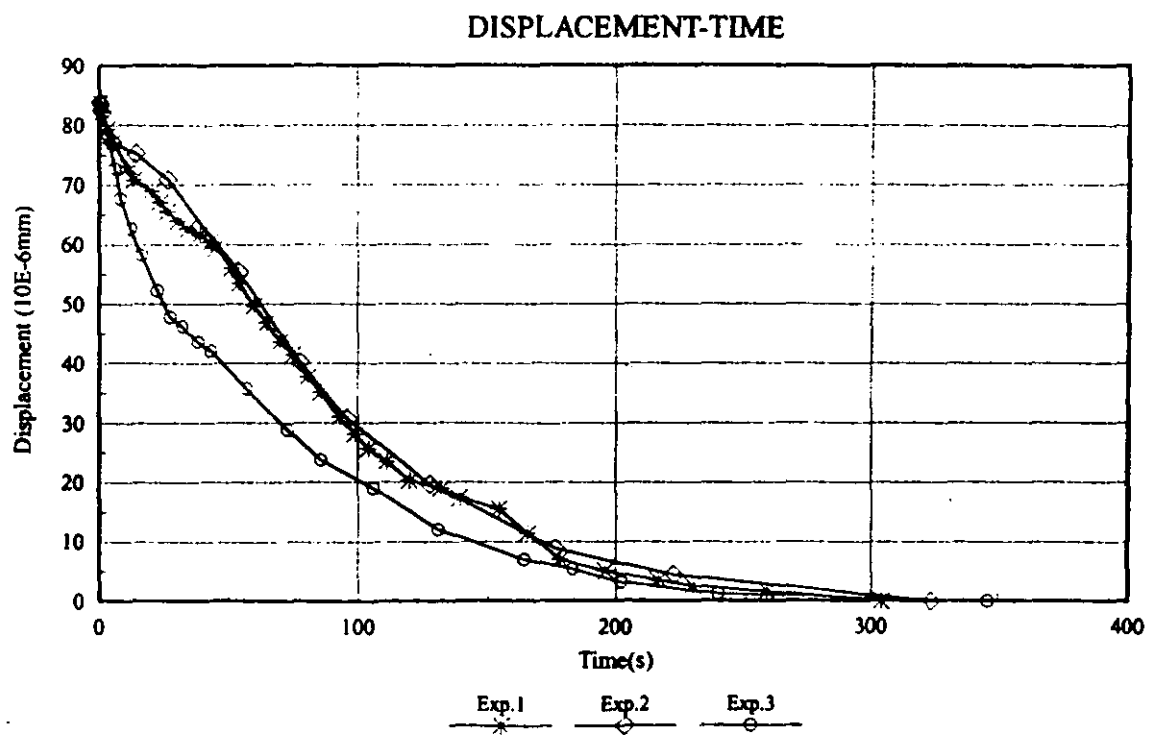

Figure 7.5: cooling and displacement characteristics

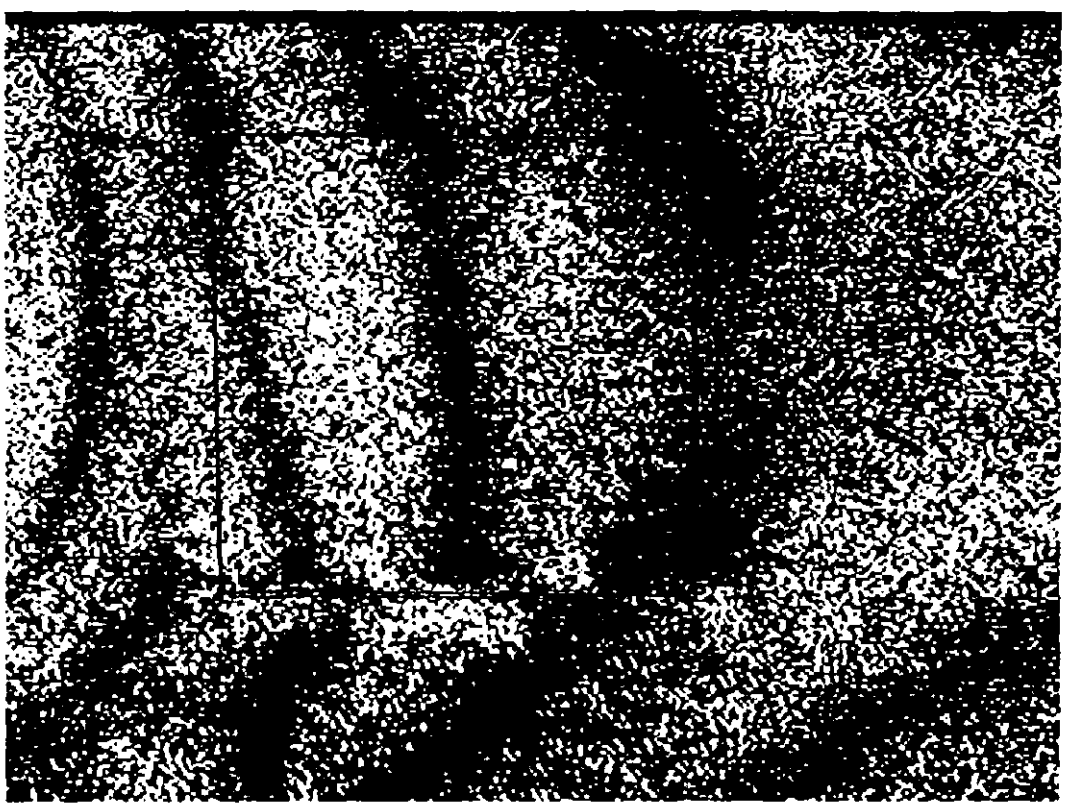

Figure 7.6: Discontinuous fringes indicating non-uniform bonding

The out-of-plane interferometer has a first order resolution of $\lambda/2$, represented as a single black fringe. Accurate counting of fringes thus imparts a maximum uncertainty of one fringe (316nm), if the rate of fringe formation is slow and even. These experiments contained two potential sources of fringe counting uncertainty. Firstly the very rapid initial cooling causes rapid movement of the associated fringe sets, often exceeding the temporal resolution of one camera frame. Secondly, each frame refresh operation takes a finite time (dependant on the speed of the operator), hence fringe data may be lost during earlier stages of the experiments, although this will be in the order of a few fringes only. The analysis leads to the conclusion that the fringe count values will be minimum counts. A realistic estimate of the potential uncertainty for each count is plus ten fringes (3.2 μm or 4%). Similarly evaluation of results and indeed elimination of errors can be improved upon by developing vision systems capable of counting the fringes automatically.

An important issue that has been overlooked by the approximation is the effect of the thermal coefficient of expansion of the thick film resistor on the out of plane displacement of the die attach system. It is however difficult to quantify this effect as the resistor is needed to supply heat to the system. Similarly, the assembly was heated from the back only creating a thermal gradient across the thickness of the assembly. This is in contrast to the model in which every point in the model was assumed to be at the same temperature. This assumption in the model is expected to contribute to the discrepancy in the experimental and modelling results.

7.9. Conclusion

The results of this experiment shows that the result of the models are qualitatively correct and in reasonable quantitative agreement given the fact that the there will be some discrepancies in measured material properties (as in the model) and the real property exhibited by the materials during the experiment. The non linear and temperature dependent properties of both the silicon die and the adhesive have not been modelled because of the lack of sufficient information on the non-linear materials properties.

ESPI has been successfully applied as a method for calibrating Finite Element models and an inspection method. The results shows remarkable improvement on strain gauges as it eliminates the calibration problem constantly faced by the users of strain gauges for experimental validation.

Chapter 8

Conclusions

8.1. Introduction

This thesis has described the use of finite element analysis to investigate the effect of manufacturing processes on electronics interconnection. The approach has used both global and local models. The global model addressed the heat transfer from the reflow furnace to the printed circuit board which may contain thousands of interconnections. This stage of the work demonstrated the feasibility of modelling a commercial reflow furnace using finite element analysis. The local model addressed the thermal stress arising from the heat distribution in a typical assembly. The local model used in this thesis concentrated on conductive adhesives because these materials are relatively new when compared to solder which has received considerable attention over the years. Relevant materials property that affects the structural integrity of such interconnections were also identified.

Overall this thesis has demonstrated the feasibility of using finite element analysis to model the thermal and thermo-mechanical effects of manufacturing processes on electronics interconnection. This chapter summarises the contributions of the investigation. An assessment of electrically conductive adhesives for electronics interconnection is made in the light of these results. The contributions and limitations of the modelling method applied in this work are also discussed and opportunities for further work identified.

8.2. Summary of Results

Before discussing the conclusions from this work in greater depth, the contributions of the various aspects of the work, discussed in the earlier chapters are summarised below.

8.2.1. Literature Review

A review of literature outlined in chapter 2 shows that the effect of manufacturing processes on electronics interconnection has not been well addressed when compared to studies on the reliability of products in service. This is highlighted by the relative shortage of technical publications on the issue. Similarly, reports of experimental stress analysis for reliability in service, identifies modes of failure but fails to explain their mechanism. Constitutive equations and other forms of analytical methods excluding finite element analysis can identify mechanisms but often fail to adequately map stress to specific locations on realistic geometries of electronic interconnections. However, a combination of relevant experimental methods with the finite element method, as shown in this work, can be used to fully investigate the effect of manufacturing processes on electronics interconnection. Balance of this thesis forms two groups of work, global-local modelling programme supported by experimental verification.

8.2.2. The Reflow Furnace Trials

The set of trials reported in this work evaluates the contribution of the different modes of heat transfer found in a commercial reflow furnace to the temperature distribution of the printed circuit board (PCB) as it goes through the furnace. The furnace used was a state of the art commercial furnace which enabled the evaluation of components like the edge heaters, which were believed to help improve heat distribution on the PCB. The trials and the data collected gave the major parameters for the computer model of the furnace and its calibration. The experiment also gives a better understanding of the reflow furnace and the mechanism of heat transfer to the board. The knowledge gained in this area can be used to improve the design of the furnace and the layout of the board so as to avoid adverse consequences of excessive heat on the board.

8.2.3. The Development of a Process Model of the Senju Reflow furnace at IBM Greenock

The development and use of the model significantly improves upon the sole use of data loggers to predict the temperature distribution of the PCB as it goes through the reflow furnace. The model gives a visual account of the temperature distribution on the PCB for the whole of its presence in the furnace and over the whole area of the board. It enables the prediction of the temperature distribution during reflow, while offering the conven-

ience and economic advantage of the investigation of a variety of reflow profiles in a short time, and with considerable savings in experimental hardware and allows more informed design decisions. The output from this model can also be used to identify critical areas of the board and the temperature distribution used as boundary condition for a localised model of the particular areas and interconnection. Although, in this work, the temperature distribution used in the modelling of the die attach assembly was not taken from the model of the PCB through the reflow furnace, the former model is an example of a localised model of the latter.

8.2.4. Materials Property Measurements

The materials property measurements enable the characterisation of the materials used for this work. The materials properties are the most important variable used by the finite element method to predict the behaviour of a structure because the material properties determine the mechanical characteristics of the components. The major contribution from this chapter is the characterisation of the conductive adhesives used in this work. A novel way of preparing conductive adhesive samples for property testing was also developed. The materials properties determined included the glass transition temperature and the comparison of the variation of the modulus of elasticity with temperature for range of conductive adhesives. The creep study also allowed the comparison of the behaviour of the adhesives indicating that conductive adhesives are capable of higher mechanical strength than solders in service.

8.2.5. Modelling of the Conductive Adhesive Die-Attach Assembly

The modelling of the conductive adhesive die attach assembly quantifies the sensitivity of the assembly to design variables. The results indicate that the bondline thickness should be above 30μm for good stress management. Similarly the sensitivity of the stresses in the assembly to the material properties of the conductive adhesive was quantified. The presence of voids in the adhesive layer, was found to not, as a mechanical entity, act as stress raisers, however, further work is required in this area in order to fully quantify the effect of voids. Similarly, a sawn through die was found to be better for stress management while the level of stress in the die does not change significantly for sizes greater than 4mm x 4mm. Until this work, the fear that the larger the die, the greater the stress has been a major factor discouraging the use of conductive adhesives for large

area die attach.

The models revealed that silicon die with <110> orientation will not be appropriate for stress sensitive applications because the level of stress on the surface of such die is higher than other orientations. The modelling methodology also shows that axisymmetric models offer a good approximation to 3-dimensional models with considerable savings in time and computer resources during analysis.

8.2.6. The Use of Electronic Speckle Pattern Interferometry to calibrate Finite Element Models

Any process model needs to be calibrated to avoid unreliable predictions. The use of Electronic Speckle Pattern Interferometry to calibrate the adhesive die attach model demonstrates the part to be played by this optical method in future experimental stress analysis. It also shows that the models in this work are qualitatively correct and quantitatively accurate to within 15%. The quantitative discrepancies are due to the cumulative experimental errors in the materials property measurement and the ESPI procedure. It is also perhaps worth mentioning that the non-linear properties of the conductive adhesives as exhibited in real life, and the materials properties changes as a result of changes in chemistry of the components of the assembly due to the manufacturing processes (especially, adhesion and adhesive cure) cannot be incorporated in the model. For example, formation of intermetallics from absorption of elements from adjacent materials and the effect of contamination from flux and solvent during processing are difficult to incorporate in the analysis.

Overall, the use of ESPI as a method for calibrating finite element models of electronics interconnection and as an inspection method for good bonds was successfully demonstrated. The results also show an improvement on the use of strain gauges because it can be applied to smaller components without the usual calibration problems and the errors of the physical presence of the strain gauge.

8.3. Solder or Electrically Conductive Adhesive?

The use of conductive adhesive for electronics interconnection is an attractive technology involving fewer process steps and a lower curing temperature than soldering. It also avoids the environmental issues surrounding the use of CFC-based flux cleaners and the use of lead. The prospect of anisotropically conductive adhesives which conduct electricity only along one axis promises very fine pitch interconnection beyond the practical capabilities of soldering. However, conductive adhesive technology is in its infancy and very little is known about the behaviour of the product and manufacturing process. Most of the processing issues are actively being investigated and this work has been carried out as part of efforts to address technical issues arising from the effect of the manufacturing processes on the structural integrity of assemblies constructed using conductive adhesives.

The results of the work outlined particularly in this thesis indicate that conductive adhesives are capable of higher mechanical strength than solders at elevated temperature. This is particularly highlighted by the results of the strain creep measurements where conductive adhesives were shown to creep less than solders, and DMTA measurements where the modulus of elasticity of some conductive adhesives at 200°C, a temperature past the eutectic range for solders, were shown to be as high as 75% of their values at room temperature.

A consequence of this result is that while solder is capable of relieving stress (arising from manufacturing processes) over a period of time, the stresses are locked into the structure for a longer time in the conductive adhesive interconnection. However, the model has shown that the stresses arising from the manufacturing processes only are not capable of permanent damage unless aided by flaws or defects in the components. These stresses are perhaps the highest instantaneous thermal stress to be experienced by the assembly as thermal stresses due to operation will be much lower. Similarly, the results of the model show that there is no significant increase in stress with increasing die sizes above 4mm x 4mm suggests that size will not be a limiting factor for the application of conductive adhesives. With increasing demands for interconnections capable of operating at higher temperatures (typically 175°C and above), conductive adhesives appear to be the ideal candidates for high temperature applications in the automotive and aerospace applications.

It was also mentioned in the earlier chapters that the current generation of conductive adhesives are been engineered for specific applications. There are low T_g epoxies for stress management, where stress levels are a major concern, high T_g epoxies for high temperature application and thermoplastic adhesives for ease of rework. Conductive adhesives are therefore more versatile than lead-tin solders. At present, the difficulty with rework is a major factor mitigating against the use of other types of conductive adhesives except the thermoplastic polyimide.

8.4. Modelling

The feasibility of modelling an oven with true commercial complexities (with mixed mode of heat transfer) has been demonstrated in this work. This is a step forward in resolving the temperature related issues in the problems of solder reflow and adhesive curing. The nature of the temperature related problem requires a complete understanding of the temperature distribution of the printed circuit board in question. A visual account as well as point to point data is produced by the modelling process, a procedure that is almost impossible experimentally, due to the cumbersome setup and the practicalities associated with collecting the amount of data needed. The application of modelling in studying the effect of manufacturing processes on the die-attach assembly highlights the versatility of this method as a valuable tool in the investigation of a range of problems encountered in electronics manufacturing.

Materials property and validation of models remain a critical issue in the application of this method. The accuracy of the results of the model depends mainly on accurate material properties and a model which accurately captures appropriate boundary conditions. Verification of the models showed that the appropriate boundary condition has been applied and the predicted results are reasonable. Materials properties are difficult to find or establish and the accuracy of such data when available are often questionable as in many cases there are variations in values of properties depending on the method of measurement. Similarly, with the miniaturisation of electronic components, the small size of components is making it difficult to verify models with the known experimental measurement techniques such as strain gauges. The more relevant optical methods also have limitations arising from factors like the wavelength of light from available sources

and the resolution of images. The discrepancy between experiments and modelling are often due to a cumulative error arising from approximations in modelling, which may include inaccurate materials properties, and experimental errors from the verification method.

The approach in this work has been the application of commercially available finite element software as it was inappropriate to generate a new solver when well developed, versatile and user friendly software was already available. This work also sought to be industrially relevant and it was intended that the results of the work, including the model could be used by such industry. This required it to be based upon a robust commercial system. There are however limitations to the use of commercial packages and indeed the use of finite element analysis, as outlined below.

8.4.1. Practical size limits

There are limits to the amount of finite elements/nodes that typical software can handle. Also, the problem of scale appears when there are extreme dimensions in the model. An example from this work is the modelling of the furnace where the length of the furnace is 3.5m in length as compared to the die attach layer of 50μm. This type of extreme dimensional range will introduce numerical errors in the analysis. The general approach to overcoming this type of error is to use local or sub-models with a reasonably true dimensions.

8.4.2. Trade-offs.

The need for commercial software packages to be generic and easy to use leads to trade-offs in the accuracy and efficiency of computation in the following ways;

a. Constitutive equations that are easier to solve numerically are often used and are not necessarily totally representative of the typical situation under analysis. This can limit the validity of the results.

b. The use of iterative methods for solving equations forces value changes in data input to be gradual. This means that the detail present in real experimental data cannot be accommodated. Therefore, for example, experimental results such as the creep curves in chapter 5 have to be smoothed or pre-

sented as a step change for analysis purposes to prevent convergence errors being introduced during solution. This may reduce the accuracy of results because primary/secondary yield phenomena for example may not be adequately represented by the data.

c. In order to model special effects such as non-linear properties of materials, data that are difficult to acquire or results from unreliable experimental techniques are often needed. Such data is required for the representation of the constitutive equations that are used in the solvers because they are convenient to solve numerically.

d. The issue of the scale of dimensions limits the details of results obtainable from each analysis, for example, macroscopic and microscopic phenomena cannot be modelled together in a single model. The user has to chose the appropriate level of modelling.

e. Often, the initial bulk material properties of a typical material used as a test sample is used as input for finite element models. Other variables resulting from changes in these properties from the chemistry of materials interaction as a result of the manufacturing or other process that is been modelled cannot be accommodated in a finite element models. For example, as mentioned earlier, formation of intermetallics from absorption of elements from adjacent materials and the effect of contamination from flux and solvent during processing are difficult to incorporate in the analysis.

Although finite element analysis is an approximate method and despite all the limitations mentioned above, it is more accurate than most of the other analytical methods. It produces much useful information and more importantly enables the visualisation of the problem in question. Experience and good engineering judgement are required to effectively decipher the results of a typical analysis.

8.5. Overall Conclusions

This thesis has demonstrated the feasibility of using finite element analysis to model the thermal and thermo-mechanical effects of manufacturing processes on electronics interconnection. Similarly optical methods were demonstrated as an effective method of validating models of electronics interconnection. The thesis also demonstrated the use of

finite element modelling to investigate a wide variety of problems associated with such interconnections while the relevant material properties that affect the structural integrity of the interconnections were identified. Linear material properties have been assumed in these models, taking into consideration the non-linear properties of some of the relevant materials the results predicted are conservative and the stresses are expected to be slightly lower in real life. The thermal processes modelled in this work are manufacturing processes and as such these results are therefore only valid for these conditions. This work contributes towards efforts in the "physics of failure" approach to understanding the reliability of electronics interconnections. This approach is in contrast to the statistical approach which solely considers statistical data collected historically.

8.6. Suggestions for further work

The work reported in the preceding chapters shows that the feasibility of a predictive method of investigating the effect of manufacturing processes especially in electronics interconnection has been demonstrated. However, the work presented in this thesis is only a starting point and an improved understanding of the effect of manufacturing processes on the product is still needed. Much progress can be made continuing the approach of this work. Therefore the following suggestions are made for further work.

8.6.1. A viscoelastic modelling of conductive adhesives.

The major difference between the performance of conductive adhesives and solders can be identified by understanding the different behaviours of the materials under the same service or processing conditions. This can only be furnished by a full viscoelastic model of the conductive adhesive. In order to do this using the ABAQUS finite element solver, full experimental data from both the shear mode and bulk modulus modes of creep will be required. The designed practicality of implementing a representative test procedure remains an issue.

8.6.2. Reliability modelling.

A more accurate prediction of reliability of interconnection can be made by incorporating the combined effect of the stresses from manufacturing processes, as predicted by the models in this work, with field reliability modelling. The incorporation of the effect of manufacturing defects into such reliability models would improve their validity

should they be combined to predict the interconnection life. This will require finite element models with the appropriate boundary conditions (incorporating the effect of manufacturing processes) to simulate the operating conditions of the product. The results of such an analysis can be used in reliability constitutive equations to predict the life of the product.

8.6.3. Materials property measurements

Emphasis should be laid on the measurement of materials properties such as modulus of elasticity, thermal coefficient of expansion, creep and stress relaxation as they form the major input for finite element models. Accurate materials properties are needed for a better understanding of linear and non-linear materials property of the adhesives. However better methods of preparing samples to reflect the geometry and state of materials found in application need to be developed.

8.6.4. Improvement of the reflow furnace model

While there is a good correlation between the current model and the experimental result on the heating portion of the process cycle, the correlation is not as satisfactory on the cooling portion. The cooling models could be improved to reflect real cooling phenomenon. Perhaps the use of a computational fluid dynamics model rather than area proportional conductance, as used in this work, would improve the model.

8.6.5. Effect of rework

The effect of rework on interconnections is often neglected. The assembly is subjected to extremely harsh thermal conditions during rework. The localised heating often applied during rework may not cause visible damage but can result in residual stresses that may subsequently lead to failure during service. A finite element analysis of the rework process and the incorporation of the results of this exercise into our understanding of reliability in service could have a major impact.

References

[1]. Suhir, E., Structural Analysis in Microelectronic and Fibre -optic Systems, Volume I, Van Nostrand Reinhold, New York, 1991, Chapter 17.

[2]. Champion, E.R.,Jr., Finite Element Analysis in Manufacturing Engineering, McGraw-Hill, Inc. New York,1992, Introduction.

[3]. Baran, N.M., Finite Element Analysis on Microcomputers, McGraw-Hill, Inc. New York,1988, Chapter 1.

[4]. National Agency for Finite Element Methods & Standards(NAFEMS), A Finite Element Primer., HMSO, 1986. Chapter 1-2.

[5]. Suhir, E., Structural Analysis in Microelectronic and Fibre -optic Systems, Volume I, Van Nostrand Reinhold, New York,1991, Chapter 13.

[6]. Baran, N.M., Finite Element Analysis on Microcomputers, McGraw-Hill, Inc. New York,1988, Chapter 3.

[7]. Gilleo, K., "Solderless assembly reduces cost, hazards and pollution", Proceedings of IVF Seminar, Gottenburg, October 1991, Paper 16.

[8]. Conway P.P., Williams, D.J., Whalley, D.C., Tang, A.C.T. and Sargent P.M., "Process Variables in the Reflow Soldering of Surface Mount", Final Report of the ACME Research Grant GR/F/34596, 1991.

[9]. Katsuri, S., "Forced Convection: The Key to SMT Reflow", Technical Proceedings of Nepcon East, June 1990, p800-887.

[10]. Dow, S.J., "The use of zone segregated forced convection in SMT mass Reflow soldering", Technical Proceedings Nepcon West, June 1990, p823-840.

[11]. Zarrow, P., "IR Reflow Soldering Systems and Steps", Circuits Manufacturing, Vol. 28, 1988, p47-49.

[12]. Holloway, W. and Pignato, J., "The emergence of Multi-mode Heating For SMT mass solder Reflow Systems", Technical Proceedings Nepcon West, June 1990, p13-22

[13]. Hey, D., "Making the right choice of Reflow Technologies", Electronics

Manufacture and Test. June, 1988, p42-48

[14]. Gothard, A.,"Reflow choices Multiplying Fast", Electronics Manufacture and Test, June, 1988.

[15]. Walton, J.P, "Infrared vs. Vapour Phase Reflow", Electronic Production, Vol. 16 No. 6, June 1987, p9-14.

[16]. LoVasco, F., "Solder Joint Modelling using Finite Element Analysis", Proceedings of IEPS, 1988, p410-415.

[17]. Hall, P.M. Dudderar, T.D, Argyle, J.F., "Thermal Deformations observed in Leadless Ceramic Chip Carriers Surface Mounted to Printed Wiring Boards", IEEE Transaction on Components Hybrid and Manufacturing Technology, Vol. CHMT-6 No. 4, December 1983.

[18]. Solomon, H.D., Brzozowski, V., Thompson, D.G, "Predictions of Solder Joint Fatigue Life", Proceedings of the IEE 40th Electronics Components and Technology Conference, 1990.

[19]. Kojima Y, Sakiura, J., Matsunaga. K., "Experimental and Analytical Study of Fine Pitch QFP Solder Joint Reliability", Proceedings of IEEE Japan IEMT Symposium, June 1993. p181.

[20]. Eftychiou, M.A, Bergman, T.L and Masada, G.Y., "A Detailed Thermal Model of the Infrared Reflow Soldering Process", Journal of Electronic Packaging, Vol. 115, March, 1993., p55-62.

[21]. Whalley, D.C., Conway, P.P., and Williams, D.J.,"Thermal Modelling of Temperature Development During the Reflow Soldering of SMD Assemblies", Proceedings of the 6th ISHM International Microelectronics Conference, Tokyo, May 1990. p120-124.

[22]. Bolger, J.C. and Mooney, C. T., "Die Attach in Hi-Rel P-Dips: Polyimides or Low Chloride Epoxies?", IEEE Transactions on Components, Hybrids and Manufacturing Technology, Vol. CHMT-7. No. 4, December 1984. p394-398.

[23]. Bolger, J.C. and Mooney, C. T., "Failure Mechanisms for epoxy die attach adhesives in plastic encapsulated I.C's", Proceedings of IEEE 33nd Electronics Components conference, May 1983. p227-231.

[24]. Riemer, D.E., "Electrical Equivalent Method of Thermal Stress Analysis"

Proceedings of the 39th Electronic Component Conference, Texas, May 1989, p869-874.

[25]. Suhir, E., Structural Analysis in Microelectronic and Fibre -optic Systems, Volume I, Van Nostrand Reinhold, New York,1991, Chapter 17.

[26]. Hu, J.M., Pecht, M. and Dasgupta, A., "Design of Reliable Die Attach", The International Journal of Microcircuits and Electronic Packaging, Vol.16, 1993.

[27]. Suhir, E.,"Calculated Thermally induced Stresses in Adhesively bonded and soldered Assemblies" Presented at International Symposium on Microelectronics, ISHM, 1986.

[28]. Suhir, E., "Stress in Adhesively Bonded Bi-material Assemblies used in Electronic Packaging", Proceedings of Material Research Society Symposium, No. 72,1986. p133-138.

[29]. Suhir, E., "Die Attachment Design and its Influence on Thermal Stresses in the Die and the Attachment", Proceedings of IEEE 37th Electronic Components Conference, 1987. p508-517.

[30]. INSPEC, Properties of Silicon. Institute of Electrical Engineers, London, 1992.

[31]. Tumala R.R. and Rymaszewski, E.J, Microelectronics Packaging Handbook, Van Nostrand Reinhold, New York, 1989.

[32]. Minges, M.L., Electronics Materials Handbook, Vol.1-Packaging, ASM International, Materials Park, Ohio, 1989.

[33]. Seraphim, D.P., Lasky, R.C and Li, C.Y., Principles of Electronic Packaging, Design and Materials Science, McGraw-Hill, New York, 1989.

[34]. Pecht, M., Handbook of Electronic Packaging Design, Marcel Dekker, New York, 1991.

[35]. American Society of Testing and Materials, Annual Book of ASTM Standards, Philadelphia (Updated annually).

[36]. Institute of Interconnecting and Packaging Electronic Circuits, Test Methods Manual, IPC-TM-650, (Updated Intermittently).

[37]. Touloukian, Y.S, Kirby, R.K., Taylor, R.E., Lee, T.Y.R., Thermophysical Properties of Matter, Vol.13: Thermal Expansion, Nonmetallic Solids, Ple-

num Publishing Corporation, New York 1977, p12a-37a.

[38]. Saraf, R.F., Tong, H.M, Poon, T.W. Silverman, B.D., Ho, P.S. and Rossi, A.R, Thickness-Direction Thermal Expansion Measurements", Journal of Applied Polymers, Vol.46, 1992, p1329-1337.

[39]. Synder, W.B., Sutton, W.H., Iskander, M.F. and Johnson, D.L., Microwave Processing of Materials II, Materials Research Society, Pittsburgh, PA, 1991, p117-119.

[40]. Chen, W.T and Abel H., Advances in Electronic Packaging, Vol. 1, EEP-Vol. 1-1" American Society of Mechanical Engineers, New York,1992, p463-468.

[41]. Beatty, C.L and Weaver, J.L., "Effect of temperature on the compressive stress-strain properties of Polystrene", Polymer Engineering Science, Vol. 18, 1978, p1109.

[42]. Darveaux, R. and Barneji, K., "Constitutive Relations for Tin Based Solder Joints", Proceedings of the 42nd Electronic Components and Technology Conference, Institute of Electrical and Electronic Engineers, New York, 1992, p538-551.

[43]. Bernier, G.A. and Kline, D.E., "Dynamic mechanical behaviour of a polyimide", Journal of Applied Polymer Science, Vol. 12, 1968, p.593

[44]. Aklonis, J.A and Macknight, W.J., Introduction to Polymer Viscoelasticity, Wiley-Interscience Publication 1983.

[45]. Ferry, D.J., Viscoelastic Properties of Polymers, Wiley, New York, 1961

[46]. McCrum, N.G, Read, B.Eand Williams, G., "Anaelastic and Dielectric Effects in Polymeric Solids", John Wiley & Sons, 1967.

[47]. Wetton, R.E., Marsh, R.D.L. and Van-de-Velde, J.G., "Theory and Application of Dynamic Mechanical Thermal Analysis", Thermochimica Acta, 175, 1-11, Elsvier Science Publishers B.V., Amsterdam, 1992, p1-11

[48]. Bauer, C.L and Farris, R.J., "Determination of Poisson's ratio for polyimide films," Polymer Engineering and Science, vol. 29, 1989, p1107.

[49]. Fernades, N.J., Bergman, T.L., and Masada, G.Y., "Thermal Effects During Infrared Solder Reflow-Part 1: Heat Transfer Mechanisms", Journal of Electronic Packaging, Vol.114 March 1992, p41-47.

[50]. Ennis, T.J., Brady, N., Keane, B. and Donnelly, A., "A Study of the Effects of Infra-red Reflow Profile on Solder Joint Strength and Structure", Soldering and Surface Mount Technology, No. 12, October 1992.

[51]. Spencer, J., "Calculating Stress and Mobility in Silicon Chips using strain gauge measurements," Semiconductor Engineering Journal, Vol. 1981, p34-37,

[52]. Guo, Y. and Woychik, G.C., "Thermal Strain Measurements of Solder Joints in Second Level Interconnections Using Moire Interferometry", Journal of Electronic Packaging, Vol. 114, March 1992, p88-92.

[53]. Gee, S.A, Van Den Bogert, W.F., Akylas, V.R. and Shelton, R.J., "Strain-Gauge Mapping of Die Surface Stresses ", IEEE Transactions on components, Hybrids and Manufacturing Technology, Vol. CHMT-12, No.4, December 1989,p343-350,

[54]. Lim C.K., "Mechanical and Materials Modelling /Simulation/Verification Trend for Electronics Packaging Products", Proceedings of Electronic Component and Technology Conference 1993, Orlando Florida. p238-248.

[55]. Window, A.L. and Holister, G.S., Strain Gauge Technology, Applied Science Publishers Ltd., Essex, 1982, p2.

[56]. Suhir, E., Structural Analysis in Microelectronic and Fibre -optic Systems, Volume I, Van Nostrand Reinhold, New York, 1991, p375

[57]. Pfann, W.G. and Thurston, R.N., "Semiconducting Stress Transducers Utilizing the Transverse and Shear Piezoresistance Effects", Journal of Applied Physics, Vol. 32. No. 10. 1961. p2008-2019.

[58]. Steel, D.V., "Internal Stresses Developed in an Epoxy Resin Potting Compound During Long-Term Storage", Polymer Engineering & Science, Oct. 1965, p280

[59]. Jordan, R.B. "Determination of Encapsulated Strains", presented at Semicon West Hysol Symposium, May 1978.

[60]. Usell, R.J. Jr. and Smiley, S.A. "Experimental and Mathematical Determination of Mechanical Strains within Plastic IC Packages and their effect on Devices during Environmental Tests", Proceedings of the IEEE on Microelectronic Test Structure, Orlando, Florida, 1981, p65-73.

[61]. Akylas, V.R.,Gee, S.A., and Van Den Bogert, W.F., "The Design and Calibration of a Semiconductor Strain Gauge Array", Proceedings of the IEEE International Conference on Microelectronic Test Structures, February 22-23, Long Beach, California, 1988.

[62]. Lanchberry, J.F. and Shorthouse, G., "Measurement of Stress and Temperature Distribution in Large Area Dies", 8th International Electronic Manufacturing Technology Symposium, May 1990, Bavieno, Italy, p287-293.

[63]. Woisetschlager, J., Sheffer, D.B., Mikati, H., Somasundaram, K., Loughry, C.W., Chawla, S.K. and Wesolowski, P.J., "Breast Cancer Detection by Holographic Interferometry", Proceedings of SPIE-The international Society for optical Engineering, Vol. 1756, July 1992, p176-182.

[64]. Pryputniewicz, R.J.," Holographic and Finite element studies of vibrating beams", Proceedings of SPIE-The international Society for optical Engineering, Vol. 599, July 1985, p54-62.

[65]. Juptner, W.P.O., Geldmacher, J., Bischof, T. and Kreis, T., "Measurement of the deformation of a pressure vessel above a weld point", Proceedings of SPIE-The international Society for optical Engineering, Vol. 1756, July 1992, p98-105.

[66]. Han, B. "Higher Sensitivity Moire Interferometry for Micromechanics studies", Optical Engineering, Vol. 31, No. 7, 1992, p1517-1526,

[67]. Batawros, A.F., Voloshin, A.S. and Rodogoveski, P., "Experimental Validation of Fractional Fringe Moire Interferometry", Proceedings 1989 SEM Spring Conference on experimental Mechanics, Cambridge, MA, May 1989, p401-406.

[68]. Bastawros, A.F. and Voloshin, A.S., "Thermal Strain measurements in Electronic Packages through Fractional Fringe Moire Interferometry", Journal of Electronic Packaging, Vol. 112 December 1990, p303-308.

[69]. Lim, C.K., "Mechanical and Materials Modelling/Simulation/Verification Trend for Electronics Packaging Products", Proceedings of IEEE Electronic Component and Technology Conference, Orlando, Florida, 1993. p238-248.

[70]. Biederman, S.W. and Pryputniewicz, R.J., "Holographic study of vibrations of a wing section", Proceedings of SPIE-The international Society for optical Engineering, Vol. 1756, July 1992, p153-163.

[71]. Charette, P., Hunter, I.W., Hunter, P.J., "Biaxial Testing of pericardium using electronic speckle pattern interferometry (ESPI)", Proceedings of SPIE-The international Society for optical Engineering, Vol. 1756, July 1992, San Diego, U.S.A. p196-197.

[72]. Jones, R. & Wykes, C., Holographic and speckle interferometry, Cambridge studies in modern optics, Cambridge University Press, 1989.

[73]. Wykes, C., "Use of electronic speckle Pattern Interferometry (ESPI) in the measurement of static and dynamic surface displacements", Optical Engineering, Vol. 21, No. 3, May 1982. p400-406.

[74]. Flattery, D.K., "Infrared Reflow for the solder Attachment of Surface Mount Devices", Hybrid Circuits, No.9 1986. p32-40.

[75]. Lea, C., A scientific Guide to Surface Mount Technology, Electrochemical Publications Ltd., 1988, p223-228.

[76]. Personal Communication with Process Engineer at IBM Greenock, August 1991.

[77]. Ogunjimi, A.O, Boyle O., Whalley, D.C, and Williams, D.J, "A review of the impact of conductive adhesive technology on interconnection", Journal of Electronics Manufacturing Vol. 2 1992, p109-118.

[78]. Conway, P.P, Ogunjimi, A.O., Sargent, P.M., Tang, A.C.T, Whalley, D.C, Williams, D.J, and Chisholm, A.W.J., "SMD Reflow Soldering: A Thermal Process Model", Annals of the CIRP Vol. 40, January 1991, p21 - 24.

[79]. Whalley, D.C, Ogunjimi, A.O., Conway, P.P and Williams, D.J., "A Process Model of the Infra-red Reflow Soldering of Printed Circuit Board Assemblies"., Journal of Electronic Manufacturing, Volume 2, No. 1, March 1992, p23-30

[80]. Ward, I. M., Mechanical Properties of Solid Polymer, John Wiley &Sons, London 1971, p15.

[81]. Personal Communication with Dr. J.C Duncan of Polymer Laboratories, Loughborough, U.K, March 1993.

[82]. Folkes, M.J. and Hope, P.S., Polymer Blends and Alloys, Chapman & Hall, Glasgow, 1993. p146.

[83]. Kinloch, A.J., Thrusabanjong, E., and Williams, J.G., "Fracture at bimate-

rial interfaces: the role of residual stresses", Journal of Materials Science, Vol. 26, p6260-6270, 1991.

[84]. Chung, K.K.T. and Koehn, W., "Low Tg Epoxy Adhesives for Thermal Management", 4th International SAMPE Electronics Conference, p241-254, June 1990.

[85]. Nguyen, M.N. and Wood, J.H., "Silver Filled Polyimidesiloxane Die Attach Material", 4th International SAMPE Electronics Conference, p291-412, June 1990.

[86]. Farag, M.M., Selection of Materials and Manufacturing Processes for Engineering Design, Prentice Hall International (UK) Ltd.

[87]. Kinloch, A.J., Adhesion and Adhesives, Chapman and Hall, London, 1986. p264-313.

[88]. Hall, P.M., "Forces, Moments, and Displacements During Thermal Chamber Cycling of Leadless Ceramic Chip Carriers Soldered to Printed Boards", Vol CHMT-7, p314-327, December 1984.

[89]. Ghandi, S.K., "VLSI Fabrication Principles: Silicon and Galium Arsenide", John Wiley & Sons, New York 1993. p10-12.

[90]. Ogunjimi, A.O., Whalley, D.C. and Williams, D.J., "A Comparison of Modelling Methods for Electronic Interconnect Structures", Proceedings of the 43 IEEE Components, Hybrids and Manufacturing Technology Conference, Orlando, June 1993, p871-876.

[91]. Hu, J.M., Pecht, M. and Dasgupta, A., "Design of reliable die-attach", The International Journal of Microcircuits and Electronic Packaging, Vol. 16, Number 1, 1993 p1-21.

[92]. Kinloch, A.J., Adhesion and Adhesives. New York: Chapman and Hall, 1987, ch. 6.

Appendix 1

Time Varying temperature profile for the infrared panels of the radiation only model

The program reads, from an input file, the label for the finite elements of the infrared panels and their length, number of heater zones for the top and bottom, conveyor belt speed and the duration of the PCB in the furnace. Based on this information, a temperature history table for each element (identified by its label) is created for the duration of the PCB in the furnace.

```
# include <stdio.h>

float   limit(z, zz) /* limit z to between 0 and zz */
float   z, zz;
{
        if (z < 0)
                z = 0;
        if (z > zz)
                z = zz;
        return(z);
}


main(argc, argv)

int     argc;

char    *argv[];

#define max_no_of_zones 20
#define max_no_of_elements 250


{
        int     count,
        count2,
        no_of_elements,
        no_of_zones;

        float   element_length,
        belt_speed,
        maximum_time,
        distance[max_no_of_zones],
        top[max_no_of_zones],
        bottom[max_no_of_zones],
        x, y;

        char    dummy[100],
        spacer[2];

        FILE * input_file, *output_file;

        if ( (input_file = fopen(argv[1], "r")) == NULL) {
                perror(argv[1]);
                exit(1);
        }
        output_file = fopen(argv[2], "w");
        fscanf(input_file, "%e %s", &element_length, dummy);
        fscanf(input_file, "%i %s", &no_of_elements, dummy);
        fscanf(input_file, "%e %s", &belt_speed, dummy);
        fscanf(input_file, "%i %s", &no_of_zones, dummy);
        fscanf(input_file, "%e %s", &maximum_time, dummy);
        fscanf(input_file, "%s,%s,%s", dummy, dummy, dummy);
        count = 0;

        while (count < no_of_zones) {
                count++;
                fscanf(input_file, "%e,%e,%e", &distance[count], &top[count], &bottom[cou
        }
        distance[no_of_zones+1] = 1E6;
        count = 0;
        while (count < no_of_elements) {
                count++;
                fprintf(output_file, "INTERP   %d         %d          %3d  1.00000E+00\n"
        }
        count = 0;
```

```
        while (count < no_of_elements) {
                count++;
                fprintf(output_file, "TABTYPE   %3d TEMP         TIME\n", count);
        }
        count = 0;
        while (count < (no_of_elements / 2)) {
                count++;
                count2 = 0;
                while (count2 < no_of_zones) {
                        count2++;
                        x = (distance[count2] - distance[no_of_zones] + count * element_
                        x = limit(x, maximum_time);
                        fprintf(output_file, "TABDATA   %3d  %.5E  %.5E\n", count, top[c
                        y = (distance[count2+1] - distance[no_of_zones] + (count - 1) * e
                        y = limit(y, maximum_time);
                        fprintf(output_file, "TABDATA   %3d  %.5E  %.5E\n", count, top[c
                }
        }
        while (count < no_of_elements) {
                count++;
                count2 = 0;
                while (count2 < no_of_zones) {
                        count2++;
                        x = (distance[count2] - distance[no_of_zones] + (count - no_of_e
                            belt_speed;
                        x = limit(x, maximum_time);
                        fprintf(output_file, "TABDATA   %3d  %.5E  %.5E\n", count, botto
                        y = (distance[count2+1] - distance[no_of_zones] + (count - 1 - n
                            / belt_speed;
                        y = limit(y, maximum_time);
                        fprintf(output_file, "TABDATA   %3d  %.5E  %.5E\n", count, botto
                }
        }
        fprintf(output_file, "-1\n");
        fprintf(output_file, "-1\n");

        fclose(input_file);
        fclose(output_file);

}
```

Appendix II

Time varying temperature profile for the edge heaters of the radiation + edge heaters model of the senju furnace

The first and last finite element labels for each edge heater on either side, the length of each element, the heat flux from or temperature of the edge heaters, belt speed and the duration of the PCB in the furnace are read from the input file. Based on this information, a temperature or heat flux history table for each element (identified by its label) is created for the duration of the PCB in the furnace. This table is combined with the table generated from Appendix I in the model

```
#include <stdio.h>
#include <math.h>

main(argc, argv)

int     argc;

char    *argv[];

{
        int     fle,
        lle,
        fre,
        lre,
        count,
        count1,
        count2,
        count3,
        prv,
        j,
        jl,
        y;

        float   flux,
        bs,
        tdt,
        swot,
        fnlt,
        elt;

        double  x;

        char    dummy[100];


        FILE     * input_file, *output_file;

        if ( (input_file = fopen(argv[1], "r")) == NULL) {
                perror(argv[1]);
                exit(1);
        }
        output_file = fopen(argv[2], "w");
        fscanf(input_file, "%d %s", &fle, dummy);
        fscanf(input_file, "%d %s", &lle, dummy);
        fscanf(input_file, "%d %s", &fre, dummy);
        fscanf(input_file, "%d %s", &lre, dummy);
        fscanf(input_file, "%f %s", &flux, dummy);
        fscanf(input_file, "%f %s", &bs, dummy);
        fscanf(input_file, "%f %s", &elt, dummy);
        fscanf(input_file, "%f  %s", &fnlt, dummy);

        count2 = 1000;


        for (count = fle; count <= lle; count++) {
                fprintf(output_file, "INTERP  %i  %i  %i  1.00000E+00\n",
                    count, count, count2);
                count2++;
        }

        for (count = fre; count <= lre; count++) {

                fprintf(output_file, "INTERP  %i  %i  %i  1.00000E+00\n",
                    count, count, count2);
                count2++;
        }
```

```
            count, count, count2);
        count2++;
}

for (count = fre; count <= lre; count++) {

        fprintf(output_file, "INTERP  %i  %i  %i  1.00000E+00\n",
            count, count, count2);
        count2++;
}

/* the tabtype table */

count2 = 2000;

for (count = fle; count <= lle; count++)                    {
        fprintf(output_file, "TABTYPE  %i  QNODE  TIME\n", count2);
        count2++;
}

for (count = fre; count <= lre; count++) {
        fprintf(output_file, "TABTYPE  %i  QNODE  TIME\n", count2);
        count2++;
}

/* calculating flux per node, switch off time and first nodes */
/* to be switched on */

flux = flux / (2 * fnlt) * elt;
swot = fnlt / bs;
j = fle + (lle - fle) / 2;
j1 = fre + (lre - fre) / 2;
count2 = 2000;
count = fre;
count3 = fle;

prv = 0;
for (count1 = 0; count1 <= (int) (swot + 1); count1++) {
        x = j + (bs * count1 / elt);
        y = irint(x);

        while (count3 <= y && count3 > prv && count3 <= lle) {
                fprintf(output_file, "TABDATA  %i 0.0000   0.0000\n",
                    count2);
                if (count1 > 0)
                        fprintf(output_file, "TABDATA %i   0.0000  %i\n", count2,
                            count1);
                fprintf(output_file, "TABDATA %i   %f  %i\n", count2,
                    flux, count1);
                fprintf(output_file, "TABDATA   %i  %f  %f\n", count2,
                    flux, swot);
                fprintf(output_file, "TABDATA %i   0.0000  %f\n", count2,
                    swot);
                fprintf(output_file, "TABDATA %i   0.0000  %i\n", count2,
                    mt);
                prv = count3;
                count2++;
                count3++;
        }


}
printf("completed firstloop\n");
prv = 0;
for (count1 = 0; count1 <= (int) (swot + 1); count1++) {
```

Appendix III

Time varying conductance value for the lumped masses finite elements used to model convection in the complete model of the Senju furnace.

The program is combined with the program in Appendix II for use in the complete model of the Senju furnace. While the first section is the same as in Appendix II, the last section of the program generates a conditional time varying temperature conductance value for the thermal link between the lumped masses and infrared panels. The term conditional is used because the conductance value is dependent on the temperature of the infrared panel elements, being lowest for the elements representing the gap in order to avoid the hot PCB from losing heat to the colder gaps.

```
#include <stdio.h>
#include <math.h>

main(argc, argv)

int     argc;

char    *argv[];

{
        int     fle,
        lle,
        fre,
        lre,
        count,
        count1,
        count2,
        count3,
        prv,
        j,
        j1,
        y;

        float   flux,
        bs,
        tdt,
        swot,
        fnlt,
        elt;

        double  x;

        char    dummy[100];


        FILE     * input_file, *output_file;

        if ( (input_file = fopen(argv[1], "r")) == NULL) {
                perror(argv[1]);
                exit(1);
        }
        output_file = fopen(argv[2], "w");
        fscanf(input_file, "%d %s", &fle, dummy);
        fscanf(input_file, "%d %s", &lle, dummy);
        fscanf(input_file, "%d %s", &fre, dummy);
        fscanf(input_file, "%d %s", &lre, dummy);
        fscanf(input_file, "%f %s", &flux, dummy);
        fscanf(input_file, "%f %s", &bs, dummy);
        fscanf(input_file, "%f %s", &elt, dummy);
        fscanf(input_file, "%f  %s", &fnlt, dummy);

        count2 = 1000;


        for (count = fle; count <= lle; count++) {
                fprintf(output_file, "INTERP  %i  %i  %i  1.00000E+00\n",
                    count, count, count2);
                count2++;
        }

        for (count = fre; count <= lre; count++) {

                fprintf(output_file, "INTERP  %i  %i  %i  1.00000E+00\n",
                    count, count, count2);
                count2++;
        }
```

```
                x = jl + (bs * count1 / elt);
                y = irint(x);


                while (count <= y && count > prv && count <= lre) {

                        fprintf(output_file, "TABDATA  %i 0.0000   0.0000\n",
                            count2);
                        if (count1 > 0)
                                fprintf(output_file, "TABDATA %i   0.0000  %i\n", count2,
                                    count1);
                        fprintf(output_file, "TABDATA   %i %f  %i\n", count2,
                            flux, count1);

                        fprintf(output_file, "TABDATA   %i %f  %f\n", count2,
                            flux, swot);
                        fprintf(output_file, "TABDATA %i   0.0000  %f\n", count2,
                            swot);
                        fprintf(output_file, "TABDATA %i   0.0000  %i\n", count2,
                            mt);
                        prv = count;
                        count++;
                        count2++;
                }

        }
        printf("completed secondloop\n");

        /* convection table */

        count = radtopel;
        count1 = 1000;

        fprintf(output_file, "INTERP  %i  %i  %i  1.00000E+00\n", count, count + 5, count
        fprintf(output_file, "INTERP  %i  %i  %i  1.00000E+00\n", radbotel, radbotel + 5,
        fprintf(output_file, "TABTYPE  %i  COND  TEMP\n", count1);
        fprintf(output_file, "TABTYPE  %i  COND  TEMP\n", count1 + 1);

        while (count1 <= 1001) {
                fprintf(output_file, "TABDATA  %i   0.0000  0.000\n", count1);
                fprintf(output_file, "TABDATA %i   0.0000  100.000\n", count1);
                fprintf(output_file, "TABDATA %i   1.000  100.000\n", count1);
                fprintf(output_file, "TABDATA %i   1.0000  %i\n", count1, mt);
                count1++;
                count = radbotel;
        }

        fprintf(output_file, "-1\n");
        fprintf(output_file, "-1\n");

        fclose(input_file);
        fclose(output_file);

}
```